MULTIPLEX IMMUNOHISTOCHEMISTRY/ IMMUNOFLUORESCENCE TECHNIQUE: THE POTENTIAL AND PROMISE FOR CLINICAL APPLICATION

EDITED BY: Joe Yeong, Bernard A. Fox, Houssein A. Sater, Jaime A. Rodriguez-Canales and Trevor David McKee

PUBLISHED IN: Frontiers in Molecular Biosciences

frontiers Research Topics

frontiers

ISSN 1664-8714
ISBN 978-2-88974-718-4
DOI 10.3389/978-2-88974-718-4

About Frontiers

Frontiers is more than just an open-access publisher of scholarly articles: it is a pioneering approach to the world of academia, radically improving the way scholarly research is managed. The grand vision of Frontiers is a world where all people have an equal opportunity to seek, share and generate knowledge. Frontiers provides immediate and permanent online open access to all its publications, but this alone is not enough to realize our grand goals.

Frontiers Journal Series

The Frontiers Journal Series is a multi-tier and interdisciplinary set of open-access, online journals, promising a paradigm shift from the current review, selection and dissemination processes in academic publishing. All Frontiers journals are driven by researchers for researchers; therefore, they constitute a service to the scholarly community. At the same time, the Frontiers Journal Series operates on a revolutionary invention, the tiered publishing system, initially addressing specific communities of scholars, and gradually climbing up to broader public understanding, thus serving the interests of the lay society, too.

Dedication to Quality

Each Frontiers article is a landmark of the highest quality, thanks to genuinely collaborative interactions between authors and review editors, who include some of the world's best academicians. Research must be certified by peers before entering a stream of knowledge that may eventually reach the public - and shape society; therefore, Frontiers only applies the most rigorous and unbiased reviews.
Frontiers revolutionizes research publishing by freely delivering the most outstanding research, evaluated with no bias from both the academic and social point of view. By applying the most advanced information technologies, Frontiers is catapulting scholarly publishing into a new generation.

What are Frontiers Research Topics?

Frontiers Research Topics are very popular trademarks of the Frontiers Journals Series: they are collections of at least ten articles, all centered on a particular subject. With their unique mix of varied contributions from Original Research to Review Articles, Frontiers Research Topics unify the most influential researchers, the latest key findings and historical advances in a hot research area! Find out more on how to host your own Frontiers Research Topic or contribute to one as an author by contacting the Frontiers Editorial Office: frontiersin.org/about/contact

MULTIPLEX IMMUNOHISTOCHEMISTRY/ IMMUNOFLUORESCENCE TECHNIQUE: THE POTENTIAL AND PROMISE FOR CLINICAL APPLICATION

Topic Editors:
Joe Yeong, Institute of Molecular and Cell Biology (A*STAR), Singapore
Bernard A. Fox, Earle A. Chiles Research Institute, United States
Houssein A. Sater, National Institutes of Health (NIH), United States
Jaime A. Rodriguez-Canales, AstraZeneca (United States), United States
Trevor David McKee, STTARR Innovation Centre, Canada

Citation: Yeong, J., Fox, B. A., Sater, H. A., Rodriguez-Canales, J. A., McKee, T. D., eds. (2022). Multiplex Immunohistochemistry/Immunofluorescence Technique: The Potential and Promise for Clinical Application. Lausanne: Frontiers Media SA. doi: 10.3389/978-2-88974-718-4

Table of Contents

frontiers in Molecular Biosciences

EDITORIAL
published: 25 February 2022
doi: 10.3389/fmolb.2022.831383

Editorial: Multiplex Immunohistochemistry/ Immunofluorescence Technique: The Potential and Promise for Clinical Application

Rachel Elizabeth Ann Fincham[1,2†], *Hamed Bashiri*[2†], *Mai Chan Lau*[2*] *and Joe Yeong*[2,3,4*]

[1]Centre for Tumour Biology, Barts Cancer Institute—A CRUK Centre of Excellence, Queen Mary University of London, London, United Kingdom, [2]Institute of Molecular Cell Biology (IMCB), Agency of Science, Technology and Research (A*STAR), Singapore, Singapore, [3]Singapore Immunology Network, Agency of Science (SIgN), Technology and Research (A*STAR), Singapore, Singapore, [4]Department of Anatomical Pathology, Singapore General Hospital, Singapore, Singapore

Keywords: multiplex immunofluorescence, multiplex immunohistochemistry, immunotherapy, spatial technology, spatial biology, digital pathology, clinical translation

OPEN ACCESS

Edited by:
William C. Cho, QEH, Hong Kong SAR, China

Reviewed by:
Takahiro Tsujikawa, Kyoto Prefectural University of Medicine, Japan

***Correspondence:**
Mai Chan Lau
Lau_Mai_Chan@imcb.a-star.edu.sg
Joe Yeong
yeongps@imcb.a-star.edu.sg

†*These authors share first authorship*

Specialty section:
This article was submitted to Molecular Diagnostics and Therapeutics, a section of the journal Frontiers in Molecular Biosciences

Received: *08 December 2021*
Accepted: *07 February 2022*
Published: *25 February 2022*

Citation:
Fincham REA, Bashiri H, Lau MC and Yeong J (2022) Editorial: Multiplex Immunohistochemistry/ Immunofluorescence Technique: The Potential and Promise for Clinical Application. Front. Mol. Biosci. 9:831383. doi: 10.3389/fmolb.2022.831383

Editorial on the Research Topic

Multiplex Immunohistochemistry/Immunofluorescence Technique: The Potential and Promise for Clinical Application

Conventional immunohistochemistry (IHC) has long been regarded as the "gold standard" for the diagnosis of tissue pathology. However, the diagnostic-prognostic value of this technique is limited by factors such as high inter-observer variability, restricted labeling potential and insufficient availability of samples for testing (Tan et al., 2020). However, the emergence of multiplex immunohistochemistry/immunofluorescence (mIHC/IF) techniques has provided an opportunity to overcome many of these challenges. These techniques facilitate investigation of multiple biomarkers on a single slide as well as exploration of tissue-level biology, classification of cell-cell interactions, and identification of rare cellular phenotypes. mIHC/IF is also a powerful supplement to technologies such as next generation sequencing. As such, mIHC/IF holds the potential to revolutionize cancer therapies and diagnostic pathology (Tan et al., 2020; Hernandez et al.; Lazcano et al.; Parra). In this special edition of Frontiers in Molecular Biosciences we review the importance and clinical translational potential of mIHC/IF.

The COVID-19 pandemic has resulted in an urgent need to understand the implications of myocardial involvement in disease mortality, necessitating detection of viral components within tissue samples. Chong et al., used a combination of mIHC/IF and molecular techniques to examine cardiac autopsy specimens from 12 intensive care unit (ICU) naïve, SARS-CoV-2 PCR-positive patients. These novel findings revealed histopathologic changes in coronary vessels, as well as inflammation of the myocardium in these patients. This study provided crucial insights into the characteristics of COVID-19 patients at risk of sudden death, and suggested the possibility of long-term complications in patients with persistent virus (Chong et al.).

As well as detecting viral particles within tissue samples, mIHC/IF can be used to explore the tumour immune microenvironment (TIME). Through the development of a multiplex panel for the identification of proliferating B cells, follicular helper T cells, and follicular regulatory T cells, Boisson et al., demonstrated the power of mIHC/IF for studying marker co-localization in

individual tissue sections and highlighted the potential application of this technique in clinical practice (Boisson et al.).

To exploit the translational potential of mIHC/IF, Wharton et al., proposed that, until greater levels of standardization across mIHC/IF protocols and pipelines are established, diagnostic laboratories will play a critical role in driving the adoption of multiplex tissue diagnostics through retrospective analysis of clinical trial samples and development of reproducible diagnostic assays (Wharton et al.). In addition, Hoyt provided a discussion of the requirements for the use of mIHC/IF in medical applications and offered suggestions on assay development/improvement. In light of growing health economic concerns in the field of immuno-oncology and the need for tests that precisely predict responses to costly immunotherapies/cell therapies, the translation of mIHC/IF into clinical practice is of paramount importance (Hoyt).

Analysis of the spatial distribution of cells within the tumor microenvironment by mIHC/IF provides important, clinically relevant information; however, with the availability of multiple spatial analysis tools, choosing the correct algorithm remains a challenge. As such, development of robust, standardized analysis pipelines and consensus on their application is necessary to fully exploit the benefits of this technique (Lazcano et al.). In this regard, Parra discussed the analysis of mIHC/IF, with a particular focus on interrogating spatial cellular distribution and concluded that assessment of cell phenotype compartmentalisation and nearest neighbour analysis is the simplest approach to identification of patterns of distribution and cellular interaction (Parra). Similarly, Hernandez et al., noted that in-depth spatial analysis of formalin-fixed, paraffin-embedded patient samples using mIHC/IF facilitates patient stratification for immunotherapy, as well as identification of prognostic and predictive immune biomarkers. Despite these obvious benefits, several limitations were also revealed, including tyramide signal over-reactions, fluorophore constraints and the challenges associated with accurate data interpretation. Thus, a thorough understanding of both the technique and cellular biology are necessary to achieve optimum high-quality data with mIHC/IF (Hernandez et al.).

Apaolaza et al., also highlighted the need for standardized, reproducible image analysis tools for understanding disease pathology and combating the propensity for bias associated with manual analysis. Implementation of such tools may be informative for the improvement and design of novel therapeutic strategies (Apaolaza et al.).

The importance of standardization and quality control is further emphasized by Laberiano-Fernández et al., who highlighted the importance of refining, standardizing and validating the mIHC/IF workflow at the pre-analytical, analytical and post-analytical stages. Laberiano-Fernández et al. also emphasized the importance of antibody selection, optimization and validation as well as the need for the extensive review of panel design and multiplex staining. Similarly, through retrospective assessment, Lazcona et al., demonstrate the importance of assessing tumor content, sample size, and percentages of necrosis and fibrosis for pathology quality control (PQC) in mIHC/IF image analysis (Lazcano et al.). Through workflow standardization and robust PQC, it is hoped that mIHC/IF will become a cornerstone of diagnosis and prognosis in the clinical setting through its incorporation in Clinical Laboratory Improvement Amendments (CLIA) (Laberiano-Fernández et al.).

In conclusion, this special edition encompasses the whole spectrum of current mIHC/IF work, from discovery findings (Boisson et al.; Chong et al.) to translational research (Apaolaza et al.; Hernandez et al.; Hoyt), to guidelines for actual clinical implementation (Laberiano-Fernández et al.; Lazcano et al.). The majority of articles included in this research topic demonstrate the desire of both researchers and clinicians to implement this revolutionary technique into daily clinical practice to ultimately benefit patients. Currently, multiple taskforces and working groups including the Society for Immunotherapy of Cancer (SITC) (Taube et al., 2020) and the Joint Effort to Develop multiplex Immunofluorescence standards (JEDI) council (Nelson et al., 2021; Surace et al., 2021) are working to pave the way for clinical mIHC/IF implementation. Their work includes the writing of expert consensus guidelines and assay checklists; extensive investigation of potential technique errors and generation of technical solutions; standardisation of analysis and evaluation tools; and continued communication with regulatory agents and authorities to understand the gaps and challenges faced in meeting the requirements for clinical application.

With all these efforts, we anticipate that the clinical implementation of mIHC/IF, under proper guidelines and quality assurance/control programs, will come to fruition within the next couple of years.

AUTHOR CONTRIBUTIONS

All authors listed have made a substantial, direct, and intellectual contribution to the work and approved it for publication.

REFERENCES

Nelson, M. S., Jensen, S., Lau, M. C., Surace, M., McKee, T., and Yeong, J. (2021) A Spatial Biology Startup Guide—Part 2. Inside the lab: Biochemistry and Molecular Biology, Technology and Innovation. *The Pathologist*. (https://thepathologist.com/inside-the-lab/a-spatial-biology-startup-guide-part-2 (Accessed January 12, 2022).

Surace, M., Sater, H. A., Andrea, C., Lim, J. C. T., Ballesteros-Merino, C., Canales, J. R., et al. (2021) A Spatial Biology Startup Guide—Part 1. Inside the lab: Biochemistry and Molecular Biology, Technology and Innovation. *The Pathologist*. (https://thepathologist.com/inside-the-lab/a-spatial-biology-startup-guide-part-1 (Accessed January 12, 2022).

Tan, W. C. C., Nerurkar, S. N., Cai, H. Y., Ng, H. H. M., Wu, D., Wee, Y. T. F., et al. (2020). Overview of Multiplex Immunohistochemistry/immunofluorescence

Techniques in the Era of Cancer Immunotherapy. *Cancer Commun.* 40, 135–153. doi:10.1002/cac2.12023

Taube, J. M., Akturk, G., Angelo, M., Engle, E. L., Gnjatic, S., Greenbaum, S., et al. (2020). The Society for Immunotherapy of Cancer Statement on Best Practices for Multiplex Immunohistochemistry (IHC) and Immunofluorescence (IF) Staining and Validation. *J. Immunother. Cancer* 8, e000155. doi:10.1136/jitc-2019-000155

Conflict of Interest: The authors declare that the research was conducted in the absence of any commercial or financial relationships that could be construed as a potential conflict of interest.

Publisher's Note: All claims expressed in this article are solely those of the authors and do not necessarily represent those of their affiliated organizations, or those of the publisher, the editors and the reviewers. Any product that may be evaluated in this article, or claim that may be made by its manufacturer, is not guaranteed or endorsed by the publisher.

frontiers in Molecular Biosciences

REVIEW
published: 29 April 2021
doi: 10.3389/fmolb.2021.667067

Multiplex Immunofluorescence Tyramide Signal Amplification for Immune Cell Profiling of Paraffin-Embedded Tumor Tissues

*Sharia Hernandez, Frank Rojas, Caddie Laberiano, Rossana Lazcano, Ignacio Wistuba and Edwin Roger Parra**

Department of Translational Molecular Pathology, The University of Texas MD Anderson Cancer Center, Houston, TX, United States

Every day, more evidence is revealed regarding the importance of the relationship between the response to cancer immunotherapy and the cancer immune microenvironment. It is well established that a profound characterization of the immune microenvironment is needed to identify prognostic and predictive immune biomarkers. To this end, we find phenotyping cells by multiplex immunofluorescence (mIF) a powerful and useful tool to identify cell types in biopsy specimens. Here, we describe the use of mIF tyramide signal amplification for labeling up to eight markers on a single slide of formalin-fixed, paraffin-embedded tumor tissue to phenotype immune cells in tumor tissues. Different panels show different markers, and the different panels can be used to characterize immune cells and relevant checkpoint proteins. The panel design depends on the research hypothesis, the cell population of interest, or the treatment under investigation. To phenotype the cells, image analysis software is used to identify individual marker expression or specific co-expression markers, which can differentiate already selected phenotypes. The individual-markers approach identifies a broad number of cell phenotypes, including rare cells, which may be helpful in a tumor microenvironment study. To accurately interpret results, it is important to recognize which receptors are expressed on different cell types and their typical location (i.e., nuclear, membrane, and/or cytoplasm). Furthermore, the amplification system of mIF may allow us to see weak marker signals, such as programmed cell death ligand 1, more easily than they are seen with single-marker immunohistochemistry (IHC) labeling. Finally, mIF technologies are promising resources for discovery of novel cancer immunotherapies and related biomarkers. In contrast with conventional IHC, which permits only the labeling of one single marker per tissue sample, mIF can detect multiple markers from a single tissue sample, and at the same time, deliver extensive information about the cell phenotypes composition and their spatial localization. In this matter, the phenotyping process is critical and must be done accurately by a highly trained personal with knowledge of immune cell protein expression and tumor pathology.

Keywords: immune microenvironment, multiplex immunofluorescence, immune profiling, cell phenotyping, immunotherapy

OPEN ACCESS

Edited by:
Joe Yeong,
*Institute of Molecular and Cell Biology (A*STAR), Singapore*

Reviewed by:
Jincheng Zeng,
Guangdong Medical University, China
Jacopo Junio Valerio Branca,
University of Florence, Italy

***Correspondence:**
Edwin Roger Parra
erparra@mdanderson.org

Specialty section:
This article was submitted to Molecular Diagnostics and Therapeutics, a section of the journal Frontiers in Molecular Biosciences

Received: *11 February 2021*
Accepted: *29 March 2021*
Published: *29 April 2021*

Citation:
Hernandez S, Rojas F, Laberiano C, Lazcano R, Wistuba I and Parra ER (2021) Multiplex Immunofluorescence Tyramide Signal Amplification for Immune Cell Profiling of Paraffin-Embedded Tumor Tissues. Front. Mol. Biosci. 8:667067. doi: 10.3389/fmolb.2021.667067

INTRODUCTION

Recently, crucial developments in cellular immunology helped facilitate the translation of immunologic concepts into new immunotherapies. In cancer immunotherapies, the immune system is activated to strike tumor cells through natural mechanisms that were lost or evaded during disease progression (Riley et al., 2019). Instead of directly killing cancer cells, these therapies aim to improve antitumor immune responses, with fewer off-target effects than are observed with chemotherapy agents, shifting the cancer treatment paradigm (Mitchison, 1955; Rosenberg, 2014; Parra et al., 2018; Riley et al., 2019).

The tumor microenvironment consists of tumor cells, immune cells, fibroblasts, tumor vasculature, and the extracellular matrix. Their interactions can promote tumor transformation, tumor protection from host immunity, tumor growth, and tumor invasion and can foster therapeutic resistance (Yu and Cui, 2018). To determine the effect of the host immune response to tumor formation and invasion, researchers can analyze immune components and their organization within human tumors. Because immune infiltrates differ between tumor types and even between patients, an analysis of the location, density, and spatial orientation of the different immune cell populations in large annotated collections of human tumors allows for the identification of beneficial immune components, as well as those that might indicate a poor prognosis (Fridman et al., 2012; Pilla and Maccalli, 2018).

An increasing number of studies have characterized immune infiltrates for T-cell subsets, B cells, macrophages, etc., and some studies have also included activation and functional markers (Bethmann et al., 2017). Immune profiling can be achieved through various technologies, such as conventional technologies [e.g., single immunohistochemistry (IHC) and early-generation fluorescence-based flow cytometry] and multiplex technologies (Parra et al., 2016; Taube et al., 2020; Wang et al., 2020). Conventional technologies, such as single IHC, have many limitations, including fewer available analysis parameters, a greater sample quantity requirement, and sometimes overlapping detection signals. The newer and higher-dimensional technologies avoid many of these limitations (Chuah and Chew, 2020).

Over the last years, multiplex techniques are widely defined as technologies used to identify multiple biological markers in different tissue samples (Dixon et al., 2015; Taube et al., 2020). Using these technologies, individual cells can be assessed with extraordinary fidelity, and rare cell populations can be studied, providing unique biological information that, in many cases, cannot be obtained by conventional techniques (Parra et al., 2019a). Multiplex technologies are based on the analysis of the expression of proteins of interest, which correspond to specific cell types and biological processes, providing an insight about cell characteristics and their biological interactions. Additionally, the resulting single-cell data can be analyzed using qualitative and quantitative approaches in the context of the original spatial arrangement of the tissue cells (Rashid et al., 2019). The spatial cell distributions can be analyzed to link their biological interactions with the morphological characteristics of tumoral tissues (Barua et al., 2018). Compared to previous tissue analysis methods, multiplex technologies provide a more comprehensive view of tissue composition and marker distribution (Bodenmiller, 2016).

In this setting, we find multiplex immunofluorescence (mIF) a powerful and useful tool to identify different cell phenotypes in biopsy specimens. In this article, we describe the use of mIF tyramide signal amplification to for immune cell profiling of formalin-fixed, paraffin-embedded tumor tissues.

PANEL DESIGN AND SELECTION

Designing a mIF panel for a specific project requires selecting and validating appropriate antibodies chosen by a multidisciplinary team of experts in oncology, pathology, and immunology, to ensure that the panel will appropriately address the aims of the project and be able to comprehensively and coherently identify the specific cell phenotypes of interest (Parra et al., 2017, 2020b). Researchers can create panels with groups of markers to study different immune cell populations [using programmed cell death ligand 1 (PD-L1) and programmed cell death 1 (PD-1)], T-cell behavior (using stimulatory and regulatory T-cell markers), and myeloid cell populations (using more targeted panels). Besides, every panel can be customized depending on the type of tumor. For example, cytokeratin antibody can be used as an epithelial tumoral marker (Krishna, 2010), glial fibrillar acidic protein as a glioblastoma marker (Guichet et al., 2016), SOX10/S100 as a melanoma marker (Mohamed et al., 2013), and vimentin as a marker for some sarcomas (**Figure 1**). We can use different immune markers in the mIF panels to identify more specific phenotypes, such as using TMEM119 to identify microglia in brain tissues (Satoh et al., 2016).

TISSUE SELECTION

Ideally, formalin-fixed, paraffin-embedded tumor samples should be at least 10 mm × 2 mm, with tumor cells accounting for at least 10% of the biopsy specimen. Furthermore, a threshold of 100 malignant cells identified by markers is considered necessary to minimize the risk of errors in the analysis and interpretation of the samples, as is the case of PD-L1 expression (Tsao et al., 2018). During the analysis, necrotic areas, such as those observed in tumors treated with neoadjuvant therapies, should be excluded, as should material secreted by tumors, such as mucus, that can limit the quality of the analysis, and the results containing these characteristics should be excluded. Thus, a pathology quality assessment is a very important and necessary step for the selection of oncology samples (Parra et al., 2017).

TISSUE AND CELL SEGMENTATION FOR CELL PHENOTYPING

Overall, the image analysis software, Inform software (Akoya Biosciences), needs to have tools for different purposes, such as

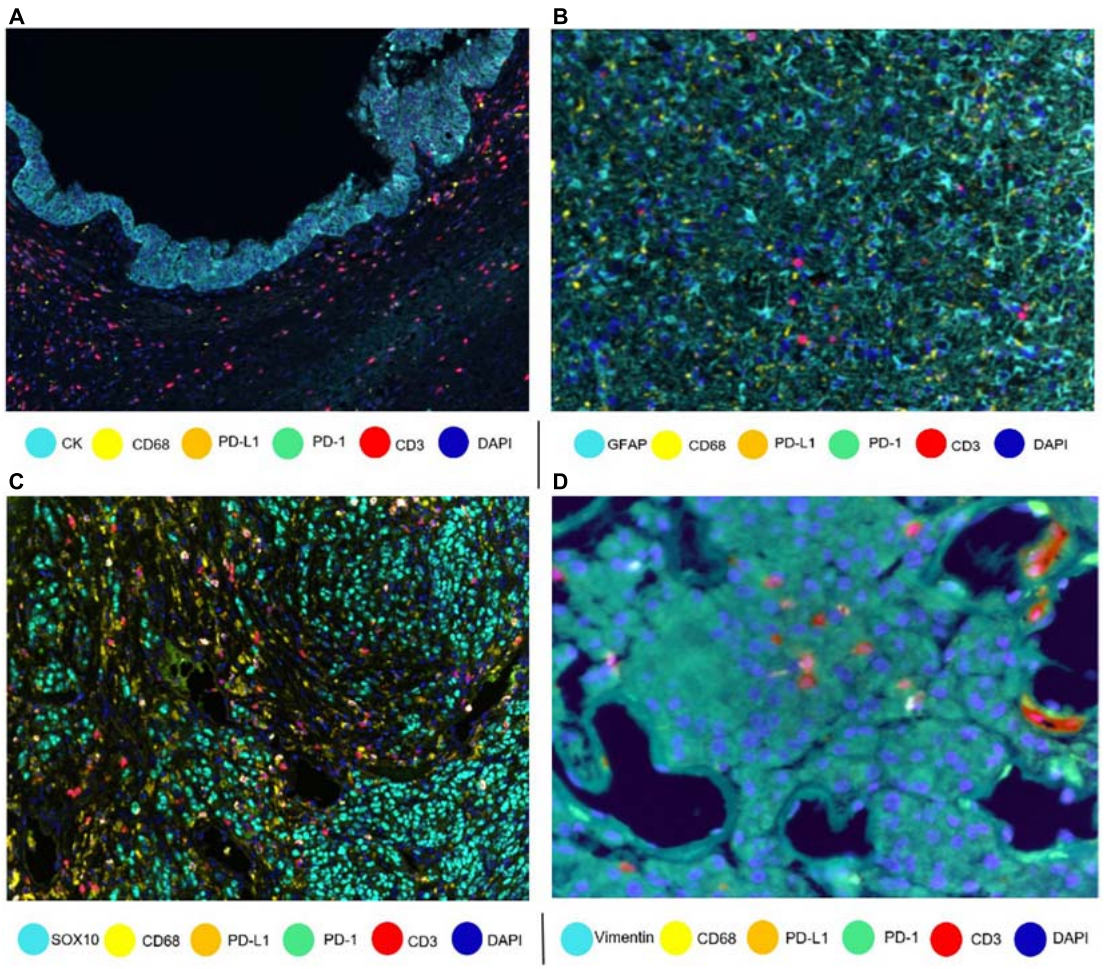

FIGURE 1 | Composites of tumor samples stained with different tumor and epithelium antibodies. **(A)** Intraductal papillary mucinous neoplasm epithelium with cytokeratin (CK). **(B)** Glioblastoma glial cells with glial fibrillar acidic protein (GFAP). **(C)** Melanoma with nuclear SOX10. **(D)** Sarcoma with vimentin.

tumor compartmentalization. Tumor compartmentalization will depend on the markers included in a panel. For this purpose, and based on the expression or absence of tumor markers (e.g., cytokeratin and SOX10/S100), we can divide the image into tumor cell nests and the stromal compartment (Parra et al., 2020b). The tools need to be flexible enough to identify other compartments, such as vessel areas, necrotic areas, and empty space as glass areas (areas without tissue).

Training a software to individualize the cells is crucial and one of the key steps to obtain accurate data. For this purpose, 4',6-diamidino-2-phenylindole is useful, and it is used for nuclear quantitation to visualize nuclear DNA in formalin-fixed, paraffin-embedded tissues (Tarnowski et al., 1991). It can be used alone or in combination with membrane markers, such as CD3, or cytoplasmic markers, such as cytokeratin, to better identify and individualize the cells. Modifying parameters, such as nuclear size and nuclear staining thresholds, or using tools that combine such parameters is essential to better identify and individualize cells. Because every tumor and sample are different, adjusting these parameters based on tumor type will probably be necessary (**Supplementary Figure 1**).

IMPORTANCE OF MARKER IDENTIFICATION

Correct understanding of the individual markers in a mIF panel is crucial to identify different cell phenotypes in tumor tissues. Identifying individual markers and identification of the combination of different markers at different levels are distinct approaches that have a similar goal: cell phenotyping, or the final identification of the marker's co-expression by the same cells. Individual markers, such as the ones used in mIF panels, are complex and can be co-expressed in multiple cells. The image analysis tools can facilitate the creation of thresholds for individual markers, based on the pathology visualization and multiple rounds of software training (**Figure 2**). To create such thresholds, both the morphology of the stained cells and the subcellular compartment that is stained must be considered.

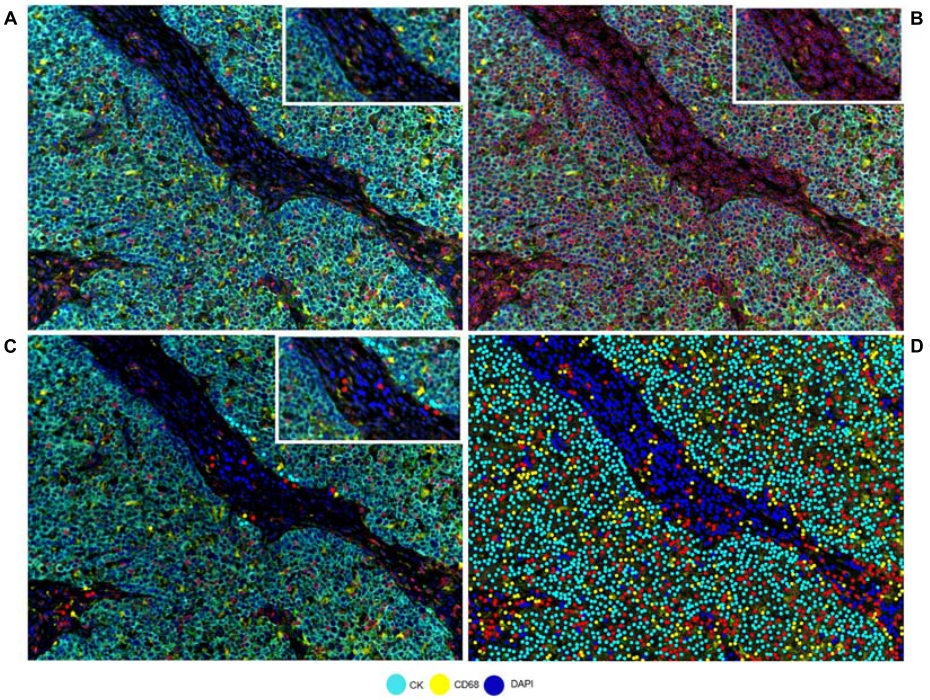

FIGURE 2 | Developing a phenotyping algorithm for an intraductal papillary mucinous neoplasm image. **(A)** Composite image. **(B)** Cell segmentation with red lines surrounding the cells. **(C)** Phenotyping examples. **(D)** Phenotype result of the software after training. White-framed rectangles on the images identify the same area in the four images, and this area has been amplified in the white-framed rectangles on the upper right of each panel.

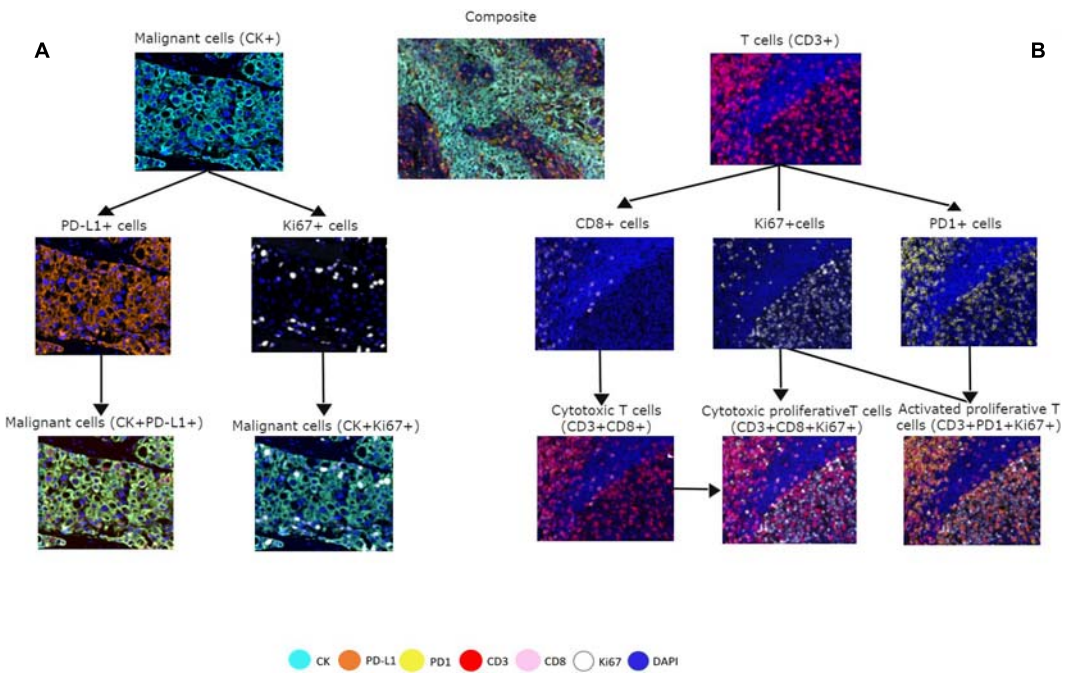

FIGURE 3 | Multiplex immunofluorescence panel showing different cell phenotype co-localizations in tumor and immune cells from a non-small cell lung cancer sample. **(A)** Marker expression of malignant cells with cytokeratin (CK) and co-localization with PD-L1 + and Ki67 +. **(B)** Marker expression of CD3 + on immune T-cells, expression of CD8 + cells, expression of PD-1 + cells, and co-localization with CD3 + CD8 + for cytotoxic T-cells, Ki67 + CD3 + CD8 + for cytotoxic proliferative T-cells, and CD3 + Ki67 + PD-1 + for activated proliferative T-cells. The composite image with all the markers is localized in the upper center of the image.

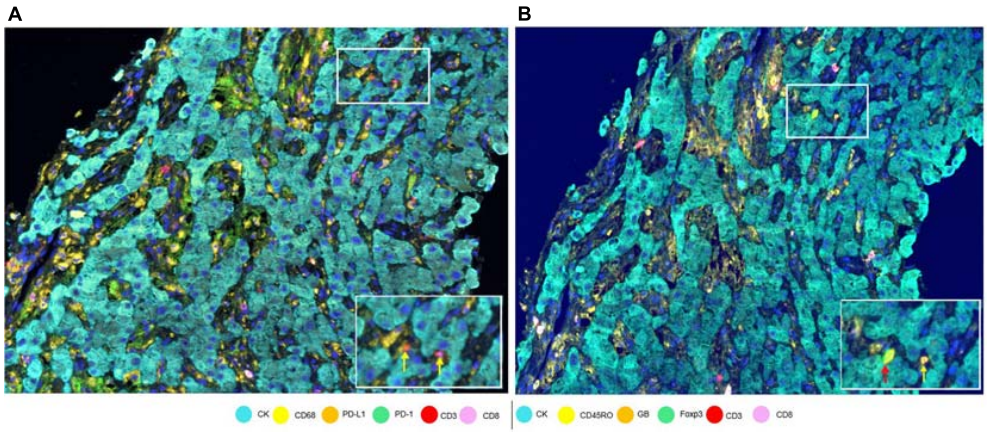

FIGURE 4 | Marker expression in a hepatocellular carcinoma sample. **(A)** Low-magnification image with white-framed rectangles showing two CD3 + cells (indicated by yellow arrows) seen with high magnification at the bottom right of the panel. **(B)** Low-magnification image with white-framed rectangles showing the same two CD3 + cells with co-localizations: CD3 + Foxp3 + CD45Ro (indicated by a red arrow) and CD3 + CD45Ro (indicated by a yellow arrow) seen with high magnification at the bottom right of the panel.

As an example, PD-L1 is expressed by the membrane of tumor cells and macrophages, but because lymphocytes are small cells with very scarce cytoplasm that cannot always be distinguished from the cell membrane, we consider strong lymphocyte cytoplasmic and/or membrane expression to be positive expression. As another example, some cells, such as hepatocytes, can constitutionally express arginase-1 (Yan et al., 2010). However, myeloid cells also express arginase-1 (Grzywa et al., 2020), so co-localization of arginase-1 with cytokeratin in hepatocytes or with CD68 in macrophages helps us to identify the cell phenotype of interest. Also, co-localization can help to distinguish between real staining and artifacts or background. If we have doubts in a subset of cells (e.g., some that express CD8, Foxp3, or PD-1, which can all also be expressed by T-cells), we can always visualize the CD3 co-expression to be sure of the marker expression of that specific cell. Nevertheless, negative controls always need to be included to avoid the autofluorescence that certain tissues emit during the preparation of the image and to obtain a clearer signal, taking off any interference of the autofluorescence.

MARKER CONSOLIDATION AND ASSESSMENT OF CELL PHENOTYPES

Because a single cell can express many immune markers, individual marker analysis is usually a very efficient approach and can result in a large variety of cell phenotypes in the consolidation step, which uses consolidation software, such as R-studio (Ye, 2016) and SAS (Dembe et al., 2011). The data need to be placed in a comprehensive table categorizing immune cell phenotype (co-expression of markers) densities or percentages. The data also need to be reviewed and pass a quality control to ensure their accuracy. For example, the total number of cells should be similar to the quantity of cells observed while processing the image samples. We have also found that processing images, while qualitative, allows a pathologist to become familiar with the images and detect "odd" numbers that do not correlate with the nature of cases. When using multiple mIF panels to study samples, it is important to incorporate a common marker as an internal control in each panel. For example, CD3 is usually used in different mIF panels to study lymphocyte subpopulations. Although different levels of the formalin-fixed, paraffin-embedded biopsy specimens are used, we always try to obtain close cut levels during the staining process of the sample to achieve similar cellularity between panels. This goal makes it possible to compare immune cell phenotypes or total tumor cell numbers to detect a consolidation or processing error. Granted, there is always the possibility of finding differences between similar levels of the same biopsy specimen related to the natural geographic changes of the cells. Pathology comments added to the different samples are very important not only to explain those changes but also to have a retrospective record of what happened with a specific image analysis sample.

To assess cell phenotypes according to the markers in a panel, we use the information given by the image analysis software about the marker expression of each individual cell according to their X and Y coordinates on the image. In this way, with the data consolidation, we can determine all the markers expressed by a single cell and, with this information, identify specific cell phenotypes. Commonly, many cell phenotypes can be identified according to markers in a mIF panel. Panels aimed to study lymphocytes can identify specific cell phenotypes (**Figure 3**), such as cytotoxic T-cells (CD3 + CD8 +), regulatory T-cells (CD3 + CD4 + FOXP3 +), memory T-cells (CD3 + CD45RO +), or T-cells expressing immune checkpoint markers, such as CD3 + PD-1 + or CD3 + PD-L1 + (**Figure 4**). The marker combinations are unlimited and, depending on the panel and markers, are able to show activation of markers, such as OX40 in tumor cells (CK + OX40 +) and rare cells, such as cytotoxic T-cells that express immune checkpoints (e.g., CD3, CD8, PD-1, and PD-L1; **Figure 5**).

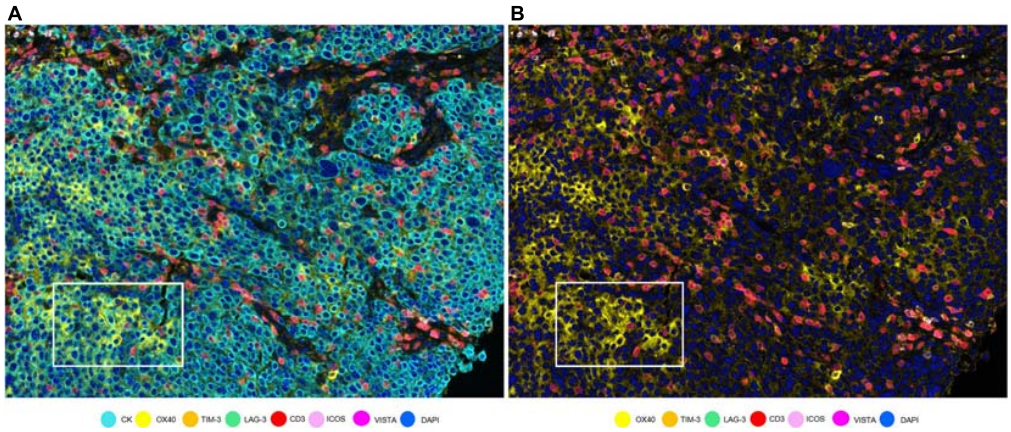

FIGURE 5 | OX40 expression in tumor cells in a non-small cell lung cancer sample. **(A)** Composite with all the markers. White rectangle shows tumor cells with co-localization of cytokeratin (CK, cyan) and OX40 (yellow). **(B)** Composite with all markers except cytokeratin. The white-framed rectangle is the same area as in **(A)**.

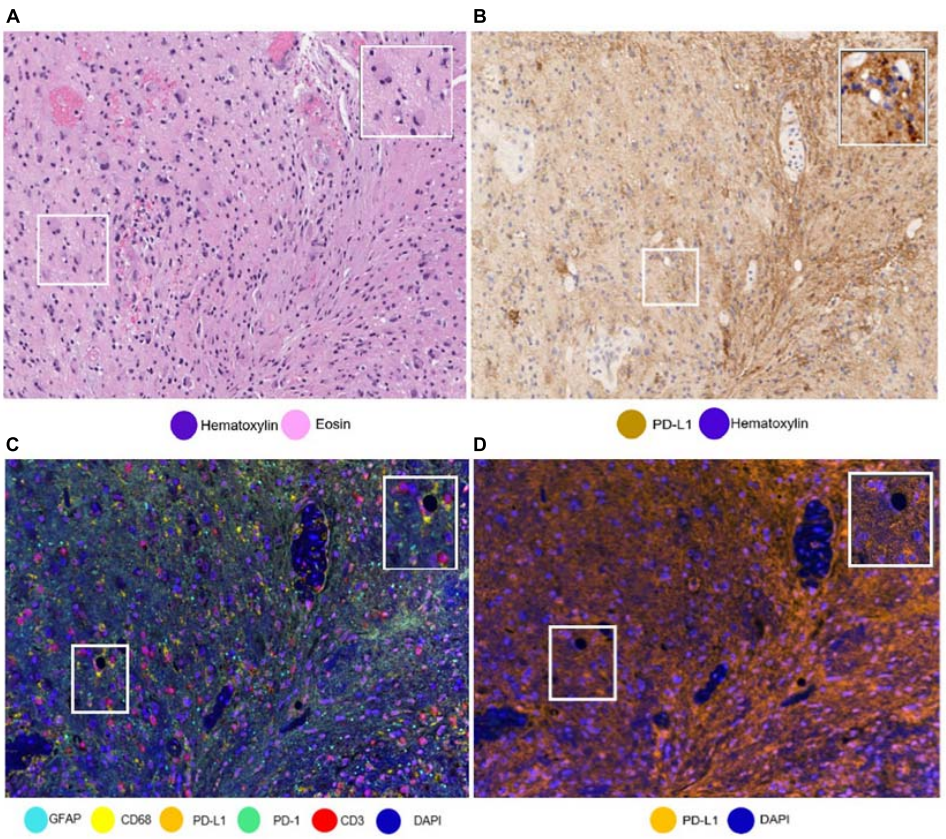

FIGURE 6 | Same areas of a glioblastoma sample with different stainings. The glioblastoma sample stained with **(A)** hematoxylin and eosin and with **(B)** PD-L1 immunohistochemistry. It is important to note the challenge to differentiate immune cells from tumoral cells. **(C)** The glioblastoma sample stained using multiplex immunofluorescence (mIF). Using mIF allows us to differentiate lymphocytes from tumor cells (as seen in 3 CD3 + lymphocytes staining red and glial fibrillar acidic protein staining cyan). **(D)** mIF with only PD-L1-positive cells. White-framed rectangles in all the images highlight the same area of the sample, which is augmented in the rectangles on the upper right of each panel.

The availability of unlimited combinations of markers opened new ways to study tumor tissues, making the study of multiple markers possible. Additionally, while being a challenge when using standard methods, such as single IHC, differentiating the cell types that express these markers (e.g., tumor cells from immune cells) has also been made possible (Parra, 2018;

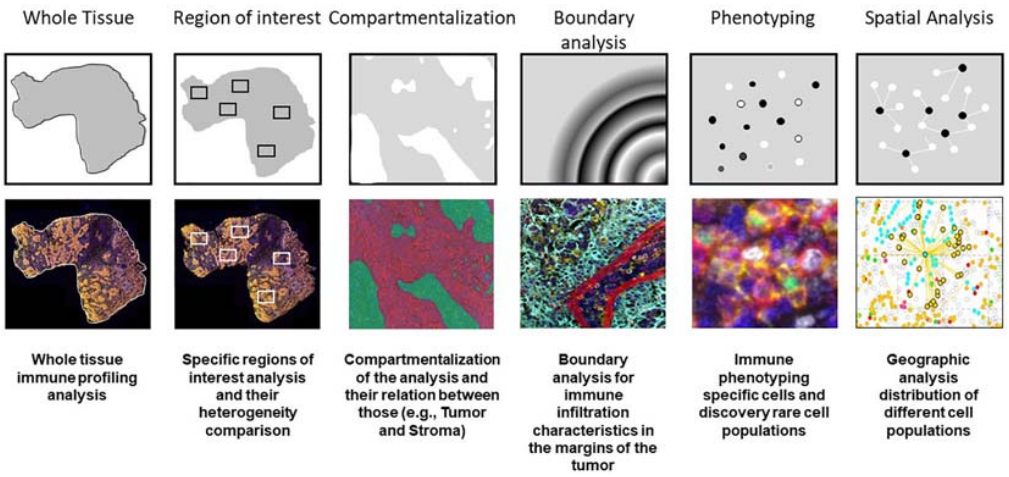

FIGURE 7 | Examples of multiplex immunofluorescence capabilities for tissue immune cell phenotyping spatial analysis.

Parra et al., 2019b). We have found this ability to differentiate the cells very useful in the study of PD-L1 in glioblastoma samples, because PD-L1 can be expressed by tumor cells, microglia, macrophages, and lymphocytes, with a wide range of patterns of tumoral morphology, making it very challenging to discriminate a cell with only single IHC (**Figure 6**) (Chen et al., 2018).

When we perform data consolidation, we can study not only the density of cell phenotypes but also the spatial placement of those cells in the tumor, allowing for the study of possible excitatory or inhibitory signals related by their proximity with the tumor cells or their neighbors. Phenotyping of cells *in situ* allows to establish those cells located close enough to interact with each other in immune activity. This approach is achieved using a different software, such as R-studio or SAS with the X and Y coordinates of each cell given by the image analysis software (Nagl et al., 2016; Lazarus et al., 2018). Other methods can be used, such as spatial metrics from the G-function (Barua et al., 2018) or infiltration analysis, to determine the number of objects or cells within a set range of an annotated region of interest (Kather et al., 2018) (**Figure 7**).

TUMOR IMMUNE PROFILING

In recent years, many studies have demonstrated the significance of tumor immune infiltrate densities, cell phenotypes, and spatial localization for the prediction of clinical outcomes, survival, and response to treatment (Pilla and Maccalli, 2018; Parra et al., 2020a). The direct simultaneous evaluation of immune tumor-related interactions and their spatial localization in a single tissue sample using multiplex techniques may allow a more accurate patient stratification for immunotherapy (Cascone et al., 2020; Provencio et al., 2020). A study that used multiplex IHC in head and neck squamous cell carcinomas showed a high infiltration of CD8 + T-cells and other T-helper type 1-associated immune infiltrates, indicating the presence of anti-tumor immunoreactivity. Furthermore, portion of these tumors exhibited the high myeloid cell infiltration profiles, and these tumors were associated with a poor prognosis. In the same study, the authors revealed that the response of pancreatic ductal adenocarcinomas to neoadjuvant vaccination therapy correlated with the grade of mono-myelocytic cell density and percentages of CD8 + T-cell exhaustion markers (Tsujikawa et al., 2017).

In the study of rare tumors, such as sarcomas, which in some cases may exhibit poor prognosis and adverse clinical outcomes (Dangoor et al., 2016), immune profiling has become a powerful tool in the characterization and understanding of tumor behavior. For example, immune profiling of Ewing sarcomas has demonstrated an association between higher densities of immunosuppressive M2 macrophages and a shorter event-free survival. Moreover, high frequency of T-cells and activated natural killer cells correlated with prolonged overall survival. Targeting macrophages, alone or in combination with other treatments, could be an interesting novel strategy for personalized medicine (Stahl et al., 2019). The rationale for immunotherapy in sarcomas is also explained by the presence of possible treatment targets, such as chromosomal alterations, or the cancer antigens resulting from genetic mutations. The presence of lymphoid tertiary structures and the rest of a naturally occurring immune infiltrate in sarcomas suggest that immunotherapy, such as cancer vaccines, adoptive cell therapy, and immune checkpoint blockade, may be feasible (Tseng et al., 2014). Because of this, we have found that analysis of the immune tumor microenvironment provides profound understanding of tumor behavior and novel treatment options.

Multiplex technologies provide unique sample-sparing analytical tools to characterize limited clinical tissue samples by allowing for *in situ* profiling and for the simultaneous profiling of multiple targets of interest (Hofman et al., 2019; Cascone et al., 2020; Provencio et al., 2020). We find the ability to study multiple markers in one specific cell especially useful in the study of cell densities, cell distribution, immune pathway marker expression in tumor cells, and recognition of new cell phenotypes, which

can help explain the biological behavior of the immune system in relation to certain cancers. To accomplish this, we have created many mIF panels using six to eight markers to study cells according to their biological lineage (e.g., lymphoid or myeloid), immune activity (e.g., activated, pro-inflammatory, and regulatory), and presence of immune checkpoints (e.g., PD-1, PD-L1, B7-H3, B7-H4, and IDO-1). It is important to acknowledge that every mIF panel can and must be adapted to the purpose of the study and the type of sample being profiled.

One of the biggest advantages of mIF platforms is the ability to get a great deal of data from one slide, without the necessity of multiple sections as in IHC (Tan et al., 2020) or multiple staining followed by denaturalization steps as in sequential immunofluorescence staining (Wahlby et al., 2002). However, we do face certain challenges because tyramide signal amplification does not recognize the intensity of the antibody expression, which is conventionally used in the qualitative study of certain markers (Fedchenko and Reifenrath, 2014). Nevertheless, this same amplification has helped us to recognize weak signals that are difficult to evaluate in conventional IHC, such as arginase-1 in macrophages. Furthermore, the cell phenotyping (co-localization) tool is very handy to evaluate the immune score of PD-L1 in certain challenging malignancies, such as glioblastoma multiforme, in which differentiating tumor cells, lymphocytes, and macrophages is difficult. In cases like these, the combination of co-expression markers, such as glial fibrillar acidic protein, CD3, and CD68, can help to obtain very accurate results compared to single IHC.

CONCLUSION

The advantages of mIF technologies are notable. The detection of multiple markers from a single tissue sample is both useful and necessary to provide comprehensive information about the cell nature, expression of prognostic markers, and even interactions between cells in the context of the tumor microenvironment. For imaging mIF with TSA, the ideal system is a scanner able to discriminate the different spectrums of the fluorophores used in a panel, giving us high-resolution images. As an example, the VectraPolaris scanner that combines the multispectral camera, the fluorescence cubes, and a resolution of 20 and 40x is able to capture high-quality images. Of course, other scanner systems can be used but probably those systems will be limited according to their assay-based specifications.

This technology is not exempt from limitations. For mIF, which currently uses tyramide signal amplification-based reagents, there is always the risk of tyramide overaction causing an umbrella effect. For this reason, it is important to evaluate the individual staining of each marker to recognize this possible effect during the optimization process. mIF methodology is also considerably more time consuming than a single bright field staining and subsequent imaging and digital pathology-related analysis. Also, there is the limitation of the number of antibodies in a panel which is basically the limitation in the spectrum of the fluorophores used. Eight markers per panel is the secure number of antibodies recommended in the workflow of the vendor in order to avoid any challenges in the optimization of new fluorophores and that can be discriminated easily by the scanner. However, new fluorophores can be tested and incorporated into the system. Nevertheless, a panel with less markers is more accurate and easily evaluated during the pathology image analysis compared with high plex technologies as imaging mass spectrometry or barcoding system that are used for exploratory purposes. In conclusion, the phenotyping process is complex, but mIF gives us tools to overcome many of the challenges that may arise. These tools and a deep understanding of immune cell protein expression and tumoral pathology are the key factors in the contribution of phenotyping and immune profiling to the study of tumor behavior and the development of new immunotherapies.

AUTHOR CONTRIBUTIONS

SH wrote most of the manuscript. FR, CL, RL, and IW contributed to the writing with their expertise on digital image analysis and immune profiling. EP developed the mIF technology in our laboratory and edited the manuscript according to his experience. All authors contributed to the article and approved the submitted version.

FUNDING

This manuscript was partially supported by the Cancer Prevention and Research Institute of Texas Multi-Investigator Research Award grant (MIRA) (RP160668), the Lung Specialized Programs of Research Excellence (SPORE) (P50CA070907), MD Anderson Cancer Center Support Grant (CA016672), and the National Cancer Institute (NCI) Cooperative Agreement CIMAC-CIDC Network (U24CA224285) (to the University of Texas MD Anderson Cancer Center CIMAC).

ACKNOWLEDGMENTS

The authors would like to acknowledge the Translational Molecular Pathology Immunoprofiling Laboratory members, who contribute daily to quality multiplex immunoflourescence and IHC processing. The authors also thank Stephanie Deming, Senior Scientific Editor, and Ashli Nguyen-Villarreal, Associate Scientific Editor, in the Research Medical Library at The University of Texas MD Anderson Cancer Center, for editing this article.

SUPPLEMENTARY MATERIAL

The Supplementary Material for this article can be found online at: https://www.frontiersin.org/articles/10.3389/fmolb.2021.667067/full#supplementary-material

Supplementary Figure 1 | IPMN images with **(A)** tissue segmentation in different colors representing glass (blue), epithelium (red), and stroma (green) and **(B)** cell segmentation with cell nuclei (green center) and cell membrane (red border).

REFERENCES

Barua, S., Solis, L., Parra, E. R., Uraoka, N., Jiang, M., Wang, H., et al. (2018). A functional spatial analysis platform for discovery of immunological interactions predictive of low-grade to high-grade transition of pancreatic intraductal papillary mucinous neoplasms. *Cancer Inform.* 17:1176935118782880. doi: 10.1177/1176935118782880

Bethmann, D., Feng, Z., and Fox, B. A. (2017). Immunoprofiling as a predictor of patient's response to cancer therapy-promises and challenges. *Curr. Opin. Immunol.* 45, 60–72. doi: 10.1016/j.coi.2017.01.005

Bodenmiller, B. (2016). Multiplexed epitope-based tissue imaging for discovery and healthcare applications. *Cell Syst.* 2, 225–238. doi: 10.1016/j.cels.2016.03.008

Cascone, T., Sepesi, B., Lin, H. Y., Kalhor, N., Parra, E. R., Jiang, M., et al. (2020). A phase I/II study of neoadjuvant cisplatin, docetaxel, and nintedanib for resectable non-small cell lung cancer. *Clin. Cancer Res.* 26, 3525–3536. doi: 10.1158/1078-0432.CCR-19-4180

Chen, R. Q., Liu, F., Qiu, X. Y., and Chen, X. Q. (2018). The prognostic and therapeutic value of PD-L1 in glioma. *Front. Pharmacol.* 9:1503. doi: 10.3389/fphar.2018.01503

Chuah, S., and Chew, V. (2020). High-dimensional immune-profiling in cancer: implications for immunotherapy. *J. Immunother. Cancer* 8:e000363. doi: 10.1136/jitc-2019-000363

Dangoor, A., Seddon, B., Gerrand, C., Grimer, R., Whelan, J., and Judson, I. (2016). UK guidelines for the management of soft tissue sarcomas. *Clin. Sarcoma Res.* 6:20. doi: 10.1186/s13569-016-0060-4

Dembe, A. E., Partridge, J. S., and Geist, L. C. (2011). Statistical software applications used in health services research: analysis of published studies in the U.S. *BMC Health Serv. Res.* 11:252. doi: 10.1186/1472-6963-11-252

Dixon, A. R., Bathany, C., Tsuei, M., White, J., Barald, K. F., and Takayama, S. (2015). Recent developments in multiplexing techniques for immunohistochemistry. *Expert Rev. Mol. Diagn.* 15, 1171–1186. doi: 10.1586/14737159.2015.1069182

Fedchenko, N., and Reifenrath, J. (2014). Different approaches for interpretation and reporting of immunohistochemistry analysis results in the bone tissue – a review. *Diagn. Pathol.* 9:221. doi: 10.1186/s13000-014-0221-9

Fridman, W. H., Pages, F., Sautes-Fridman, C., and Galon, J. (2012). The immune contexture in human tumours: impact on clinical outcome. *Nat. Rev. Cancer* 12, 298–306. doi: 10.1038/nrc3245

Grzywa, T. M., Sosnowska, A., Matryba, P., Rydzynska, Z., Jasinski, M., Nowis, D., et al. (2020). Myeloid cell-derived arginase in cancer immune response. *Front. Immunol.* 11:938. doi: 10.3389/fimmu.2020.00938

Guichet, P. O., Guelfi, S., Ripoll, C., Teigell, M., Sabourin, J. C., Bauchet, L., et al. (2016). Asymmetric distribution of GFAP in glioma multipotent cells. *PLoS One* 11:e0151274. doi: 10.1371/journal.pone.0151274

Hofman, P., Badoual, C., Henderson, F., Berland, L., Hamila, M., Long-Mira, E., et al. (2019). Multiplexed immunohistochemistry for molecular and immune profiling in lung cancer-just about ready for prime-time? *Cancers (Basel)* 11:283. doi: 10.3390/cancers11030283

Kather, J. N., Suarez-Carmona, M., Charoentong, P., Weis, C. A., Hirsch, D., Bankhead, P., et al. (2018). Topography of cancer-associated immune cells in human solid tumors. *Elife* 7:e36967. doi: 10.7554/eLife.36967

Krishna, M. (2010). Diagnosis of metastatic neoplasms: an immunohistochemical approach. *Arch. Pathol. Lab. Med.* 134, 207–215. doi: 10.1043/1543-2165-134.2.207

Lazarus, J., Maj, T., Smith, J. J., Perusina Lanfranca, M., Rao, A., D'Angelica, M. I., et al. (2018). Spatial and phenotypic immune profiling of metastatic colon cancer. *JCI Insight* 3:e121932. doi: 10.1172/jci.insight.121932

Mitchison, N. A. (1955). Studies on the immunological response to foreign tumor transplants in the mouse. I. The role of lymph node cells in conferring immunity by adoptive transfer. *J. Exp. Med.* 102, 157–177. doi: 10.1084/jem.102.2.157

Mohamed, A., Gonzalez, R. S., Lawson, D., Wang, J., and Cohen, C. (2013). SOX10 expression in malignant melanoma, carcinoma, and normal tissues. *Appl. Immunohistochem. Mol. Morphol.* 21, 506–510. doi: 10.1097/PAI.0b013e318279bc0a

Nagl, S., Haas, M., Lahmer, G., Buttner-Herold, M., Grabenbauer, G. G., Fietkau, R., et al. (2016). Cell-to-cell distances between tumor-infiltrating inflammatory cells have the potential to distinguish functionally active from suppressed inflammatory cells. *Oncoimmunology* 5:e1127494. doi: 10.1080/2162402X.2015.1127494

Parra, E. R. (2018). Novel technology to assess programmed death-ligand 1 expression by multiplex immunofluorescence and image analysis. *Appl. Immunohistochem. Mol. Morphol.* 26, e22–e24. doi: 10.1097/PAI.0000000000000610

Parra, E. R., Behrens, C., Rodriguez-Canales, J., Lin, H., Mino, B., Blando, J., et al. (2016). Image analysis-based assessment of PD-L1 and tumor-associated immune cells density supports distinct intratumoral microenvironment groups in non-small cell lung carcinoma patients. *Clin. Cancer Res.* 22, 6278–6289. doi: 10.1158/1078-0432.CCR-15-2443

Parra, E. R., Francisco-Cruz, A., and Wistuba, I. I. (2019a). State-of-the-art of profiling immune contexture in the era of multiplexed staining and digital analysis to study paraffin tumor tissues. *Cancers (Basel)* 11:247. doi: 10.3390/cancers11020247

Parra, E. R., Jiang, M., Machado-Rugolo, J., Yaegashi, L. B., Prieto, T., Farhat, C., et al. (2020a). Variants in epithelial-mesenchymal transition and immune checkpoint genes are associated with immune cell profiles and predict survival in non-small cell lung cancer. *Arch. Pathol. Lab. Med.* 144, 1234–1244. doi: 10.5858/arpa.2019-0419-OA

Parra, E. R., Jiang, M., Solis, L., Mino, B., Laberiano, C., Hernandez, S., et al. (2020b). Procedural requirements and recommendations for multiplex immunofluorescence tyramide signal amplification assays to support translational oncology studies. *Cancers (Basel)* 12:255. doi: 10.3390/cancers12020255

Parra, E. R., Uraoka, N., Jiang, M., Cook, P., Gibbons, D., Forget, M. A., et al. (2017). Validation of multiplex immunofluorescence panels using multispectral microscopy for immune-profiling of formalin-fixed and paraffin-embedded human tumor tissues. *Sci. Rep.* 7:13380. doi: 10.1038/s41598-017-13942-8

Parra, E. R., Villalobos, P., and Rodriguez-Canales, J. (2019b). The multiple faces of programmed cell death ligand 1 expression in malignant and nonmalignant cells. *Appl. Immunohistochem. Mol. Morphol.* 27, 287–294. doi: 10.1097/PAI.0000000000000602

Parra, E. R., Villalobos, P., Behrens, C., Jiang, M., Pataer, A., Swisher, S. G., et al. (2018). Effect of neoadjuvant chemotherapy on the immune microenvironment in non-small cell lung carcinomas as determined by multiplex immunofluorescence and image analysis approaches. *J. Immunother. Cancer* 6:48. doi: 10.1186/s40425-018-0368-0

Pilla, L., and Maccalli, C. (2018). Immune profiling of cancer patients treated with immunotherapy: advances and challenges. *Biomedicines* 6:76. doi: 10.3390/biomedicines6030076

Provencio, M., Nadal, E., Insa, A., Garcia-Campelo, M. R., Casal-Rubio, J., Domine, M., et al. (2020). Neoadjuvant chemotherapy and nivolumab in resectable non-small-cell lung cancer (NADIM): an open-label, multicentre, single-arm, phase 2 trial. *Lancet Oncol.* 21, 1413–1422. doi: 10.1016/S1470-2045(20)30453-8

Rashid, R., Gaglia, G., Chen, Y. A., Lin, J. R., Du, Z., Maliga, Z., et al. (2019). Highly multiplexed immunofluorescence images and single-cell data of immune markers in tonsil and lung cancer. *Sci. Data* 6:323. doi: 10.1038/s41597-019-0332-y

Riley, R. S., June, C. H., Langer, R., and Mitchell, M. J. (2019). Delivery technologies for cancer immunotherapy. *Nat. Rev. Drug Discov.* 18, 175–196. doi: 10.1038/s41573-018-0006-z

Rosenberg, S. A. (2014). IL-2: the first effective immunotherapy for human cancer. *J. Immunol.* 192, 5451–5458. doi: 10.4049/jimmunol.1490019

Satoh, J., Kino, Y., Asahina, N., Takitani, M., Miyoshi, J., Ishida, T., et al. (2016). TMEM119 marks a subset of microglia in the human brain. *Neuropathology* 36, 39–49. doi: 10.1111/neup.12235

Stahl, D., Gentles, A. J., Thiele, R., and Gutgemann, I. (2019). Prognostic profiling of the immune cell microenvironment in Ewing s Sarcoma family of tumors. *Oncoimmunology* 8:e1674113. doi: 10.1080/2162402X.2019.1674113

Tan, W. C. C., Nerurkar, S. N., Cai, H. Y., Ng, H. H. M., Wu, D., Wee, Y. T. F., et al. (2020). Overview of multiplex immunohistochemistry/immunofluorescence techniques in the era of cancer immunotherapy. *Cancer Commun.* 40, 135–153. doi: 10.1002/cac2.12023

Tarnowski, B. I., Spinale, F. G., and Nicholson, J. H. (1991). DAPI as a useful stain for nuclear quantitation. *Biotech. Histochem.* 66, 297–302.

Taube, J. M., Akturk, G., Angelo, M., Engle, E. L., Gnjatic, S., Greenbaum, S., et al. (2020). The society for immunotherapy of cancer statement on best

practices for multiplex immunohistochemistry (IHC) and immunofluorescence (IF) staining and validation. *J. Immunother. Cancer* 8:e000155. doi: 10.1136/jitc-2019-000155

Tsao, M. S., Kerr, K. M., Kockx, M., Beasley, M. B., Borczuk, A. C., Botling, J., et al. (2018). PD-L1 immunohistochemistry comparability study in real-life clinical samples: results of blueprint phase 2 project. *J. Thorac. Oncol.* 13, 1302–1311. doi: 10.1016/j.jtho.2018.05.013

Tseng, W. W., Somaiah, N., and Engleman, E. G. (2014). Potential for immunotherapy in soft tissue sarcoma. *Hum. Vaccin. Immunother.* 10, 3117–3124. doi: 10.4161/21645515.2014.983003

Tsujikawa, T., Kumar, S., Borkar, R. N., Azimi, V., Thibault, G., Chang, Y. H., et al. (2017). Quantitative multiplex immunohistochemistry reveals myeloid-inflamed tumor-immune complexity associated with poor prognosis. *Cell Rep.* 19, 203–217. doi: 10.1016/j.celrep.2017.03.037

Wahlby, C., Erlandsson, F., Bengtsson, E., and Zetterberg, A. (2002). Sequential immunofluorescence staining and image analysis for detection of large numbers of antigens in individual cell nuclei. *Cytometry* 47, 32–41.

Wang, S., Rong, R., Yang, D. M., Fujimoto, J., Yan, S., Cai, L., et al. (2020). Computational staining of pathology images to study the tumor microenvironment in lung cancer. *Cancer Res.* 80, 2056–2066. doi: 10.1158/0008-5472.CAN-19-1629

Yan, B. C., Gong, C., Song, J., Krausz, T., Tretiakova, M., Hyjek, E., et al. (2010). Arginase-1: a new immunohistochemical marker of hepatocytes and hepatocellular neoplasms. *Am. J. Surg. Pathol.* 34, 1147–1154. doi: 10.1097/PAS.0b013e3181e5dffa

Ye, J. J. (2016). Pathology report data extraction from relational database using R, with extraction from reports on melanoma of skin as an example. *J. Pathol. Inform.* 7:44. doi: 10.4103/2153-3539.192822

Yu, Y., and Cui, J. (2018). Present and future of cancer immunotherapy: a tumor microenvironmental perspective. *Oncol. Lett.* 16, 4105–4113. doi: 10.3892/ol.2018.9219

Conflict of Interest: The authors declare that the research was conducted in the absence of any commercial or financial relationships that could be construed as a potential conflict of interest.

frontiers in Molecular Biosciences

REVIEW
published: 02 June 2021
doi: 10.3389/fmolb.2021.674747

Multiplex Immunofluorescence and Multispectral Imaging: Forming the Basis of a Clinical Test Platform for Immuno-Oncology

Clifford C. Hoyt[1]*

[1]*Akoya Biosciences Inc., Malborough, MA, United States*

As immuno-oncology (I/O) emerges as an effective approach in the fight against cancer, multispectral imaging of multiplex immunofluorescence (mIF) is maturing as an analytical platform. The timing is fortuitous. Due to health economic considerations surrounding the use of I/O, there is an urgent need for tests that accurately predict response to the growing list of available therapies. Multispectral mIF provides several advantages over other biomarker modalities by enabling deeper interrogation of the intricate biology within the tumor microenvironment, including detection of cell-to-cell spatial interactions that correlate with clinical outcomes. It also provides a practical path for generating reliable and reproducible results in a clinically suitable, high-throughput workflow. In this article, we (1) describe the principles behind multispectral mIF; (2) provide advice and recommendations on assay development and optimization and highlight characteristics of a well-performing assay; and (3) discuss the requirements for translating this approach into clinical practice.

Keywords: Predictive biomarkers, multiplex immunofluorescence, multispectral imaging, immuno-oncology, clinical workflow, image analysis, automated staining, spatial biology

OPEN ACCESS

Edited by:
Joe Yeong,
*Institute of Molecular and Cell Biology (A*STAR), Singapore*

Reviewed by:
Thomas Pfister,
University Health Network, Canada
Mai Chan Lau,
Brigham and Women's Hospital and Harvard Medical School, United States

***Correspondence:**
Clifford C. Hoyt
choyt@akoyabio.com

Specialty section:
This article was submitted to Molecular Diagnostics and Therapeutics, a section of the journal Frontiers in Molecular Biosciences

Received: *01 March 2021*
Accepted: *04 May 2021*
Published: *02 June 2021*

Citation:
Hoyt CC (2021) Multiplex Immunofluorescence and Multispectral Imaging: Forming the Basis of a Clinical Test Platform for Immuno-Oncology. Front. Mol. Biosci. 8:674747. doi: 10.3389/fmolb.2021.674747

INTRODUCTION

Tissue biopsies and surgical resections offer a critical insight into a patient's cancer and are the basis of prognostic evaluations and therapy selection. Yet a wealth of information remains largely inaccessible due to the limitations of established tools and methods for evaluating formalin-fixed, paraffin-embedded (FFPE) tissue sections. For example, immunohistochemistry (IHC), the established tool for characterizing the biology present in the tumor and its microenvironment, lacks the capability to capture the complexity of cell-to-cell biology because it reveals only one or two proteins at a time. Pathologist assessment of tissues is done primarily by visual inspection and includes review of the tissue morphology, and positivity of one or two proteins, or of two to three genes targeting DNA or RNA molecules. Its application to assessments of expression in cellular subgroups is also inconsistent because it relies solely on visual interpretation which may vary greatly between individuals (Hirsch et al., 2017; Ilie and Hofman, 2017; Rimm et al., 2017).

Recent advances in tissue image analysis are helping address the variability and limitations of human perception. Measuring biologically significant parameters that are substantially out of reach of human perception, such as cellular co-expression, cellular spatial relationships, tissue heterogeneity, and expression of low abundance molecules, is now possible. However, progress to date with the application of quantitative image analysis, including deep learning and artificial

intelligence approaches, has focused mainly on conventional IHC and hematoxylin and eosin (H&E)–stained slides, which does not leverage the wealth of data that can be captured through multiplex immunofluorescence (mIF) (Effner et al., 2019; Niazi et al., 2019).

Understanding the cellular composition and spatial distribution in tissue sections, termed "spatial biology," is particularly valuable in the age of immunotherapy. Immune checkpoint inhibitors have revolutionized cancer treatment, especially for metastatic disease, for which patients have little recourse. Immune checkpoint inhibitors reduce T-cell inhibition, allowing them to attack cancers unhindered. In instances where a patient positively responds to the therapy, the benefits often last for years rather than months, which has led to excitement for potential cures for cancer (Wilky, 2019).

While lifesaving for some, current I/O treatments offer little benefit to more than 80% of patients (Haslam and Prasad, 2019; Wilky, 2019). With costs typically twice that of other types of cancer treatments, with frequent and impactful side effects, and with often precious little time for metastatic patients to try different approaches, there is an urgent need for better predictive assays that can be used to determine which drug or combination of treatments is most likely to help (Mehnert et al., 2017). This is particularly important with the rapid increase in the number of trials involving combination therapy approaches. Combination therapies target multiple proteins and/or cellular signaling cascades to provide more impactful treatment. Clinical trials have not only shown that patients can have significantly higher response rates but have also shown higher frequency of severe side effects. Predictive tests to help oncologists identify likelihood of response for monotherapy vs. combination therapy will have significant health economic benefits.

However, predicting whether a patient will respond or not to immunotherapies has proven difficult. This is probably due to how complex cancer is and how it uses multiple mechanisms to evade the immune system and survive. Currently, few approved diagnostic approaches exist that can accurately determine the likelihood of response to the ever-expanding list of FDA-approved immunotherapy drugs.

There is mounting evidence that the spatial biology occurring within the tumor microenvironment (TME) holds the answers as to why some patients respond to immunotherapy and others do not. Early in the I/O era, Tumeh et al. used quantitative IHC and mIF to investigate advanced melanoma patient responsiveness to pembrolizumab. They found that the presence of $CD8^+$ cytotoxic T-cells present along the invasive margin of the tumor, as well as the close proximity of programmed death receptor 1 (PD-1, located on $CD8^+$ T-cells) to programmed death ligand 1 (PD-L1), predicted the therapeutic response to anti–PD-1 blockade and subsequent tumor regression (Tumeh et al., 2014). In another study, Johnson et al. demonstrated a similar finding in melanoma based on PD-1 and PD-L1 proximity to other cell types within the TME (Johnson et al., 2016). Since then, there have been several biomarker studies performed that highlight the performance of mIF and the value of spatial biology (Gettinger et al., 2018; Giraldo et al., 2018; Mazzaschi et al., 2018; Wong et al., 2018; Althammer et al., 2019).

An interdisciplinary team led by Johns Hopkins University recently conducted a meta-analysis on data pooled from more than 50 studies, spanning more than 10 cancer types and over 8,000 patients (Lu et al., 2019). Each study assessed the predictive value of one or more biomarker assays intended to determine the likelihood of response to anti–PD-1/PD-L1 therapy, the leading class of immunotherapy. The meta-analysis revealed that three of the four assays most commonly utilized in I/O research, PD-L1 IHC, tumor mutation burden (TMB), and gene expression profiling (GEP), had moderate, comparable performance when predicting response to anti–PD-1/PD-L1 therapy. Interestingly, it revealed that the category of multiplex IHC or immunofluorescence (IF), which includes multispectral mIF, performed significantly better than the other three assay types.

The researchers concluded that the spatial biology revealed by mIHC or mIF, including cellular protein co-expression, localization, and arrangement, correlated better with patient response than information gathered with the other approaches. These findings support the premise that determining or predicting a patient's likelihood to respond to a specific therapy will be aided by detailed cell-level evaluation of the TME-specific cell presence, their functional status, and how they interact within the TME.

Ideally, to satisfy the urgent need for predictive I/O biomarkers, one would want to leverage the well-established attributes and benefits of conventional IHC and IF while taking advantage of new technologies for multiplex staining, high-throughput slide imaging, and computer vision, to provide an automated, reliable, and practical analysis workflow. To that end, we developed the multispectral mIF platform described here using a range of technologies to achieve an assay that is rapid, reproducible, and customizable to support research, clinical trials, and eventually standard of care. The platform consists of automated mIF staining using tyramide signal amplification (TSA), high-throughput multispectral slide image acquisition, and advanced machine learning–based image analysis algorithms for segmenting and characterizing the cell-level immuno-biology occurring in the TME (Stack et al., 2014). Example imagery is shown in **Figure 1**.

The goal of this article was to provide (1) the principles behind multispectral mIF; (2) high-level guidance on assay optimization to achieve sensitive reproducible multiplex assays; (3) performance metrics that typify well-optimized assays; and (4) a list of considerations for translating this method and methods like it into clinical standard of care. The perspectives and recommendations provided within this article are based on our experience with the Akoya mIF platform. We are sharing with the expectation that they might be useful generally for anyone developing mIF assays for translational work and eventual clinical use.

PRINCIPLES OF MULTISPECTRAL MIF

Before discussing the principles behind multispectral mIF, we will discuss assay performance goals as they drive the selection of the necessary technologies to perform the assay.

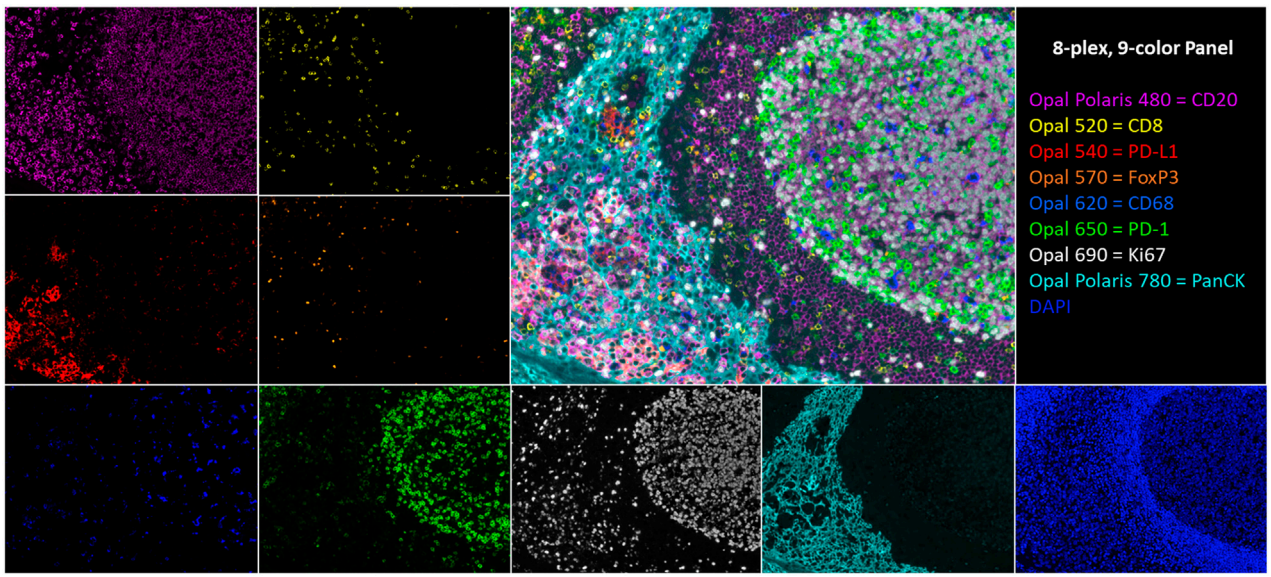

FIGURE 1 | An 8-plex, 9-color tonsil composite image with respective channel monoplex images: Opal Polaris 480 = CD20 (purple), Opal 520 = CD8 (yellow), Opal 540 = PD-L1 (red), Opal 570 = FoxP3 (orange), Opal 620 = CD68 (blue), Opal 650 = PD-1 (green), Opal 690 = Ki67 (white), Opal Polaris 780 = PanCK (teal), and DAPI counterstain.

Assay Performance Goals

Multiplex immunofluorescence methods have become a standard in I/O research, to understand cell-level biology occurring in the TME. However, little standardization has occurred. Up until now, IF and in situ hybridization approaches have been generally used to create imagery for qualitative visual assessment or to be analyzed ad hoc in the research setting with image analysis software packages designed to be open and flexible to suite individual project goals.

To advance quantitative mIF forward to support translational research and eventual clinical use, analytical performance standards are required at a level suitable for cancer diagnostic testing where accurate detection of cell types and biology depends on reliable detection of multiple proteins. The goal, effectively, is to create a quantitative multiplex imaging enzyme-linked immunosorbent assay (ELISA). Each pixel in an image of multiplex-stained samples should hold calibrated and precise data that indicate relative abundance of the multiple proteins of interest. If ELISAs are the analytical gold standard of protein measurement, the goal is to have percent co-efficient of variation (CV) of approximately 10% for detecting truly positive cells for one or more markers (Gupta et al., 2017). Analytical performance at this level is needed to support the following: (1) discovery of biomarkers that are real and reproducible; (2) the quality, regulatory, and analytical requirements for research studies and clinical trials; and (3) practical and reliable clinical deployment.

Principles

The first of three guiding principles of current multispectral mIF, thanks to valuable insights provided by collaborators at leading academic medical institutions, is that the mIF assay matches the sensitivity of highly optimized conventional chromogenic IHC staining (Kim et al., 2016; Parra et al., 2017). Conventional IHC is the prevailing clinical standard and has served the medical community well. One might think initially that replicating conventional DAB staining sensitivity with a fluorescence assay would be straightforward; however, it poses technical challenges. Conventional IHC is often saturated to reveal weak expressing cells, driven by clinical evidence that low-level expression correlates with response (Caruana et al., 2020). Saturated DAB staining supports how a pathologist would visually assess a sample because it reveals both high- and low-level expressing cells, which is what the pathologist cares about. Visual acuity is also adept at distinguishing specific staining in the presence of diffuse nonspecific background staining. Visual analysis combined with IHC presents a very sensitive method for detecting positive cells, wherein positivity is determined using visual acuity to detect specific staining above background staining.

However, as mentioned earlier, visual assessment of conventional IHC is predominantly limited by multiplexing level and the subjectivity of human perception (Sapino et al., 2013; Troncone and Gridelli, 2017; Santana MFCdLF, 2018). When transitioning to a quantitative mIF assay, analytical performance needs to support all of the attributes of fluorescence detection compared to chromogenic, including quantitative measure of expression through linear dynamic range, and independent staining of each marker to support accurate and reproducible machine vision–based assessments of cellular co-expression, arrangement, and localization within the TME architecture and across whole sections.

The second guiding principle is that multispectral mIF staining needs to support consistent and accurate image

analysis along with practical and fast process workflows. Analytical performance of a multispectral mIF assay depends on the integration of panel design and image analysis algorithms. While imagery can be visually enticing because of the biology it reveals, reliable and specific biomarker signatures are needed for translation. They form the basis of scores that will be used to make critical drug trial, and eventual clinical, decisions once appropriate regulatory certifications are obtained.

To this end, it is advantageous to include markers in multiplex assay panels that support image analysis functions to segment tissues and cellular compartments. This is critical given the variability of human tissues. For example, a tumor-specific marker or cocktail is essential to segment tumor regions and separate them from stroma. Also, if multiplexing bandwidth affords, including a cocktail of markers to serve as a "membrane counterstain" supports more robust cell segmentation by revealing cell surfaces to assist with assigning measured signals accurately to individual cells and with cell splitting, which can be challenging in tertiary lymphoid structures.

Another important attribute of robust assays is that they have strong and stable fluorescence signals to support rapid slide scanning and subsequent rescanning if needed, which may be needed months later. Stability includes two considerations—photostability to avoid bleaching from strong excitation light and stability of slides in storage. Two other attributes of robust assays are low background and independence of individual stains. These support accurate identification of cells-of-interest, frequency of colocalized markers, percent positivity, determination specific cell types within tissue microenvironments, proximities between certain cells, and other cellular distribution measures.

The third guiding principle is that the assay workflow needs to be practical, economical, and aligned with study and research laboratory standards so that this method is accessible to the entire research community, to accelerate and increase the likelihood of finding the most effective biomarkers. Furthermore, having a workflow that fits into clinical laboratory standards and workflows supports (1) pathologists who will continue to play a critical quality control and data review role, (2) laboratory and clinical personnel who will run the assays, and (3) physicians who need reliable and actionable information with rapid turnaround times.

TECHNICAL APPROACH

To achieve these goals, we developed an end-to-end workflow based on the Akoya mIF platform that includes reagents for automated and manual staining (antibodies and detection reagents), image acquisition instruments capable of both field-of-view and multispectral whole-slide imaging, software applications for image analysis, data reduction, and a cloud-based image storage, sharing, and viewing solution. In the workflow described here, we used the Leica BOND RX autostainer for automated staining. Additional R-script packages help consolidate field-of-view datasets and investigate whole-slide parameters that support the research and clinical trial objectives of today (Stack et al., 2014). Developing an effective workflow requires careful and seamless integration of each individual component. Assay panels are designed and optimized to work with the image acquisition instruments and image analysis programs. The imaging instrument is configured to isolate and measure signals, which are spatially and spectrally overlapping. Lastly, the image analysis software is built from the ground up to support multispectral unmixing and tissue and cell segmentation based on specific staining patterns, with algorithms for cell phenotyping and expression thresholding, that are robust across the variability of human diseased tissue types.

This approach was selected as a focus for translational, and eventual clinical, work rather than other higher-plex options, including Akoya's CODEX platform, other cycled mIF technologies, and approaches based on imaging mass spectrometry, because these platforms have attributes that would make it challenging to advance discovered biomarkers into a suitable clinical workflow. Contributing attributes that would make other approaches challenging are throughput, cost, and, in most cases, sensitivity which is needed to capture the intricate biology occurring in the TME related to therapy response.

Other mIF staining technologies, such as those from Ultivue, offer a single component of an end-to-end solution that could support translational work and eventual clinical application. The approach we describe in this review offers integration of a complete workflow which is important for assay reproducibility, accuracy, and standardization as each component of the workflow is optimized to support the other components. It also offers flexibility to discover and validate signatures among an almost infinite array of biological mechanisms to explore.

The multispectral mIF platform described here utilizes TSA to support biomarker detection. TSA is a technology invented more than 20 years ago that amplifies IF detection through the use of horse radish peroxidase (HRP) to enzymatically convert TSA molecules into free radicals that then covalently bind to tyrosine residues on and in the immediate vicinity of the protein epitope targeted by the primary antibody (**Figure 2**) (Bobrow et al., 2001). Today, TSA technology has been optimized for integration into the multispectral mIF platform and is available under the Opal trademark (www.akoyabio.com). This technology enables the detection of low-level expression by elevating signal above background tissue autofluorescence. TSA is also very photostable relative to conventional IF methods, enabling the storage and re-scanning of slides a year after slides are stained without appreciable loss of signal. As each color is amplified individually, signals can be balanced for measurement with negligible spectral channel-to-channel bleed-through.

The fluorophores selected for Opal detection support up to 8-plex staining (9-colors including DAPI counterstain) and have been carefully selected to provide optimum spectral separation across the visible wavelength range. Fluorophore selection was based on detailed models of total system spectral response covering the entire optical train of the imaging system.

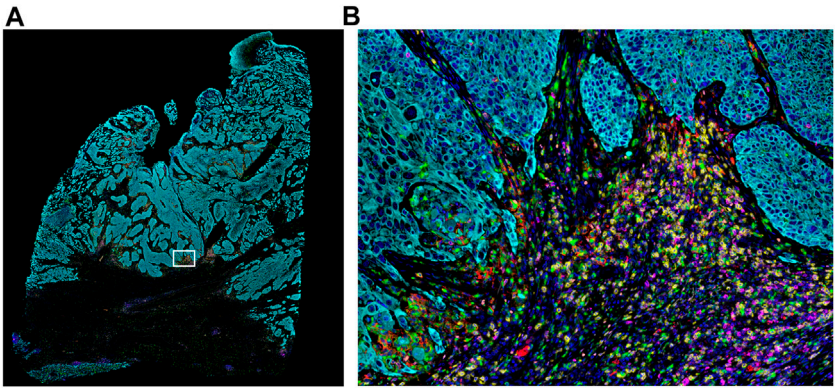

FIGURE 2 | Whole-slide MOTiF image of lung cancer FFPE tissue. **(A)** Markers stained for this 6-plex, 7-color assay include CD8 (yellow), PD-L1 (red), FoxP3 (orange), PD-1 (magenta), cytokeratin (cyan), and CD68 (green). White box indicates **(B)** selected area from whole tissue section image at 20× magnification highlighting the interactions between the immune system and the tumor (i.e., "hotspot"). The cellular composition and distribution reveal immune engagement with the tumor, evidenced by tumor-infiltrating lymphocytes (TILs), PD-L1+ macrophages, PD-L1− tumor cells, and an abundance of para-tumoral regulator T-cells and cytotoxic T-cells, including several that are PD-1+. Elucidating the interplay between these different cell types is key to understanding the variance in patient responsiveness to therapeutic treatments.

Amplified detection signals enable rapid slide scanning rates, typically with camera exposure times in the millisecond range for each fluorophore. This signal level translates to slide scan times of approximately 15 min per 7-color assay at 20× performed on a typical resection biopsy with an area of 1.5 × 1.5 cm (0.5 × 0.5 micron pixel size).

Having adjustable amplification gives researchers the flexibility to tailor assays to characterize biological mechanisms of interest, which may be best assessed by either high amplification to detect weak expressing cells or optimization to measure a large dynamic of expression if different expression levels have biological meaning. For example, if detecting very low expression is important, one can amplify aggressively. On the contrary, if a user wanted to capture as many gray-scale levels as possible, including at the high end of expression, one could amplify less aggressively.

There is a common belief that TSA-based amplification leads to variability in measured signals. This may be due, in part, to users not fully understanding all of the important parameters that need to be optimized to assure consistent, reproducible results. Careful assay development and optimization leads to reproducible measured signals, as evidenced by over 200 peer-reviewed articles that utilize the AQUA technology (McCabe et al., 2005), one of the first demonstrations of quantitative mIF, and by the rapidly growing number of more than 100 peer-reviewed articles describing results using the Opal technology. Just recently, a six-center inter-site comparison study, termed the multi-institutional TSA-amplified mIF reproducibility evaluation (MITRE) study, was undertaken to demonstrate the reproducibility of this integrated workflow system. The results revealed that multispectral mIF is not only transferable among different sites, but it is also reproducible at a level comparable to that of quantitative ELISAs, with CVs of <15% (Hoyt et al., 2019).

The MITRE study utilized the multispectral mIF workflow described in this article, including staining automation using the Leica BOND RX autostainer. The BOND RX autostainer is

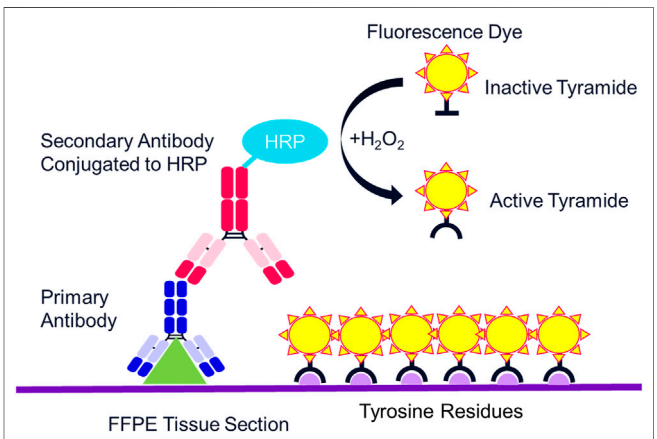

FIGURE 3 | Mechanism of tyramide signal amplification (TSA) staining. Opal dyes allow for the use of any standard unlabeled primary antibody, including multiple antibodies raised in the same species. After introduction of the primary antibody, the Opal polymer HRP is applied. The Opal system uses TSA to amplify IHC detection by covalently depositing multiple fluorophores near that targeted antigen. After labeling is complete, antibodies are removed in a manner that does not disrupt the Opal fluorescence signal, allowing for the next target to be detected without antibody cross-reactivity.

capable of staining 30 slides in a single run. Each run takes approximately 12–13 h, which fits into a daily schedule that includes sample and instrument preparation during the day and slide staining at night.

Once the slides are stained, they are scanned on a multispectral digital slide imaging system, the Vectra Polaris. The Vectra Polaris uses patented multispectral imaging technology to compensate for optical spectral bleed-through among channels and to isolate signal from background autofluorescence, which is particularly important for fluorophores at the blue-to-green end of the visible spectrum (**Figure 3**). In an internal quantitative

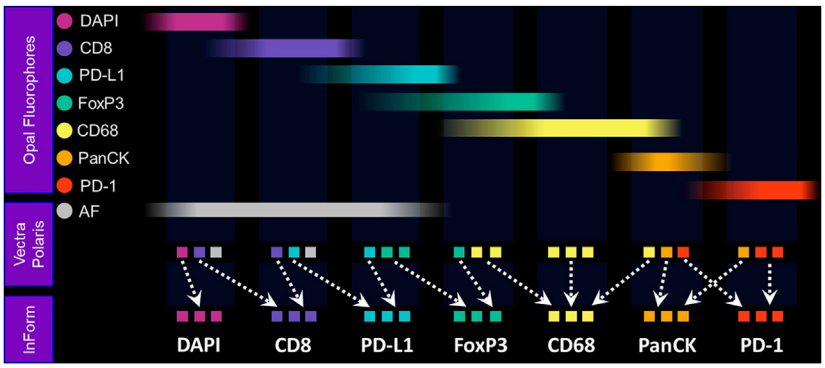

FIGURE 4 | Fundamentals of MOTiF imaging and spectral unmixing. With the MOTiF workflow, a tissue is stained with Opal fluorophores using a Leica BOND RX autostainer. The 6-plex, 7-color assay is then imaged using the Vectra Polaris slide scan protocol, wherein whole-slide scan images can be acquired in 10 min. Using inForm, designated library slides are used to isolate the exact spectral signature of each fluorophore to properly unmix each whole-slide composite image, as well as isolate and remove tissue autofluorescence. Spectral unmixing of signals is key to the Phenoptics technology and critical to ensuring accurate data for analysis.

assessment investigating the ability of multispectral unmixing to compensate for spectral bleed-through, we found that the average optical bleed-through was 8.7% for an optimized 6-plex assay and 13% for an optimized 8-plex assay. With multispectral unmixing, residual bleed-through was reduced to <1% in both cases. If a signal is 10 times its spectral neighbor, a 10% bleed-through from the stronger channel into the weaker channel would be equivalent to the signal in the weaker channel, leading to significant false-positive cell classifications.

The Vectra Polaris was designed from the ground up to be an IF quantification system. Recent advances have been incorporated into the instrument to further support translational workflows, including a whole-slide multispectral imaging capability called MOTiF™, enabling the rapid 15-min scanning of 1.5 cm^2 tissue areas for 6-plex, 7-color assays (**Figure 4**).

Following whole-slide image acquisition, images are analyzed with inForm image analysis software to quantify the cell-level biological features. The inForm software program was developed to integrate multispectral capabilities with image analysis to (1) spectrally unmix and isolate multiple Opal signals and background autofluorescence; (2) detect different tissue architecture (e.g., tumor, stroma, vessels, and necrosis) using a machine learning–based neural network pattern recognition function; (3) segment individual cells starting with nuclei, based on DAPI, and using other markers to detect membranous and cytoplasmic regions of cells; and (4) identify cell types of interest based on marker signal levels and cellular staining pattern using user-trained multinomial logistic regression algorithms.

To assist with image storage, sharing, and whole-slide image processing, a cloud-based platform called Proxima has been developed. Proxima is a hybrid solution consisting of a network-attached server (NAS) connected locally to the Vectra Polaris. Images generated on the Vectra Polaris are automatically transferred to the NAS and then uploaded to the cloud for remote viewing and data processing. The NAS can be used for rapid algorithm development and analysis of smaller projects, avoiding time delays associated with downloading images from cloud storage. Once image analysis algorithms are developed and validated locally, they can then be uploaded to Proxima for rapid batch whole-slide analysis, leveraging the computational power and speed of the cloud.

Analyzing whole-slide imagery generates very large data tables of single cell data, consisting of each individual cell's classification according to the cell phenotyping function; all measured attributes, including signal levels in cellular compartments, staining pattern statistics, spatial coordinates, and tissue region designations; and any other spatial parameter established in the image analysis protocol. To reduce and consolidate these datasets into per-sample or per-slide statistics that can be used as bases for sample scoring, we have developed a library of open-source R-script packages, including phenoptr and phenoptrReports (akoyabio.github.io/phenoptr/; akoyabio. github.io/phenoptrReports/). These scores are often selected and optimized to quantitate the specific biological attributes, including spatial measurements, which correlate best with clinical parameters such as response to therapy.

Assay Development Recommendations

In this section, we provide recommendations for assay development and optimization. Much of these insights were gained while developing and refining a rigorous assay optimization process and high-throughput slide analysis workflow in Akoya's contract services laboratory. Additional detailed guidance can be found here: www.akoyabio.com/support/reagents/.

First, we suggest starting with validated IHC chromogenic assays for each of the markers. A validated assay, to us, refers to antibodies that have been tested using multiple titers and antigen retrieval conditions on control tissues to screen for markers which produce the best staining patterns. This usually includes cross-validation with other clones targeting the same epitope, with Western blots, and with a pathologist who is familiar with the target and can confirm the associated biology and staining pattern. It is also important that IHC assay be amplified to the

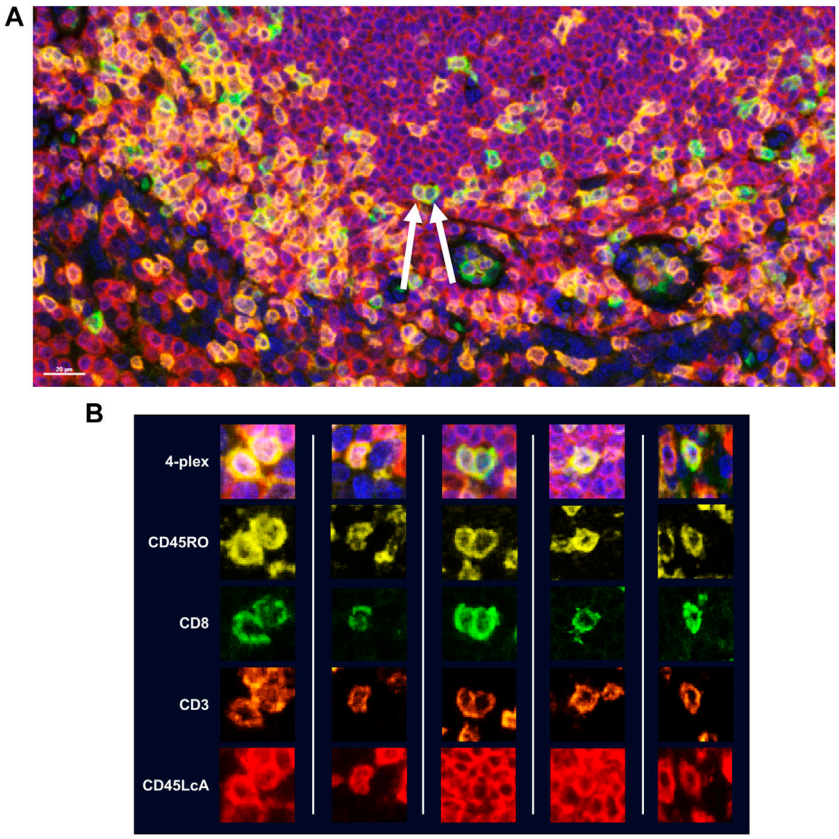

FIGURE 5 | Assessment of TSA staining interference in detection of multiple markers within the same cellular compartment. Four membrane markers were chosen for this experiment which are known to have significant co-localization with one another: CD8 (Opal 520), CD3 (Opal 620), CD45RO (Opal 570), and CD45LcA (Opal 690). All reagents were double dispensed using the BOND RX and scanned using the Vectra Polaris. **(A)** Image with arrows indicates cells that display all four markers. **(B)** Additional representative images of cells displaying all four markers without any reduction in signal intensity demonstrating that TSA does not interfere with detection of three or more markers co-localized to the cell membrane.

point where the nonspecific background is on the verge of becoming apparent and interfering with the weakest specific staining. It is believed that at this point, the maximum sensitivity of the assay is achieved.

The next step in assay panel development is to design the multiplex panel by pairing Opal fluorophores with markers. It is recommended to pair the brightest Opal fluorophores with the weaker expressing proteins, and vice versa. More detailed information is available about Opal-marker pairing recommendations using the Assay Development Guide: www.akoyabio.com/support/reagents/.

While manual staining can achieve excellent results, it is recommended that autostainers be used to achieve quicker, consistent results. If using a BOND RX to perform the staining, double-dispensing primary antibodies, secondary antibody-HRPs, and Opal fluorophores are recommended. Double dispensing provides a more complete and uniform distribution of reagents across the tissue section, delivering uniform staining across large samples, regardless of where the section is mounted on the slide. Double dispensing of these reagents also appears to substantially eliminate "umbrella effect," which is a term commonly used to describe when a previously applied marker impedes the application of an additional marker that co-localizes with the first. This is particularly important in instances where a user is interested in studying more than three markers of interest on the same cellular compartment. To demonstrate the effectiveness of the BOND RX double-dispense approach, an experiment was devised using CD3, CD8, CD45RO, and CD45LcA, membrane markers known to have significant co-localization with one another, to assess staining interference (**Figure 5A**). Results indicate negligible interference between the four markers, demonstrating reliable and clean detection of quad-positive cells, confirming that the "umbrella effect" is not an inherent limitation of TSA-based biomarker detection (**Figure 5B**).

It is recommended that one start with converting each IHC protocol to a monoplex IF (monoIF) protocol using the same primary antibody concentration established in the IHC assay and adjusting Opal TSA concentration to achieve fluorescence intensity signals at levels within suggested ranges. Reducing the primary antibody concentration should only be done in instances of where fluorescent signals continually remain high despite reducing the TSA concentrations, or if background staining becomes an issue.

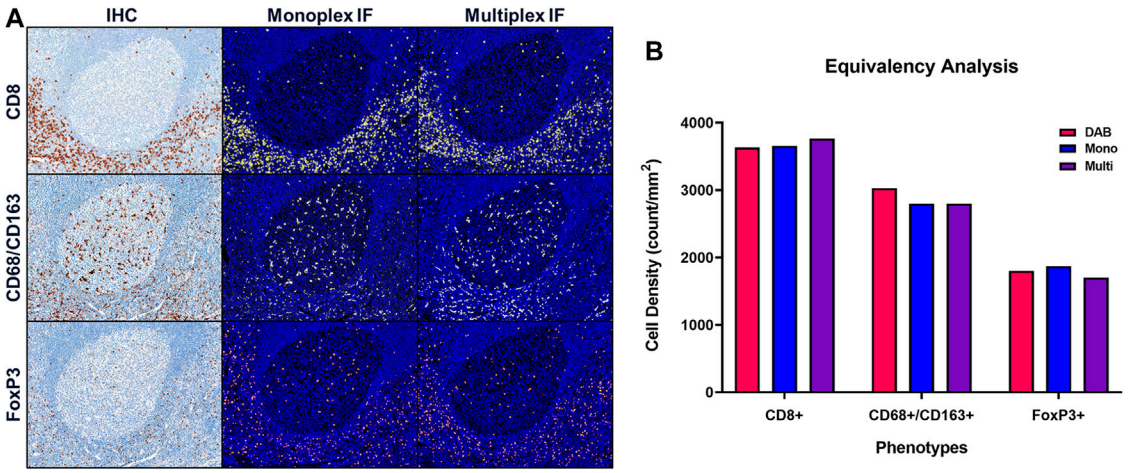

FIGURE 6 | Quantitative assessment of equivalence to chromogenic IHC staining. Staining parameters for each antibody are first optimized using single stain, chromogenic IHC on tonsil sections. Next, each primary antibody was paired to a select TSA fluorophore and a single-stain, monoplex IF (monoIF) was performed. Lastly, all of the monoplex conditions are combined into a multiplex IF (mIF) panel. **(A)** Representative image showing serial sections with each marker for IHC, monoIF, and mIF staining. **(B)** Quantitative assessment of each image demonstrating the equivalence of staining for each marker across the three staining parameters, wherein monoIF and mIF are consistent with DAB.

To assess equivalence between chromogenic IHC and monoIF, we suggest rigorous image analysis to count positive cells and to confirm that the number of cells revealed with IF is equivalent to the number revealed by IHC, within a range of 10%–20%. Since one image type is of brightfield chromogenic staining and the other IF, each requires very different image analysis approaches.

If measured cell counts with the chromogenic IHC are significantly higher than that detected with IF, despite the fact that the fluorescent signals are within the recommended range, it may be helpful to try other secondary-HRP systems that come in a more concentrated form than the current Akoya commercially available secondary HRP system. Opal users find that products such as Powervision from Leica increase the signal from lower expressing cells while not overly amplifying signal from stronger expressing cells. If the signals for higher expressing cells become too bright beyond recommended levels, reducing the primary antibody concentration can return the fluorescent signals back into the recommended ranges.

Increasing the signal of lower expressing cells while not significantly increasing the signal from higher expressing cells suggests that there is some level of saturation occurring. The tradeoff between dynamic range and sensitivity should be considered when optimizing an assay. Is it more important to see every low expression cell or to maximize dynamic range? In our experience, using a more sensitive secondary detection system to reveal low expressors retains at least two orders of magnitude of signal to resolve low, medium, or high expression levels when important to the biomarker assay.

Once equivalence between chromogenic IHC and monoIF is achieved, the monoIF protocols are then combined into a multiplex IF (mIF) protocol. The equivalency test, illustrated in **Figure 6A**, consists of a 15-slide serialization as described and is an efficient approach for evaluating IHC/monoIF/mIF equivalence (**Figure 6B**).

Lastly, routine maintenance and regular performance testing of the BOND RX is critical for obtaining consistent and reliable data. A basic challenge of any IHC or IF assay is distinguishing true negative staining from staining failures. In Akoya's Contract Research Services division, we perform monthly performance tests on every BOND RX instrument, consisting of one batch of 30 tonsil serial sections stained with a monoIF protocol labeling CD20 (**Figure 7A**) and a second batch of 10 tonsil serial sections that are stained with a standard PD-1/PD-L1 6-plex, 7-color mIF protocol (**Figure 7B**).

To gauge staining performance, we carefully select a minimum of five fields of view that are aligned across serial sections to reduce the impact of tissue heterogeneity on the staining reproducibility measurement. The stain intensity for each slide is then determined as the average of the top 20 brightest cells. When instruments are well maintained and a high-quality tissue control is used, such as healthy tonsil, percent CVs should be in the 5%–15% range. When using this methodology, it is important to always inspect the imagery as well because either approach cannot detect issues related to staining artifacts such as folds or other staining errors.

Characteristics of an Optimized Assay

The key performance parameters of a well-optimized assay are signal strength, signal balance, marker independence, staining uniformity, reproducibility over time, and most importantly from a translational perspective, the ability to transfer assays across sites with equivalent results.

Signal Intensity

As measured by inForm or Phenochart software, the target range for positively stained pixels is in the 10–30 normalized count range for all Opal fluorophores, with the exception of Opal Polaris 780, where the recommended range is from 1 to 10

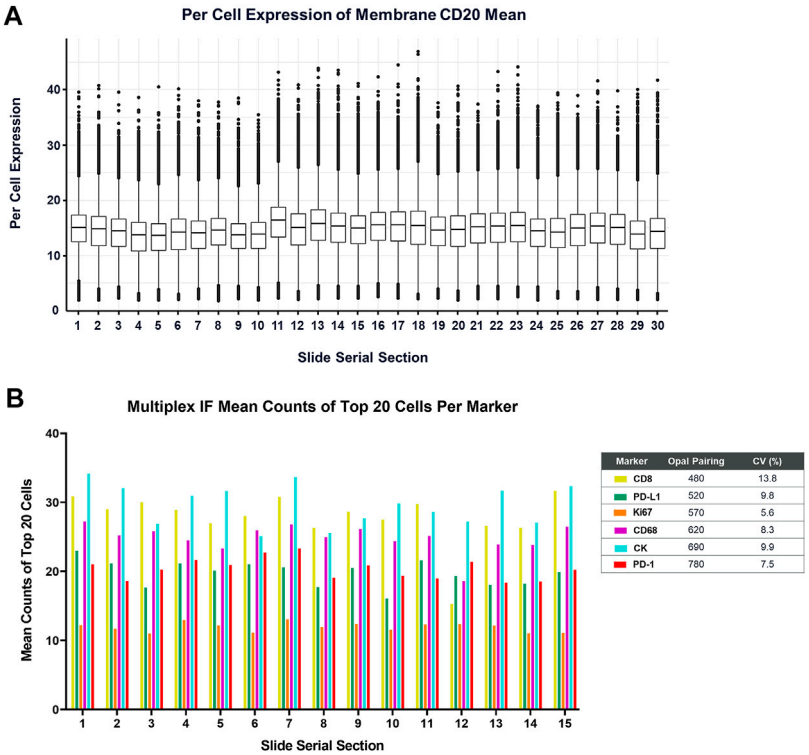

FIGURE 7 | Measurement of the BOND RX performance is captured by **(A)** running a CD20-Opal 520 monoplex assay across 30 serial sections. The percent coefficient of variation (%CV) is calculated by determining the mean expression of the top 20 brightest expressing cells across five matching annotations on all the serial sections. **(B)** Similarly, an optimized 6-plex, 7-color assay is also run on 15 serial sections, and the mean IF counts of the top 20 cells per marker are measured and the mean, standard deviation, and %CV are calculated.

cell counts. These ranges support reliable and accurate data analysis. It is worth noting that viable data can still be obtained when signals are as low as a few counts or as high as 50 or more counts, but risks are higher for crosstalk issues.

Dynamic Range

Our standard approach assessing dynamic range is to calculate a signal-to-background (SNR) ratio by dividing the average of the top 20 brightest cells by the average intensity of the weakest 10% of cells. An SNR of 10 or more supports reliable image analysis, including accurate counting of positive cells and quantifying expression levels. While we recommend an SNR of 10 or greater, typical ratios are well in the 100s with high-performing antibodies, or as low as 3-to-1 that still provide analytical value.

Signal Balance

With the classic Opal line-up (Opals 520, 540, 570, 620, 650, and 690), the rule of thumb was to aim for ratios of signals between neighboring channels of 3:1 or less. This rule was particularly useful for the 520, 540, and 570 channels. This was just a guide. Most of the time when ratios exceeded 3, the assays performed very well with negligible crosstalk.

With the introduction of MOTiF 6-plex, 7-color capability, which replaces Opal 540 with Opal Polaris 480 and Opal 650 with Opal Polaris 780, the rule of thumb substantially goes away because the six fluorophores are more spectrally distinct. As a result, there is little residual crosstalk after unmixing, even if neighboring signals are significantly imbalanced. As discussed in the signal intensity section, normalized counts within the 10–30 range for all Opals except Opal Polaris 780 are key to achieving optimal signal balance and an SNR of 10 or more. In the end, the goal of signal balancing is to achieve negligible crosstalk.

Crosstalk

Crosstalk should be minimized or eliminated because it can cause false positives and can limit dynamic range for important expression markers when crosstalk inaccurately contributes to a neighboring signal channel. There are two main sources of crosstalk: (1) instrumental crosstalk occurring when fluorescence signals leak from one channel to another due to imperfect filter optics or from inadequate crosstalk compensation algorithms and (2) staining crosstalk from actual fluorophore inaccurately labeling proteins on the sample, resulting in residual fluorophores inadvertently binding to epitopes intended to be labeled by other fluorophore. It is very important to distinguish the two causes because resolving each is a very different process.

When optimizing a multiplex assay, visual assessment for spectral bleed-through should always be part of the evaluation

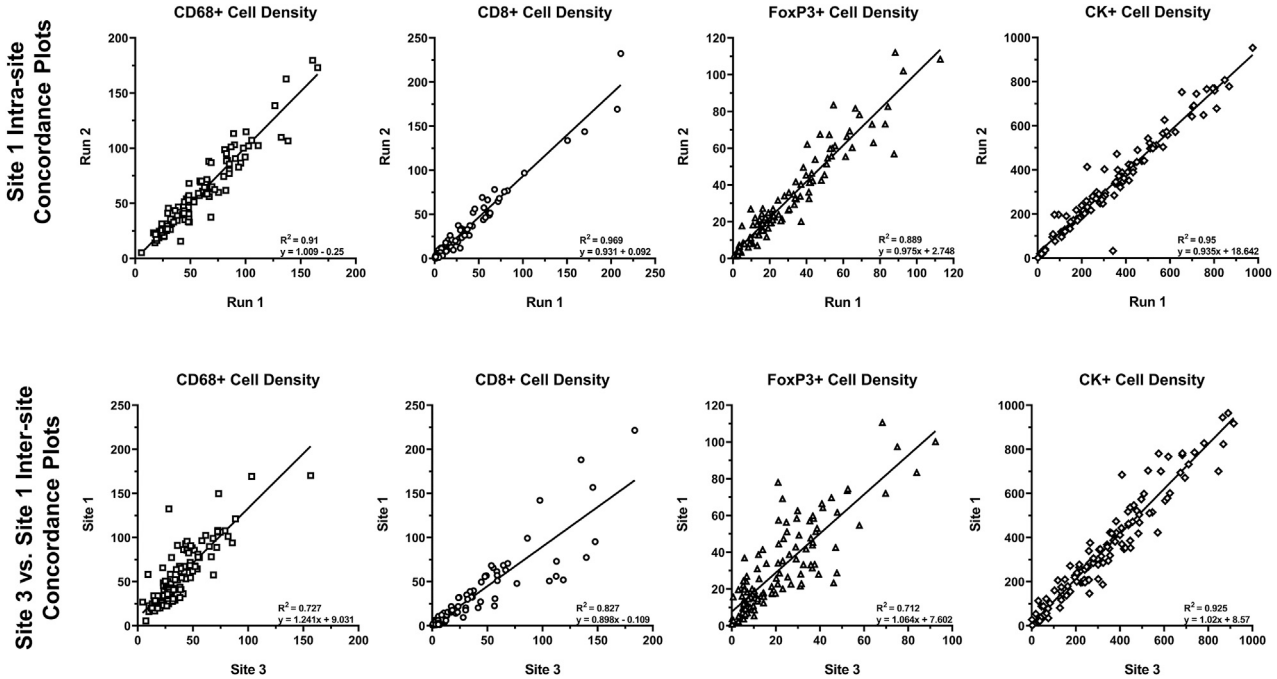

FIGURE 8 | Intra- and inter-site concordance assessment of cell densities. Average intra- and inter-site concordance plots comparing Run 1 vs. Run 2 (intra-site) and Site 1 vs. Site 3 (inter-site) cell densities for $CD68^+$, $CD8^+$, FoxP3+, and CK+. Data shown as R^2 (slope and standard deviation (SD) of slope). Graphs depict data presented as part of a study investigating multiplex IF reproducibility across multiple institutions (Hoyt et al., 2019).

process because trained human perception is very good at distinguishing actual signal from crosstalk.

Crosstalk can be assessed with a set of monoIF slides, one for each Opal fluor. It is then determined by dividing the signal in its respective channel from an image of the monoIF sample corresponding to that channel by the signal in that channel from an image of a sample that is only stained with the neighboring fluorophore. For a robust assay, residual crosstalk of less than 1% is recommended to ensure minimal interference with image analysis. More often than not, there is no measurable crosstalk.

Specific guidance on this topic is provided in our guide available on the Akoya website: https://www.akoyabio.com/support/reagents/.

Reproducibility

Reproducibility of approximately 10% CV or better is typical of well-optimized panels and run on the Leica BOND RX that is well maintained. To assess the analytical performance of multispectral mIF and its suitability to support future clinical applications, the MITRE study was conducted, as previously discussed (Hoyt et al., 2019). Serial sections of tonsil and tissue microarrays and reagent kits were distributed to six sites, each equipped with a Leica BOND RX and a Vectra Polaris. Slides were stained with an optimized assay panel for PD-1, PD-L1, CD8, CD68, Foxp3, and CK using the recommendations described. Intra- and inter-site concordance analysis of signal intensities was assessed (**Figure 8**).

Comparison of the multispectral mIF and IHC cell counts showed equivalence of 90% on average. Intra-site equivalence assessment showed an average slope of 0.93 and R-squared value of 0.86. Inter-site assessment showed a slope of 0.98 and R-squared value of 0.76, confirming analytical robustness.

Beyond demonstrating that the staining was reproducible across sites, we were able to establish that image analysis substantially addresses the inconsistencies of human visual assessments. Agreement among sites for assessing percent positivity of PD-L1 in immune cells, using the TMA samples, was demonstrated by an R-squared value of 0.81 and slope of 0.82. In contrast, ICC values of <0.3 were demonstrated for a similar assessment of reproducibility in the NCCN and Blueprint 2 PD-L1 IHC harmonization studies (Hirsch et al., 2017; Rimm et al., 2017).

Photostability

To assure analytical robustness and support eventual clinical applications, it is important that fluorescence signals are not only photostable to allow for repeated scanning but also temporally stable so that slides can be stored for months without appreciable loss of signal. Multiplex assays using Opal TSA detection can be scanned repeatedly over the course of 6 months while being stored at room temperature with <10% loss of signal. In an internal assessment, we determined that signal intensity across repeated scanning decreased linearly by <6% over 30 scans. This consistent level of photostability is due to the nature of TSA-based labeling that involves covalent binding of fluorophores to tyrosine residues, in addition to the pulsed LED excitation in the Vectra Polaris imaging instrument, which illuminates the sample only during imaging, reducing total

light exposer by many factors of magnitude compared to conventional fluorescence microscope excitation systems.

TRANSLATING MULTISPECTRAL MIF INTO THE CLINIC

With well over 100 peer-reviewed publications that utilize multispectral mIF, the I/O research community has embraced mIF as a primary tool to uncover and characterize cell-level biological interactions in the TME, to help understand how cancer survives and grows, and to uncover its potential biological mechanisms to target with new therapies. Moreover, multispectral mIF has become the leading candidate to support identification of urgently needed predictive biomarkers to make I/O more efficient and precise. As the predictive power of biomarkers based on the spatial biology is revealed by mIF methods, we fully expect mIF to translate into clinical practice as an essential tool in a physician's diagnostic toolkit.

The purpose of this final section is to suggest remaining steps to translate multispectral mIF into a fully validated clinical platform. Requirements can be summarized into five categories: (1) flexibility to fully explore co-expression and spatial information; (2) analytical performance providing reproducibility and robustness; (3) workflow and standardization to support laboratory needs; (4) demonstrated clinical validation and utility; and (5) reimbursement from payers to support laboratory economics and clinical adoption.

Flexibility to Fully Explore Co-Expression and Spatial Information

The academic and medical research setting where oncologists, pathologists, immunologists, cancer biologists, and image analysis scientists work together to solve challenging life science problems is ideal for exploring the full dimensionality of spatial biology. Supporting these interdisciplinary teams in their pursuit of effective biomarkers requires a research platform that is open and flexible and that fits into research budgets and laboratory workflows. Open and flexible in this context refer to the ability to freely select antibodies, design multiplex panels, adjust amplification to capture expression levels that correlate best with clinical parameters, and follow the data to explore the intricate biology behind I/O responsiveness.

The objective of I/O research is to quickly converge on optimum biomarker signatures, which typically means integrating (1) hypothesis-driven sets of markers; (2) staining protocols, including optimized antigen retrieval and amplification to observe the range of expression related to response; (3) image analysis measurements of co-expressions and spatial parameters; and (4) calculations or algorithms to reduce large cellular datasets to operator-independent and actionable scores, which we define as scores based on measurements of TME cell-level biology that have sufficient utility to justify use in making therapeutic decisions. The platform should have the flexibility to freely adjust parameters for each of these steps, allowing researchers to effectively integrate a translational workflow into their daily routine and fully explore the spatial biology to identify optimum predictive biomarkers.

Analytical Performance Providing Reproducibility and Robustness

Analytical performance provides confidence that assay results are accurate, regardless of when, where, or by whom the assay is performed. Performance standards need to be at a level typified by, at a minimum, the regulatory analytical standards of a laboratory in compliance with the US Clinical Laboratory Improvement Amendments (CLIA) and, ideally, the analytical component of a Food and Drug Administration *In Vitro* Diagnostic (IVD) Class III Medical Device Pre-Market Approval submission. Components of these standards include (1) precision and reproducibility (e.g., CV) of the test readout over time, across instruments, across operators, across sites, and so on; (2) shelf life and stability; and (3) robustness, which is a measure of a platform's capacity to remain unaffected by small but deliberate variations in method parameters.

Analytical performance applies to image analysis as well, but in a different way. Image analysis algorithms will provide the same answer every time for a given sample, but it can be challenging to provide accurate data due to the variability of staining, tissue morphology, and tissue conditions. Accuracy across sample variability needs to be assessed, preferably using a pathologist's manual assessments and/or annotations as a gold standard.

Although there has yet to be an IVD-level validation of an mIF assay, results from the MITRE study described above suggest that multispectral mIF has the performance attributes suitable to support the analytical requirements of an FDA-approved IVD.

Workflow and Standardization to Support Laboratory Needs

As mIF matures and moves toward the clinic, there is a push to define standards for developing and validating predictive biomarkers, including multispectral mIF. In 2017, the National Institutes of Health launched a $220 million initiative called the Partnership for Accelerating Cancer Therapies (PACT) in which drug companies facilitated systematic and uniform clinical testing of biomarker assays (https://fnih.org/what-we-do/programs/partnership-for-accelerating-cancer-therapies). The Society for Immunotherapy of Cancer (SITC) launched a benchmark effort of its own in 2019, establishing a 21-member task force to develop best practices surrounding the use of multiplex IHC and additional multiplex imaging tools (https://www.sitcancer.org/membership/volunteer/task-forces/pathology).

Platform providers meanwhile will need to design assays that are robust across the variability of human tissue specimens, incorporate suitable controls to compensate for staining variations, automate and integrate components of the assay to reduce the likelihood of errors, and create levels of access to assure platform configurations are controlled and locked down.

Once these items are accomplished, the next critical step is to provide the platform with a configuration that satisfies the needs

of the clinical laboratory setting. Processing a sample must be reduced to a simple, streamlined workflow that resembles, as much as possible, an automated sample-in, score-out process. Given the complexity of mIF or IHC, the measurement, and the variability of tissues, there will be a few points during the process that will need pathologist input, including quality assessment, tumor annotation, and results review. Since the platform performance depends on the proper execution of each step and as the success of subsequent steps depends heavily on the performance of previous steps, the entire end-to-end workflow needs to be automated and locked down to prevent operator dependencies. Some recommendations to improve performance and reduce assay variability at each step include full integration into a laboratory information management system to automate information management and avoid errors by using a database to indicate autostainer protocol, confirm appropriate reagents, select image acquisition protocols (exposures, colors, sequence, etc.), and develop image analysis and reporting algorithms.

This workflow also needs to support laboratory staff who operate the instruments and pathologists who provide valuable quality control and oversight function to confirm the sample is sufficient for testing, and to review and approve results in the form of a report.

Providing an H&E view of the sample will be critical for the pathologist's tissue quality inspection, annotation of tumor, and results review. mIF imagery, while visually stunning, is foreign to most classically trained pathologists and does not present the anatomical and morphological features in a format that most pathologists are accustomed to. Ideally, the H&E view will be of the exact same section that is analyzed with multispectral mIF, rather than of another section from the biopsy sample. Although there will probably be a representative H&E-stained section from each sample tissue block, the representative H&E section may be from a very different depth into the block and may contain significantly different tissue morphology, thus not providing sufficient visual guidance about the makeup and quality of the section being characterized with mIF. Additionally, as the reference H&E slide is a different section, it may have different sectioning artifacts such as tears, folds, and lost areas. To address this issue, we have incorporated into our workflow a method to capture an H&E whole-slide image of the section to be stained and analyzed with multispectral mIF. The H&E view and the appropriate representations of the multispectral mIF views will be used by the overseeing pathologist as part of his or her review of the results and final sign-off of a report.

Other basic requirements for translation are that (a) instruments, reagents, and software are designed and manufactured within an ISO13485-certified quality system and according to good manufacturing principles, typically audited by the FDA for Class-III medical devices; (2) the platform workflow is compatible with common and custom laboratory information management systems; and (3) data processing workflows support remote viewing and annotation and are capable of handling the scale and size of images and datasets, probably requiring a cloud-based platform that is HIPAA compliant. A key attribute of a cloud-based solution is that the computational power supports rapid automated whole-slide image analysis taking on average 10 min per slide, which will be needed to provide sufficient turnaround time and reduce the massive amount of raw data for each tissue section to an operator-independent and actionable score.

Clinical Validation and Utility

Potentially, the most important element of translating these methods to clinical practice is demonstrating analytical validation, clinical validation, and clinical utility in the clinical trial setting. Having a platform and assays that support the rigors and quality and regulatory requirements of clinical trials, coupled with clinical-grade analytical performance, are critical. Additionally, laboratories running the trials need to have appropriate documentation and controls in place, as well as be CLIA/GCP/GCLP certified or compliant. They also need to have daily slide analysis throughput to support trial timelines.

Clinical Test Reimbursement to Support Laboratory Economics and Clinical Adoption

Reimbursement is also a key milestone in the path to clinical adoption, as important as demonstrating clinical validation and utility. Despite significant attention being paid to personalized (i.e., precision) medicine, there is still significant pressure to reduce testing costs. Obtaining reimbursement is a complicated process and requires significant time and resources to demonstrate rigorously real value. Regulatory and reimbursement bodies, such as CMS and NCCN, have made the hurdles higher because of the lack of performance of many over-sold testing platforms. On the other hand, there are several examples of tests, such as next-gen sequencing–based tests for microsatellite instability and tumor mutation burden, that are garnering healthy reimbursement and that have predictive power at levels that will be potentially superseded by assays based on mIF assessments.

Obtaining approvals and support for reimbursement from regulatory agencies requires clinical utility studies that demonstrate significant statistical evidence that patients and the health system benefit from taking the test. An example of a clinical utility study that effectively demonstrates the clinical utility of a multispectral mIF was performed by Peabody et al. for a prostate cancer prognostic test (Peabody et al., 2017).

Lastly, the cost of performing the test must fit within the economic imperatives of academic and commercial reference laboratories. Simply put, the initial investment, per-test cost, and volume need to support healthy business for the laboratory, certainly enough to cover costs, but optimally to support healthy gross and profit margins.

CONCLUSION–MULTIPLEX IMMUNOFLUORESCENCE HAS A BRIGHT FUTURE

In the ongoing battle against cancer, there are two major developments that give us reason to be optimistic about improving the lives of cancer patients. First, I/O has drastically

changed the game and created an extensive list of new efficacious avenues of attack by harnessing the immune system and enabling new drug combinations that work synergistically together. Second, thanks to new detection and imaging technologies, our understanding of the TME and cancer immunology is advancing at a rapid pace, revealing driver biology behind progression and responses to therapy.

In addition to the multispectral mIF approach described here, there are many other new and higher-plex discovery platforms taking root in cancer research (Tan et al., 2020; Taube et al., 2020). These platforms leverage novel detection approaches to multiplex tens of proteins in single tissue section, such as cycled steps of staining and imaging, faster scanning of laser or ion beams coupled to mass spectrometers to analyze antibody-metal atom conjugates, spatially indexed beads for imaging "trans-scriptomics," and spatially resolved oligo-barcoded snipping technologies to look at proteins and RNA in optically masked areas. These approaches give researchers a comprehensive tool kit to explore and understand the intricate details of how cells behave in the TME.

Fortunately, biomarker discoveries made with these higher-plex approaches, which have workflows and economics that are not well suited to translation into the clinic, can be reduced to the most informative markers in a multispectral mIF workflow providing rapid, whole-slide analysis that is automated and operator-independent for trials and clinical deployment. They provide a rich pipeline of new biomarker signatures that can be converted to a multispectral mIF assay which is suitable for clinical trials and translation into eventual standard of care. The new frontier of biomarker discovery based on spatial biology has a practical path toward the clinic, based on practically, economically, and analytically robust workflows, which promises to have material benefit for cancer patients.

AUTHOR CONTRIBUTIONS

The author confirms being the sole contributor of this work and has approved it for publication.

ACKNOWLEDGMENTS

The author acknowledges help from Bethany Remeniuk, a colleague at Akoya Biosciences, with the editing, formatting and submission of this manuscript.

REFERENCES

Aeffner, F., Zarella, M., Buchbinder, N., Bui, M., Goodman, M., Hartman, D., et al. (2019). Introduction to Digital Image Analysis in Whole-Slide Imaging: A White Paper from the Digital Pathology Association. *J. Pathol. Inform.* 10, 9. doi:10.4103/jpi.jpi_82_18

Althammer, S., Tan, T. H., Spitzmuller, A., Rognoni, L., Wiestler, T., Herz, T., et al. (2019). Automated Image Analysis of NSCLC Biopsies to Predict Response to Anti-PD-L1 Therapy. *J. Immunother. Cancer.* 7, 121. doi:10.1186/s40425-019-0589-x

Bobrow, M. N., and Moen, P. T., Jr. (2001). Tyramide Signal Amplification (TSA) Systems for the Enhancement of ISH Signals in Cytogenetics. *Curr. Protoc. Cytometry*. Chapter 8, Unit 8 9. doi:10.1002/0471142956.cy0809s11

Caruana, D., Wei, W., Martinez-Morilla, S., Rimm, D. L., and Reisenbichler, E. S. (2020). Association between Low Estrogen Receptor Positive Breast Cancer and Staining Performance. *NPJ Breast Cancer*. 6, 5. doi:10.1038/s41523-020-0146-2

Gettinger, S. N., Choi, J., Mani, N., Sanmamed, M. F., Datar, I., Sowell, R., et al. (2018). A Dormant TIL Phenotype Defines Non-small Cell Lung Carcinomas Sensitive to Immune Checkpoint Blockers. *Nat. Commun.* 9 (1), 3196. doi:10.1038/s41467-018-05032-8

Giraldo, N. A., Nguyen, P., Engle, E. L., Kaunitz, G. J., Cottrell, T. R., Berry, S., et al. (2018). Multidimensional, Quantitative Assessment of PD-1/pd-L1 Expression in Patients with Merkel Cell Carcinoma and Association with Response to Pembrolizumab. *J. Immunotherapy Cancer*. 6 (1), 99. doi:10.1186/s40425-018-0404-0

Gupta, S., Richards, S., Amaravadi, L., Piccoli, S., Desilva, B., Pillutla, R., et al. (2017). 2017 White Paper on Recent Issues in Bioanalysis: a Global Perspective on Immunogenicity Guidelines & Biomarker Assay Performance (Part 3 - LBA: Immunogenicity, Biomarkers and PK Assays). *Bioanalysis* 9 (24), 1967–1996. doi:10.4155/bio-2017-4974

Haslam, A., and Prasad, V. (2019). Estimation of the Percentage of US Patients with Cancer Who Are Eligible for and Respond to Checkpoint Inhibitor Immunotherapy Drugs. *JAMA Netw. Open* 2 (5), e192535. doi:10.1001/jamanetworkopen.2019.2535

Hirsch, F. R., McElhinny, A., Stanforth, D., Ranger-Moore, J., Jansson, M., Kulangara, K., et al. (2017). PD-L1 Immunohistochemistry Assays for Lung Cancer: Results from Phase 1 of the Blueprint PD-L1 IHC Assay Comparison Project. *J. Thorac. Oncol.* 12 (2), 208–222. doi:10.1016/j.jtho.2016.11.2228

Hoyt, C., Roman, K., Engle, E., Wang, C., Ballesteros-Merino, C., Jensen, S. M., et al. (2019). *Multi-institutional TSA-Amplified Multiplexed Immunofluorescence Reproducibility Evaluation (MITRE Study): Reproducibility Assessment of an Automated Multiplexed Immunofluorescence Slide Staining, Imaging, and Analysis Workflow*. Atlanta, GA: American Association of Cancer Research. doi:10.1158/1538-7445.sabcs18-lb-318

Ilie, M., and Hofman, P. (2017). Reproducibility of PD-L1 Assessment in Non-small Cell Lung Cancer-Know Your Limits but Never Stop Trying to Exceed Them. *Transl. Lung Cancer Res.* 6, S51–S54. doi:10.21037/tlcr.2017.10.13

Johnson, D. B., Frampton, G. M., Rioth, M. J., Yusko, E., Xu, Y., Guo, X., et al. (2016). Targeted Next Generation Sequencing Identifies Markers of Response to PD-1 Blockade. *Cancer Immunol. Res.* 4 (11), 959–967. doi:10.1158/2326-6066.CIR-16-0143

Kim, S.-W., Roh, J., and Park, C.-S. (2016). Immunohistochemistry for Pathologists: Protocols, Pitfalls, and Tips. *J. Pathol. Transl Med.* 50 (6), 411–418. doi:10.4132/jptm.2016.08.08

Lu, S., Stein, J. E., Rimm, D. L., Wang, D. W., Bell, J. M., Johnson, D. B., et al. (2019). Comparison of Biomarker Modalities for Predicting Response to PD-1/pd-L1 Checkpoint Blockade. *JAMA Oncol.* 5, 1195. doi:10.1001/jamaoncol.2019.1549

Mazzaschi, G., Madeddu, D., Falco, A., Bocchialini, G., Goldoni, M., Sogni, F., et al. (2018). Low PD-1 Expression in Cytotoxic CD8+ Tumor-Infiltrating Lymphocytes Confers an Immune-Privileged Tissue Microenvironment in NSCLC with a Prognostic and Predictive Value. *Clin. Cancer Res.* 24 (2), 407–419. doi:10.1158/1078-0432.Ccr-17-2156

McCabe, A., Dolled-Filhart, M., Camp, R. L., and Rimm, D. L. (2005). Automated Quantitative Analysis (AQUA) of In Situ Protein Expression, Antibody Concentration, and Prognosis. *J. Natl. Cancer Inst.* 97 (24), 1808–1815. doi:10.1093/jnci/dji427

Mehnert, J. M., Monjazeb, A. M., Beerthuijzen, J. M. T., Collyar, D., Rubinstein, L., and Harris, L. N. (2017). The Challenge for Development of Valuable Immuno-Oncology Biomarkers. *Clin. Cancer Res.* 23 (17), 4970–4979. doi:10.1158/1078-0432.CCR-16-3063

Niazi, M. K. K., Parwani, A. V., and Gurcan, M. N. (2019). Digital Pathology and Artificial Intelligence. *Lancet Oncol.* 20 (5), e253–e261. doi:10.1016/S1470-2045(19)30154-8

Parra, E. R., Uraoka, N., Jiang, M., Cook, P., Gibbons, D., Forget, M.-A., et al. (2017). Validation of Multiplex Immunofluorescence Panels Using Multispectral

Microscopy for Immune-Profiling of Formalin-Fixed and Paraffin-Embedded Human Tumor Tissues. *Sci. Rep.* 7 (1), 13380. doi:10.1038/s41598-017-13942-8

Peabody, J. W., DeMaria, L. M., Tamondong-Lachica, D., Florentino, J., Czarina Acelajado, M., Ouenes, O., et al. (2017). Impact of a Protein-Based Assay that Predicts Prostate Cancer Aggressiveness on Urologists' Recommendations for Active Treatment or Active Surveillance: a Randomized Clinical Utility Trial. *BMC Urol.* 17 (1), 51. doi:10.1186/s12894-017-0243-1

Rimm, D. L., Han, G., Taube, J. M., Yi, E. S., Bridge, J. A., Flieder, D. B., et al. (2017). A Prospective, Multi-Institutional, Pathologist-Based Assessment of 4 Immunohistochemistry Assays for PD-L1 Expression in Non-small Cell Lung Cancer. *JAMA Oncol.* 3 (8), 1051–1058. doi:10.1001/jamaoncol.2017.0013

Santana MFCdLF, L. (2018). *Errors in Surgical Pathology Laboratory*. IntechOpen: Quality Control in Laboratory. doi:10.5772/intechopen.72919

Sapino, A., Goia, M., Recupero, D., and Marchiò, C. (2013). Current Challenges for HER2 Testing in Diagnostic Pathology: State of the Art and Controversial Issues. *Front. Oncol.* 3, 129. doi:10.3389/fonc.2013.00129

Stack, E. C., Wang, C., Roman, K. A., and Hoyt, C. C. (2014). Multiplexed Immunohistochemistry, Imaging, and Quantitation: a Review, with an Assessment of Tyramide Signal Amplification, Multispectral Imaging and Multiplex Analysis. *Methods.* 70 (1), 46–58. doi:10.1016/j.ymeth.2014.08.016

Tan, W. C. C., Nerurkar, S. N., Cai, H. Y., Ng, H. H. M., Wu, D., Wee, Y. T. F., et al. (2020). Overview of Multiplex Immunohistochemistry/immunofluorescence Techniques in the Era of Cancer Immunotherapy. *Cancer Commun.* 40 (4), 135–153. doi:10.1002/cac2.12023

Taube, J. M., Akturk, G., Angelo, M., Engle, E. L., Gnjatic, S., Greenbaum, S., et al. (2020). The Society for Immunotherapy of Cancer Statement on Best Practices for Multiplex Immunohistochemistry (IHC) and Immunofluorescence (IF) Staining and Validation. *J. Immunother. Cancer.* 8 (1), e000155. doi:10.1136/jitc-2019-000155

Troncone, G., and Gridelli, C. (2017). The Reproducibility of PD-L1 Scoring in Lung Cancer: Can the Pathologists Do Better?. *Transl. Lung Cancer Res.* 6 (Suppl. 1), S74–S77. doi:10.21037/tlcr.2017.10.05

Tumeh, P. C., Harview, C. L., Yearley, J. H., Shintaku, I. P., Taylor, E. J. M., Robert, L., et al. (2014). PD-1 Blockade Induces Responses by Inhibiting Adaptive Immune Resistance. *Nature.* 515 (7528), 568–571. doi:10.1038/nature13954

Wilky, B. A. (2019). Immune Checkpoint Inhibitors: The Linchpins of Modern Immunotherapy. *Immunol. Rev.* 290 (1), 6–23. doi:10.1111/imr.12766

Wong, P. F., Smithy, J. W., Blenman, K. R., Kluger, H. M., and Rimm, D. L. (2018). Abstract 3638: Quantitative Assessment of Tumor-Infiltrating Lymphocytes and Immunotherapy Outcome in Metastatic Melanoma. *Cancer Res.* 78 (13). doi:10.1158/1538-7445.Am2018-3638

Conflict of Interest: Author CH was employed by Akoya Biosciences Inc.

frontiers in Molecular Biosciences

METHODS
published: 11 June 2021
doi: 10.3389/fmolb.2021.689799

Whole-Slide Image Analysis of Human Pancreas Samples to Elucidate the Immunopathogenesis of Type 1 Diabetes Using the QuPath Software

Paola S. Apaolaza[1,2†], *Peristera-Ioanna Petropoulou*[1,2†] *and Teresa Rodriguez-Calvo*[1,2*]

[1]*Institute of Diabetes Research, Helmholtz Diabetes Center at Helmholtz Zentrum München, Munich, Germany,* [2]*German Center for Diabetes Research (DZD), Helmholtz Zentrum Munich, Munich, Germany*

OPEN ACCESS

Edited by:
Joe Yeong,
*A*STAR, Singapore*

Reviewed by:
Bernett Lee,
*A*STAR, Singapore*
Carmen Ballesteros-Merino,
Earle A. Chiles Research Institute, United States

***Correspondence:**
Teresa Rodriguez-Calvo
teresa.rodriguez@helmholtz-muenchen.de

†These authors have contributed equally to this work and share first authorship

Specialty section:
This article was submitted to Molecular Diagnostics and Therapeutics, a section of the journal Frontiers in Molecular Biosciences

Received: *01 April 2021*
Accepted: *18 May 2021*
Published: *11 June 2021*

Citation:
Apaolaza PS, Petropoulou P-I and Rodriguez-Calvo T (2021) Whole-Slide Image Analysis of Human Pancreas Samples to Elucidate the Immunopathogenesis of Type 1 Diabetes Using the QuPath Software. Front. Mol. Biosci. 8:689799. doi: 10.3389/fmolb.2021.689799

Type 1 diabetes is a chronic disease of the pancreas characterized by the loss of insulin-producing beta cells. Access to human pancreas samples for research purposes has been historically limited, restricting pathological analyses to animal models. However, intrinsic differences between animals and humans have made clinical translation very challenging. Recently, human pancreas samples have become available through several biobanks worldwide, and this has opened numerous opportunities for scientific discovery. In addition, the use of new imaging technologies has unraveled many mysteries of the human pancreas not merely in the presence of disease, but also in physiological conditions. Nowadays, multiplex immunofluorescence protocols as well as sophisticated image analysis tools can be employed. Here, we described the use of QuPath—an open-source platform for image analysis—for the investigation of human pancreas samples. We demonstrate that QuPath can be adequately used to analyze whole-slide images with the aim of identifying the islets of Langerhans and define their cellular composition as well as other basic morphological characteristics. In addition, we show that QuPath can identify immune cell populations in the exocrine tissue and islets of Langerhans, accurately localizing and quantifying immune infiltrates in the pancreas. Therefore, we present a tool and analysis pipeline that allows for the accurate characterization of the human pancreas, enabling the study of the anatomical and physiological changes underlying pancreatic diseases such as type 1 diabetes. The standardization and implementation of these analysis tools is of critical importance to understand disease pathogenesis, and may be informative for the design of new therapies aimed at preserving beta cell function and halting the inflammation caused by the immune attack.

Keywords: pancreas, type 1 diabetes, pathology, multiplex immunofluorescence, whole-slide image analysis, QuPath

INTRODUCTION

The pancreas is mainly divided into exocrine and endocrine tissue. The islets of Langerhans, which account for 1–4% of the total pancreatic volume, form the endocrine portion and contain several cell populations (secreting distinct proteins): alpha cells (glucagon), beta cells (insulin), delta cells (somatostatin), epsilon cells (ghrelin), and pancreatic polypeptide cells (PP) (Dolenšek et al., 2015; Noguchi and Huising, 2019). In physiological conditions, beta cells constitute approximately 50–70% of the total endocrine cells, followed by alpha cells (20–40%), delta cells (<10%), and a few epsilon and PP cells (Steiner et al., 2010); however these proportions vary from region to region (e.g., PP cells can reach 80% in the pancreatic head, whereas beta cells are <20% in the same region) or with disease stage (Rahier et al., 1983; Steiner et al., 2010). The exocrine pancreas accounts for 96–99% of the total volume and is organized into lobes, lobules, and acini (dome-like structures consisting of acinar cells); single endocrine cells can be found throughout the acinar and ductal tissue (Dolenšek et al., 2015). Both endocrine and exocrine tissue are affected in type 1 diabetes (T1D) (Rodriguez-Calvo et al., 2014; Campbell-Thompson et al., 2015; Alexandre-Heymann et al., 2019; Bender et al., 2020), but the disease is characterized by a chronic autoimmune destruction of insulin-producing beta cells (Rowe et al., 2011). Recently, in individuals with recent onset T1D, a decrease in pancreatic volume has been observed compared to healthy controls (Williams et al., 2012), indicating that pancreatic atrophy might be an important contributing factor to disease pathogenesis and bringing the often-neglected study of the pancreas as a whole to T1D research.

Beta cells are the main source of insulin biosynthesis, storage, and secretion (Vasiljević et al., 2020). Insulin is a peptide hormone of 51 amino acids consisting of two chains (A and B chain, linked by two disulfide bonds), which is initially synthesized from a single-chain precursor—preproinsulin. After synthesis in the ribosomes, preproinsulin is transferred to the endoplasmic reticulum (ER), where proinsulin is created by cleavage of the signal peptide. When folding and disulfide bonds are completed, proinsulin is transferred to the Golgi, where it is packaged in clathrin-coated vesicles (Steiner et al., 2009; Vasiljević et al., 2020). In these granules, proinsulin is cleaved sequentially by 1) prohormone convertase 1/3 (PC1/3), which shows preference for the C-peptide/A-chain junction, but cleaves also at the C-peptide/B-chain junction, 2) prohormone convertase 2 (PC2), which cleaves at the C-peptide/B-chain junction, and 3) carboxypeptidase E (CPE), which cleaves away the connecting segment and removes any remaining C-terminal basic residues from both insulin and C-peptide (Steiner et al., 2009; Vasiljević et al., 2020). In T1D and other pancreatic diseases, alterations at the level of these enzymes in beta cells have a major impact in proinsulin processing, proinsulin and insulin secretion (Sims et al., 2019), and overall beta cell function.

Infiltrating immune cells can be found scattered in the exocrine and endocrine pancreas in physiological conditions and their numbers increase prior to, at the time of diagnosis, and after T1D onset (Willcox et al., 2009; Rodriguez-Calvo et al., 2014; Bender et al., 2020). Insulitis, which is a hallmark of T1D, has been defined over the years as infiltration by ≥15 CD45+ cells (Campbell-Thompson et al., 2013) or ≥6 CD3+ cells (Campbell-Thompson et al., 2016) located immediately adjacent to or within the islet, in a minimum of three islets of standard size (150 µm of diameter). In addition, pseudoatrophic islets (insulin deficient) should be present in the tissue section (Campbell-Thompson et al., 2013). T cells are the major cell type found in insulitis, and their presence is significantly higher in T1D subjects, not only in the islets, but also in the exocrine compartment (Rodriguez-Calvo et al., 2014). Up to this date, the events leading to the autoimmune attack and the consequent beta cell destruction are not well elucidated. However, increasing evidence suggests a potential self-involvement of beta cells in their own demise (Mallone and Eizirik, 2020; Roep et al., 2020). In individuals with genetic predisposition, intrinsic properties of beta cells such as high ER stress, vascularization, and hormone secretion, might intensify the presentation of self-antigens on beta cells, which could increase the recruitment of immune cells to the islets.

Early research in T1D was originally based on limited human pancreatic specimens (Foulis and Stewart, 1984; Foulis et al., 1986), experimental mouse models [mainly the non-obese diabetic (NOD) mouse (Anderson and Bluestone, 2005)], or on beta cell lines (Scharfmann et al., 2019). During the last decades, the scientific community realized the importance of systematic organ collection and distribution for research and founded several biobanks, such as the Exeter Archival Diabetes Biobank (EADB) (Foulis et al., 1986), the Dutch Pancreas Biobank (Strijker et al., 2018), and the IMIDIA Biobank (Solimena et al., 2018). The National Institutes of Health established the Human Pancreas Analysis Program (HPAP), which aims to distribute high quality molecular data derived from human pancreata in order to enable scientific discovery (Kaestner et al., 2019). The biggest and well-known biobank in the T1D field is the Network for Pancreatic Organ Donors with Diabetes (nPOD), founded by the Juvenile Diabetes Research Foundation (JDRF) in 2007, and based in the United States (Campbell-Thompson et al., 2012). nPOD's main goals are to obtain and distribute pancreatic or disease-relevant tissue samples from organ donors to affiliated researchers around the globe, as well as to foster and promote collaboration between research teams, leading ultimately to a quicker elucidation of the disease pathogenesis (Pugliese et al., 2014).

One of the biggest challenges in the study and analysis of pancreas pathology is the heterogeneity of the human pancreas, which is evident at the beta cell, the islet, and the organ level (Dybala and Hara, 2019). Manual analysis of multiple regions of interest (ROIs) has been traditionally performed, which faced a lack of robustness and reproducibility. This type of analysis is prone to bias and cannot capture the variability in size, endocrine composition, architecture, vasculature and immune cell infiltration in islets, and exocrine tissue (Dybala and Hara, 2019). Several algorithms and workflows for the analysis of 2D (Wang et al., 2013; Kilimnik et al., 2012) and 3D (Poudel et al., 2016; Fowler et al., 2018) images of the pancreas have been proposed using specific Fiji plugins and MATLAB. However, most of these algorithms are not intuitive and require a considerable amount of computer proficiency. Nowadays,

whole-slide image analysis of tissue sections, provided by the biobanks mentioned above, is becoming increasingly accessible to researchers. To date, analysis of such images required either specialized commercial software (Tang et al., 2020) or was limited to a small ROI, due to the inability of existing open-source software to handle large 2D images (Aeffner et al., 2019). QuPath (http://qupath.github.io) is an open-source, user-friendly software developed by Bankhead et al. (2017) in 2016 in order to enable whole-slide image analysis and digital pathology, by addressing the unique requirements in the visualization and analysis of such data.

Here, we show that QuPath can automatically and accurately detect, quantify and distinguish cell populations in the endocrine and the exocrine compartments of the pancreas using a series of detection algorithms based on intensity thresholding, pixel classification, and machine learning. We provide the groundwork for a standardized, semi-automated analysis of the human pancreas using QuPath, which can lead to a more efficient and reproducible analysis of tissue images, reducing inter-observer variability, and bringing researchers closer to elucidating the etiology of T1D.

MATERIALS AND EQUIPMENT

QuPath Software

Multiplexed fluorescence images from tissue sections were analyzed with QuPath version 0.2.3, an open-source software for digital pathology and whole-slide image analysis described by Bankhead et al. (2017). Briefly, the software was developed using Java 8, with a JavaFX interface for annotation and visualization, built-in algorithms for common tasks, including cell and tissue detection, and interactive machine learning for object and pixel classification. It is compatible with ImageJ, OpenCV, Java Topology Suite, and OMERO. The software supports several image formats through Bio-Formats and OpenSlide, including whole-slide images and multiplexed data.

Pancreatic Specimens

Six 4-μm-thick pancreatic formalin-fixed paraffin-embedded (FFPE) sections from the tail of the pancreas of a female non-diabetic donor, were obtained through nPOD. All the sections were obtained from the same tissue block. Slides #1, #2, #3, #4, and #6 were consecutive, while section #5 was not. Briefly, the donor was 64 years old, Caucasian, with a BMI of 31.2 and an HLA-A*02/03, B*07/60, DR*13/15, DQ*06 phenotype, who was hospitalized for 2.67 days due to a cerebrovascular accident. The histopathology record showed insulin and glucagon positive normal islets. All experimental procedures were approved by the ethics committee at the Technical University of Munich (protocol #215/17 S) and the Helmholtz Center Munich, Institute of Diabetes Research.

Immunofluorescence and Imaging

FFPE sections were stained for insulin, proinsulin, glucagon, CD3, CD8, CD45, chromogranin A (CHGA), PC1/3, PC2, and CPE by immunofluorescence (**Supplementary Figure S1**). Tissue sections were deparaffinized with an alternative to xylene clearing agent (H2779, Sigma-Aldrich, MO, United States) and rehydrated in ethanol baths of decreasing ethanol content. Antigen retrieval and multiplexing of primary antibodies of the same species was performed using the Opal kit according to the manufacturer's instructions (NEL811001KT, Akoya Biosciences, CA, United States). Specifically, a 2-step microwave antigen retrieval process preceded the primary antibody incubations and was the same for all the stainings. Slides were first microwaved at 900 W for 45–65 s (until retrieval buffer reached the boiling point), followed by a second step, where the sections were microwaved for 15 min at 160 W. The following primary antibodies were incubated for 1 h at room temperature or overnight at 4°C depending on the protocol: mouse anti-proinsulin (1:200, GS-9A8 supernatant, DSHB, IA, United States), mouse anti-CD45 (1:100, M070101, Agilent Technologies, CA, United States), rabbit anti-CD3 (1:200, A045229, Agilent Technologies), rabbit anti-CD8 (1:900, ATA-HPA037756, Atlas Antibodies, Bromma, Sweden), mouse anti-insulin (1:300, 5-1108, Merck, Darmstadt, Germany), guinea pig anti-insulin (1:500; A056401-2, Agilent Technologies), rabbit anti-glucagon (1:1200; ab92517, Abcam, Cambridge, United Kingdom), rabbit anti-CHGA (1:500; ab15160, Abcam), mouse anti-PCSK1N (1:500, ATA-HPA064734, Atlas Antibodies), rabbit anti-PC2 (1:800, Merck), and rabbit anti-CPE (1:100, ATA-HPA003819, Atlas Antibodies). Detection was performed by 1 h incubation at room temperature with the following secondary antibodies at 1:1,000 dilution (all from Life technologies, Darmstadt, Germany): Goat Anti-Guinea Pig IgG Alexa Fluor 488 (A11073), Goat Anti-Rabbit IgG Alexa Fluor 750 (A21039), Goat Anti-Mouse IgG Alexa Fluor 750 (A21037), F(ab')2-Goat anti-Rabbit IgG Alexa Fluor 488 (A11070), Goat Anti-Mouse IgG1 Alexa Fluor 555 (A21127), F(ab')2-Goat anti-Rabbit IgG Alexa Fluor 555 (A21430), and Goat Anti-Mouse IgG1 Alexa Fluor 647 (A21240). Sections were counterstained with Hoechst 33342 (1:5,000; Invitrogen, CA, United States) and mounted with Prolong Gold Antifade reagent (Invitrogen). Whole tissue sections were scanned by an Axio Scan.Z1 slide scanner (Zeiss, Jena, Germany) using a 20x/0.8NA Plan-Apochromat (a = 0.55 mm) objective.

Statistics

All the graphs show the median and 95% confidence interval of the median. Analyses were performed using GraphPad Prism version 9, GraphPad Software, La Jolla, CA, United States, www.graphpad.com.

Standard Operating Procedure for Whole Slide Image Analysis

A step by step guide and detailed information on how to analyze whole-slide pancreatic tissue sections is provided as a supplementary document (**Supplementary Data S1**).

METHODS

Tissue, Islet and Cell Detection

First, tissue area and islets were automatically identified based on average values of all channels for the labeled proteins (antibody

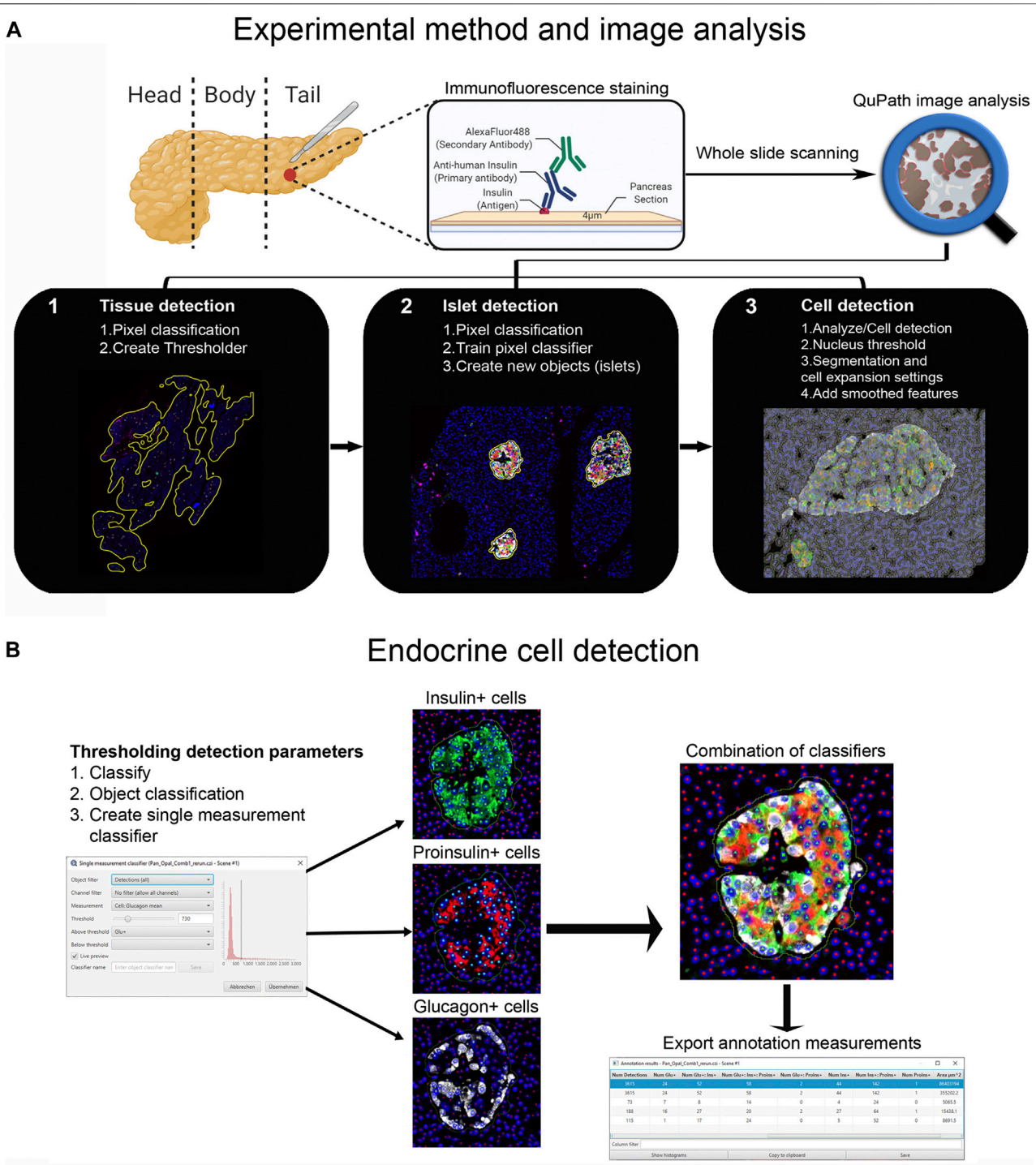

FIGURE 1 | Schematic illustration of the whole-slide image analysis workflow using QuPath. **(A)** Experimental method and image analysis. Multiple immunofluorescence protocols were employed for the staining of tissue sections from the pancreatic tail of a single non-diabetic donor. Whole-slide image analysis was carried out with QuPath, version 0.2.3 1); tissue was detected using an intensity thresholder based on average values of all channels for the labeled proteins 2), Objects (islets) were then created using the pixel classifier, and 3) cells were detected and smoothed features were added. **(B)** The *Single measurement classifier tool* was employed to detect positive cells for the marker of interest. Cells were identified as areas of staining above the background level by applying optimized *Cell mean* intensity thresholds. Combination of single classifiers was necessary for the accurate detection of beta and alpha cells. Annotation measurements were exported as CSV files and were subsequently processed in Excel spreadsheets.

TABLE 1 | Characterization of the endocrine and the exocrine pancreas of a non-diabetic donor according to different staining combinations.

Slide ID	Tissue area (mm^2)	Exocrine area (mm^2)	Endocrine area (mm^2)	No. islets	No. islet cells	No. beta cells	No. alpha cells
1-PI/CD45/INS/GCG	80.9	79.8	1.2	260	13,625	9,571	4,537
2-INS/PI/GCG	71.8	70.6	1.3	262	13,129	7,581	4,163
3-INS/PC1/PI	84.6	83.4	1.1	234	12,441	9,040	3,401
4-INS/CPE/PI	92.9	91.7	1.2	273	14,616	11,682	2,934
5-INS/PC2/PI	130.6	128.3	2.3	432	26,655	17,579	9,076
6-CD3/CD8/CHGA	75.0	74.14	0.9	241	13,203	NA	NA
Total mean ± SD	89.3 ± 19.7	87.9 ± 19.2	1.3 ± 0.5	283.7 ± 67.6	15,611.5 ± 4,981.8	11,090.6 ± 3,500.9	4,822.2 ± 2,199.8

combinations are shown in **Supplementary Table S1**) using thresholding detection and machine learning. Information on the whole tissue section, exocrine and endocrine areas, number of islets per section, as well as the total number of alpha and beta cells was obtained. Independent workflows and settings for 1) tissue, 2) islet, and 3) cell detection are shown in **Figure 1A** and **Supplementary Figure S2**. Only islets formed by ≥10 cells were included in the analysis in order to avoid scattered single endocrine cells present in the exocrine tissue and possible detection errors derived from small artefacts. First, for tissue detection, the command *Pixel classification → Create thresholder* was used (**Figure 1A**). After applying the *fill holes* function, the tissue was manually checked for the presence of artifacts. Then, a small ROI was created, and islets were recognized as a new class by *Pixel classification*. For this purpose, the command *Train pixel classifier* was used and new objects (islets) were created. Once the new islet classifier was saved, *Cell detection* was performed in the entire tissue section. Cells were identified as areas of staining above the background level, by applying optimized *nucleus threshold*, segmentation parameters (*Median filter radius and Sigma*), and cell expansion (**Figure 1A** and **Supplementary Figure S2**). Last, *smoothed features* were added in order to obtain new measurements considering the cell features within a 25 μm range. After cells were detected, the islet pixel classifier, initially applied to a small ROI, was applied to the whole tissue area, and the newly created islet areas, defined as objects, were filled automatically following the path *Objects→ Annotations→ Fill holes*.

Endocrine Cell Detection

Thresholding detection was applied to create unique classifiers for every staining combination due to fluorescence channel dependency. After islet detection, the path *Classify → Object classification → Create single measurement classifier tool* was applied to detect cells positive for insulin, proinsulin, glucagon, PC1/3, PC2 or CPE (**Figure 1B**). Cells were identified as areas of staining above the background level by applying optimized *Cell mean* intensity thresholds. To identify beta cells, the new classifiers were combined to obtain the number of cells positive for both insulin and proinsulin together with different proteins of interest like PC1/3, PC2 or CPE. Data on alpha cells were obtained by using glucagon positive cells as reference. Chromogranin A was used for complete islet cell detection for slide #6. *Annotation measurements* were exported and information on islet size, cell composition and number of positive cells was obtained (**Table 1** and **Supplementary Table S2**).

Immune Cell Detection and Spatial Analysis of Immune Infiltration

Different image analysis protocols were generated for the study of CD45+ (leucocyte marker), CD3+ (T cell marker) and CD8+ cells (CD8+ T cell marker) and their localization in the islets and exocrine tissue. CD4+ T cells were calculated as the total number of CD3+ cells minus the number of CD8+ cells (CD3+ CD8−cells). The use of thresholding vs. machine learning was compared (**Figure 2A**). First, the membrane marker CD45, which is expressed in all leucocytes, was detected. For thresholding, a *single measurement classifier* for the *cell mean* intensity value of the CD45 marker was used. Using this method, an overestimation in the number of islet-infiltrating cells was observed, and manual correction was applied. For machine learning, the following path was used: *Classify → Object classification → Train object classifier*. For the classifier training, the option *Points only* was selected. Then, the *Points* tool was used to assign two different classes to the corresponding cells, one for the marker of interest (CD45+), and one for unclassified objects (*ignore**). For each class, negative (*ignore**) and positive (CD45+), three different ranges of training points were tested (≥50, ≥80, and over 100). Overall, classifying between 50 and 80 points and using machine learning was comparable to applying the best threshold and subsequent manual correction. Moreover, when the whole section was analyzed, the total number of CD45+ cells detected by thresholding was lower than the one obtained by machine learning using 100 training points (8,078 vs. 17,116 cells), indicating that immune cells with low intensity values were not properly detected when thresholding was used (**Table 2**). Machine learning using ≥100 points showed higher accuracy than thresholding and was subsequently used for the detection of CD3+ and CD8+ cells. However, the most suitable number of training points should be defined by the user based on staining, intrinsic characteristics of the tissue and quality of the specimen. Last, measurements were exported and the number, proportion of

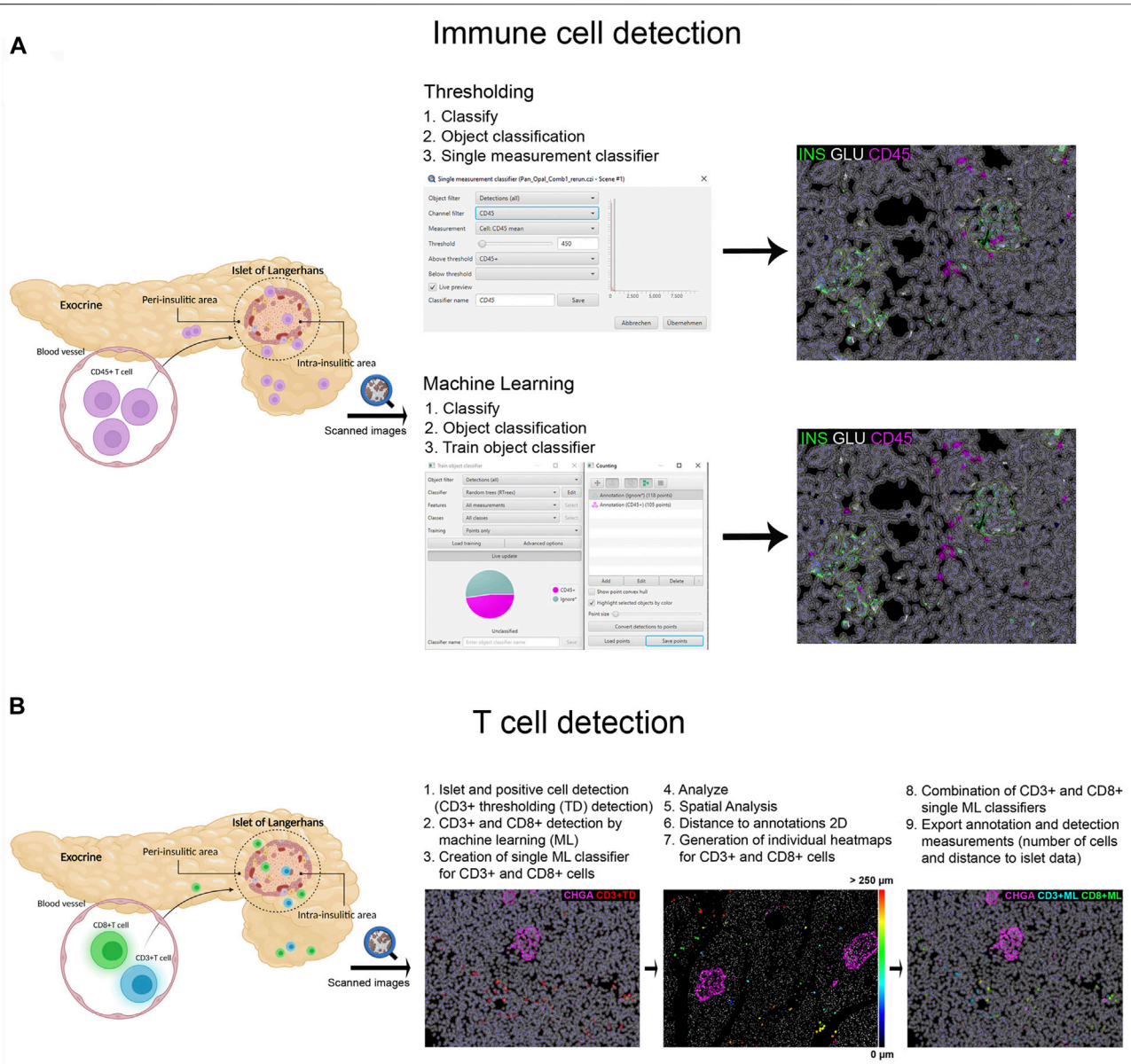

FIGURE 2 | Schematic illustration of the immune cell detection workflow using QuPath. **(A)** Comparison of the thresholding (single measurement classifier) and the machine learning (train object classifier) option for the detection of CD45+ cells. **(B)** Workflow for the detection and distance analysis of CD3+ and CD8+ cells detected with thresholding and machine learning. Heatmaps were created to depict the relative distance of CD3+ and CD8+ cells (either individually or combined as one class) to the annotated islets.

TABLE 2 | Comparison of the number of CD45+ cells in the whole tissue, the exocrine and endocrine area of slide #1, depending on the detection method (thresholding vs. machine learning).

QuPath method	Total no. CD45+	No. CD45+ in exocrine	No. CD45+ in endocrine
Thresholding	8,107	8,069	38
Thresholding manually corrected	8,078	8,067	11
Machine learning (≥50 points)	6,801	6,800	1
Machine learning (≥80 points)	12,874	12,870	4
Machine learning (≥100 points)	17,116	17,098	18

TABLE 3 | Number, proportion and density of immune cells in the whole tissue, the exocrine and endocrine area. CD45+ cell values correspond to the analysis of slide #1, and CD3+, CD8+, and CD4+ cell analysis to slide #6.

	No. CD45+	No. CD3+	No. CD8+	No. CD4+	% CD45+	% CD3+	% CD8+	% CD4+	CD45+/ mm^2	CD3+/ mm^2	CD8+/ mm^2	CD4+/ mm^2
Tissue	17,116	8,643	3,911	4,732	100	100	100	100	211.5	115.2	52.1	63.1
Exocrine	17,098	8,639	3,909	4,730	99.9	99.95	99.95	99.96	214.3	116.7	52.8	63.9
Endocrine	18	4	2	2	0.1	0.05	0.05	0.04	15.5	4.1	2	2

infiltrated islets and density of CD45+ cells (expressed as number of positive cells per mm^2) were calculated in the whole tissue, and the exocrine and endocrine compartments (**Table 3** and **Figure 6**).

In order to characterize T cell infiltration, a modified version for cell detection was applied as follows (**Figure 2B**): After islets were detected, the option *Positive cell detection* was used to identify by thresholding all CD3+ cells. However, as cell detection by thresholding was not completely accurate, a second classifier for CD3+ or CD8+ membrane markers was created using machine learning. As explained above, the object classifier was trained with a minimum of 100 training points for CD3+ and CD8+ cell detection, and was applied over the CD3+ cells detected by thresholding, creating a single machine learning classifier for CD3+ and CD8+ cells. Then, once T cells were identified, their localization with respect to the islets was analyzed (**Figure 2B**). Distance analysis was performed using the command *Spatial analysis*. This tool was applied as follows: *Analyze→ Spatial analysis→ Distance to annotations 2D*. Next, we generated individual heatmaps for CD3+ and CD8+ cells based on the distance of the cells to the islets. Finally, both single machine learning classifiers were combined and different classes were automatically created; the first one corresponding to all CD3+ cells, the second class for cells positive for both markers (CD3+CD8+), representing CD8+ cells, and the third one representing CD4+ cells (CD3+CD8−). Last, *annotation* and *detection measurements* were exported. Data on T cell numbers, endocrine and exocrine T cell density, proportion of infiltrated islets, as well as the distance of T cells to the islets were obtained (**Table 3** and **Figures 6**, **7**).

RESULTS

Characterization of the Endocrine and Exocrine Pancreas in a Non-diabetic Donor

To characterize pancreas tissue sections, thresholding detection and machine learning were used as described above (*Tissue, Islet and Cell Detection*) and applied to define the whole tissue as well as the exocrine and endocrine areas. For this purpose, six tissue sections from a non-diabetic donor were analyzed as shown in **Table 1**. Data regarding islet density, the number of cells per islet as well as their cellular composition (beta and alpha cells) were obtained (**Figure 3** and **Table 1**). There were minimal differences in endocrine cell density, expressed as number of endocrine cells per islet area (mm^2), between the sections (**Figure 3A**). Analysis of the cellular composition showed that the majority of islets contain between 10 and 100 endocrine cells (**Figure 3B**). As observed in **Table 1**, the mean area value of whole tissue, exocrine and endocrine compartments (including all slides) was 89.3 ± 19.7, 87.9 ± 19.2, and 1.3 ± 0.5 mm^2 respectively. A similar number of islets was detected in the majority of tissue sections, even when individual pixel classifiers for each section were applied (283.7 ± 67.6 islets, **Table 1**). Only section #5, which had a bigger area, contained more islets than slide #1 to 4 and slide #6 (**Figure 3B**, **Supplementary Figure S3** and **Supplementary Table S3**). There was a large variability in the proportion of alpha and beta cells per islet which ranged from 0 to 100% (**Figures 3C, E** and **Supplementary Figure S4**), as well as in endocrine cell density per islet (**Figure 3D** and **Supplementary Figure S4**). A mean of 70.1% of beta cells (range 57.7–79.9%) were present in the whole section versus a mean of 28.1% of alpha cells (range 20.1–33.3%) (**Figure 3F**). Cell density profiles showed a similar distribution for alpha and beta cells in different sections (**Supplementary Figure S4**).

Assessment of the Reproducibility and Accuracy of Insulin (INS) and Proinsulin (PI) Positive Cell Detection

As shown above, insulin-producing beta cells are the predominant islet cell population. To further characterize them, the total number of cells positive for insulin (INS+) and proinsulin (PI+) was first measured in the whole tissue area of slides #1, #2, #3, #4, and #5 (**Supplementary Table S2**). The proportion of INS + cells was lower for sections #1, #2, and #5 (64.8, 56.2, and 53.5% respectively) compared to sections #3 (71.5%) and #4 (77.8%) (**Supplementary Table S2**). Slight differences between sections were expected: sections #1 and #2 were stained with a different insulin antibody and section #5 belonged to the same tissue block, but was not consecutive to the other slides (**Supplementary Tables S2, S3**). Conversely, the proportion of PI+ cells was comparable between sections, as the same antibody was used for all the slides (**Supplementary Table S2**). Then, the proportion and density of INS+ and PI+ cells per islet were calculated (**Figure 4**). Overall, there were mild differences in INS+ and PI+ cell distribution per islet between tissue sections.

As intraindividual differences could also be observed, the ratio PI/INS was calculated for each section (**Figure 4F**). Comparable results were obtained with median ratios that ranged from 0.79 to 1.02. In two sections (#2 and #3) the ratios were close to 1, indicating an equal detection of INS and PI in beta cells, whereas

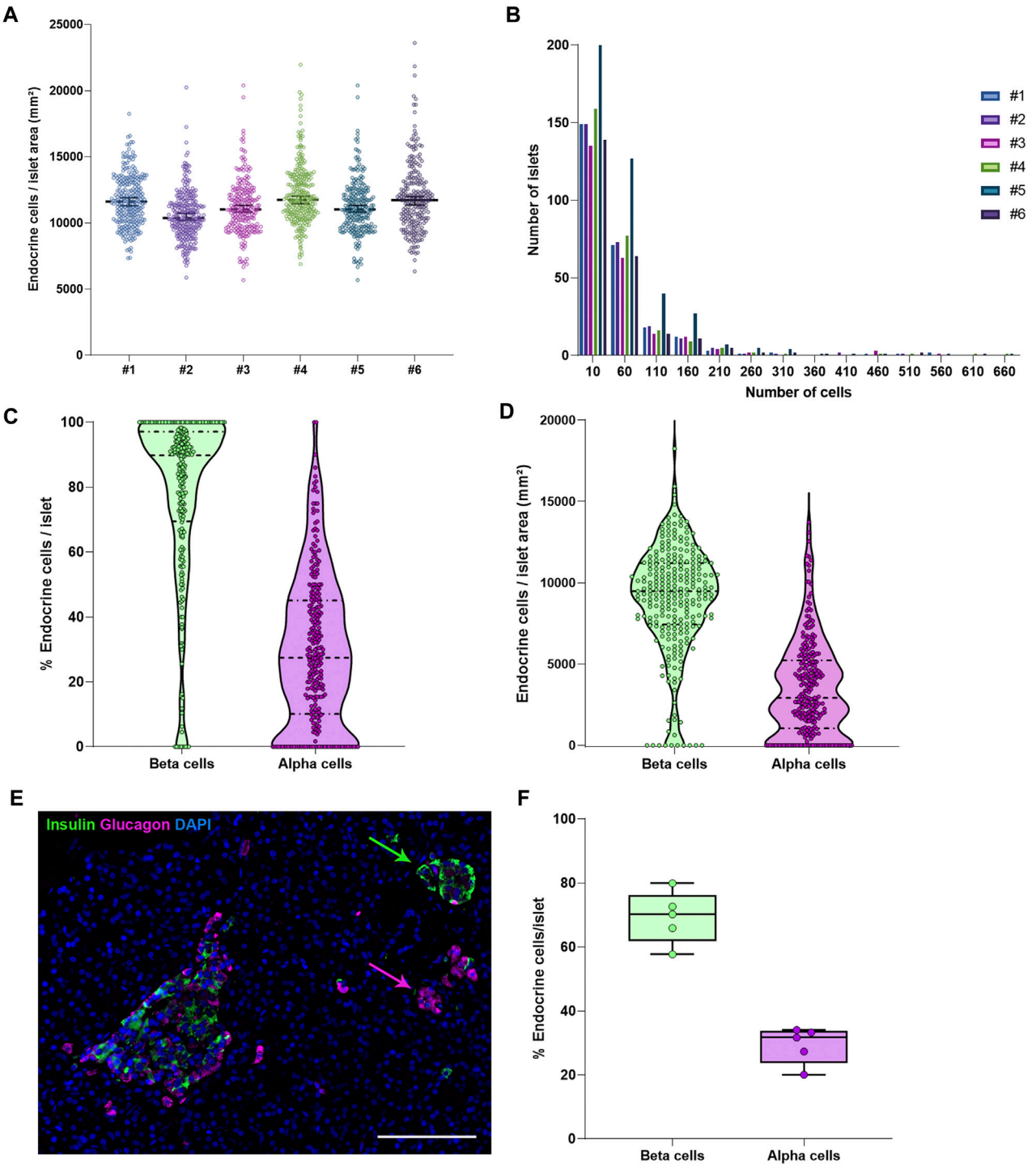

FIGURE 3 | Characterization of the endocrine and exocrine pancreas in a non-diabetic donor. **(A)** Comparison of islet density expressed as number of endocrine cells per islet area in mm^2 among the different staining combinations. Each dot represents an islet. **(B)** Histograms showing the cellular content of islets in pancreatic sections stained with different antibody combinations. The different staining IDs are shown as #1–6. Each bar represents a different slide. More details can be found in **Supplementary Table S1**. **(C)** Violin plots showing the percentage of endocrine cells (beta and alpha cells) per islet analyzed in the whole pancreatic section, stained with antibody combination #1. Each dot colored represents an islet. **(D)** Violin plots showing the density of beta and alpha cells in the same section, expressed as number of endocrine cells per mm^2 of islet area. Each dot represents an islet. **(E)** Representative image showing two islets, one containing mainly beta cells (green) and one containing mainly alpha cells (magenta). **(F)** Boxplots showing the mean percentage of beta or alpha cells per islet. Each dot represents the mean from a single slide. Scale bar: 100 μm.

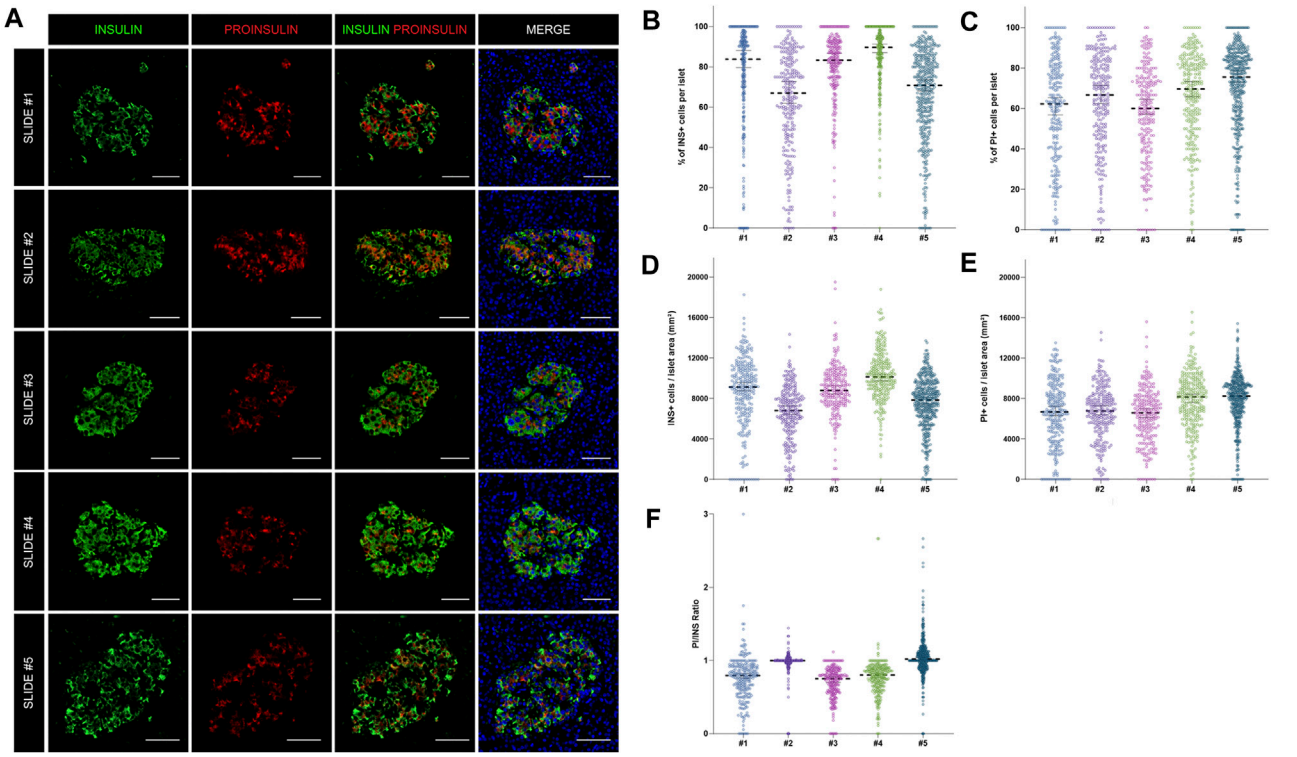

FIGURE 4 | Assessment of the reproducibility and accuracy of insulin (INS) and proinsulin (PI) positive cell detection. **(A)** Representative images showing insulin (INS) and proinsulin (PI) staining in islets from different pancreatic sections stained with different antibody combinations (slides #1–5). **(B)** Dot plots showing the proportion of insulin and **(C)** proinsulin positive cells per islet in slides #1–5. Each dot represents an islet. **(D)** Dot plots showing the density of insulin and **(E)** proinsulin positive cells expressed as number of positive cells per islet area in mm^2. Each dot represents an islet. **(F)** Comparison of the proinsulin to insulin ratio (PI/INS) among the different samples. Each dot represents an islet. Scale bar: 50 μm.

in other sections, lower ratios were observed. Therefore, mild variations in INS and PI expression from islet to islet and cell to cell are expected, even within the same individual.

Analysis of the Proinsulin Processing Enzymes Prohormone Convertase 1/3, Prohormone Convertase 2 and Carboxypeptidase E

As shown above, interindividual, inter-islet (among different islets of the same donor) and intra-islet (between cells within the same islet) differences in protein expression are expected. Therefore, establishment of reference expression levels for proteins like insulin, proinsulin, and their processing enzymes in non-diabetic individuals is of great interest. Thus, the expression of the enzymes PC1/3, PC2, and CPE was evaluated. The proportion of PC1/3+, PC2+, and CPE+ cells per islet was calculated in beta and alpha cells (**Figure 5**). Overall, the three prohormone enzymes were expressed in a higher percentage of beta cells compared to alpha cells, although there was high inter-islet variability (**Figure 5B**). CPE was expressed in a higher proportion of beta cells compared to PC1/3 and PC2 (mean CPE+ 78.5 ± 21.9%, mean PC1/3+ 68.2 ± 20.1%, and mean PC2+ 62.4 ± 24.1%). CPE and PC2 were expressed in a higher proportion of alpha cells compared to PC1/3 (mean PC1/3+ 49.3 ± 33.4%, mean PC2+ 58.4 ± 33.4%, and mean CPE+ 63.9 ± 35.9%).

Analysis of the Proportion and Density of Immune Infiltration in the Exocrine and Endocrine Pancreas

To investigate immune cell infiltration in the pancreas, cells were detected using the machine learning protocol described above (*Immune Cell Detection and Spatial Analysis of Immune Infiltration*). A minimum of 100 training points for each class of interest were assigned, and the proportion of CD45+, CD3+, CD8+, and CD4+ (CD3+CD8−) cells was calculated in the exocrine and the endocrine compartments using different sections from the same donor. As expected in a non-diabetic pancreas, there were no signs of insulitis, as currently defined. However, as observed in **Figure 6**, a few immune cells could be found close to, or infiltrating some islets. To evaluate immune infiltration in both compartments (exocrine and endocrine), the proportion of infiltrated islets, the proportion of immune cells, and immune cell density in the whole section were calculated (**Figure 6** and **Table 3**). First, CD45+ cells were analyzed. In a total of 260 islets, only 18 CD45+ cells could be found within or

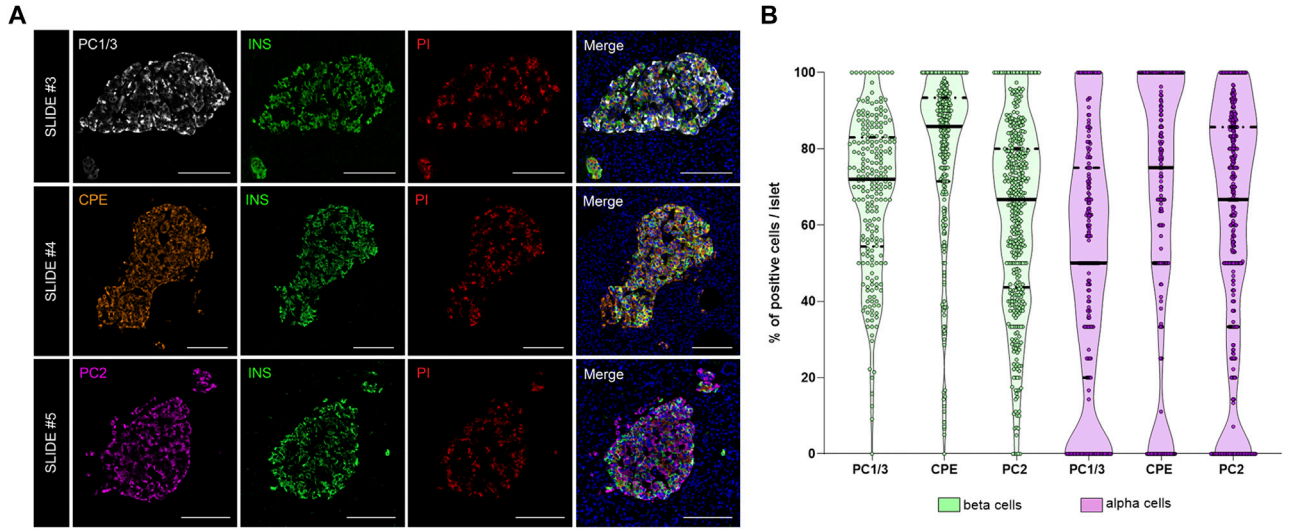

FIGURE 5 | Analysis of the prohormone processing enzymes PC1/3, CPE and PC2 in the endocrine pancreas. **(A)** Representative images showing the distribution and localization of the proinsulin processing enzymes PC1/3 (slide #3, upper row), CPE (slide #4, middle row) and PC2 (slide #5, lower row) in the islets. **(B)** Violin plots showing the proportion of PC1/3+, PC2+, and CPE+ cells in beta (green) and alpha cells (violet). Each dot represents an islet. Scale bar: 100 μm.

immediately adjacent to islets (1% of the total number of CD45+ cells). Then, the proportion of CD3+, CD8+, and CD4+ cells per islet was calculated. In a total of 241 islets, 4 CD3+ cells (0.05%) could be found, of which two cells were CD8+ (0.05%) and two cells were CD8− (considered CD4+, 0.04%) (**Table 3**). The majority of immune cells were found in the exocrine tissue or in close proximity to blood vessels. Next, the proportion of islets that were infiltrated by at least one cell was calculated (**Figure 6B**). Only a few infiltrated islets were found in the whole section (5% by CD45+, 1.7% by CD3+, 0.8% by CD8+, and 0.8% by CD4+ cells).

Last, to evaluate the magnitude of the infiltration, T cell density was calculated as the number of infiltrating cells divided by the total exocrine or endocrine area (**Table 3** and **Figure 6C**). As expected, density values were higher for CD45+ and CD3+ cells in both the exocrine and endocrine compartments (214.3 and 15.5 cells/mm^2 for CD45+ cells; 116.7 and 4.1 cells/mm^2 for CD3$^+$ cells, respectively) while CD8+ (52.8 cells/mm^2 in the exocrine and 2 cells/mm^2 in the endocrine tissue) and CD4+ cell density (63.9 cells/mm^2 in the exocrine and 2 cells/mm^2 in the endocrine tissue) were lower.

Two-Dimensional Spatial Analysis of the Localization and Distance of Immune Cells to the Islets

The current definition of insulitis takes into account both peri-islet (peri-insulitis), as well as intra-islet infiltration (intra-insulitis). Therefore, the location and distance of immune cells to the islets is an interesting feature for the analysis of immune infiltration in the context of T1D. As explained above (*Immune Cell Detection and Spatial Analysis of Immune Infiltration*), heatmaps were generated for CD3+ and CD8+ cells, which were color coded based on their distance to the closest islet. The majority of T cells were located far from islets while just a few cells were located close to islets (**Figures 7A,B**). Subsequently, the total number of CD3+CD8+ and CD3+CD8− (CD4+) T cells were grouped based on their distance to the islets (**Figure 7**). Five categories were defined: 1) between 0 and 1 μm; 2) between 1 and 50 μm; 3) between 50 and 200 μm; 4) between 200 and 500 μm, and 5) higher than 500 μm to the closest islet. The majority of T cells were found at a distance of 200–500 μm (4029 CD3+, 1728 CD8+, and 2301 CD4+ T cells). The distance range 1–50 μm represented the diameter of 3–5 acinar cells and it was considered the peri-islet area. For all T cell populations, a low number of cells was found in the periphery of the islets (619 CD3+, 315 CD8+, and 304 CD4+ T cells). As observed in **Figures 7F–H**, the number was low for cells infiltrating the islet parenchyma (distance of 0–1 μm: 5 CD3+, 3 CD8+, and 2 CD4+ T cells). This analysis revealed that under physiological conditions, immune cells can be found predominantly in the exocrine tissue at distances over 50 μm from the islets, whereas a low number of cells is located within and around the islet parenchyma.

DISCUSSION

The histological analysis of tissue sections has been historically challenging for pathologists due to time requirements, inter-observer variability, and the risk of biased interpretation (Aeffner et al., 2019). In T1D research, there is still a lot of ground to cover in deciphering the immunopathogenic mechanisms of the disease. In the last decade, the nPOD repository addressed the need for high quality human pancreatic specimens. Around the globe, researchers can now perform sophisticated multiplexed immunostainings, and acquire high-resolution whole-slide digitized images. This

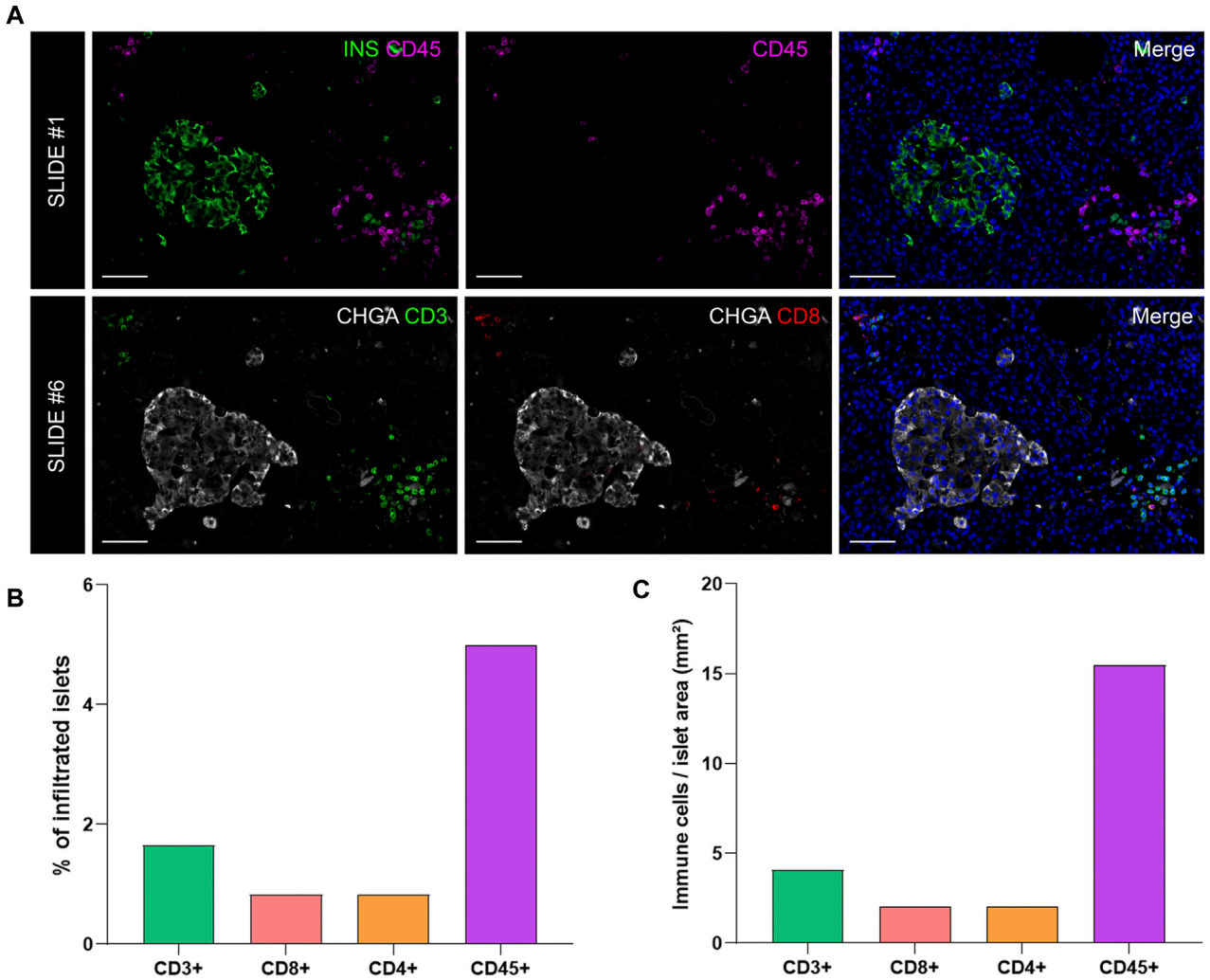

FIGURE 6 | Analysis of the proportion and density of immune infiltration in the exocrine and endocrine pancreas. **(A)** Representative images of slide #1 showing $CD45^+$ cells in the vicinity of an insulin-containing islet (upper row) and representative images of slide #6 showing CD3+ (lower row left) and CD8+ (lower row middle) cells close to a chromogranin A positive (CHGA+) islet. **(B)** Bar graphs show the proportion of infiltrated islets by CD3+, CD8+, CD4+, and CD45+ positive cells expressed as percentage of total islets. **(C)** Bar graphs show the density of CD3+, CD8+, CD4+, and CD45+ cells expressed as number of cells per islet area (mm^2). Scale bar: 50 μm.

automatically creates a need for a quick, standardized and reproducible image analysis method. QuPath is an open-source software that enables whole-slide image analysis with time-saving and variability-reducing, semi-automated workflows (Bankhead et al., 2017). Interestingly, whole-slide image analysis is widely used in pancreatic malignancies for the detection of infiltrating immune cells or for annotation of tumor areas (Carstens et al., 2021; Zacarías-Fluck et al., 2021; Bulle et al., 2020), yet in the T1D research field this is still not a common practice. To date, out of the 552 publications citing QuPath (Bankhead, 2021), 27 used it for analysis of images from the pancreas or from isolated pancreatic islets (human or rodent): 24 were found related to pancreatic cancer, 3 to diabetes (Rajendran et al., 2020; Rubey et al., 2020; Apaolaza et al., 2021) and, to our knowledge, only 2 of them describe results from whole-image analysis of donors with T1D (Rajendran et al., 2020; Apaolaza et al., 2021).

Besides QuPath, whole-slide image analysis can be achieved with other open-source software, such as ImageJ [using the SlideJ plugin (Della Mea et al., 2017)], Orbit (Stritt et al., 2020), and Icy (de Chaumont et al., 2012). However, we are not aware of any studies comparing the reproducibility of the results, the time requirements for analysis or the ease of use among the three aforementioned software. HALO image analysis platform is a proprietary software from Indica Labs that can also handle whole-slide images; recently, scientists from the nPOD network analyzed whole-slide images from pancreata of non-diabetic, autoantibody-positive and T1D donors using the HALO platform, and reported alterations in the number and density of the acinar cells in donors with T1D (Tang et al., 2020).

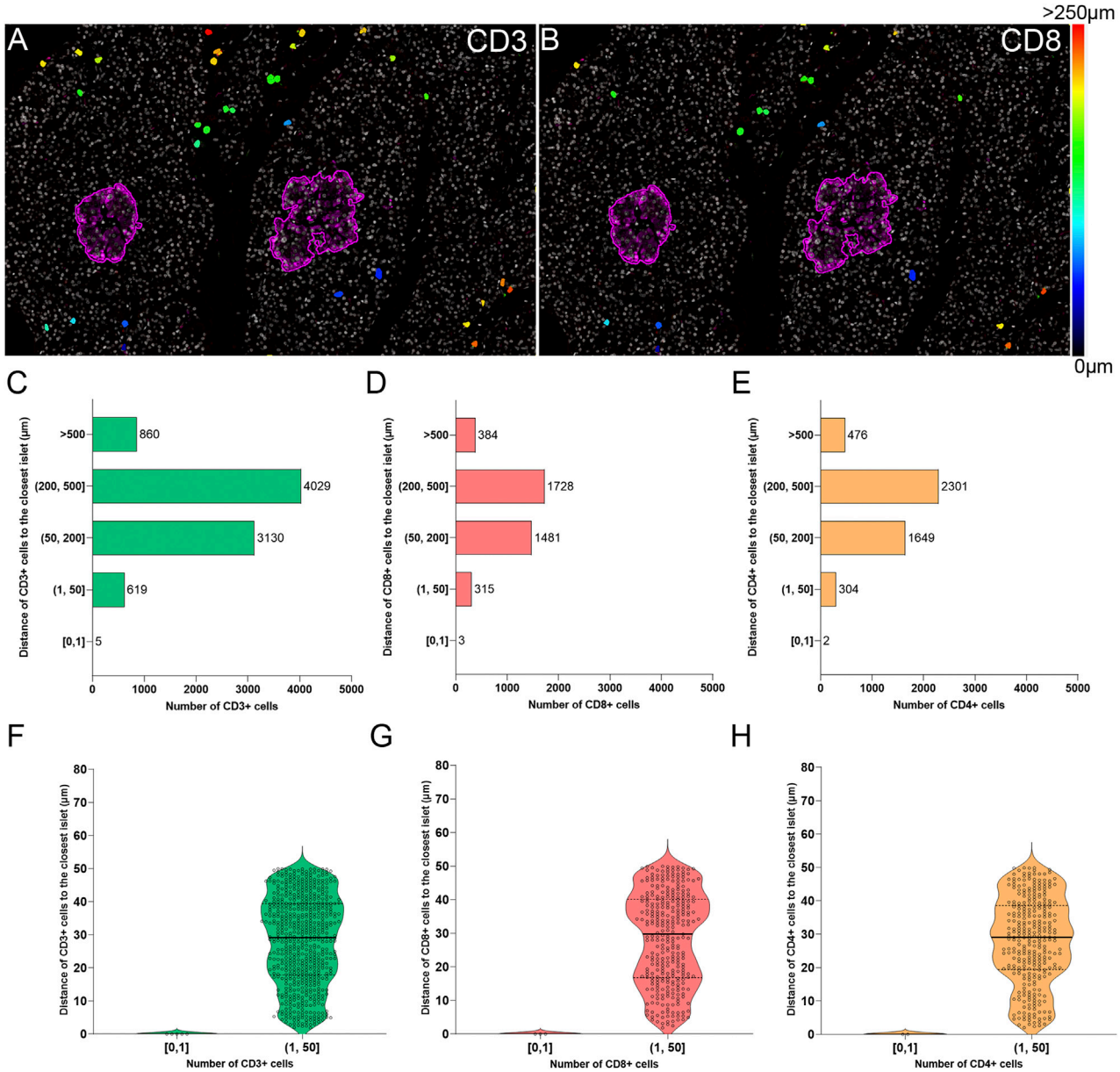

FIGURE 7 | Two-dimensional spatial analysis of the localization and distance of immune cells to the islets. Heatmaps showing the distance of **(A)** CD3+ and **(B)** CD8+ cells to the closest islet. Scale: 0 (black-blue)—>250 (red) µm. **(C)** Bar graph showing the distribution of CD3+, **(D)** CD8+, and **(E)** CD4+ cells in five different distance categories to the closest islet: [0, 1), (1, 50], (50, 200], (200, 500], and >500 µm. **(F)** Violin plots showing the number of CD3+, **(G)** CD8+, and **(H)** CD4+ cells in the intra-islet [0, 1) and peri-islet (1, 50 µm]. Each dot represents a cell.

In a recent study, the reproducibility of the Ki67 measurement and the subsequent predictability of cancer prognosis were compared among three image analysis platforms: HALO, QuantCenter (from 3D Histech), and QuPath. While Ki67 scoring can prove useful for the prediction of cancer prognosis, the variability in pre-analytical, analytical (experimental), and especially in manual scoring protocols has discouraged pathologists from implementing it in the clinical practice. Conversely, using the mentioned Image analysis platforms yielded excellent results. Ki67 scoring and prognosis predictability were "indistinguishable" among the three platforms even when different operators were employed, thus urging scientists to opt for automated analysis solutions, in order to avoid the variability of manual analysis and thus accelerate the implementation of digital Ki67 scoring in the clinic (Acs et al., 2019).

In this study, we used intensity thresholding, pixel classification and machine learning algorithms in QuPath to precisely and automatically detect different structures in the pancreas from multiplexed immunofluorescence images

regardless the staining protocols. We were able to run an accurate anatomical (tissue size, islet areas, etc.) and physiological characterization (insulin, proinsulin, and prohormone enzyme profiles) of whole pancreas sections from a non-diabetic donor, establishing an image analysis pipeline that can be applied not only to the study of T1D but also to other diseases of the pancreas. Importantly, we found similar islet numbers and densities, as well as similar distribution for alpha and beta cells between sections, demonstrating the validity of the parameters implemented in our protocols. In line with previous studies (Steiner et al., 2010; Dolenšek et al., 2015; Da Silva Xavier, 2018; Noguchi and Huising, 2019), we confirmed that insulin-producing beta cells constitute 60–70% of the islet cell population, whereas around 30–40% are alpha cells. In addition, we showed that in a non-diabetic condition the majority of the islets contain between 10 and 100 endocrine cells. This parameter is worth to be considered, as differences in the number of endocrine cells forming the islets can also indicate beta cell decay. Independently of the antibody combination used, the median values for INS+ and PI+ cells, as well as the PI/INS ratio were comparable, with few exceptions.

Furthermore, changes in the expression and distribution of the proinsulin processing enzymes can indicate failure of these specific prohormone conversion mechanisms. Differences may exist even in non-diabetic individuals, which can be extended to high intra-individual or even intra- and inter-islet heterogeneity under pathogenic conditions (Teitelman, 2019). Proteomic analysis of islets obtained by laser capture microdissection (LCM) indicated that PC1/3 and CPE are reduced in islets from donors with T1D with long disease duration (Wasserfall et al., 2017; Sims et al., 2019). Impaired proinsulin conversion accompanied by elevated proinsulin secretion is characteristic of T2D and T1D, and defects in proinsulin processing result in alteration of the PI/C-peptide and PI/INS ratios (Sims et al., 2019; Sims et al., 2019). Of note, there has been some controversy regarding the role of PC2 in proinsulin processing in humans; a recent paper, Ramzy and colleagues (Ramzy et al., 2020) provide evidence that PC2 is neither abundant nor plays a significant role in the processing of proinsulin in human beta cells, whereas other groups have reported the abundancy of PC2 in human pancreata (Scopsi et al., 1995; Teitelman, 2019). However, a limitation of these analyses is that they were not performed in whole pancreas sections, thus capturing the majority of islet types in an individual, but in isolated islets and beta cell lines. Here, we provide an analysis pipeline to estimate the proportion and density of beta and alpha cells, as well as of the processing enzymes PC1/3, PC2, and CPE in the islets or endocrine compartment, which could uncover important alterations in insulin production under inflammatory or stressful conditions and provide comprehensive evidence to fundamental mechanistic questions of proinsulin processing.

Modern lifestyle and diet have placed an enormous amount of metabolic pressure on beta cells, which are constantly hyper-functioning to produce and secrete insulin. This metabolic stress could lead to mistakes in the translational and post-translational processing of insulin and other beta cell proteins, which could in turn lead to the generation of neoantigens and to the ultimate recruitment of the immune cells to the pancreas (Rodriguez-Calvo et al., 2021). Insulitis is a hallmark of T1D; CD8+ T cells are the most abundant cell population in an insulitic lesion, followed by CD68+ macrophages, CD20+ B cells, and CD4+ T cells (Willcox et al., 2009). Even though insulitis seems to matter most because of the consequent destruction of beta cells and the loss of insulin, it has been shown that the exocrine compartment is also infiltrated by CD8+, CD4+, and CD11c+ cells (Rodriguez-Calvo et al., 2014; Campbell-Thompson et al., 2015). Despite these observations, the immunopathological course from health to disease, as well as the importance of the crosstalk between the endocrine and the exocrine tissue are still unclear. The detection of T cells around or within the islets, as well as their dynamic distribution in the endocrine and the exocrine pancreas are of great interest. Here, we described two ways of detecting immune cells using QuPath: 1) using the *single measurement classifier* based on thresholding or 2) by *machine learning*. Our results show that the machine learning option is quicker and more accurate and we recommend its use for the detection of infiltrating immune cells in the pancreas. In this study, we have evaluated their number, density and distance to the islets. Distance-wise, the majority of the T cells are found between 50 and 500 μm away from the closest islet in a non-diabetic pancreas. However, as disease progresses, a higher number of immune cells might be found closer to or inside the islets. This type of analysis can help to understand the dynamics of immune infiltration in the pancreas in individuals with prediabetes, as well as after onset of disease, and could inform clinical trials aiming to halt the autoimmune attack in T1D (Herold et al., 2019). As reported recently (Berben et al., 2020), the semi-automated methods offered by QuPath are equally reliable and considerably quicker than manual counting of immune infiltrating cells—a method that is still considered the gold standard in the clinical setting.

From a practical point of view, the working time with QuPath ranges between 1.5 and 2 h per slide, depending on computer processing power, memory and user's experience level. Most of this time is devoted to finding the correct settings in cell detection and intensity thresholds for each channel that will work for different sections. In our experience, these two parameters can strongly influence cell segmentation and subsequent positive or negative identification of cells for markers of interest. Thus, we advise researchers to test these parameters in small areas, and in different types of donor sections (control, disease, etc), in order to find which ones will work for most, if not all, types of samples. Despite slowing the process at the beginning of the analysis, the aforementioned preliminary testing will save time during the actual analysis, and prevent the occurrence of segmentation or detection issues among the different types of samples. Besides the actual working time with QuPath, the user should plan time for data-processing, grouping, and analysis, which depending on the number of desired readouts, may range from 2 to 5 h per slide. Overall, the time invested in whole-slide image analysis yields high quality data and we hope that, together with the step-wise guide provided here, it will encourage the performance of large-scale image analysis studies.

We believe that researchers should take advantage of the increasingly available digitized whole-slide pancreatic images and of the numerous open-source tools offered by QuPath. Taken together, we established several image analysis workflows that provide a basic guide to improve the characterization of the exocrine and endocrine compartments, islet cell populations, and immune infiltration. We acknowledge that other methods and analytical tools within QuPath could be used to obtain similar datasets, and that these should be customized based on quality of the sample, staining parameters and analytical goals. In addition, intra-individual variability should be assessed, as there are several factors that could contribute to it: 1) the use of different antibody combinations and/or protocols on different sections; 2) even though some sections might be consecutive, it does not necessarily mean that all the sections contain the same islets or cells; 3) stainings might not be performed on the same day, and this could add inter-staining variability. The fact that we were able to detect and quantify the extent of this variability through the use of QuPath makes us more confident that we provide an objective workflow for large-scale studies. Moreover, samples from different donor groups and disease status need to be included in the first steps of the image analysis workflow to assess inter-donor variability and to ensure that all the parameters are applicable to the different experimental conditions. Therefore, we invite other scientists to share their image analysis pipelines with the scientific community to maximize the impact of open-access tools. Here, we provide an analysis pipeline customized for the analysis of pancreas specimens with the aim of improving the accuracy, reproducibility and objectivity of image analysis while shortening the analysis time. These tools should help to gain new insights into the pathogenesis of diabetes and other pancreatic diseases, and could accelerate research on biomarker discovery and pharmacological interventions aimed at the diagnosis and cure of T1D.

DATA AVAILABILITY STATEMENT

The original contributions presented in the study are included in the article/**Supplementary Material**, further inquiries can be directed to the corresponding author.

ETHICS STATEMENT

The studies involving human pancreatic tissue samples were reviewed and approved by the ethics commitee at the Technical University of Munich (protocol #215/17 S) and the Helmholtz Center Munich, Institute for Diabetes Research.

AUTHOR CONTRIBUTIONS

PA analyzed and interpreted the data, and wrote the manuscript. P-IP performed experiments, interpreted the data, and wrote the manuscript. TR-C designed experiments, interpreted the data, and wrote the manuscript. TR-C is the guarantor of this work and, as such, had full access to all of the data in the study and takes responsibility for the integrity of the data and the accuracy of the data analysis.

FUNDING

Related research in the TR-C laboratory is supported by IMI2-JU under grant agreement No. 115797 (INNODIA) and No. 945268 (INNODIA HARVEST). This Joint Undertaking receives support from the Union's Horizon 2020 research and innovation program and "EFPIA," "JDRF" and "The Leona M. and Harry B. Helmsley Charitable Trust". TR-C is supported by JDRF (5-CDA-2020-949-A-N) and Helmholtz Zentrum Munich junior group funding. Research in the laboratory of TR-C is performed with the support of the Network for Pancreatic Organ donors with Diabetes (nPOD; RRID:SCR_014641), a collaborative T1D research project supported by JDRF (nPOD: 5-SRA-2018-557-Q-R) and The Leona M. and Harry B. Helmsley Charitable Trust (Grant#2018PG-T1D053). The content and views expressed are the responsibility of the authors and do not necessarily reflect the official view of nPOD. Organ Procurement Organizations (OPO) partnering with nPOD to provide research resources are listed at http://www.jdrfnpod.org/for-partners/npod-partners/.

ACKNOWLEDGMENTS

We thank the organ donors and their families. **Figures 1**, **2** and **Supplementary Figure S2** were created with BioRender.com.

SUPPLEMENTARY MATERIAL

The Supplementary Material for this article can be found online at: https://www.frontiersin.org/articles/10.3389/fmolb.2021.689799/full#supplementary-material

REFERENCES

Acs, B., Pelekanou, V., Bai, Y., Martinez-Morilla, S., Toki, M., Leung, S. C. Y., et al. (2019). Ki67 Reproducibility Using Digital Image Analysis: an Inter-platform and Inter-operator Study. *Lab. Invest.* 99 (1), 107–117. doi:10.1038/s41374-018-0123-7

Aeffner, F., Zarella, M., Buchbinder, N., Bui, M., Goodman, M., Hartman, D., et al. (2019). Introduction to Digital Image Analysis in Whole-Slide Imaging: A white Paper from the Digital Pathology Association. *J. Pathol. Inform.* 10 (1), 9. doi:10.4103/jpi.jpi_82_18

Alexandre-Heymann, L., Mallone, R., Boitard, C., Scharfmann, R., and Larger, E. (2019). Structure and Function of the Exocrine Pancreas in Patients with Type 1 Diabetes. *Rev. Endocr. Metab. Disord.* 20 (2), 129–149. doi:10.1007/s11154-019-09501-3

Anderson, M. S., and Bluestone, J. A. (2005). THE NOD MOUSE: A Model of Immune Dysregulation. *Annu. Rev. Immunol.* 23 (1), 447–485. doi:10.1146/annurev.immunol.23.021704.115643

Apaolaza, P. S., Balcacean, D., Zapardiel-Gonzalo, J., Nelson, G., Lenchik, N., Akhbari, P., et al. (2021). Islet Expression of Type I Interferon Response Sensors Is Associated with Immune Infiltration and Viral Infection in Type 1 Diabetes. *Sci. Adv.* 7 (9), eabd6527. doi:10.1126/sciadv.abd6527

Bankhead, P. (2021). How to Cite Qupath [Internet]. Available at: https://qupath.readthedocs.io/en/latest/docs/intro/citing.html#publications-using-qupath (Accessed March 29).

Bankhead, P., Loughrey, M. B., Fernández, J. A., Dombrowski, Y., McArt, D. G., Dunne, P. D., et al. (2017). QuPath: Open Source Software for Digital Pathology Image Analysis. *Sci. Rep.* 7 (1), 16878. doi:10.1038/s41598-017-17204-5

Bender, C., Rodriguez-Calvo, T., Amirian, N., Coppieters, K. T., and von Herrath, M. G. (2020). The Healthy Exocrine Pancreas Contains Preproinsulin-specific CD8 T Cells that Attack Islets in Type 1 Diabetes. *Sci. Adv.* 6 (42), eabc5586. doi:10.1126/sciadv.abc5586

Berben, L., Wildiers, H., Marcelis, L., Antoranz, A., Bosisio, F., Hatse, S., et al. (2020). Computerised Scoring Protocol for Identification and Quantification of Different Immune Cell Populations in Breast Tumour Regions by the Use of QuPath Software. *Histopathology* 77 (1), 79–91. doi:10.1111/his.14108

Bulle, A., Dekervel, J., Deschuttere, L., Nittner, D., Libbrecht, L., Janky, R., et al. (2020). Gemcitabine Recruits M2-Type Tumor-Associated Macrophages into the Stroma of Pancreatic Cancer. *Transl. Oncolo.* 13, 100743. doi:10.26508/lsa.201900490

Campbell-Thompson, M., Rodriguez-Calvo, T., and Battaglia, M. (2015). Abnormalities of the Exocrine Pancreas in Type 1 Diabetes. *Curr. Diab Rep.* 15 (10), 79. doi:10.1007/s11892-015-0653-y

Campbell-Thompson, M., Fu, A., Kaddis, J. S., Wasserfall, C., Schatz, D. A., Pugliese, A., et al. (2016). Insulitis and β-Cell Mass in the Natural History of Type 1 Diabetes. *Diabetes* 65 (3), 719–731. doi:10.2337/db15-0779

Campbell-Thompson, M. L., Atkinson, M. A., Butler, A. E., Chapman, N. M., Frisk, G., Gianani, R., et al. (2013). The Diagnosis of Insulitis in Human Type 1 Diabetes. *Diabetologia* 56 (11), 2541–2543. doi:10.1007/s00125-013-3043-5

Campbell-Thompson, M., Wasserfall, C., Kaddis, J., Albanese-O'Neill, A., Staeva, T., Nierras, C., et al. (2012). Network for Pancreatic Organ Donors with Diabetes (nPOD): Developing a Tissue Biobank for Type 1 Diabetes. *Diabetes Metab. Res. Rev.* 28 (7), 608–617. doi:10.1002/dmrr.2316

Carstens, J. L., Yang, S., Correa de Sampaio, P., Zheng, X., Barua, S., McAndrews, K., et al. (2021). Stabilized Epithelial Phenotype of Cancer Cells in Primary Tumors Leads to Increased Colonization of Liver Metastasis in Pancreatic cancer. *Cell Rep.* 35, 108990. doi:10.1016/j.celrep.2021.108990

Da Silva Xavier, G. (2018). The Cells of the Islets of Langerhans. *J. Clin. Med.* 7 (3), 54. doi:10.3390/jcm7030054

de Chaumont, F., Dallongeville, S., Chenouard, N., Hervé, N., Pop, S., Provoost, T., et al. (2012). Icy: an Open Bioimage Informatics Platform for Extended Reproducible Research. *Nat. Methods* 9 (7), 690–696. doi:10.1038/nmeth.2075

Della Mea, V., Baroni, G. L., Pilutti, D., and Di Loreto, C. (2017). SlideJ: An ImageJ Plugin for Automated Processing of Whole Slide Images. *PLOS ONE* 12 (7), e0180540. doi:10.1371/journal.pone.0180540

Dolenšek, J., Rupnik, M. S., and Stožer, A. (2015). Structural Similarities and Differences between the Human and the Mouse Pancreas. *Islets* 7 (1), e1024405. doi:10.1080/19382014.2015.1024405

Dybala, M. P., and Hara, M. (2019). Heterogeneity of the Human Pancreatic Islet. *Diabetes* 68 (6), 1230–1239. doi:10.2337/db19-0072

Foulis, A. K., and Stewart, J. A. (1984). The Pancreas in Recent-Onset Type 1 (Insulin-dependent) Diabetes Mellitus: Insulin Content of Islets, Insulitis and Associated Changes in the Exocrine Acinar Tissue. *Diabetologia* 26 (6), 456. doi:10.1007/BF00262221

Foulis, A. K., Liddle, C. N., Farquharson, M. A., Richmond, J. A., and Weir, R. S. (1986). The Histopathology of the Pancreas in Type I (Insulin-dependent) Diabetes Mellitus: a 25-year Review of Deaths in Patients under 20 Years of Age in the United Kingdom. *Diabetologia* 29 (5), 267–274. doi:10.1007/bf00452061

Fowler, J. L., Lee, S. S.-Y., Wesner, Z. C., Olehnik, S. K., Kron, S. J., and Hara, M. (2018). Three-Dimensional Analysis of the Human Pancreas. *Endocrinology* 159 (3), 1393–1400. doi:10.1210/en.2017-03076

Herold, K. C., Bundy, B. N., Long, S. A., Bluestone, J. A., DiMeglio, L. A., Dufort, M. J., et al. (2019). An Anti-CD3 Antibody, Teplizumab, in Relatives at Risk for Type 1 Diabetes. *N. Engl. J. Med.* 381 (7), 603–613. doi:10.1056/nejmoa1902226

Kaestner, K. H., Powers, A. C., Naji, A., Atkinson, M. A., and Atkinson, M. A. (2019). NIH Initiative to Improve Understanding of the Pancreas, Islet, and Autoimmunity in Type 1 Diabetes: The Human Pancreas Analysis Program (HPAP). *Diabetes* 68 (7), 1394–1402. doi:10.2337/db19-0058

Kilimnik, G., Jo, J., Periwal, V., Zielinski, M. C., and Hara, M. (2012). Quantification of Islet Size and Architecture. *Islets* 4 (2), 167–172. doi:10.4161/isl.19256

Mallone, R., and Eizirik, D. L. (2020). Presumption of Innocence for Beta Cells: Why Are They Vulnerable Autoimmune Targets in Type 1 Diabetes? *Diabetologia* 63 (10), 1999–2006. doi:10.1007/s00125-020-05176-7

Noguchi, G. M., and Huising, M. O. (2019). Integrating the Inputs that Shape Pancreatic Islet Hormone Release. *Nat. Metab.* 1 (12), 1189–1201. doi:10.1038/s42255-019-0148-2

Poudel, A., Fowler, J. L., Zielinski, M. C., Kilimnik, G., and Hara, M. (2016). Stereological Analyses of the Whole Human Pancreas. *Sci. Rep.* 6 (1), 34049. doi:10.1038/srep34049

Pugliese, A., Yang, M., Kusmarteva, I., Heiple, T., Vendrame, F., Wasserfall, C., et al. (2014). The Juvenile Diabetes Research Foundation Network for Pancreatic Organ Donors with Diabetes (nPOD) Program: Goals, Operational Model and Emerging Findings. *Pediatr. Diabetes* 15 (1), 1–9. doi:10.1111/pedi.12097

Rahier, J., Goebbels, R. M., and Henquin, J. C. (1983). Cellular Composition of the Human Diabetic Pancreas. *Diabetologia* 24 (5), 366. doi:10.1007/BF00251826

Rajendran, S., Anquetil, F., Quesada-Masachs, E., Graef, M., Gonzalez, N., McArdle, S., et al. (2020). IL-6 Is Present in Beta and Alpha Cells in Human Pancreatic Islets: Expression Is Reduced in Subjects with Type 1 Diabetes. *Clin. Immunol.* 211, 108320. doi:10.1016/j.clim.2019.108320

Ramzy, A., Asadi, A., and Kieffer, T. J. (2020). Revisiting Proinsulin Processing: Evidence that Human β-Cells Process Proinsulin with Prohormone Convertase (PC) 1/3 but Not PC2. *Diabetes* 69 (7), 1451–1462. doi:10.2337/db19-0276

Rodriguez-Calvo, T., Johnson, J. D., Overbergh, L., and Dunne, J. M. (2021). Neoepitopes in Type 1 Diabetes: Etiological Insights, Biomarkers and Therapeutic Targets. *Front. Immunol.* 12, 667989. doi:10.3389/fimmu.2021.667989

Rodriguez-Calvo, T., Ekwall, O., Amirian, N., Zapardiel-Gonzalo, J., and von Herrath, M. G. (2014). Increased Immune Cell Infiltration of the Exocrine Pancreas: A Possible Contribution to the Pathogenesis of Type 1 Diabetes. *Diabetes* 63 (11), 3880–3890. doi:10.2337/db14-0549

Roep, B. O., Thomaidou, S., van Tienhoven, R., and Zaldumbide, A. (2020). Type 1 Diabetes Mellitus as a Disease of the β-cell (Do Not Blame the Immune System?). *Nat. Rev. Endocrinol.* 17, 150. doi:10.1038/s41574-020-00443-4

Rowe, P. A., Campbell-Thompson, M. L., Schatz, D. A., and Atkinson, M. A. (2011). The Pancreas in Human Type 1 Diabetes. *Semin. Immunopathol* 33 (1), 29–43. doi:10.1007/s00281-010-0208-x

Rubey, M., Chhabra, N. F., Gradinger, D., Sanz-Moreno, A., Lickert, H., Przemeck, G. K. H., et al. (2020). DLL1- and DLL4-Mediated Notch Signaling Is Essential for Adult Pancreatic Islet Homeostasis. *Diabetes* 69 (5), 915–926. doi:10.2337/db19-0795

Scharfmann, R., Staels, W., and Albagli, O. (2019). The Supply Chain of Human Pancreatic β Cell Lines. *J. Clin. Invest.* 129 (9), 3511–3520. doi:10.1172/jci129484

Scopsi, L., Gullo, M., Rilke, F., Martin, S., and Steiner, D. F. (1995). Proprotein Convertases (PC1/PC3 and PC2) in normal and Neoplastic Human Tissues: Their Use as Markers of Neuroendocrine Differentiation. *J. Clin. Endocrinol. Metab.* 80 (1), 294–301. doi:10.1210/jc.80.1.294

Sims, E. K., Bahnson, H. T., Nyalwidhe, J., Haataja, L., Davis, A. K., Speake, C., et al. (2019). Proinsulin Secretion Is a Persistent Feature of Type 1 Diabetes. *Dia Care* 42 (2), 258–264. doi:10.2337/dc17-2625

Sims, E. K., Syed, F., Nyalwidhe, J., Bahnson, H. T., Haataja, L., Speake, C., et al. (2019). Abnormalities in Proinsulin Processing in Islets from Individuals with Longstanding T1D. *Translational Res.* 213, 90–99. doi:10.1016/j.trsl.2019.08.001

Solimena, M., Schulte, A. M., Marselli, L., Ehehalt, F., Richter, D., Kleeberg, M., et al. (2018). Systems Biology of the IMIDIA Biobank from Organ Donors and Pancreatectomised Patients Defines a Novel Transcriptomic Signature of Islets from Individuals with Type 2 Diabetes. *Diabetologia* 61 (3), 641–657. doi:10.1007/s00125-017-4500-3

Steiner, D. F., Park, S.-Y., Støy, J., Philipson, L. H., and Bell, G. I. (2009). A Brief Perspective on Insulin Production. *Diabetes Obes. Metab.* 11, 189–196. doi:10.1111/j.1463-1326.2009.01106.x

Steiner, D. J., Kim, A., Miller, K., and Hara, M. (2010). Pancreatic Islet Plasticity: Interspecies Comparison of Islet Architecture and Composition. *Islets* 2 (3), 135–145. doi:10.4161/isl.2.3.11815

Strijker, M., Gerritsen, A., van Hilst, J., Bijlsma, M. F., Bonsing, B. A., Brosens, L. A., et al. (2018). The Dutch Pancreas Biobank within the Parelsnoer Institute. *Pancreas* 47 (4), 495–501. doi:10.1097/mpa.0000000000001018

Stritt, M., Stalder, A. K., and Vezzali, E. (2020). Orbit Image Analysis: An Open-Source Whole Slide Image Analysis Tool. Carpenter AE. *PLOS Comput. Biol.* 16 (2), e1007313. doi:10.1371/journal.pcbi.1007313

Tang, X., Kusmartseva, I., Kulkarni, S., Posgai, A., Speier, S., Schatz, D. A., et al. (2020). Image-Based Machine Learning Algorithms for Disease Characterization in the Human Type 1 Diabetes Pancreas. *Am. J. Pathol.* 191, 454. doi:10.1016/j.ajpath.2020.11.010

Teitelman, G. (2019). Heterogeneous Expression of Proinsulin Processing Enzymes in Beta Cells of Non-diabetic and Type 2 Diabetic Humans. *J. Histochem. Cytochem.* 67 (6), 385–400. doi:10.1369/0022155419831641

Vasiljević, J., Torkko, J. M., Knoch, K. P., and Solimena, M. (2020). The Making of Insulin in Health and Disease. *Diabetologia* 63 (10), 1981–1989. doi:10.1007/s00125-020-05192-7

Wang, X., Zielinski, M. C., Misawa, R., Wen, P., Wang, T-Y., Wang, C-Z., et al. (2013). Quantitative Analysis of Pancreatic Polypeptide Cell Distribution in the Human Pancreas. *PLoS ONE* 8 (1), e55501. doi:10.1371/journal.pone.0055501

Willcox, A., Richardson, S. J., Bone, A. J., Foulis, A. K., and Morgan, N. G. (2009). Analysis of Islet Inflammation in Human Type 1 Diabetes. *Clin. Exp. Immunol.* 155 (2), 173–181. doi:10.1111/j.1365-2249.2008.03860.x

Williams, A. J. K., Thrower, S. L., Sequeiros, I. M., Ward, A., Bickerton, A. S., Triay, J. M., et al. (2012). Pancreatic Volume Is Reduced in Adult Patients with Recently Diagnosed Type 1 Diabetes. *J. Clin. Endocrinol. Metab.* 97 (11), E2109–E2113. doi:10.1210/jc.2012-1815

Wasserfall, C., Nick, H. S., Campbell-Thompson, M., Beachy, D., Haataja, L., Kusmartseva , I., et al. (2017). Persistence of Pancreatic Insulin mRNA Expression and Proinsulin Protein in Type 1 Diabetes Pancreata. *Cell Metab.* 26, 568–575.e3. doi:10.1016/j.cmet.2017.08.013

Zacarías-Fluck, M. F., Jauset, T., Martínez-Martín, S., Kaur, J., Casacuberta-Serra, S., Massó-Vallés, D., et al. (2021). The Wnt Signaling Receptor Fzd9 is Essential for Myc-Driven Tumorigenesis in Pancreatic Islets. *Life Sci, Alliance* 4, e201900490. doi:10.26508/lsa.201900490

Conflict of Interest: The authors declare that the research was conducted in the absence of any commercial or financial relationships that could be construed as a potential conflict of interest.

frontiers in Molecular Biosciences

REVIEW
published: 14 June 2021
doi: 10.3389/fmolb.2021.668340

Methods to Determine and Analyze the Cellular Spatial Distribution Extracted From Multiplex Immunofluorescence Data to Understand the Tumor Microenvironment

Edwin Roger Parra *

Department of Translational Molecular Pathology, The University of Texas MD Anderson Cancer Center, Houston, TX, United States

Image analysis using multiplex immunofluorescence (mIF) to detect different proteins in a single tissue section has revolutionized immunohistochemical methods in recent years. With mIF, individual cell phenotypes, as well as different cell subpopulations and even rare cell populations, can be identified with extraordinary fidelity according to the expression of antibodies in an mIF panel. This technology therefore has an important role in translational oncology studies and probably will be incorporated in the clinic. The expression of different biomarkers of interest can be examined at the tissue or individual cell level using mIF, providing information about cell phenotypes, distribution of cells, and cell biological processes in tumor samples. At present, the main challenge in spatial analysis is choosing the most appropriate method for extracting meaningful information about cell distribution from mIF images for analysis. Thus, knowing how the spatial interaction between cells in the tumor encodes clinical information is important. Exploratory analysis of the location of the cell phenotypes using point patterns of distribution is used to calculate metrics summarizing the distances at which cells are processed and the interpretation of those distances. Various methods can be used to analyze cellular distribution in an mIF image, and several mathematical functions can be applied to identify the most elemental relationships between the spatial analysis of cells in the image and established patterns of cellular distribution in tumor samples. The aim of this review is to describe the characteristics of mIF image analysis at different levels, including spatial distribution of cell populations and cellular distribution patterns, that can increase understanding of the tumor microenvironment.

Keywords: multiplex immunofluorescence, matrix construction, cellular spatial distribution, nearest neighbor, correlation functions

OPEN ACCESS

Edited by:
Joe Yeong,
*Institute of Molecular and Cell Biology (A*STAR), Singapore*

Reviewed by:
WP Ng,
National Cancer Centre Singapore, Singapore
Lit-Hsin Loo,
*Bioinformatics Institute (A*STAR), Singapore*

***Correspondence:**
Edwin Roger Parra
erparra@mdanderson.org

Specialty section:
This article was submitted to Molecular Diagnostics and Therapeutics, a section of the journal Frontiers in Molecular Biosciences

Received: *16 February 2021*
Accepted: *02 June 2021*
Published: *14 June 2021*

Citation:
Parra ER (2021) Methods to Determine and Analyze the Cellular Spatial Distribution Extracted From Multiplex Immunofluorescence Data to Understand the Tumor Microenvironment. Front. Mol. Biosci. 8:668340. doi: 10.3389/fmolb.2021.668340

INTRODUCTION

Multiplex immunofluorescence (mIF) facilitates detection of cell phenotypes (Parra et al., 2020) and quantification of spatial relationships among cells within the tumor microenvironment (Barua et al., 2018). Studying the spatial distribution of tumor cells and infiltrating immune cells in tumor samples using data obtained via mIF-based digital image analysis allows for detailed characterization of cell-

cell associations and the geographic distribution of cell phenotypes, which may help in predicting clinical responses and mechanisms of resistance of cancer to immunotherapies (Yu et al., 2020). With increases in the volume and complexity of this type of data, integration of computational analysis with image analysis has become more important and relevant to better understanding the tumor microenvironment. Analysis of spatial data requires specific tools and techniques to look at these data from different angles. Over the past few years, my group has applied computational analysis tools in an exploratory way to measure the intensity of expression of cell phenotypes in cancer and the spatial distribution of cells in images obtained using mIF (Barua et al., 2018). We have also applied careful inferential methods to validate the results of cell distance analysis. In essence, we attempted to extract features from many mIF images and captured the most relevant features that can answer our questions. Once these features are extracted and checked for anomalies, hypothesis tests and mathematical models can be designed to assess the effect of certain features or patterns of cell distribution on cancer (Robinson et al., 2020). This analysis of spatial cell distribution can be used to determine whether a strong association exists between cell distribution patterns and clinicopathologic information or outcome.

Feature extraction from mIF digital image analysis begins with computing maps for individual markers using the center of the cells, which then creates a point process object. A point process from the image analysis is a collection of points that can be structured using two-dimensional coordinates in the *x*- and *y*-planes using identified cell markers (Parra et al., 2020). Creating this point process object allows us to superimpose point patterns of different markers for combined co-localization analysis, which identifies specific cell phenotypes that correspond to a unique image identifier, and each image has a corresponding case. Lastly, each cell has a binary entry for each marker that the cell expresses. This enables efficient assignment of a phenotype to each cell.

When we explore image analysis data, the cell phenotype frequencies on each mIF digital image must be counted to determine the number of pairwise phenotype incidences. We count the interaction of protein markers in every cell in the data and organize by image and case. For each cell phenotype, we estimate the intensity of another phenotype by counting the cells in a neighborhood and also increasing the radius (Illian et al., 2008). This measure of intensity is very important when adjusting for the effect of other features and computing the space between cells. Using the coordinates that the images provide after image analysis, for any image and cell phenotype, we can calculate the distance to every other cell in the image. Thus, we can construct a distance matrix that encodes the distances for all pairs of cells, giving us the opportunity to map cell pathways in every image (Illian et al., 2008). The spatial distribution of the cell phenotypes can be used to calculate several characteristics of the cells using a mathematical function that is most appropriate for the research question. Using the data provided by this method, we can model features of cellular spatial distribution to determine whether certain phenotypes differ in their patterns of distribution. For instance, we can study patterns of distribution of and distances between cells across images and cases and correlate this information with clinical data to see if the spatial distribution of these cells plays an important role in driving different responses to treatments and outcomes in the tumor microenvironment.

Herein, I describe strategies and mathematical models and functions used to study the spatial distribution of cell phenotypes in tumor tissues, demonstrating a practical approach to study the tumor microenvironment. I also discuss the integration of these analyses with their biological interpretation to answer research questions.

SPATIAL CELLULAR DISTRIBUTION

The tumor microenvironment is a complicated machinery that includes several groups of cells, such as epithelial and endothelial cells and a large variety of infiltrating immune cells, including cells involved in both the innate and adaptive immune responses to the tumor. The location and organization of these different immune cell phenotypes have emerged as important pieces of information for determining the function of these cells across tumor compartments and recognizing the possible impact of the cells on clinical outcomes in cancer patients (Masugi et al., 2019). Knowing the location of different cell populations in a tumor and the spatial distribution of the cells with other cell groups allows us to characterize a tumor to predict its response to treatment and the potential for progression and relapse. The spatial distribution of different cell phenotypes is known to be important in characterizing the tumor microenvironment, which influences recruitment of immune cells, and the microenvironment can be characterized in different regions within a tumor or studied to determine whether specific cell phenotypes are present (Tsujikawa et al., 2020). Therefore, data obtained from mIF-based digital image analysis are particularly useful for calculating functional spatial distribution metrics.

Geographic Cell Distribution in Tumors

As shown in **Figure 1**, studying different cell phenotypes according to their distribution in tumors, such as in the tumor and stromal compartments, normal tissue and tertiary lymphoid structures, vessels, or tumor periphery, can provide important information about the specific role of that cell phenotype (Bremnes et al., 2011; Dieu-Nosjean et al., 2014), and cellular distribution can be associated with outcomes in various tumor types. For example, T-cell populations in the tumor compartment, but not in the stromal compartment, are associated with favorable prognoses in colorectal cancer (Galon et al., 2006; Nazemalhosseini-Mojarad et al., 2019), ovarian cancer (Zhang et al., 2003), urothelial carcinoma (Wang et al., 2015), head and neck squamous cell carcinoma (Zhou et al., 2019), esophageal adenocarcinomas (Stein et al., 2017), triple-negative breast cancer (Sugie et al., 2020), pancreatic ductal adenocarcinoma (Masugi et al., 2019), and non-small cell lung carcinoma (Parra et al., 2016; Tuminello et al., 2019). Research has also shown that cytotoxic T-cells in the tumoral compartment are potential negative prognostic factors in invasive breast cancer (Catacchio et al., 2019). Furthermore, larger

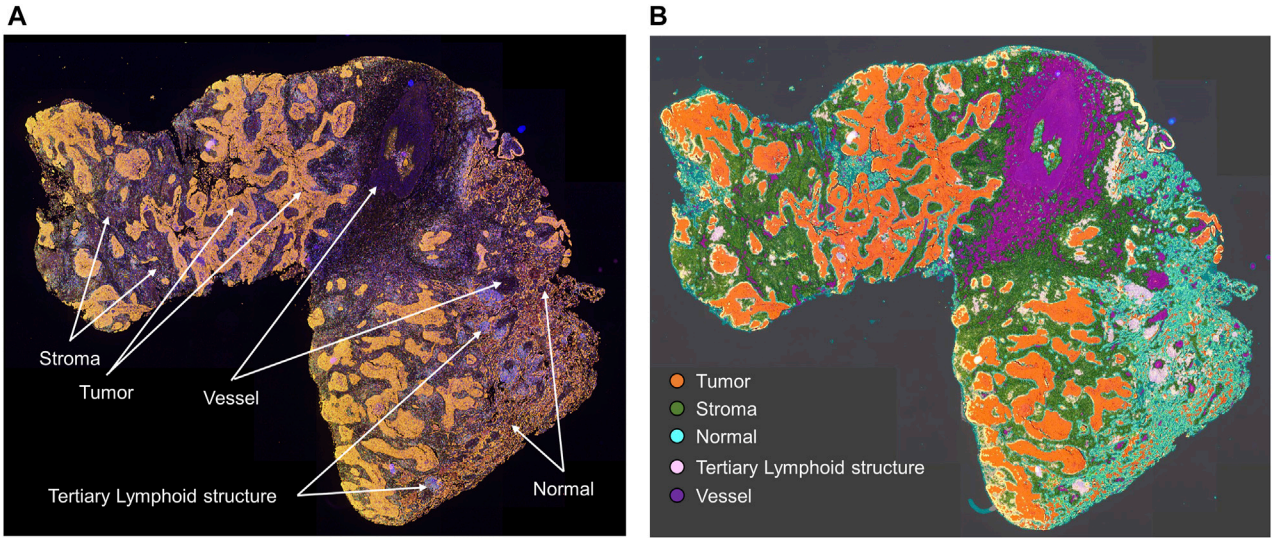

FIGURE 1 | Microphotographs of a representative whole tumor section of lung squamous cell carcinoma obtained using multiplex immunofluorescence staining. **(A)** Geographic distribution of cells in different tissue compartments. **(B)** The geographic compartments were delineated using HALO image analysis software (Indica Labs, Albuquerque, NM) to analyze cells in different compartments. Original magnification, ×4.

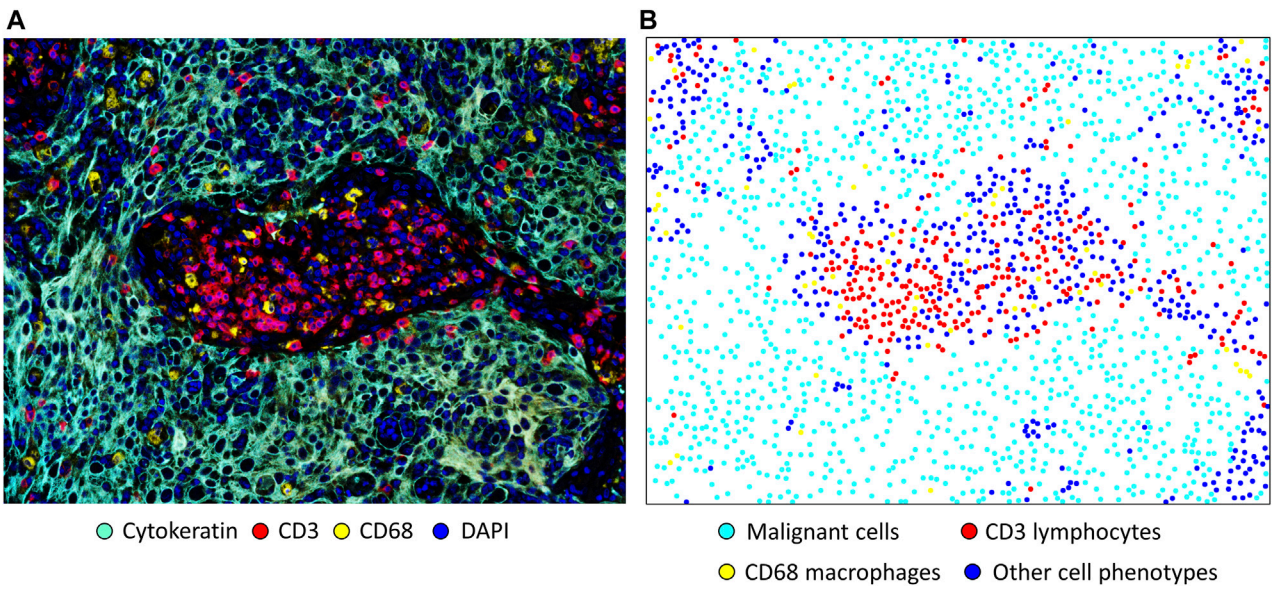

FIGURE 2 | Microphotographs of a representative section of lung squamous cell carcinoma obtained using multiplex immunofluorescence staining with a panel containing cytokeratin, $CD3^+$ T-cells, $CD68^+$ macrophages, and DAPI. **(A)** A region of interest with basic marker staining. **(B)** Colored dots representing the individual cells shown in A, showing the location of each cell in the image. Original magnification, ×20, from VectraPolaris scanner and processed by Inform software (Akoya Biosciences).

populations of specific cell phenotypes, such as FOXP3+ T-regulatory cells, in the tumoral compartment than in the peripheral compartment can correlate with aggressive tumor behavior, as observed with some papillary thyroid cancers (French et al., 2010). The distribution of T-cell phenotype populations across different geographic compartments can have therapeutic implications (Cooper et al., 2016; Feldmeyer et al., 2016; Parra et al., 2018) and drive the improvement and discovery of new treatments based on T-cell tumor tissue distribution.

Spatial Distribution at the Single-Cell Level

In spatial cellular image analysis, images show a collection of various cell phenotypes that are identified by staining for a

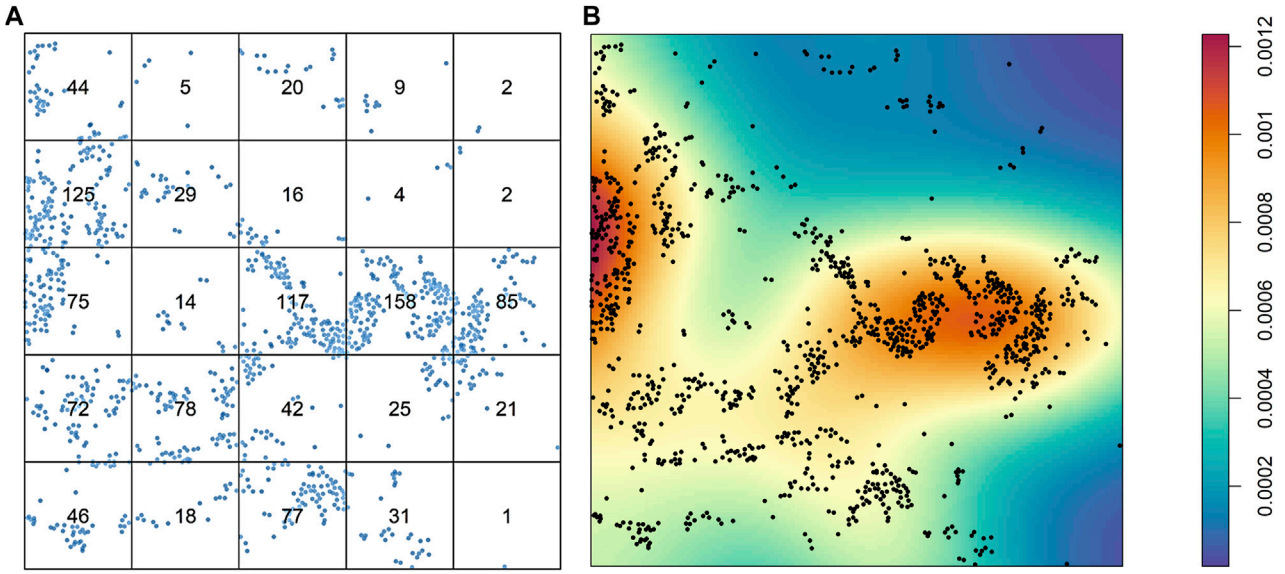

FIGURE 3 | Characterization of the distribution of cells from a sample of lung adenocarcinoma in a multiplex immunofluorescence image. **(A)** Results of quadrant analysis, with each quadrant containing the exact number of cells in a square, represented by dots. **(B)** Heat map of Kernel smoothing from the same area of the image, showing areas of high and low proliferation of cells, identified by colored regions (see color scale at right). The images were generated using R studio software version 3.6.0.

combination of markers in an mIF panel (**Figure 2A**), and these markers are translated as colored dots with x and y coordinates (**Figure 2B**). This analysis is not limited to single images but rather uses groups of images that are related to several tumor samples in a study. In our analysis, we consider the point pattern from our mIF image a non-parametric process, which assumes a stationary or homogeneous point pattern configuration independent of a specific location. Although only small or a few areas of observation can be considered non-stationary processes showing only a few groups of phenotypes, these areas, given the heterogenicity of the sample across images, ultimately generate dynamic ecologic patterns that may influence tumor progression and response to treatment (Gentles et al., 2015). Furthermore, study of spatial cell distribution has demonstrated its relationship with outcomes in cancer patients. For example, in non-small lung cancer, the proximity of macrophages to malignant cells was inversely correlated with prognosis; those with tumors in which macrophages were close to malignant cells had worse outcomes than those with tumors in which macrophages were far from the malignant cells (Zheng et al., 2020). Similarly, in a gastric cancer study, the proximity of FOXP3+ T-regulatory cells to $CD8^+$ cytotoxic T-cells was inversely correlated with prognosis (Wang et al., 2020).

FUNCTIONAL SPATIAL DISTRIBUTION METRICS

The existing methods used in spatial analysis are many and varied. Researchers have ample opportunity to explore different techniques of cellular spatial analysis for tumor tissues and implement them using mathematical models to extract mIF image data.

In spatial image analysis, consideration of intensity and density is needed. Intensity is the absolute number of cells or their abundance in an image when looking directly into it, and density is the number of cells per unit area (cells/mm^2).

After intensity and density are defined, the distribution of the cells overall is the first aspect in an image that can be studied. The cells can be distributed homogeneously or not, and a simple way to consider this variable is to divide the images into quadrants of equal size and count the cells in each quadrant. Naturally, if the number of cells varies greatly among the quadrants, the distribution of the cells is not homogeneous (**Figure 3A**). The distribution of cells in an image is very unlikely to be homogeneous, and overall, a good assumption is that patterns of cells will never be homogeneous. One obvious drawback to this approach to analyzing the distribution of cells across an image is the dependence on quadrant size or application of other geometric shapes of the partitions. If the quantification or application of the quadrants is not done carefully, no useful information will be drawn. Nonparametric approaches, such as kernel smoothing (Baddeley et al., 2015), are other popular methods of graphically determining whether cellular distribution is homogeneous, and these methods are useful for observing cell proliferation patterns or hot spots in an image (**Figure 3B**).

SPATIAL DESCRIPTIVE FUNCTIONS

In studying the spatial relationships among different cells and their patterns of distribution in an image, several spatial

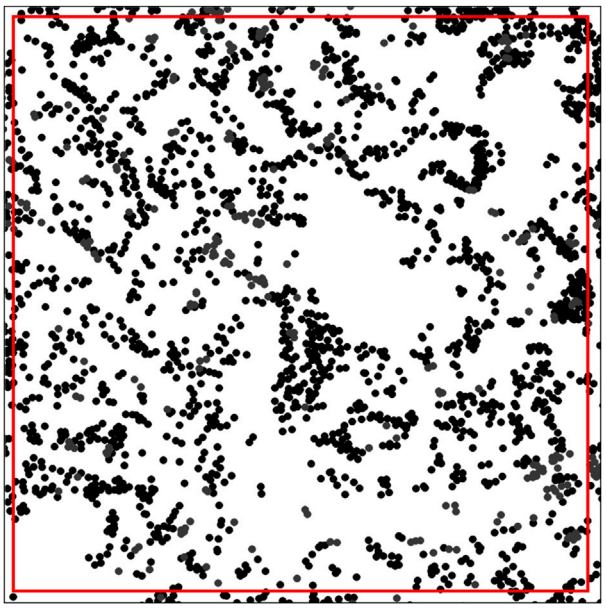

FIGURE 4 | Distribution of dots representing the cell distribution patterns in an image with edge correction, showing a square marked by a red line constructed using spatstats software in the R computing language. Only the dots inside the red line were considered in the analysis of the spatial distribution pattern. The image was generated using R studio software version 3.6.0.

descriptive functions can be applied. Basically, two groups of mathematical or computational functions can be used to analyze the data obtained in digital image analysis. One group is used to describe the measured distances between cell populations; this group includes the G-function, F-function, and J-function. The other group is used to describe the relative intensity of the cells in terms of distance measured, and this group includes the K-function, L-function, and pair correlation function. Similar principles are used to construct both function groups (Baddeley et al., 2015; Illian et al., 2008), and because these functions examine the relationship between two cell populations (*i*-to-*j*), all functions are cross-functional or mark-independent.

To apply these functions to spatial image analysis data from mIF images, users are encouraged to employ the well-known spatstats package in the R computing language (Baddeley and Turner, 2005) because it has correction tools such as edge correction, which are important for any spatial image analysis (**Figure 4**).

DISTANCE MATRIX

Construction of a distance matrix is the first step in developing any tool to reveal spatial properties of cells in an image. To maintain the simplicity of the analysis, we can assume that distances between cells are always measured in a two-dimensional Euclidean space on images that are flat. Only the cell coordinates are needed to build a distance matrix; this allows extraction of spatial information regarding the interaction between two distinct types of cells by applying various mathematical formulas on the matrix itself (**Figure 5A**).

Depending on the specific formula applied, various features of the spatial interaction between cells can be studied. In constructing a distance matrix, the coordinates of the cell phenotypes are first ordered in rows and columns, where the rows in the matrix correspond to the number of cells from one specified cell phenotype and the columns correspond to the number of cells from another specified cell phenotype. A good visual representation of the connection between cell markers in the matrix can be obtained using a chord diagram (**Figure 6**).

Each matrix entry is the distance between one cell phenotype and another cell phenotype; in this way, all entries between two groups of cell phenotypes are displayed in the distance matrix. As mentioned above, the distance is measured for every pair of cells, i.e., from one cell phenotype of interest to another cell phenotype of interest, or, in a more simplistic way, from point A (*i*) to point B (*j*) in a given radius (*r*; **Figure 5B**). The maximum distance between two cells is the farthest distance between A and B in the image; this distance is limited by the region of interest analyzed. A meaningful measure must be constructed by determining the distance between each entry in column (*i*) from one cell phenotype and each entry in row (*j*) from the other cell phenotype, for example malignant cells and $CD3^+$ T-cells (**Figure 7**). This is important when constructing other metrics for other cell phenotypes to observe the distribution of cells and to obtain a vector of distances from each cell phenotype to its nearest neighbor of another cell phenotype.

NEAREST NEIGHBOR

The nearest neighbor distance is used to determine the probability (*P*) of encountering a cell (point, *X*) of a specific phenotype (*j*; e.g., cell phenotype B, $CD3^+$) within a certain radius (*r*) centered on another cell phenotype (*i*; e.g., cell phenotype A, malignant cells; **Figure 8A**) (Barua et al., 2018). This approach allows you to determine the minimum distance between each cell of phenotype A and the nearest neighbor cell of phenotype B. Of note, this distance will be completely different if measured in the opposite direction (from cell phenotype B to cell phenotype A). The direction to be evaluated (from cell phenotype A to B or vice versa) depends on the research question and is based on biological knowledge of the tumor. For instance, a researcher may wish to measure the distance from malignant cells to the nearest neighbor T lymphocytes in a certain radius, assuming that the T lymphocytes are there because of the malignant cells.

The most common way to study the random process of cell placement, given certain intensity patterns of spatial distribution between two groups of cell phenotypes (*i*-to-*j*), is to compare the theoretical curve with the empirical nearest neighbor cross-G-function, $G_{i,j}(r) = P\{d(u,X\_j)|u \in X_i\}$ (Baddeley and Turner, 2005). Overall, there are theoretically three possible patterns of distribution when the empirical curve is above, close, or below the theoretical curve: regular, random, and cluster, respectively. However, the regular pattern does not

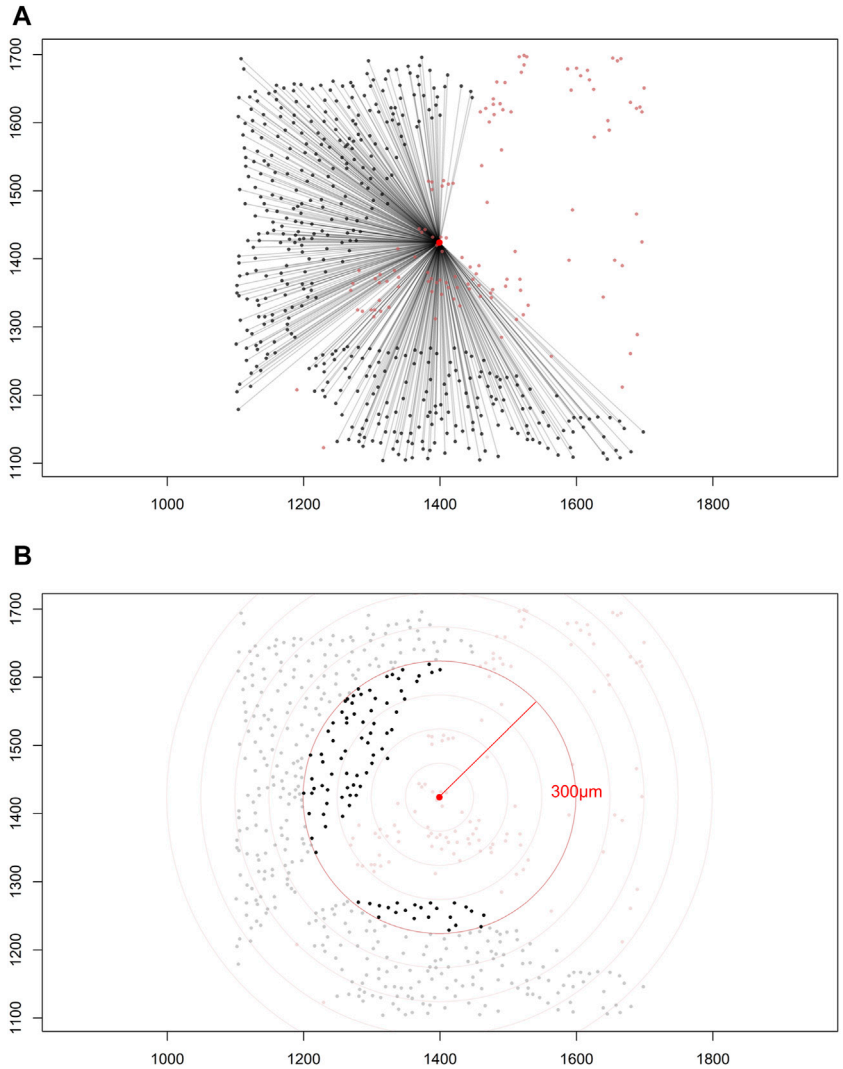

FIGURE 5 | Distance matrices. **(A)** Identified cell coordinates and distance measurements from one cell phenotype (red dots) to another cell phenotype (black dots) in a lung adenocarcinoma image. **(B)** The intensity of one cell phenotype (black dots) was calculated at a given radius (red circle, 300 µm) from the other cell phenotype (red dots). The images were generated using R studio software version 3.6.0.

tend to occur in nature, and hence a situation in which the empirical curve is very far above the theoretical curve should be used with caution. Empirical curves that occur only slightly above the theoretical curve are more accurately interpreted as close to a random pattern than as a potential regular pattern. When studying the distribution of two different cell phenotypes, such as cell phenotype A (malignant cells) and cell phenotype B (lymphocytes), a researcher should typically recognize only two patterns—random or mixed (when the empirical curve is close to the theoretical curve, either above or below) and cluster or unmixed (when the empirical curve is below the theoretical curve)—related to cell phenotype A. These two patterns of distribution can be represented graphically (**Figure 9**). Specifically, when the empirical cross-G-function is plotted against the theoretical expectation or Poisson curve, the shape of the function indicates how the events are spaced in a point pattern of two cell phenotypes. If the events of cellular distribution are random or mixed (e.g., cell phenotype B and cell phenotype A are mixed together in the plot, **Figures 9A,C**), then the nearest neighbor cross-G-function is very close to the Poisson curve because the probability of a neighbor being close is high. In contrast, as the distance increases between the empirical cross-G-function and the Poisson curve, the events are more spaced and a cluster or unmixed pattern can be identified in the plot, as shown in **Figures 9B,D**, where cell phenotype B is in separate clusters from cell phenotype A. To determine the probability that cell phenotypes have a random or cluster pattern related to the theoretical curve, the researcher must process several images from the project to ensure that a clear threshold is present to eliminate the possibility of a random pattern (Parra et al., 2021).

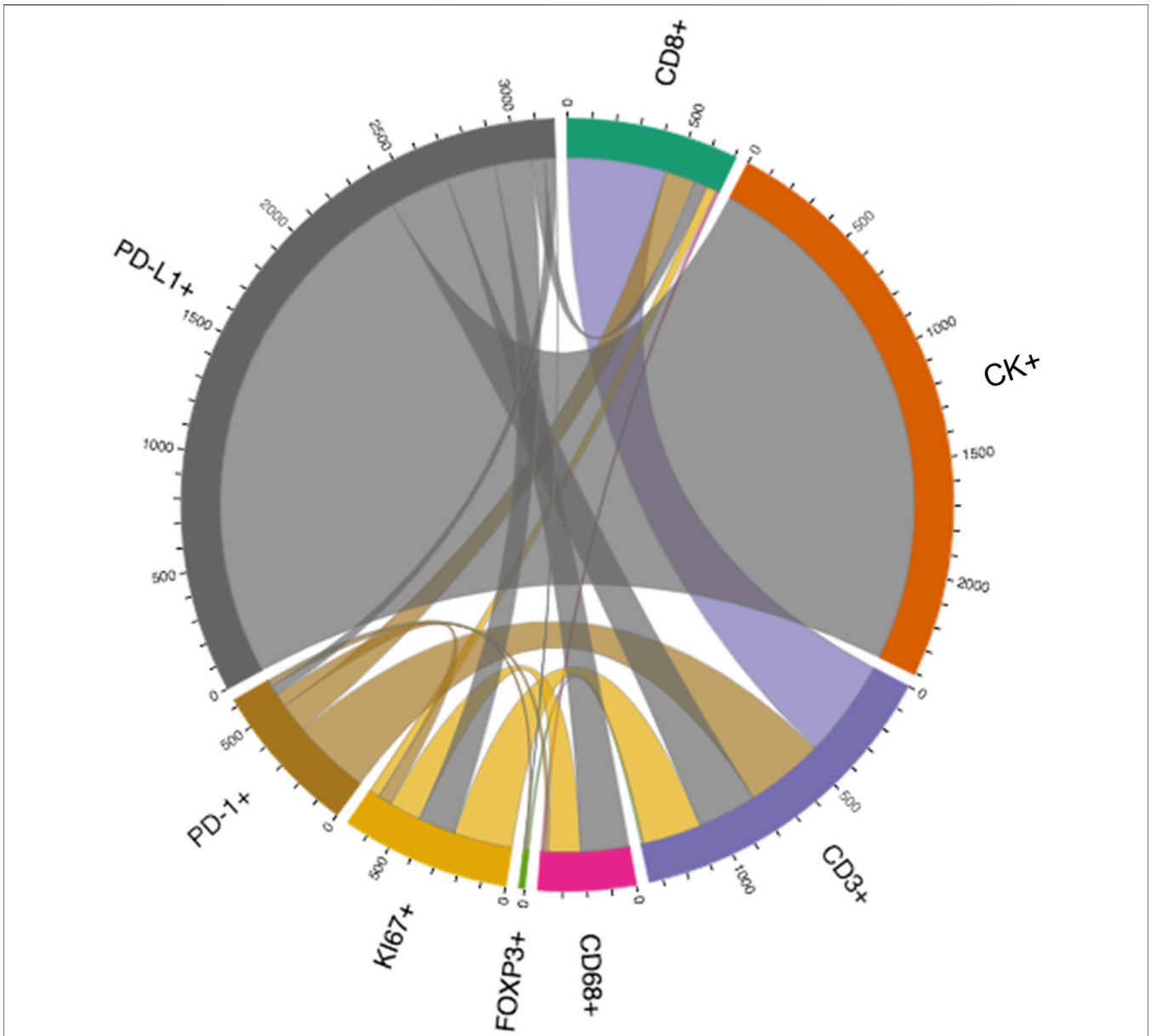

FIGURE 6 | Graphic representation of a distance matrix using a chord diagram showing the flows or connections between the markers included in a multiplex immunofluorescence panel. The chord diagram shows various connections between markers that generate cell phenotypes from a multiplex immunofluorescence panel; these markers include cytokeratin (CK), CD3, CD8, FOXP3, PD-1, PD-L1, KI67, and CD68. The graphic was generated using R studio software version 3.6.1.

CORRELATION FUNCTIONS

Correlation functions basically provide information about how many specific cells of a certain phenotype (e.g., intensity of cell phenotype B) are within a certain radius (r) from another cell phenotype (e.g., cell phenotype A) and can give a good sense of the different levels of interaction between two cell populations in terms of point intensity level (λ) or number of cells (**Figure 8B**). A commonly used correlation function for spatial analysis is the K-function: $K_{i,j}(r)=(E\{n[X_j \cap b(u,r)]|u \in X_i\})/\lambda_j$ (Baddeley and Turner, 2005; Lagache et al., 2013). The K-function essentially normalizes the spatial distribution from one cell phenotype to another cell phenotype by the intensity of the cells present in the radius. As in the cross-G-function, to determine if cell phenotype B has a distinct pattern of distribution related to cell phenotype A, one can calculate the theoretical correlation function for a random process using the same principle, and observed graphical changes can indicate that cells of phenotype B are displaced in random patterns (**Figures 10A,C**) or cluster patterns related to cells of phenotype A (**Figures 10B,D**). This function determines the consistency of the observed distribution of distances among all cells located in spatial images, using the theoretical distribution for the Poisson model as a benchmark.

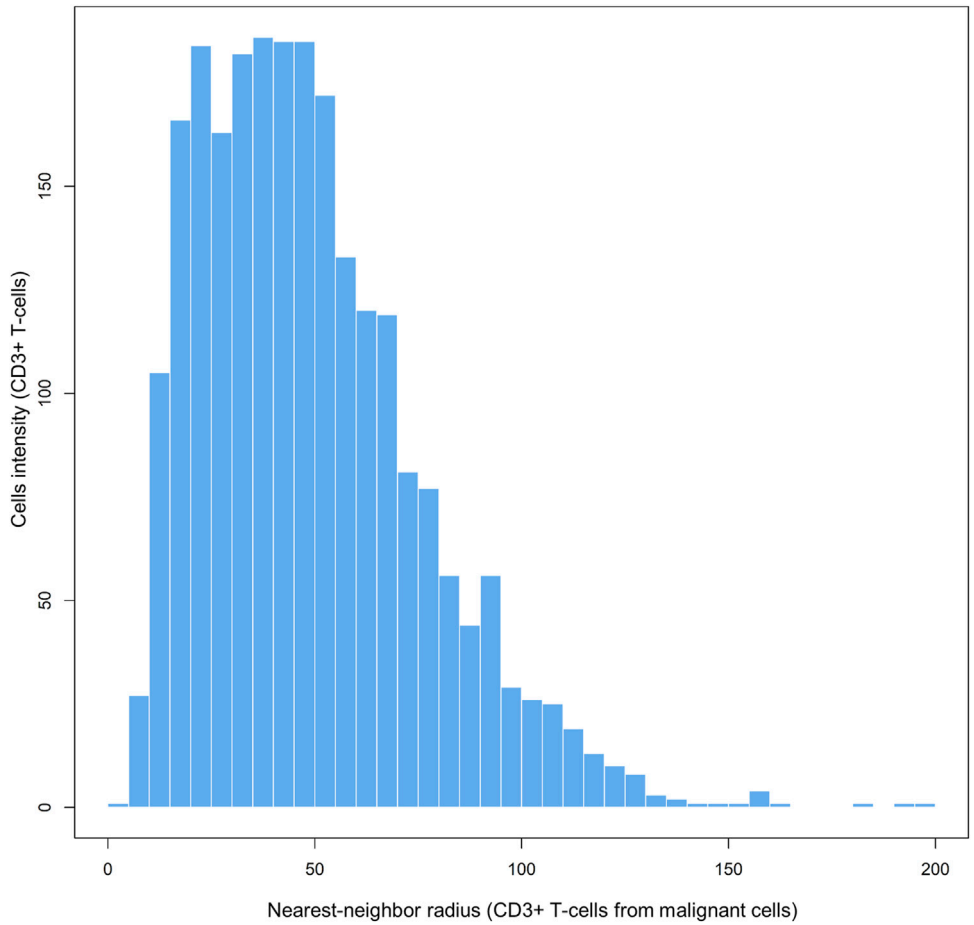

FIGURE 7 | Bar graph showing the distribution of CD3⁺ T-cell distances from malignant cells across different radii, from representative data extracted from a lung adenocarcinoma sample. The graphic was generated using R studio software version 3.6.1.

COMPLEMENTARY FUNCTIONS

Thus far, I have described two spatial functions, the G- and K-functions, which are the most common functions used for spatial image analysis. These two functions combined can provide valuable characterization of the distribution of different cell types in an image. In the learning theory literature, this is known as feature construction or extraction. The G-function provides information about the distribution of the closest cells to another cell type, and the K-function provides the context for the density of these neighbors. In some scenarios, the G-function demonstrates that cells of phenotype B are likely to be within a certain radius of cells of phenotype A, but the K-function demonstrates the intensity of the cell phenotype B distribution from cell phenotype A at the same ratio. Combined, these two distance functions can generate a compressive analysis about the tumor microenvironment, characterizing the proximity and level of interaction between one cell phenotype and another (Parra et al., 2021; Parra, Ferrufino-Schmidt, et al., 2021).

Understanding of the data provided by these two basic functions, in terms of spatial analysis of cell distribution in an image, may be improved by using a complementary function. Complementary functions are derived from the cross-G- and K-function to provide more information about cell distribution patterns and correct transformation that can occur in the image to better reflect the features observed visually.

One transformation correction that can be incorporated into the basic functions described above is the J-function: $J_{i,j}(r) = [1 - G_{i,j}(r)]/[1\ F_j(r)]$ (Baddeley and Turner, 2005). This function is used to compare distances from an arbitrary point to the nearest neighbor (empty-space F-function: $[F_j(r) = P\{d(u,X_j)\leq r\}]$) (Baddeley and Turner, 2005) and distances from a typical point in the pattern measured using the nearest neighbor distance cross-G-function (**Figure 8C**). If the distance in the J-function distribution follows the Poisson process, deviation of the J-function by more than 1 indicates spatial randomness and deviation by less than 1 indicates clustering (**Figure 11**). One can then estimate the empty-space F-function, which is identical to the G-function when the pattern is random but different from it when the probability of not observing another cell fluctuates (Kather et al., 2015; Zheng et al., 2020). Hence, this J-function aids in identifying any pockets of empty space around cells.

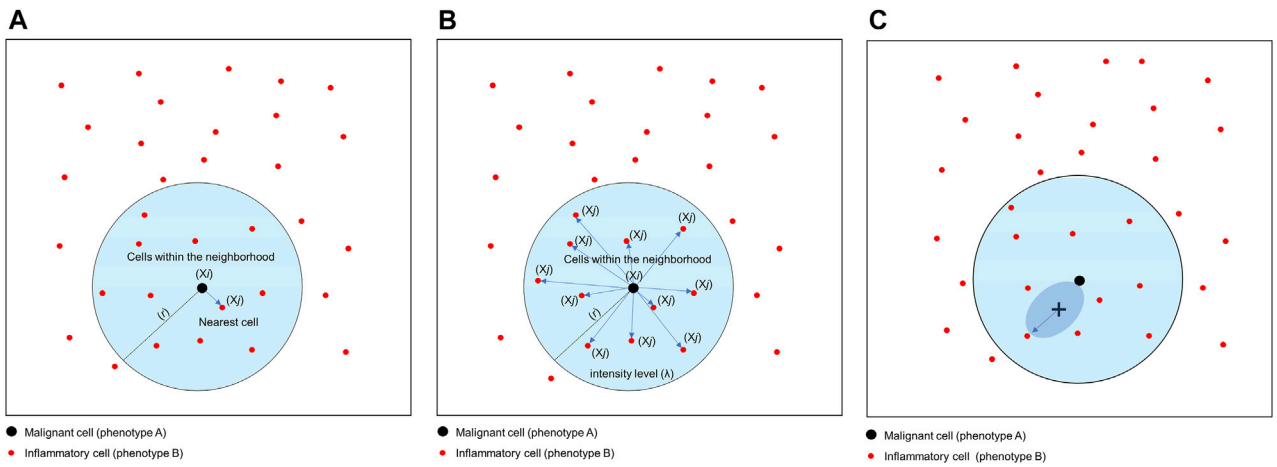

FIGURE 8 | Graphics of nearest neighbor distance, K-function and empty-space F-function. **(A)** Distance matrix showing the concept of nearest neighbor distance, used to determine the probability of encountering a cell of a specific phenotype [*Xi*, inflammatory cell (phenotype B)] within a certain radius (*r*) centered on another cell phenotype [*Xj*, malignant cell (cell phenotype A)]. **(B)** Distance matrix showing the concept of the K-function to determine the intensity level (λ) of cells of a certain phenotype within a certain radius (*r*) of another cell phenotype. In this example, the function is calculating the λ of cell phenotype B (*Xj*) from cell phenotype A (*Xi*) in a point pattern. **(C)** Graphic representation of the empty-space F-function, which compares distances from an arbitrary point (x) to the nearest neighbor cell or point. The graphics were generated using R studio software version 3.6.1.

In addition, the L-function—$L_{i,j}(r) = \sqrt{[(K_{i,j}(r)]/\pi)}$ (Baddeley and Turner, 2005)—can complement a spatial imaging study. Mathematically, this function is simply the square root of K-function divided by pi, and it helps visualize the K-function as a linear shape when it is graphically represented and can identify small differences in cell pattern distributions that are sometimes difficult to identify with the K-function. When the L-function is represented graphically, one should observe a seemingly straight line whenever the pattern is random (**Figure 12**).

Lastly, the pair correlation function—$g_{i,j}(r) = [K_{i,j}'(r)]/2\pi r$ (Baddeley and Turner, 2005)—is easy to understand but more complicated to estimate than the other functions (Gavagnin et al., 2018). The pair correlation function is related to the K- and L-functions; it is a modified version of the K-function where instead of summing all points (cell phenotypes) within a given radius, points falling within a narrow distance band are summed, and the result is the dependence between two different points or two different cell populations. If the $g(r)$ is more than 1, then the points or the correlation between the two cell groups at or around a certain radius are more clustered and the g curve is far below the Poisson curve process. If the $g(r)$ is less than 1, then the points or the correlation between the two cell groups are more dispersed and the g curve is just below the Poisson curve process (**Figure 13**). The $g(r)$ can never be less than 0.

STATISTICAL ANALYSIS MODELING

As with any other statistical analysis, the data obtained from spatial analysis can be used to perform univariate or multivariate analysis with several metrics, and data may be associated with clinicopathologic information in some meaningful way. A simple mathematical model can be applied to investigate the effect of different patterns of distribution for different cell phenotypes in the images on clinical information. Researchers would like to determine if the spatial distribution of certain cell phenotypes can be influenced by the type of tumor and, moreover, as the ultimate goal, if the cellular distribution pattern can predict response to treatment. Several statistical methods, including some of the more common methods such as generalized linear models, form the basis of most supervised machine learning methods, nonparametric testing, clustering methods, Bayesian methods, penalized regression models, survival analysis, dimensionality reduction, and others that can be applied to interpret the data (Baddeley and Turner, 2005; Illian et al., 2008; Demidenko 2020).

Cluster Analysis Methods

To characterize the tumor microenvironment data obtained from mIF imaging, researchers must identify different cell subpopulations, and this can be achieved via cluster analysis. Although cluster methods are not a measurement of distance and are not frequently used to interpret the type of data presented in this paper, cluster methods can be used for exploratory analysis of the data, in which observations are divided into different groups with standard features to ensure that the groups meaningfully differ as much as possible.

The two main types of classification are K-means clustering and hierarchical clustering. K-means clustering can be used when the number of classes is fixed; this method is infrequently used in mIF data. In contrast, hierarchical clustering can be used for an unknown number of classes and is probably more appropriate for classifying cell phenotypes.

K-means clustering comprises unsupervized learning methods of vector quantization that have an iterative process in which data are grouped into k predefined non-overlapping clusters or

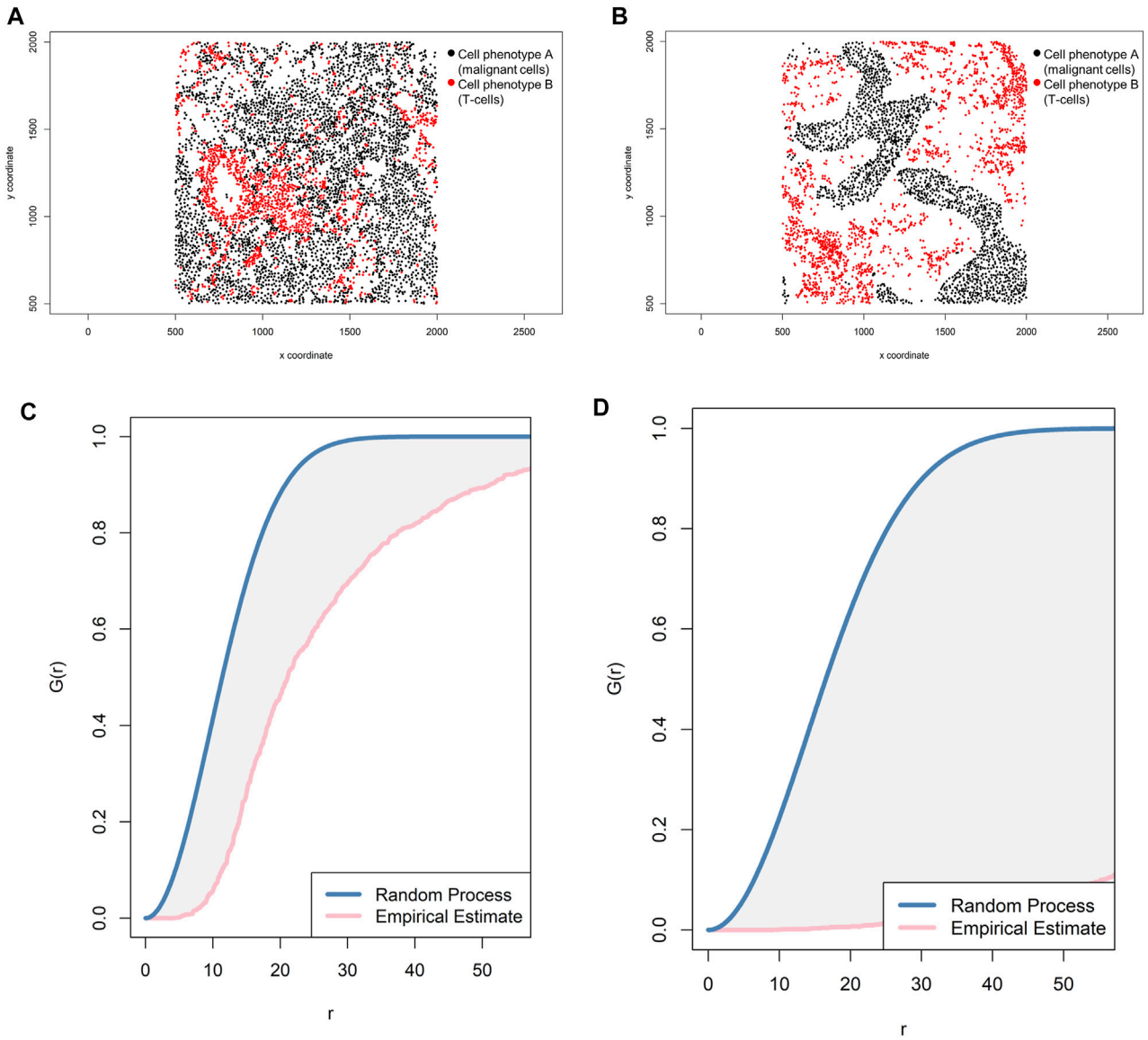

FIGURE 9 | Representative graphs showing the G-function [G(*r*)] curve of point pattern distributions for cell phenotype A (malignant cells) to cell phenotype B (T-cells) in a representative multiplex immunofluorescence image of lung adenocarcinoma. **(A)** Random point pattern distribution of cell phenotype A and B. **(C)** Graphic representation of the image shown in A using the cross-G-function, showing the proximity of the G(*r*) curve to the theoretical estimate curve (Poisson curve), characterizing a random or mixed cell distribution pattern of one cell population in relation to another cell population. **(B)** Unmixed point pattern distribution of cell phenotype A and B. **(D)** Graphic representation of the image shown in B using the cross-G-function, showing the increased distance of the G(*r*) curve from the theoretical estimate curve (Poisson curve), characterizing a clustering or unmixed cell distribution pattern of one cell population in relation to another cell population. The graphics were generated using R studio software version 3.6.1.

subgroups, making the inner points of the cluster as similar as possible (**Figure 14A**). To maintain different clusters in distinct spaces, K-means clustering allocates the data points to a cluster in such a way that each observation belongs to the cluster with the nearest mean (cluster center or centroid), so that the sum of the squared distance between the cluster centroid and the data point is minimized; at this position, the centroid of the cluster is the arithmetic mean of the data points that are in the clusters (**Figure 14B**). This results in a partitioning of the data space into Voronoi cells (Schuffler et al., 2015). Less variation in the cluster results in similar or homogeneous data points within the cluster.

To identify the number of clusters in determinate data, we use the elbow or the purpose method. In the elbow method, the sum of squares and the number of clusters are plotted into a curve resembling a human elbow; the point of the elbow in the curve indicates the optimum number of clusters and the point after the elbow point indicates the final value of the number of clusters (**Figure 14C**).

Although the K-means clustering algorithm can be used in image segmentation, image compression, vector quantization,

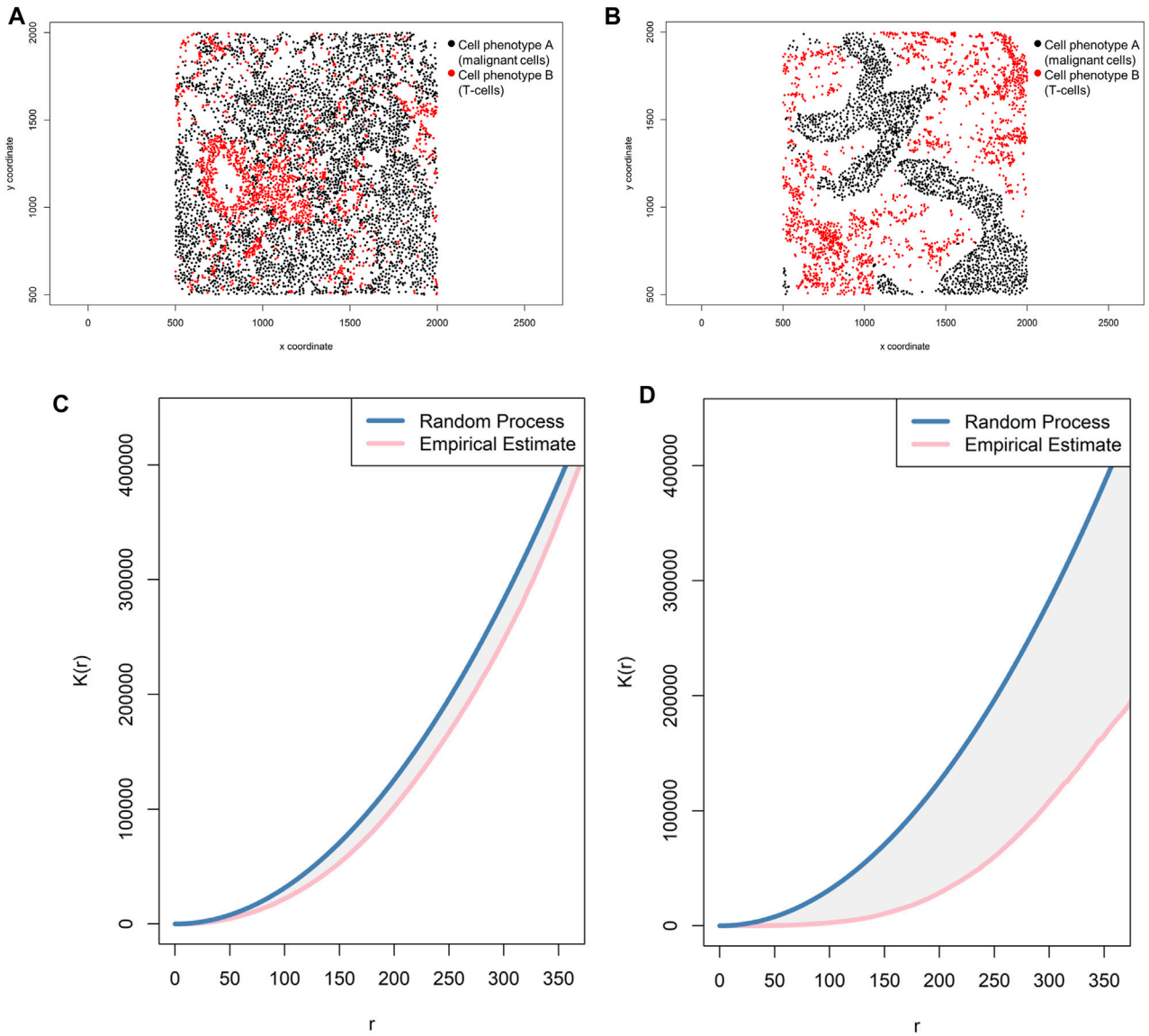

FIGURE 10 | Representative graphs showing the K-function [K(*r*)] curve of cellular distributions between two groups of cells from a representative point pattern of multiplex immunofluorescence images of lung adenocarcinoma. **(A)** Random point pattern distribution of cell phenotype A and B. **(C)** K(*r*) curve extracted from the image shown in A, showing the proximity of the curve to the theoretical estimate curve (Poisson curve), characterizing a random or mixed distribution pattern of the two cell phenotypes. **(B)** Unmixed point pattern distribution of cell phenotype A and B. **(D)** K(*r*) curve extracted from the image shown in B, showing the increased distance of the curve from the theoretical estimate curve (Poisson curve), characterizing a clustering or unmixed distribution pattern of cell phenotype A and B. The graphics were generated using R studio software version 3.6.1.

clustering analysis, machine learning, and other methods, the algorithm requires prior specification of the number of cluster centers, and if there are overlapping data the algorithm cannot distinguish clusters very well. Depending on how the data are presented, the results generated can be different every time the algorithm is run, and the Euclidean distance can unequally weight factors and can be used only if the meaning is defined. In contrast, hierarchical clustering can be agglomerative when similar objects are grouped into clusters and into a set of clusters, where each cluster is distinct from the others and the objects within each cluster are broadly similar to each other (Comin et al., 2014; Lin et al., 2015) (**Figure 15A**). Divisive hierarchical clustering is done by initially grouping all observations into one cluster and then successively splitting these clusters, typically by sequentially merging similar clusters (**Figure 15A**). The similarity here is the distance among points, which can be computed in many ways, and this distance is the crucial element of discrimination. However, in practice, divisive hierarchical clustering is rarely done. Unfortunately, it is not possible to undo the previous steps after applying the algorithm, and when the clusters have been assigned, they can no longer be moved around. In addition, this method is not suitable for large datasets, the order of the data

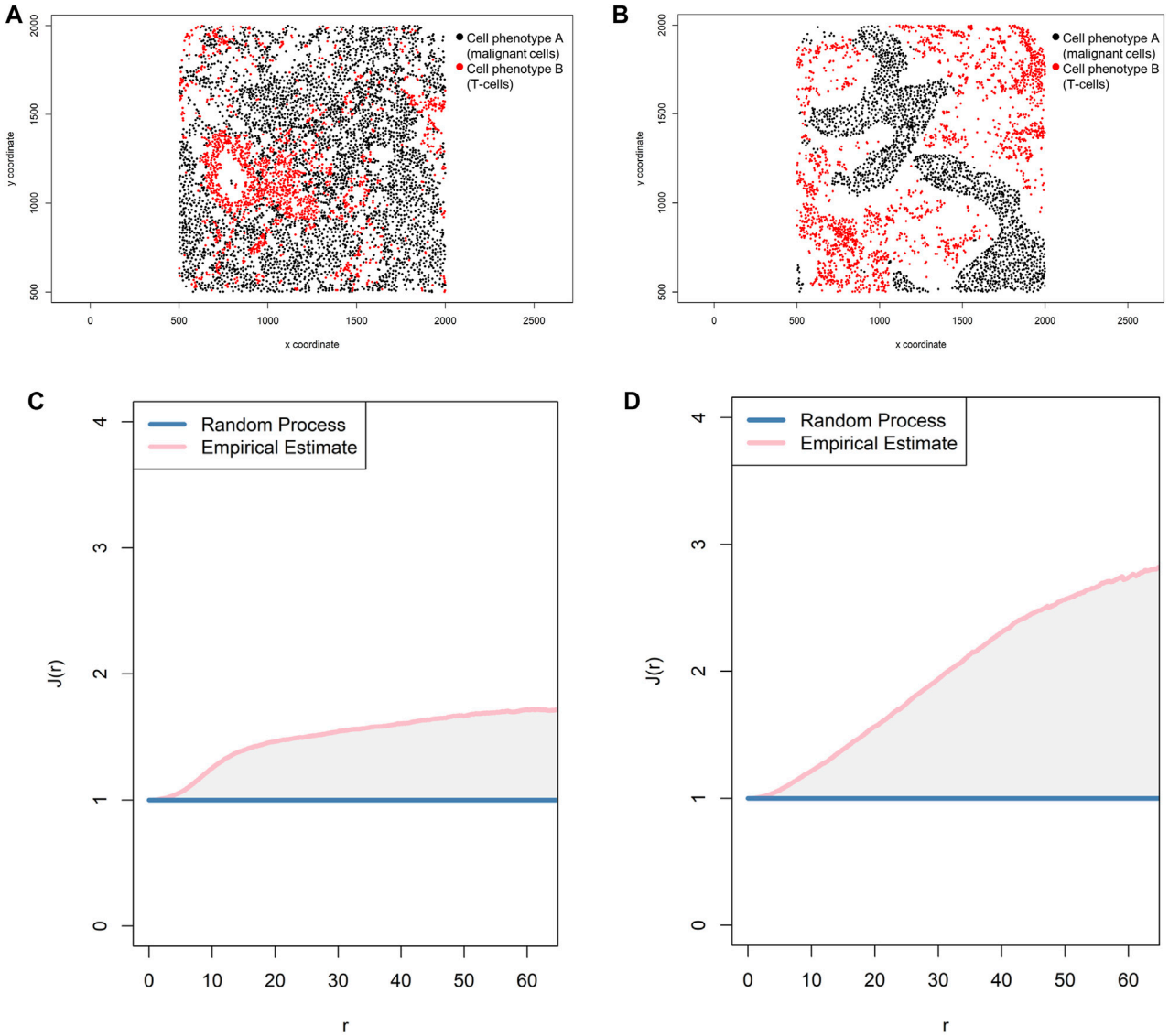

FIGURE 11 | Representative graphs showing the J-function [J(*r*)] for two different cell populations, illustrating the cellular distribution between the two groups of cells using a representative point pattern in multiplex immunofluorescence images of lung adenocarcinoma. **(A)** Random point pattern distribution of cell phenotype A and B. **(C)** Graphic representation of the J(*r*) curve showing its lineup with the theoretical estimate (Poisson line), characterizing a random or mixed pattern of one cell population in relation to another cell population. **(B)** Unmixed point pattern distribution of cell phenotype A and B. **(D)** Graphic representation of the J(*r*) curve showing highly increased distance above the theoretical estimate (Poisson line), characterizing a clustering or unmixed pattern of one cell population in relation to another cell population. The graphics were generated using R studio software version 3.6.1.

affects the results, and the method is very sensitive to data outliers.

With any data, the efficiency of multivariate parameter estimation and prediction must be increased by exploring variation of the data, which is done using envelope methods. Envelopes achieve efficiency gains by basing estimation on the variation of the data. The Monte Carlo method (**Figure 14D**) is a type of computational envelope algorithm that uses the random repletion of the sampling to obtain numeric results that optimize, integrate, and generate draws from a probability distribution of the data (Sanchez et al., 2021). Monte Carlo tests are related to the randomization tests commonly used in nonparametric statistics.

Dimensional Reduction Methods for Data Visualization

Because we generate highly multiparametric single-cell data using mIF, statistical methods can be used for better visualization and dimensional reduction, providing a location for each data point on a two- or three-dimensional map. This type of visualization through dimensional reduction algorithms tends to fall into one

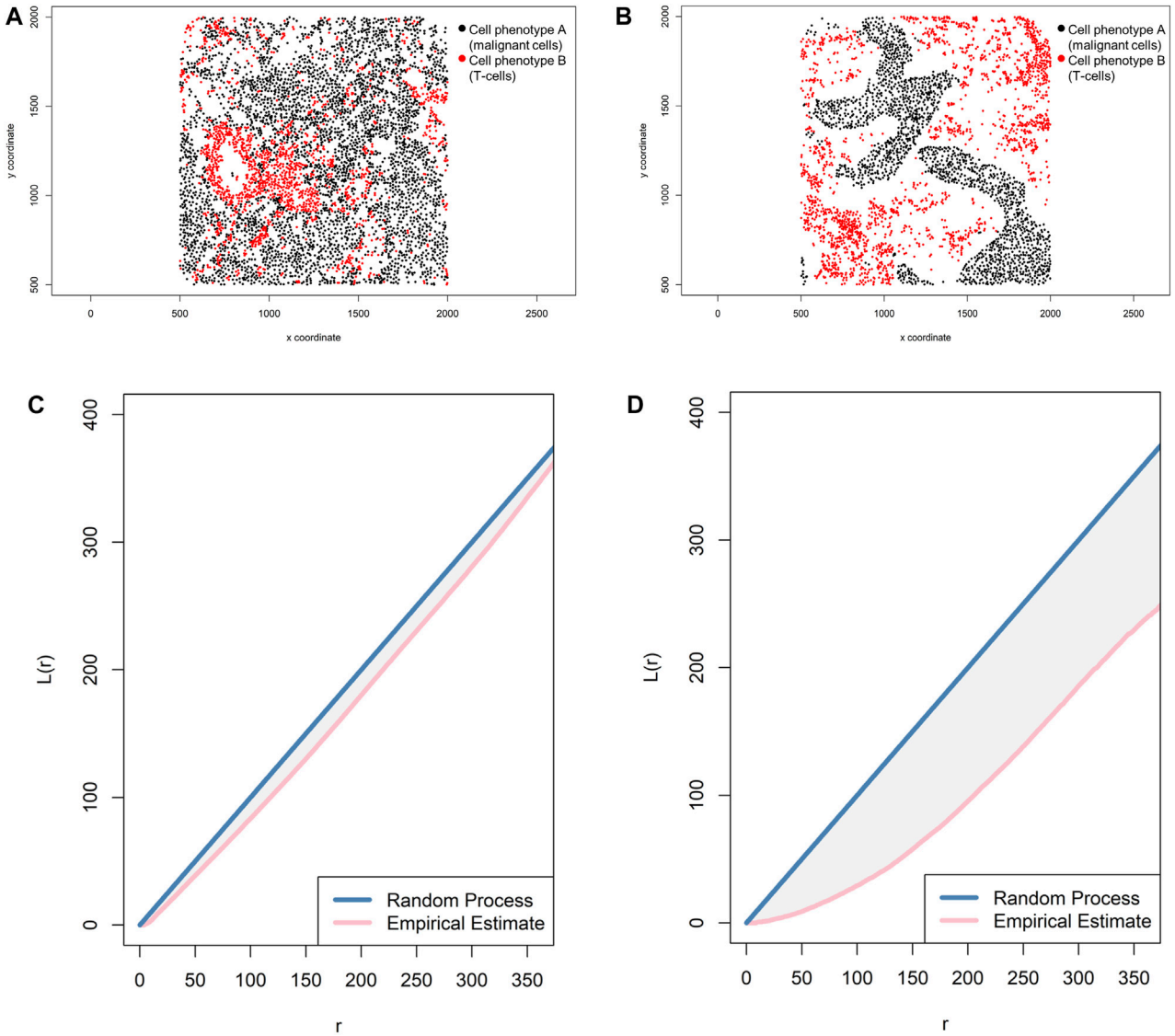

FIGURE 12 | Representative graphs showing the L-function [L(*r*)] for two different cellular distribution patterns between two group of cells from a representative point pattern in multiplex immunofluorescence images of lung adenocarcinoma. **(A)** Random point pattern distribution of cell phenotype A and B. **(C)** Graphic representation of the L(*r*) line showing its proximity to the theoretical estimate (Poisson line), characterizing a random or mixed pattern of one cell phenotype in relation to another cell phenotype. **(B)** Unmixed point pattern distribution of cell phenotype A and B. **(D)** Graphic representation of the L(*r*) line showing that it is located far from the theoretical estimate (Poisson line), characterizing a clustering or unmixed pattern of one cell phenotype in relation to another cell phenotype. The graphics were generated using R studio software version 3.6.1.

of two overall categories, algorithms that seek to preserve the distance structure within the data and algorithms that favor the preservation of local distances over global distance; these algorithms are applied for cell phenotype data visualization. Algorithms such as principal component analysis (PCA), multidimensional scaling, and Sammon mapping fall into the first category, and t-distributed stochastic neighbor embedding (t-SNE) and uniform manifold approximation and projection (UMAP), as well as others, fall into the second category (Tsogo et al., 2000).

PCA is an unsupervized algorithm that can create linear combinations of the original features, and then the new features are orthogonal, which means that they are uncorrelated (Rohde, 2002). Because the reduction of the data is dependent on scale, the dataset must be normalized before this technique can be performed (Rohde, 2002). Several algorithm variations, such as kernel PCA or sparse PCA, can be applied to compare the performance of the data, but an important disadvantage is the necessity of manually setting or tuning the threshold for cumulative explained variance.

Multidimensional scaling is another reduction method frequently used to translate information about pairwise distances obtained from data among a set number of points mapped into an abstract Cartesian space (Jackle et al., 2016). This

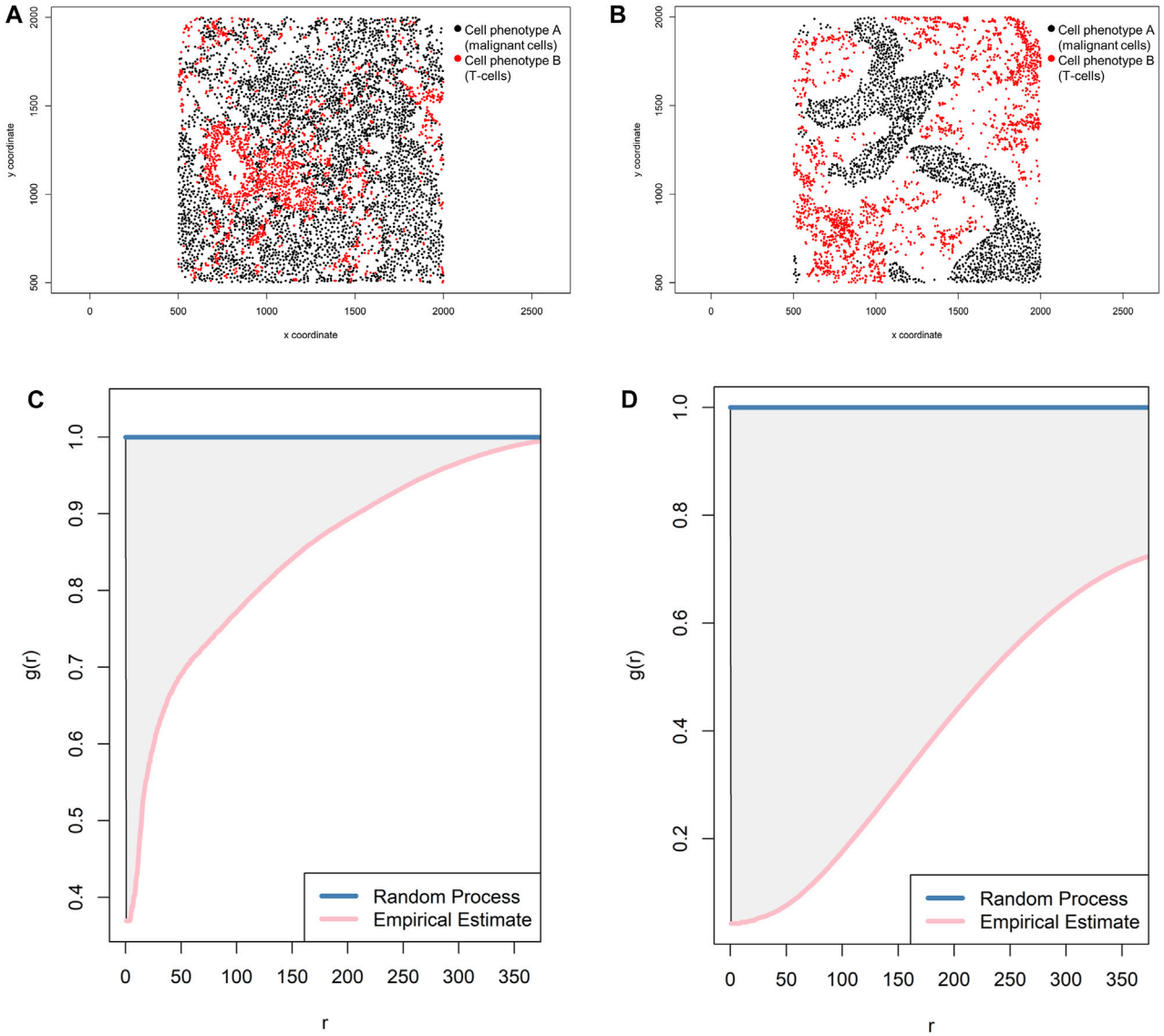

FIGURE 13 | Representative graphs showing the pair correlation function [g(*r*)] for two different cellular distribution patterns between two group of cells from a representative point pattern in multiplex immunofluorescence images of lung adenocarcinoma. **(A)** Random point pattern distribution of cell phenotype A and B. **(C)** Graphic representation of the g(*r*) curve showing a line forming downward from the theoretical estimate (Poisson line), characterizing a random or mixed pattern of one cell phenotype in relation to another cell phenotype. **(B)** Unmixed point pattern distribution of cell phenotype A and B. **(D)** Graphic representation of the g(*r*) curve showing increased distance below the theoretical estimate (Poisson line), characterizing a clustering or unmixed pattern of one cell phenotype in relation to another cell phenotype. The graphics were generated using R studio software version 3.6.1.

method allows construction of a distance matrix with the distances between each pair of objects in a set placing each object into a dimensional space, providing a point pattern to be visualized on a scatter plot.

Sammon mapping is another algorithm used in exploratory analysis. This method translates a map with a high-dimensional space to a space of lower dimensionality by trying to preserve the structure of inter-point distances from the high-dimensional space in the lower-dimension projection. Sammon mapping is considered a nonlinear approach because the mapping cannot be represented as a linear combination of the original variables, as is possible in techniques such as PCA, and this also makes Sammon mapping more difficult to use for classification applications.

For high-dimensional data such as that obtained by image analysis, a reduction and visualization can be made through t-SNE or UMAP reduction analysis (Wu et al., 2019). t-SNE is a statistical method for visualizing high-dimensional data by giving each data point a location in a two- or three-dimensional map. It is based on SNE, originally developed by Sam Roweis and Geoffrey Hinton (Van der Maaten and Rey Hinton, 2008). t-SNE constructs a probability distribution over pairs of high-dimensional objects in such a way that similar objects are assigned a higher

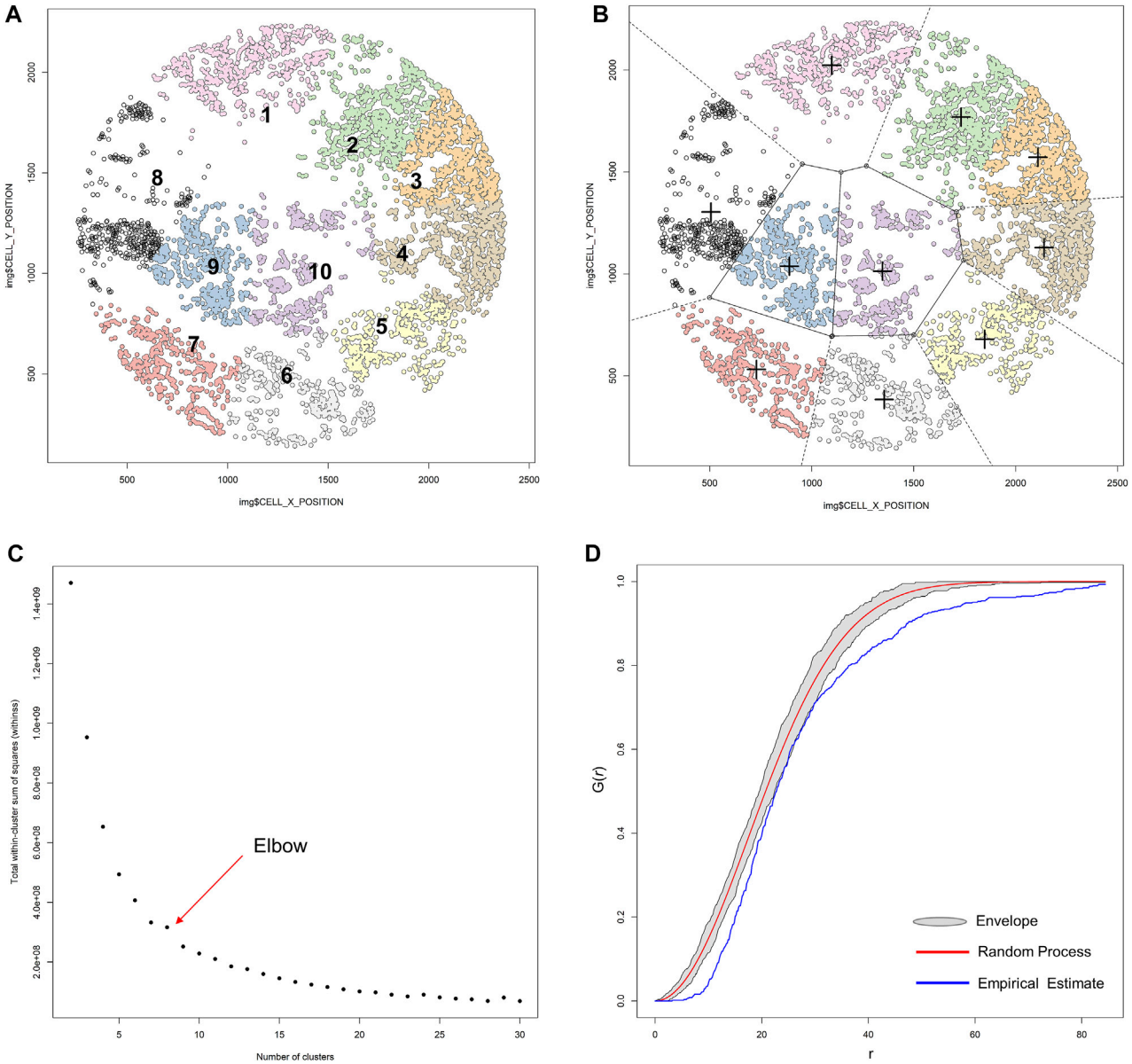

FIGURE 14 | K-means unsupervized clustering, elbow, and envelope applied in multiplex immunofluorescence image data. **(A)** K-means unsupervized clustering showing ten groups (represented by the colored points) of non-overlapping clusters in which the inner points of the cluster are as similar as possible within the image. **(B)** Different clusters are maintained in different spaces, and the center (+) of each cluster is located such that it is the arithmetic mean of the data points in the cluster. **(C)** Graphic representation of the elbow method, showing the sum of squares and the number of clusters plotted into a curve. The point of the elbow in the curve indicates the optimum number of clusters. **(D)** Graphic representation of an envelope to estimate the variation of data to achieve efficiency gains, showing the minimal variation of the envelope related to the random process curve from a representative sample of multiplex immunofluorescence data points. The graphics were generated using R studio software version 3.6.1.

probability while dissimilar points are assigned a lower probability using the Euclidian distance between objects (**Figures 15C,D**). The visual clusters often require good understanding because they can be influenced by the parameterization, forcing exploration of different parameters to validate the results. Although t-SNE is incredibly flexible and can often find structure where other dimensionality-reduction algorithms cannot, that very flexibility makes t-SNE tricky to interpret.

UMAP is another dimension reduction technique that can be used for data visualization similar to that described for t-SNE, but UMAP can be applied for general nonlinear dimension reduction (Becht et al., 2018). UMAP is based on distances between the observations obtained by the data rather than the source features, and it does not have an equivalent of the factor loadings that are required for linear techniques such as PCA. Importantly, as a way to improve the computational

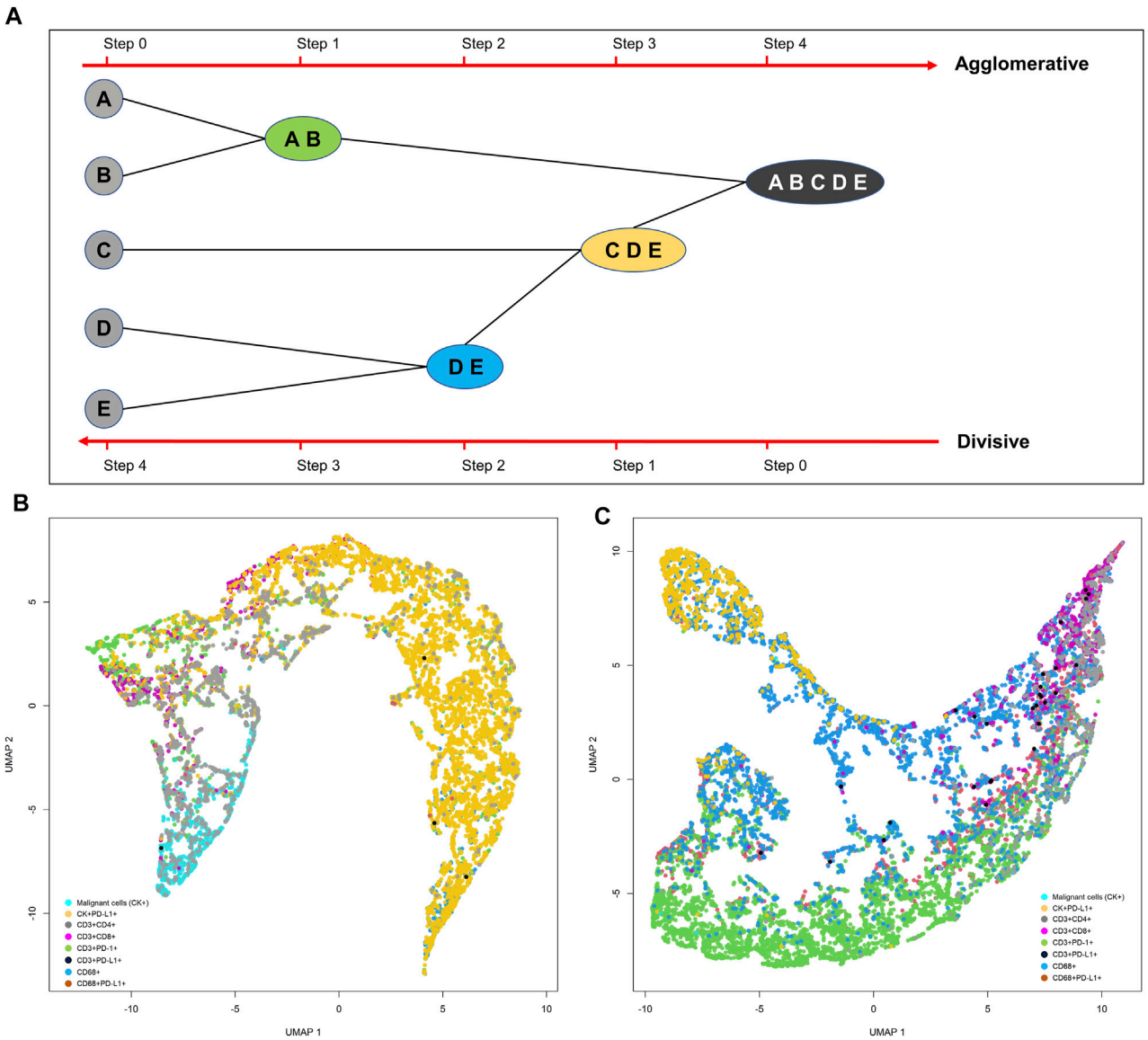

FIGURE 15 | Representative schema of hierarchical and divisive clustering to agglomerate similar objects into groups **(A)**. Uniform manifold approximation and projection (UMAP) showing different cell population distribution patterns extracted from two different lung adenocarcinoma cases analyzed with multiplex immunofluorescence against malignant cells [cytokeratin (CK)+] and CD3+, CD4+, CD8+, PD-1+, PD-L1+, and CD68+ antibodies **(B, C)**. The graphics B and C were generated using R studio software version 3.6.1.

efficiency of the UMAP algorithm, several approximations can be made and small data sizes (less than 500 samples) can be analyzed (Wu et al., 2019).

In summary, spatial distance analysis methods can be applied to analyze the spatial distribution of cells determined by mIF data. There are several methods to analyze the distribution of different cell phenotypes, but the most simple approach is a combination of cell phenotype compartmentalization at a tissue level with nearest neighbor distance measurement through the cross-G- and K-function at a cellular level to identify patterns of distribution and interaction between cell phenotypes. Although cluster analysis and visualization methods are important in exploring mIF data, overall no single cluster or visualization method described here outperforms another in terms of identifying the characteristics of the data, and for this reason researchers can choose the most convenient method for interpreting their results. Given this situation, approaches for cellular cluster identification should allow subsequent in-depth analysis to identify new clusters of special cell phenotypes and permit interpretation of features that contribute to the analysis, thus effectively answering the research question or providing a potential clinical application.

AUTHOR CONTRIBUTIONS

EP conceived the idea and the theme developed in this manuscript.

FUNDING

This study was supported in part by the scientific and financial support for the CIMAC-CIDC Network provided through the National Cancer Institute (NCI) Cooperative Agreement U24CA224285 of The University of Texas MD Anderson Cancer Center CIMAC and for the Translational Molecular Pathology Immunoprofiling Laboratory, as well as by National Institutes of Health/NCI through Cancer Center Support Grant P30CA016672 (Institutional Tissue Bank) and SPORE grant 5P50CA070907-18 from the Cancer Prevention and Research Institute of Texas through MIRA RP160688.

ACKNOWLEDGMENTS

The author acknowledges the Department of Translational Molecular Pathology at The University of Texas MD Anderson Cancer Center and the immunoprofiling laboratory members in this department. I also thank Jose de Jesus Martinez for guidance and for teaching me to apply several spatial mathematical functions for image analysis, as well as Don Norwood and Erica Goodoff from Editing Services, Research Medical Library at MD Anderson for editing this article.

REFERENCES

Baddeley, A., Rubak, E., and Turner, R. (2015). *Spatial Point Patterns: Methodology and Applications with R*. Chapman and Hall/CRC Press. doi:10.1201/b19708

Baddeley, A., and Turner, R. (2005). 'spatstat: An R Package for Analyzing Spatial Point Patterns. *J. Stat. Softw.* 12, 1–42. doi:10.18637/jss.v012.i06

Barua, S., Solis, L., Parra, E. R., Uraoka, N., Jiang, M., Wang, H., et al. (2018). A Functional Spatial Analysis Platform for Discovery of Immunological Interactions Predictive of Low-Grade to High-Grade Transition of Pancreatic Intraductal Papillary Mucinous Neoplasms. *Cancer Inform.* 17, 1176935118782880. doi:10.1177/1176935118782880

Becht, E., McInnes, L., Healy, J., Dutertre, C. A., Kwok, I. W. H., Ng, L. G., et al. (2018). 'Dimensionality Reduction for Visualizing Single-Cell Data Using UMAP. *Nat. Biotechnol.* 37, 38–44. doi:10.1038/nbt.4314

Bremnes, R. M., Dønnem, T., Al-Saad, S., Al-Shibli, K., Andersen, S., Sirera, R., et al. (2011). The Role of Tumor Stroma in Cancer Progression and Prognosis: Emphasis on Carcinoma-Associated Fibroblasts and Non-small Cell Lung Cancer. *J. Thorac. Oncol.* 6, 209–217. doi:10.1097/jto.0b013e3181f8a1bd

Catacchio, I., Silvestris, N., Scarpi, E., Schirosi, L., Scattone, A., and Mangia, A. (2019). Intratumoral, rather Than Stromal, CD8+ T Cells Could Be a Potential Negative Prognostic Marker in Invasive Breast Cancer Patients. *Transl. Oncol.* 12, 585–595. doi:10.1016/j.tranon.2018.12.005

Comin, C. H., Santos, J. R., Corradini, D., Morrison, W., Curme, C., Rosene, D. L., et al. (2014). 'Statistical Physics Approach to Quantifying Differences in Myelinated Nerve Fibers. *Sci. Rep.* 4, 4511. doi:10.1038/srep04511

Cooper, Z. A., Reuben, A., Spencer, C. N., Prieto, P. A., Austin-Breneman, J. L., Jiang, H., et al. (2016). Distinct Clinical Patterns and Immune Infiltrates Are Observed at Time of Progression on Targeted Therapy versus Immune Checkpoint Blockade for Melanoma. *Oncoimmunology* 5, e1136044. doi:10.1080/2162402x.2015.1136044

Demidenko, E. (2020). *Advanced Statistics with Applications in R*. First edition. John Wiley & Sons IncWiley Series in Probability and Statistics.

Dieu-Nosjean, M.-C., Goc, J., Giraldo, N. A., Sautès-Fridman, C., and Fridman, W. H. (2014). Tertiary Lymphoid Structures in Cancer and beyond. *Trends Immunol.* 35, 571–580. doi:10.1016/j.it.2014.09.006

Feldmeyer, L., Hudgens, C. W., Ray-Lyons, G., Nagarajan, P., Aung, P. P., Curry, J. L., et al. (2016). Density, Distribution, and Composition of Immune Infiltrates Correlate with Survival in Merkel Cell Carcinoma. *Clin. Cancer Res.* 22, 5553–5563. doi:10.1158/1078-0432.ccr-16-0392

French, J. D., Weber, Z. J., Fretwell, D. L., Said, S., Klopper, J. P., and Haugen, B. R. (2010). Tumor-Associated Lymphocytes and Increased FoxP3+ Regulatory T Cell Frequency Correlate with More Aggressive Papillary Thyroid Cancer. *J. Clin. Endocrinol. Metab.* 95, 2325–2333. doi:10.1210/jc.2009-2564

Galon, J., Costes, A., Sanchez-Cabo, F., Kirilovsky, A., Mlecnik, B., Lagorce-Pages, C., et al. (2006). Type, Density, and Location of Immune Cells within Human Colorectal Tumors Predict Clinical Outcome. *Science* 313, 1960–1964. doi:10.1126/science.1129139

Gavagnin, E., Owen, J. P., and Yates, C. A. (2018). 'Pair Correlation Functions for Identifying Spatial Correlation in Discrete Domains. *Phys. Rev. E* 97, 062104. doi:10.1103/physreve.97.062104

Gentles, A. J., Newman, A. M., Liu, C. L., Bratman, S. V., Feng, W., Kim, D., et al. (2015). The Prognostic Landscape of Genes and Infiltrating Immune Cells across Human Cancers. *Nat. Med.* 21, 938–945. doi:10.1038/nm.3909

Illian, J., Penttinen, A., Stoyan, H., and Stoyan, D. (2008). *Statistical Analysis and Modelling of Spatial Point Patterns*. Hoboken, NJ: John Wiley & Sons. doi:10.1002/9780470725160

Jackle, D., Fischer, F., Schreck, T., and Keim, D. A. (2016). Temporal MDS Plots for Analysis of Multivariate Data. *IEEE Trans. Vis. Comput. Graphics* 22, 141–150. doi:10.1109/tvcg.2015.2467553

Kather, J. N., Marx, A., Reyes-Aldasoro, C. C., Schad, L. R., Zöllner, F. G., and Weis, C.-A. (2015). Continuous Representation of Tumor Microvessel Density and Detection of Angiogenic Hotspots in Histological Whole-Slide Images. *Oncotarget* 6, 19163–19176. doi:10.18632/oncotarget.4383

Lagache, T., Lang, G., Sauvonnet, N., and Olivo-Marin, J. C. (2013). 'Analysis of the Spatial Organization of Molecules with Robust Statistics. *PLoS One* 8, e80914. doi:10.1371/journal.pone.0080914

Lin, J. R., Fallahi-Sichani, M., and Sorger, P. K. (2015). 'Highly Multiplexed Imaging of Single Cells Using a High-Throughput Cyclic Immunofluorescence Method. *Nat. Commun.* 6, 8390. doi:10.1038/ncomms9390

Masugi, Y., Abe, T., Ueno, A., Fujii-Nishimura, Y., Ojima, H., Endo, Y., et al. (2019). Characterization of Spatial Distribution of Tumor-Infiltrating CD8+ T Cells Refines Their Prognostic Utility for Pancreatic Cancer Survival. *Mod. Pathol.* 32, 1495–1507. doi:10.1038/s41379-019-0291-z

Nazemalhosseini-Mojarad, E., Mohammadpour, S., Torshizi Esafahani, A., Gharib, E., Larki, P., Moradi, A., et al. (2019). Intratumoral Infiltrating Lymphocytes Correlate with Improved Survival in Colorectal Cancer Patients: Independent of Oncogenetic Features. *J. Cel Physiol* 234, 4768–4777. doi:10.1002/jcp.27273

Parra, E. R., Behrens, C., Rodriguez-Canales, J., Lin, H., Mino, B., Blando, J., et al. (2016). Image Analysis-Based Assessment of PD-L1 and Tumor-Associated Immune Cells Density Supports Distinct Intratumoral Microenvironment Groups in Non-small Cell Lung Carcinoma Patients. *Clin. Cancer Res.* 22, 6278–6289. doi:10.1158/1078-0432.ccr-15-2443

Parra, E. R., Ferrufino-Schmidt, M. C., Tamegnon, A., Zhang, J., Solis, L., Jiang, M., et al. (2021). 'Immuno-profiling and Cellular Spatial Analysis Using Five Immune Oncology Multiplex Immunofluorescence Panels for Paraffin Tumor Tissue. *Sci. Rep.* 11, 8511. doi:10.1038/s41598-021-88156-0

Parra, E. R., Jiang, M., Solis, L., Mino, B., Laberiano, C., Hernandez, S., et al. (2020). Procedural Requirements and Recommendations for Multiplex Immunofluorescence Tyramide Signal Amplification Assays to Support Translational Oncology Studies. *Cancers* 12, 255. doi:10.3390/cancers12020255

Parra, E. R., Villalobos, P., Behrens, C., Jiang, M., Pataer, A., Swisher, S. G., et al. (2018). 'Effect of Neoadjuvant Chemotherapy on the Immune Microenvironment in Non-small Cell Lung Carcinomas as Determined by Multiplex Immunofluorescence and Image Analysis Approaches. *J. Immunother. Cancer* 6, 48. doi:10.1186/s40425-018-0368-0

Parra, E. R., Zhai, J., Tamegnon, A., Zhou, N., Pandurengan, R. K., Barreto, C., et al. (2021). 'Identification of Distinct Immune Landscapes Using an Automated Nine-Color Multiplex Immunofluorescence Staining Panel and Image Analysis in Paraffin Tumor Tissues. *Sci. Rep.* 11, 4530. doi:10.1038/s41598-021-83858-x

Robinson, M. H., Vasquez, J., Kaushal, A., MacDonald, T. J., Velazquez Vega, J. E., Schniederjan, M., et al. (2020). 'Subtype and Grade-dependent Spatial Heterogeneity of T-Cell Infiltration in Pediatric Glioma. *J. Immunother. Cancer* 8, e001066. doi:10.1136/jitc-2020-001066

Rohde, D. L. T. (2002). Methods for Binary Multidimensional Scaling. *Neural Comput.* 14, 1195–1232. doi:10.1162/089976602753633457

Sanchez, K., Kim, I., Chun, B., Pucilowska, J., Redmond, W. L., Urba, W. J., et al. (2021). Multiplex Immunofluorescence to Measure Dynamic Changes in Tumor-Infiltrating Lymphocytes and PD-L1 in Early-Stage Breast Cancer. *Breast Cancer Res.* 23, 2. doi:10.1186/s13058-020-01378-4

Schüffler, P. J., Schapiro, D., Giesen, C., Wang, H. A. O., Bodenmiller, B., and Buhmann, J. M. (2015). Automatic Single Cell Segmentation on Highly Multiplexed Tissue Images. *Cytometry* 87, 936–942. doi:10.1002/cyto.a.22702

Stein, A. V., Dislich, B., Blank, A., Guldener, L., Kröll, D., Seiler, C. A., et al. (2017). High Intratumoural but Not Peritumoural Inflammatory Host Response Is Associated with Better Prognosis in Primary Resected Oesophageal Adenocarcinomas. *Pathology* 49, 30–37. doi:10.1016/j.pathol.2016.10.005

Sugie, T., Sato, E., Miyashita, M., Yamaguchi, R., Sakatani, T., Kozuka, Y., et al. (2020). Multispectral Quantitative Immunohistochemical Analysis of Tumor-Infiltrating Lymphocytes in Relation to Programmed Death-Ligand 1 Expression in Triple-Negative Breast Cancer. *Breast Cancer* 27, 519–526. doi:10.1007/s12282-020-01110-2

Tsogo, L., Masson, M. H., and Bardot, A. (2000). Multidimensional Scaling Methods for Many-Object Sets: A Review. *Multivariate Behav. Res.* 35, 307–319. doi:10.1207/s15327906mbr3503_02

Tsujikawa, T., Mitsuda, J., Ogi, H., Miyagawa-Hayashino, A., Konishi, E., Itoh, K., et al. (2020). Prognostic Significance of Spatial Immune Profiles in Human Solid Cancers. *Cancer Sci.* 111, 3426–3434. doi:10.1111/cas.14591

Tuminello, S., Veluswamy, R., Lieberman-Cribbin, W., Gnjatic, S., Petralia, F., Wang, P., et al. (2019). Prognostic Value of Immune Cells in the Tumor Microenvironment of Early-Stage Lung Cancer: a Meta-Analysis. *Oncotarget* 10, 7142–7155. doi:10.18632/oncotarget.27392

Van der Maaten, L., and Rey Hinton, G. (2008). 'Visualizing Data Using T-SNE. *J. Machine Learn. Res.* 9, 2579–2605.

Wang, B., Wu, S., Zeng, H., Liu, Z., Dong, W., He, W., et al. (2015). CD103 + Tumor Infiltrating Lymphocytes Predict a Favorable Prognosis in Urothelial Cell Carcinoma of the Bladder. *J. Urol.* 194, 556–562. doi:10.1016/j.juro.2015.02.2941

Wang, M., Huang, Y. K., Kong, J. C., Sun, Y., Tantalo, D. G., Yeang, H. X. A., et al. (2020). High-dimensional Analyses Reveal a Distinct Role of T-cell Subsets in the Immune Microenvironment of Gastric Cancer. *Clin. Transl Immunol.* 9, e1127. doi:10.1002/cti2.1127

Wu, D., Sheng, J. Y. P., Su-En, G. T., Chevrier, M., Hua, J., Chen, J., et al. (2019). Comparison between UMAP and T-SNE for Multiplex-Immunofluorescence Derived Single-Cell Data from Tissue Sections. *BioRxiv*. doi:10.7554/elife.49599.023

Yu, C. C., Wortman, J. C., He, T. F., Solomon, S., Zhang, R. Z., Rosario, A., et al. (2020). Physics Approaches to the Spatial Distribution of Immune Cells in Tumors. *Rep. Prog. Phys.* 84, 022601. doi:10.1088/1361-6633/abcd7b

Zhang, L., Conejo-Garcia, J. R., Katsaros, D., Gimotty, P. A., Massobrio, M., Regnani, G., et al. (2003). Intratumoral T Cells, Recurrence, and Survival in Epithelial Ovarian Cancer. *N. Engl. J. Med.* 348, 203–213. doi:10.1056/nejmoa020177

Zheng, X., Weigert, A., Reu, S., Guenther, S., Mansouri, S., Bassaly, B., et al. (2020). Spatial Density and Distribution of Tumor-Associated Macrophages Predict Survival in Non-small Cell Lung Carcinoma. *Cancer Res.* 80, 4414–4425. doi:10.1158/0008-5472.can-20-0069

Zhou, C., Li, J., Wu, Y., Diao, P., Yang, J., and Cheng, J. (2019). High Density of Intratumor CD45RO+ Memory Tumor-Infiltrating Lymphocytes Predicts Favorable Prognosis in Patients with Oral Squamous Cell Carcinoma. *J. Oral Maxillofac Surg.* 77, 536–545. doi:10.1016/j.joms.2018.09.039

Conflict of Interest: The author declares that the research was conducted in the absence of any commercial or financial relationships that could be construed as a potential conflict of interest.

frontiers in Molecular Biosciences

REVIEW
published: 27 July 2021
doi: 10.3389/fmolb.2021.672531

Tissue Multiplex Analyte Detection in Anatomic Pathology – Pathways to Clinical Implementation

*Keith A. Wharton Jr. *, Douglas Wood, Mael Manesse, Kirsteen H. Maclean, Florian Leiss and Aleksandra Zuraw*

Ultivue, Inc., Cambridge, MA, United States

Background: Multiplex tissue analysis has revolutionized our understanding of the tumor microenvironment (TME) with implications for biomarker development and diagnostic testing. Multiplex labeling is used for specific clinical situations, but there remain barriers to expanded use in anatomic pathology practice.

Methods: We review immunohistochemistry (IHC) and related assays used to localize molecules in tissues, with reference to United States regulatory and practice landscapes. We review multiplex methods and strategies used in clinical diagnosis and in research, particularly in immuno-oncology. Within the framework of assay design and testing phases, we examine the suitability of multiplex immunofluorescence (mIF) for clinical diagnostic workflows, considering its advantages and challenges to implementation.

Results: Multiplex labeling is poised to radically transform pathologic diagnosis because it can answer questions about tissue-level biology and single-cell phenotypes that cannot be addressed with traditional IHC biomarker panels. Widespread implementation will require improved detection chemistry, illustrated by InSituPlex technology (Ultivue, Inc., Cambridge, MA) that allows coregistration of hematoxylin and eosin (H&E) and mIF images, greater standardization and interoperability of workflow and data pipelines to facilitate consistent interpretation by pathologists, and integration of multichannel images into digital pathology whole slide imaging (WSI) systems, including interpretation aided by artificial intelligence (AI). Adoption will also be facilitated by evidence that justifies incorporation into clinical practice, an ability to navigate regulatory pathways, and adequate health care budgets and reimbursement. We expand the brightfield WSI system "pixel pathway" concept to multiplex workflows, suggesting that adoption might be accelerated by data standardization centered on cell phenotypes defined by coexpression of multiple molecules.

Conclusion: Multiplex labeling has the potential to complement next generation sequencing in cancer diagnosis by allowing pathologists to visualize and understand every cell in a tissue biopsy slide. Until mIF reagents, digital pathology systems including fluorescence scanners, and data pipelines are standardized, we propose that diagnostic labs will play a crucial role in driving adoption of multiplex tissue diagnostics by using

OPEN ACCESS

Edited by:
Jaime A. Rodriguez-Canales, AstraZeneca, United States

Reviewed by:
Michael J. Surace, AstraZeneca, United States
José Luis Solórzano Rendón, MD Anderson Cancer Center Madrid, Spain

****Correspondence:***
Keith A. Wharton Jr.
keith.wharton@ultivue.com

Specialty section:
This article was submitted to Molecular Diagnostics and Therapeutics, a section of the journal Frontiers in Molecular Biosciences

Received: *26 February 2021*
Accepted: *14 July 2021*
Published: *27 July 2021*

Citation:
Wharton KA, Wood D, Manesse M, Maclean KH, Leiss F and Zuraw A (2021) Tissue Multiplex Analyte Detection in Anatomic Pathology – Pathways to Clinical Implementation. Front. Mol. Biosci. 8:672531. doi: 10.3389/fmolb.2021.672531

retrospective data from tissue collections as a foundation for laboratory-developed test (LDT) implementation and use in prospective trials as companion diagnostics (CDx).

Keywords: multiplex, digital pathology, whole slide image, tumor microenvironment, immunohistochemistry, immunofluorescence, pixel pathway, laboratory developed test

INTRODUCTION

In diverse human cultures, knowledge is disseminated by an esteemed individual who has achieved wisdom through discipline and sacrifice. Visualize the archetype: a wise sage, sitting on a mountain, legs folded, in meditative gaze. Advice seekers climb the mountain to pose their question or dilemma. Magic happens, wisdom is dispensed, and the seeker descends the mountain. From its origins in the mid-19th century to today, diagnostic anatomic pathology follows a similar construct. The foundation of knowledge is histopathology – examination of changes in cells and tissues viewed by microscopy to diagnose disease. The sage is the pathologist, who, through years of observation and discernment dispenses wisdom. Tissue samples and data workflows converge on the mountaintop, where the pathologist's gaze is directed in a microscope. The "magic" is the pathologist's integration, interpretation and judgment of data to establish a diagnosis that is reported in the medical record, codified in journals and textbooks, or simply Tweeted.

Rudolf Virchow, known as the father of histopathology, wrote that the body is like a state "*. . .in which every cell is a citizen. Disease is merely the conflict of citizens of the state. . .*" (Virchow, 1858). Diagnosis of disease, in particular cancer, is based on examination of cells by microscopy and on detection of specific molecules in cells. Proteins and nucleic acids are routinely identified in biopsy tissues by antibody-binding or nucleic hybridization technologies such as IHC and *in situ* hybridization (ISH). Nucleic acid amplification and sequencing technologies such as polymerase chain reaction (PCR) are routinely used in clinical practice to identify molecular alterations such as point mutations, chromosome translocations, and gene amplification/transcript overexpression. In the past decade, next generation sequencing (NGS) of hundreds to thousands of genes in parallel has entered clinical practice, increasing the efficiency of detection of abnormal genes that drive disease and impact treatment choices. Bulk transcript profiling of tissue samples over the past 2 decades has provided critical molecular insights into various cancers including lymphoma (Scott, 2015) and breast cancer (Perou et al., 2010), that have served as the basis of prognostic and predictive transcript signature tests such as OncotypeDX (Exact Sciences) (Siow et al., 2018). More recently, by deeply profiling each "citizen" involved in the conflict, single-cell profiling (transcriptomics, proteomics, etc.) has advanced understanding of cell phenotypes that drive disease, with implications for clinical practice (Marx, 2019; Aldridge and Teichmann, 2020). These data-rich sequencing and profiling techniques are powerful discovery tools, but for diagnostic use, the vast majority of data generated is extraneous and lacks the spatial context of histopathology. Nature's 2020 Method of the year, spatially resolved transcriptomics, captures spatial context, but most of the methods do not have the cellular resolution of histopathology, the size and complexity of data remains largely beyond diagnostic comprehension, and the majority of the data produced will ultimately lack clinical utility (Marx, 2021). We hypothesize that multiplex immunofluorescence (mIF) will emerge as a leading technique that allows each pathologist, within their lab and scope of practice, to answer critical questions about disease diagnosis, prognosis, and prediction of response to the next generation of targeted therapies and their combinations, particularly in immuno-oncology (Tan et al., 2020).

IHC and the Clinical Diagnostic Landscape

Despite increases in molecular diagnostic testing in recent years, IHC remains critical for histopathology diagnosis by revealing various molecular species *in situ* in a tissue sample. In IHC, antibodies against epitope(s) of a specific target (also referred to as a "marker" - most often proteins but also carbohydrates or nucleic acids – because they are used to mark cells) are applied to thin, formalin-fixed and paraffin embedded (FFPE) tissue sections mounted on glass slides. Slide pretreatment ("antigen retrieval") breaks formalin cross links, allowing the antibody to diffuse into the tissue and bind mostly linear peptide (as opposed to conformational) epitopes (Sompuram et al., 2006). Bound antibodies are then detected with visualization reagents, most commonly secondary antibodies conjugated to the enzyme horseradish peroxidase (HRP). With peroxide, HRP converts soluble 3,3′-diaminobenzidine (DAB) into an insoluble brown precipitate that reflects antigen abundance and distribution in otherwise colorless tissue. Tissue structure is then visualized with a counterstain, typically hematoxylin, which labels, predominantly nuclei, a bluish-purple color. Robotic autostainers and optimized, prediluted reagents have improved speed and reproducibility of IHC in disease diagnosis (Grogan, 1992; Prichard, 2014). ISH to detect DNA is used to identify chromosomal translocations and gene copy number changes, and RNAscope (Advanced Cell Diagnostics, BioTechne Inc.) has emerged as a sensitive ISH technique to visualize RNA in FFPE tissue, offering advantages over traditional RNA ISH techniques to detect low abundance transcripts, and over antibodies in detecting some targets such as soluble cytokines or infectious agents (Wang et al., 2012; Carossino et al., 2020; Stein et al., 2021). The DAB/hematoxylin-stained slide is interpreted by a pathologist using a microscope, or increasingly, by viewing a scanner-generated whole slide image (WSI) on a computer monitor (Gurcan et al., 2009; Dimitriou et al., 2019).

How is IHC used in clinical diagnosis? Early IHC applications in the 1970s and 80s distinguished between major categories of

neoplasia through demonstration, for example, that carcinomas express cytokeratins and lymphomas express leukocytic antigens, but not *vice versa* (Taylor, 1980; Debus et al., 1984). Over several decades the diagnostic roles for IHC have expanded to include: aiding in distinction between benign and malignant processes [e.g., p53 upregulation associated with malignancy (Yemelyanova et al., 2011), or p16 expression with HPV-positive squamous carcinomas (Shelton et al., 2017)], identification of specific cell types (e.g., CD68-positive macrophages, CD31-positive endothelial cells, Foxp3-positive regulatory T lymphocytes), subclassifying and refining diagnoses [e.g., association of marker positivity or negativity with histopathology-based differential diagnosis or molecular lesion, such as DNA mismatch repair deficient carcinomas (Wong et al., 2018) or BAP1-subtype melanomas (Shah et al., 2013)], providing information about disease drivers [e.g., C-myc translocated Burkitt's lymphoma (Nwanze et al., 2017), N-myc amplified neuroblastoma (Santiago et al., 2019), EGFR-amplified cancers (Atkins et al., 2004)], allowing inference of various cell states and behaviors (e.g., Ki67 positivity and cell proliferation, Granzyme B positivity and activated cytotoxic T lymphocytes), activity of various growth stimulating and inhibiting pathways (Ras/MAPK, Hippo, Wnt/β-catenin, Hedgehog, Notch, TGF-β, and others), and assessment of predictive biomarkers associated with response to targeted therapies (Her2, ER/PR, PD-L1). While IHC may be capable of revealing a molecule of importance within tissue, whether it is the favored diagnostic modality is dependent on clinical context and test performance relative to other options such as FISH or NGS, such as is the case with detection of NTRK-family gene translocations that occur with low frequency in a wide variety of malignancies (Solomon et al., 2020).

Diagnostic IHC tests evolve. Pathologists refine IHC tests by testing new antibody clones, platforms, and detection reagents, and create new IHC tests based on markers discovered through research, diagnostic surveys, or to recapitulate other tests such as DNA mutation sequencing [e.g., mutation-specific antibodies such as BRAF V600E (Tetzlaff et al., 2015)] or transcript profiling [IHC panels to recapitulate subtypes of diffuse large B cell lymphomas (Yan et al., 2020a)]. Candidate IHC markers start in research laboratories—and most markers stay in research applications. A new marker can enter diagnostic practice through retrospective studies that demonstrate the marker's improved utility over existing markers in defining a diagnosis or prognosis in a particular lesion type. Alternatively, the marker can enter diagnostic practice as the basis of a new standard of care through prospective investigations as a companion diagnostic (CDx) assay, as was the case with Her2 and PD-L1 IHC tests (Roach et al., 2016).

Because IHC tests are interpreted visually by a pathologist, marker choice and assay optimization is part science, part art – the intersection of truth and beauty. "Beauty" is ultimately subjective, assessed by signal strength, staining pattern, and signal to noise, whereas "truth" is assessed by biological plausibility, comparison of staining to reference standards (if they exist), and eliminating artifacts (Tsutsumi, 2021). Each IHC slide is typically scored for positivity or negativity of the tested marker in specific cell types; for cancer, whether the marker is present in cancer cells or the tumor microenvironment (TME) or both is assessed, always with reference to the location and appearance of different cell populations in the corresponding section stained with H&E. IHC CDx's are usually scored in a semiquantitative fashion, based on marker distribution, percent of positive cells and/or stain intensity. However, it is important to note that IHC marker panels only aid in establishing a diagnosis of cancer; rather, it is the appearance of individual cells and overall tissue by H&E that forms the basis of a cancer diagnosis, with interpretation of a specific set of IHC stains helping to confirm, refine, or subclassify a diagnosis. For example, a lung cancer biopsy showing "carcinoma" on the H&E section is typically stained for a set of markers to determine whether it is best classified as adenocarcinoma or squamous carcinoma, as most adenocarcinomas will be positive for TTF1 and NapsinA, but negative for p63, and *vice versa* (Inamura, 2018). For carcinomas with unambiguous squamous, ductular, or other type of differentiation, IHC stains usually confirm the histological impression, but for the not uncommon tumor that displays few or paradoxical features of differentiation (e.g., epithelioid sarcomas, which display epithelial differentiation but express mesenchymal markers, or sarcomatoid carcinomas, which display mesenchymal differentiation but express epithelial markers), IHC marker panels are crucial for accurate, state of the art histopathology diagnosis (Huey et al., 2019; Czarnecka et al., 2020).

Today, most IHCs are used as an adjunctive to diagnosis, with specific markers chosen in groups or panels based on algorithms that aim to subclassify the lesion and answer diagnostic questions relevant to the specific clinical scenario (patient age, anatomic location), specimen type (skin, soft tissue), and histologic features of the H&E-stained tissue. In the United States, IHC of adjunctive markers poses a relatively low risk to patients because they are often used redundantly, as part of a panel or suggested diagnostic algorithm. Such algorithms are typically not standardized, with variation in algorithms across institutions and geographies attributed to variation in medical practice. Thus, a testing error - a false positive or false negative result - of a single IHC assay is unlikely to impact the final diagnosis. Accordingly, adjunctive IHC tests are classified by the United States Food and Drug Administration (FDA) in the lowest risk class (Class I) of *in vitro* diagnostics (IVD) (Medical Devices, 1998). A small but critical and growing set of markers, such as Her2, ER, PR, and PD-L1, predict (or, at best enrich for) response to specific therapies and are classified as companion diagnostics (CDx) (Scheerens et al., 2017). A related category of test, a complementary diagnostic, is similar to a CDx by providing useful predictive information, but is not required to administer a particular therapy (Scheerens et al., 2017). Predictive IHC markers are often single "high stakes" tests, errors in which entail a greater risk to patient safety, and are thus classified by FDA in the highest risk class (class III) of IVD (Jørgensen, 2016). While some benign and a few malignant diagnoses do not require any IHC, the current standard of diagnosis in 2021 for most malignant diagnoses, in particular a patient's initial diagnosis, requires some IHC tests.

IHC used for patient diagnosis as a basis of medical decision making is regulated in the United States at a variety of levels. Assays must be validated and performed in a Clinical Laboratory Improvement Amendments (CLIA)-certified diagnostic laboratory, and be interpreted by qualified personnel such as a pathologist licensed to practice medicine in the state where the sample originates (Fetsch and Abati, 2010). Further lab certification by the College of American Pathologists (CAP) covers CLIA standards as well as assay performance assessment, proficiency testing, and adherence to specific practice guidelines such as processing and interpretation of breast cancer specimens (College of American Pathologists LEP, 2017). States such as New York have more rigorous laboratory standards and certification, enforced by the New York State Department of Health (NYSDOH) (New York State CLEP, 2021). A largely comparable but distinct international standard for diagnostic medical laboratories is ISO 15189 (Schneider et al., 2017). Laboratory tests are generally of two types: IVDs and Laboratory Developed Tests (LDT). While both test types require in-laboratory assay validation, IVDs are components and/or systems manufactured and distributed to laboratories for a specific purpose defined by an intended use statement, whereas LDTs are custom "single site" tests that may not be performed in laboratories other than where the test was developed. FDA regulates both IVDs and LDTs, but exercises enforcement discretion over most LDTs as constituting a part of medical practice, which is not regulated by FDA (Genzen, 2019). LDT and related regulation in the United States has been subject to attention and neglect over decades, and is not yet settled (Genzen et al., 2017). Recently, the United States VALID (Verifying Accurate, Leading-edge IVCT Development) Act, which proposes to classify all assays performed in diagnostic laboratories as *In Vitro* Clinical Tests (IVCT) and would allow the FDA to exert greater oversight of testing based on patient risk, has undergone several cycles of stakeholder feedback and revision (Konnick, 2020). In Europe, new legislation (IVDR) that applies to IVDs takes effect in May 2022, with implications for LDT development and practice (Bank et al., 2020; Stenzinger and Weichert, 2020). The language, interpretation, and enforcement of these regulations will impact global test development and deployment, particularly new tests based on innovative technologies, for decades to come (Huang et al., 2021).

Not all LDTs are equivalent, generally falling into two categories. A *de novo* or traditional LDT is a novel test "system" made from individual components, often sourced separately, each piece of equipment, input reagent, or other part of the assay system which may be labeled as an IVDs or for Research Use Only (RUO). A derived LDT is when a laboratory alters system components, instrument settings, or reaction conditions of an approved or cleared IVD, such that system definition and/or laboratory use deviates from the original product design and/or intended use statement of the parent IVD. If an LDT uses an IVD-labeled component, either type of LDT is considered an "off label" use of the IVD component. With IVDs, responsibility for test performance and thus risk of test failure is shared between the device manufacturer and the laboratory: the manufacturer is responsible for design, manufacturing, and performance of the IVD under defined conditions, and the laboratory is responsible for using the assay/device according to those conditions—only for its defined and specific purpose. In contrast, LDTs are the primary responsibility of the laboratory offering the test. Many IVD assays were first introduced to clinical practice as LDTs, so one key advantage of LDTs is the ability to quickly bring novel diagnostic technology to clinical practice. However, accompanying the lower barrier of LDTs to market entry is the possibility that poorly designed, developed, or performing tests may be used in patient care. Typically, the strict design, manufacturing, and testing requirements of IVDs are associated with more robust real-world product performance (such as accuracy, precision, multisite/multi-operator consistency, known failure modes with risk mitigation strategies in place) as well as market exclusivity that justifies a premium price or level of reimbursement. However, established IVDs can act as a barrier to rapid technological innovation by blocking competing technologies or companies who may offer superior technology or aspects of performance (e.g., lower cost, faster turn-around time, greater analytical sensitivity) but lack adequate clinical evidence to gain regulatory approval that drives adoption.

Visualizing Multiple Markers

Cells of the immune system and the majority of hematolymphoid neoplasms are defined by coexpression of multiple cell surface markers, commonly assessed by flow cytometry. However, the vast majority of IHCs used in clinical diagnosis of solid tumors interrogate a single marker per tissue section (termed "singleplex") and are thus unsuited to characterize cell phenotypes defined by coexpression of multiple markers when those markers are in the same subcellular compartment. In current diagnostic practice, many cases require multiple IHC markers, and the pathologist examines one marker at a time, one slide at a time, noting which cell populations on the slide are positive vs. negative for each marker then integrating the results to establish a final diagnosis. Occasional cases, particularly undifferentiated solid tumors and lymphomas, require more than two dozen different markers to arrive at a proper diagnosis, making the task of tallying and interpreting IHC results challenging. For such tumors, molecular profiling is playing an increasingly important diagnostic role (Yan et al., 2020b). For tumors in which sampling may be restricted to fine needle aspirates (FNA) or core needle biopsies (CNB) that yield limiting tissue, using multiple consecutive sections for singleplex IHC as well as possibly splitting the biopsy for diagnostic molecular testing such as PCR or NGS can compromise accurate diagnosis. For example, the majority of lung cancer patients present with advanced disease that is not amenable to surgical intervention, so diagnostic, prognostic, and predictive factors must be obtained from FNA or CNB of a mediastinal lymph node, or even a "liquid biopsy" (NGS to detect circulating tumor DNA in a peripheral blood sample) (Chen and Zhao, 2019). For such cases, multiplex staining allows visualization of all markers of interest using a minimal number of tissue sections.

By performing sequential or simultaneous chromogenic IHC staining reactions on a single slide, it is possible to generate

multiplex chromogenic stained slides (Morrison et al., 2020). However, there are only limited diagnostic scenarios where chromogenic multiplex staining is currently used. These are situations in which the pathologist has greater confidence in a diagnosis when two markers labeling different cell populations or tissue compartments are present in the *same slide* than when the same two markers are present in *different slides* of the same tissue block. Given the availability of >1 enzyme to detect antibodies in chromogenic IHC [in addition to HRP, alkaline phosphatase (AP) is commonly used], and various enzyme substrates with distinct absorption spectra, two or more staining reactions can be performed sequentially, creating two or more different colors (plus a counterstain), each color representing a different marker or cocktail (mixture) of markers. Such assays typically require more complex test development and validation to ensure the multiplex staining reactions recapitulate the performance of each singleplex marker. For labs requiring fast assay turn-around time, duplex assays take longer to develop, cost per slide is typically higher than an equivalent number of singleplex reactions, and, at least in the United States, reimbursement mechanisms to incentivize use do not exist. One widely used stain is "PIN4," which labels, in different colors, benign and malignant cell populations on the same slide to help the pathologist distinguish *in situ* from invasive cancer (Tacha and Miller, 2004). Most chromogenic multiplex assays are developed to label separate cell populations (e.g., cancer vs. non-cancer cells) or cell structures (plasma membrane vs. nucleus of same cell), without the intention of assessing marker colocalization, and, like adjunctive singleplex IHCs, are also interpreted in a qualitative fashion by a pathologist using light microscopy. There are many multiplex marker combinations commercially available (see e.g., BioCare Medical, Cell Marque, Mosaic Laboratory websites), and for ease of application to a wide variety of clinical scenarios most currently available kits consist of adjunctive diagnostic markers (United States FDA risk class I).

Assessment of marker coexpression (within cells) and colocalization (by x-y pixel value coordinates) with current chromogenic IHC methods can be challenging. For singleplex DAB/IHC stains, it is usually straightforward to discern whether specific *populations* of cells (e.g., cancer cells, mononuclear inflammatory cells, vascular cells) are positive or negative for each marker. However, due to the requirement for IHC of one section per marker and the size of most cells (~10 μm) relative to typical section thickness (4–5 μm), it is difficult to discern whether specific *cells* seen in an adjacent H&E-stained section are positive or negative for a given marker, and impossible to tell whether such cells viewed in the original H&E section are positive for more than two IHC markers. For current multiplex IHC assays that precipitate chromogens in tissue, when two different markers colocalize to the same subcellular compartment in the same cells, most commonly with brown and red chromogens, marker colocalization is easily overlooked. This is because mixing light-absorbing chromogens generates dark signals that to the human eye can mimic dark staining of individual chromogens, and overlapping absorption spectra of many chromogens can confound digital image collection and analysis. Another challenge is determination whether lack of marker colocalization is genuine or due to technical interference based on assay technology or design. Moreover, in triplex or higher-plex chromogenic assays, even when markers localize to completely different cell populations, it is difficult for the human brain to comprehend the multicolored patterns and to accurately quantify cell intensities and proportions of positive cells for each marker. Confidence in visual recognition of marker colocalization may be further compromised by microscope setup as well as the limited sensitivity and dynamic range of chromogenic assays. Thus, current singleplex and multiplex chromogenic IHC technologies offer only a limited capability to assess multiple marker colocalization in specific cells. Moreover, as the need to define newly recognized cell phenotypes characterized by simultaneous expression of multiple markers increases, comprehension of stained tissue sections will require automated image acquisition (slide scanning) and software-assisted marker visualization and interpretation.

Immunotherapy, the Tumor Microenvironment and Multiplex Staining

In the past decade, immunotherapies have transformed oncology research and clinical practice while revealing the importance of endogenous immune "checkpoints" such as PD-L1 and CTLA4 that prevent cytotoxic T lymphocytes in the tumor microenvironment (TME) from targeting a variety of hematological and solid malignancies (Couzin-Frankel, 2013). Despite widespread use of predictive singleplex PD-L1 IHC tests to enrich for likelihood of response to PD-1/PD-L1 axis blockade, the majority of patients do not benefit, and effectiveness is limited in several cancer types likely due to a highly immunosuppressive TME or lack of tumor-specific antigens (Xu-Monette et al., 2017; Hack et al., 2020). By contrast, ipilimumab, targeting CTLA4, does not have an accompanying predictive IHC CDx, although expression of MHC class I has been associated with response to ipilimumab in melanoma (Rodig et al., 2018). Immunoscore® (HalioDx) is an image analysis-based IHC assessment of CD3 and CD8 positive T lymphocytes in defined regions of a tumor biopsy sample, which has shown clinical utility in colon cancer (Angell et al., 2020; Bruni et al., 2020). In recognition of this and other work, tumor immune microenvironment has been added as a prognostic factor by the WHO tumor classification of colon cancer (Digestive System Tumours, 2019). It is important to note that development of Immunoscore preceded successful blockade of immune checkpoint targets in human (Galon et al., 2006), so these and other immune checkpoints as well as other TME immune cell phenotypes of known importance are not assessed by Immunoscore. A better understanding of the interactions among tumor, immune cell subsets, immune checkpoint pathways and other cell types in the TME, including response and resistance mechanisms, will be crucial to develop effective cancer therapies.

The TME is a complex ecosystem consisting of tumor cells, endogenous and tumor-induced stromal cells, vasculature (including vascular endothelia, pericytes, and perivascular cells), nerves and other sensory structures, and various organ/tissue-resident and recruited immune cell types as well

as non-cellular components of the extracellular matrix such as collagen, fibronectins, and proteoglycans (Li et al., 2021; Rameshbabu et al., 2021; Vitale et al., 2021). The TME promotes tumor stem cell renewal, proliferation, invasion, and angiogenesis while creating an immunosuppressive environment (Nicholas et al., 2016; Najafi et al., 2019). In solid tumors, dense stromal collagen (desmoplasia) creates a physical barrier that supports cancer growth, in part by promoting hypoxia and precluding entry of immune cells into the tumor mass while maintaining blood vessels that allow tumor cells to metastasize (Mortezaee, 2021), a particularly common feature of pancreatic cancer (Bulle and Lim, 2020). Other components of the TME, such as tumor-associated macrophages (TAMs) (Vitale et al., 2019) and intercellular signals such as IL10 (Ouyang and O'Garra, 2019) and TGF-β (Ganesh and Massagué, 2018) represent therapeutic targets responsible for primary resistance to immune checkpoint blockade (Bulle and Lim, 2020).

Recent advances in cell profiling technologies, data analysis, and visualization tools have unveiled a hitherto unappreciated complexity of the TME and its constituent cell phenotypes (Galon et al., 2006; Digestive System Tumours, 2019; Angell et al., 2020; Bruni et al., 2020). As many TME cell phenotypes most relevant to immuno-oncology are defined by simultaneous detection of more than two markers, singleplex IHC panels will be inadequate to unambiguously identify these cell types in a single tissue section. Several technologies have recently been employed to characterize the TME in research investigations, including multiplexed immunohistochemistry (mIHC) and immunofluorescence (mIF) (Hofman et al., 2019; Parra et al., 2019), mass spectrometry (IMC/CyTOF, MIBI) (Baharlou et al., 2019), single-cell RNA sequencing (scRNAseq) (de Vries et al., 2020), and spatial transcriptomics (Ji et al., 2020).

Several recent studies have employed multiplex methods to investigate the relationship between TME and treatment efficacy as part of exploratory or retrospective analyses of tissue biopsies from clinical trial cohorts. Chaudhary et al. evaluated both short- and long-term effects of prexasertib, a CHEK1 checkpoint kinase inhibitor, on TME of head and neck squamous cell carcinoma, coupling transcriptomics with multiplex mIHC (Chaudhary et al., 2021). Acutely, treated tumors demonstrated increased expression of T-cell activation and immune cell trafficking transcripts and decreased expression of immunosuppression-related transcripts, but over the longer time points there was an increase in immunosuppression-related transcripts suggesting evasion of immune surveillance that correlated with acquired prexasertib resistance. Schwarze et al. used IHC and mIF on cancer biopsies from a phase IB trial of immune checkpoint inhibition combined with administration of myeloid dendritic cells, revealing treatment-related immune cell infiltration into tumor (Schwarze et al., 2020). Sathe et al. integrated scRNAseq with mIHC to demonstrate dramatic increases in exhausted and regulatory T lymphocytes in gastic carcinoma compared to normal mucosa (Sathe et al., 2020). Gundle et al., in reporting microdosing of drug combinations in soft tissue sarcoma (STS), used mIHC and GeoMx Digital Spatial Profiling (Nanostring) to reveal putative mechanisms of tumor resistance to drug treatment (Gundle et al., 2020). These studies highlight the power of multiplex analysis to reveal a variety of immune cell phenotypes and their spatial arrangements in the TME from a single cancer biopsy, and based on these reports we anticipate growing use of multiplex technologies to probe patient tumor biopsies.

Multiplex Technologies and the Path From Research to the Clinic

We hypothesize that multiplex technologies most likely to reach clinical application, at least initially, will need to fit in existing histopathology sample workflow with results able to be viewed and interpreted on computer monitors. Many multiplex technologies use fluorescence emission as a means of marker visualization, with some combination of simultaneous and/or cyclic sequential labeling and detection (Lin et al., 2018; Tan et al., 2020). Because fluorescence microscopy is a mature research technique that is already used for a limited number of clinical applications, we believe fluorescence detection will be best suited for initial clinical use.

Diagnostic fluorescence microscopy in use today

The use of fluorescence microscopy in routine diagnostic anatomic pathology is currently limited to DNA ISH to detect chromosomal abnormalities (translocations, gene amplifications) and to antibody-based investigations of specific immune and genetic diseases in dermatopathology and nephropathology. A fluorescence microscope and its accompanying viewing monitor are typically located in a darkroom, outside of the main lab, in order for users' eyes to accommodate viewing images with a dark background. In contrast, the background of the H&E or DAB-stained image viewed in a brightfield microscope is usually white, and such images can be comfortably viewed for hours in a brightly lit room. Typically, dedicated technicians gather images from fluorescent diagnostic assays (e.g., DNA FISH) for the pathologist to review for case sign-out, freeing the pathologist from the dark room. One solution to the "dark room" problem is for the pathologist to review and interpret fluorescent WSI, possibly with false coloring or color inversion to create an artificial white background on a computer screen. Such images can be obtained from whole slide fluorescence scanners, that, unlike the fluorescent microscope, are not required to sit in a darkroom, but rather feature automated workflows and high throughput for enhanced viewing and analysis on computer monitors.

Differences between brightfield and fluorescence microscopy

In addition to these practical differences between fluorescence microscopy and brightfield microscopy, there are important differences in the relevant laws of physics that underlie viewing stained tissue by each type of microscopy. To the detector, whether a camera or the human eye, brightfield microscopy measures an absorption process (subtraction of light), while fluorescence microscopy measures an emissions process (addition of light). Radiative transfer, which accounts

for the emission and transport of electromagnetic radiation (light) through a medium, confers significant advantages for fluorescence over brightfield imaging in terms of dynamic range, sensitivity, and the ability to measure multiple signals at once (multiplexing):

Dynamic range

With chromogenic staining and brightfield microscopy, transmitted light passes through the sample, and light intensity in each "column" of absorption [i.e., tissue thickness (z) at each x-y coordinate of the tissue plane] is inversely proportional to the abundance of deposited chromogen. Once the absorption column has become optically thick ($e^{-\tau}$ where the optical depth, $\tau > 1$), the ability to detect additional chromogen in a heavily stained column becomes exponentially more difficult (i.e., the stain "shadows" itself). Consequently, with heavy staining, section thickness and enzyme reaction time can dramatically impact perceived stain intensity and can create challenges in consistently distinguishing between moderate vs. strong staining in semiquantitative IHC assays. In addition, chromogen diffusion can leave a lightly stained "diffusion halo" of several hundred nanometers or more around intensely stained structures (more prominent with fast-red based detection by alkaline phosphatase). In areas with low levels of chromogenic staining, focal plane, objective lens magnification and numerical aperture, and other features of the optical system can impact detection sensitivity. A recent study on focus standardization of H&E-stained WSI, obtained from different scanners, revealed that a substantial amount of out of focus information is retained by an "in focus" brightfield image (Kohlberger et al., 2019). Fluorescence imaging uses a completely different method to detect marker abundance, with the intensity of the emission column at each x-y position in the sample being directly proportional to amount of the fluorophore in the column. Because a thin tissue section is nearly optically transparent, essentially all emitted light from fluorophores passes easily through the column and is detected by the camera. As discussed above, colocalization of chromogenic dyes increases the darkness of tissue when viewed by brightfield microscopy, whereas with fluorescence based detection overlapping signals become brighter with increased marker abundance. These differences in the physics of brightfield vs. fluorescence imaging contribute to the fact that, in practice, HRP/DAB is limited to ~2 orders of magnitude of dynamic range while fluorescence can detect ~5–6 orders of magnitude, approaching the intrinsic dynamic range of the protein concentration in biological specimens of ~7 orders of magnitude or more (Rimm, 2006; Zimak et al., 2012; Vani et al., 2017).

Sensitivity

In fluorescence imaging, to achieve higher sensitivity one can increase the excitation light intensity to further increase the flux of emitted light and/or increase camera exposure time to collect additional signal. Autofluorescence of some FFPE tissues can limit sensitivity by increasing background emissions at different wavelengths (Lazarus et al., 2019). With chromogenic imaging, above a certain level of absorption there is little sensitivity gained with brighter illumination. The fluorescent signal can also be amplified by introducing more fluorophores per antibody in the staining assay (Zimak et al., 2012), while for chromogenic staining, adding more absorbing molecules has a fast-diminishing effect once the optical depth of the stain column is above a certain amount.

Higher-order marker multiplexing

Higher order multiplexing is possible for fluorescence imaging because the absorption and emission spectra of fluorescent probes are generally narrower than those of chromogenic stains. Given the finite bandwidth of the optical spectrum, this property allows for a greater number of multiplexed signals to be simultaneously detected—typically five fluorescent channels with conventional filter sets and up eight or nine channels with special filter sets and "spectral unmixing" (defined below) as compared with two or three simultaneous colocalized colors in a chromogenic image. DAB, the most commonly used chromogen, has a broad transmission spectrum overlapping with red and yellow (Gordon, 1988), making it difficult to accurately quantify DAB when other chromogens are present. Spectral unmixing is a mathematical operation, a nonlinear least-squares fit, that estimates the proportion of each fluorophore's contribution (and any tissue autofluorescence) to the overall spectrum at each wavelength when there is spectral overlap (spectral bleed-through) (Dickinson et al., 2001). But, when considering potential diagnostic uses of fluorescence, a requirement for spectral unmixing in the detection system may compromise consistent tracing of information through the so-called "pixel pathway" - the framework, described below, that governs how regulatory bodies view WSI systems for diagnostic use (Abels and Pantanowitz, 2017).

Standardization of multiplex immunofluorescence workflows. Fluorescence microscopy as a technique is far less standardized than brightfield microscopy, with each microscope manufacturer offering distinct lens materials, light sources, optical paths, filter and mirror sets, detection cameras, and viewing software. With mIF, microscopists can generate images that maximize signal to noise ratios for the given marker, antibody clone, fluorophore, tissue/sample type, preparation method, strength of emission light, camera exposure time, and experimental aim—all too frequently with only the goal of generating a beautiful and visually striking image for a publication, journal cover, or marketing material. However, these parameters require simultaneous optimization to achieve an optimal result—which might be very different for the next experimental condition, set of tissue samples, equipment setup, or laboratory. There are increasing options for whole slide fluorescence scanners that create multiplex WSIs, but these are not yet standardized with respect to how images are generated or how the output files are formatted. A critical aspect of diagnostic development and validation, even in a single laboratory, is defining the diagnostic system, locking it down, and then testing performance on scaled sample sets in relation to the assay's expected use. Thus, one major challenge of implementing

fluorescence-based tissue marker detection in clinical practice is defining the best system parameters from a wide variety of system components and configurations so that the fluorescent images can be compared to ground truth, typically "gold standard" brightfield IHC images.

Thus, for diagnostic use mIF has numerous potential advantages over enzyme-based chromogenic staining, allowing simultaneous detection of multiple markers in individual cells and reducing the number of tissue sections necessary for complete assessment of markers currently tested with IHC. As noted, this may be advantageous in situations where diagnostic tissue is limiting, such as lung cancer. Most importantly, as deep profiling methods (transcriptomics, proteomics) are used to probe individual cells in normal and diseased tissues, most notably as part of the Human Cell Atlas (Regev et al., 2017), it should be possible to specify a standard, minimal set of markers to unambiguously identify specific and well-defined pathogenic cell types and their locations using mIF on tissue biopsies.

Phases of multiplex immunofluorescence testing. A useful framework to consider mIF assays is the preanatlytic, analytic, and postanalytic phases of testing. For DAB/IHC assays, the analytic phase is staining itself, either manually by a technician or by an autostainer. Preanalytic factors include all steps from sample procurement to staining, including fixation, processing, embedding, slide preparation, and any manual tissue pretreatment. It is estimated there are over 100 discrete steps in the preanalytic phase, and beyond formalin fixation past a certain time (e.g., 8 h for ER/PR IHC of breast biopsies per CAP recommendations), practices are not standardized and thus vary widely (Agrawal et al., 2018; Compton et al., 2019). Importantly, antigen retrieval steps that lyse formalin cross links and expose epitopes prior to staining allow many singleplex IHC assays to retain robust assay performance, at least for qualitative interpretation, despite variation in preanalytics (Bogen et al., 2009). The analytic phase on the autostainer includes any automated pretreatments, antibody blocking and incubation steps, washes, and enzyme-based signal detection. The postanalytic phase includes applying the slide coverslip, any post-run slide labeling, and interpretation by the pathologist. Variation in any of these test phases can cause variation in results, as well as false positive or false negative results. Over 4 decades of practice experience with DAB-based IHCs has led to improved diagnostic assay standardization that—considering disparate reagent sources and automation platforms – allows for some degree of comparability between assays across antibody clones, platforms, and laboratories. Such inter-assay comparability is emphasized by FDA in IHC guidance documents and IHC-based product approvals (Guidance for Industry, 1998) as well as CAP-recommended updates in assay interpretation [e.g., for the Her2 IHC and FISH assays (Wolff et al., 2018)]. mIF workflows are far less standardized, and quantitation of images requires additional analytic and post-analytic steps such as fluorescent slide scanning and image capture, image processing and analysis, and viewing on a computer monitor. Thus, for mIF the diagnostic workflow is expanded relative to traditional IHC, such that the postanalytic steps of staining become the preanalytic steps for slide scanning and analysis. Tissue and slide quality impacts scan quality, which can vary widely between vendors, models, and laboratories; scan quality in turn influences image analysis (Dunstan et al., 2011; Webster and Dunstan, 2014) as well as performance of AI algorithms (Cui and Zhang, 2021).

Multiplex fluorescence technologies. Several multiplex assay platforms, technologies, and protocols have been recently reviewed (Lin et al., 2018; Hofman et al., 2019; Francisco-Cruz et al., 2020; Tan et al., 2020; McGinnis et al., 2021). Traditional mIF assays use fluorophores directly conjugated to primary or secondary antibodies. With traditional IHC, sensitivity is enhanced by increasing the number of HRP molecules per primary antibody, such as by avidin/biotin complexes or HRP-polymers. The same principle holds for mIF, with sensitivity enhanced by increasing the number of fluorophores per primary antibody molecule, allowing generation of quantitative data across analyte concentration ranges that reflect relevant physiologic or pathological states in tissue (Zimak et al., 2012). In newer mIF methods, application and detection of antibodies can be sequential, simultaneous, or some combination thereof. Some methods can be performed manually, but recent data suggests automation improves precision and reproducibility (Surace et al., 2019; Taube et al., 2020), performance attributes that will be essential to build confidence in diagnostic use. In each method, specific fluorophores need to be matched to antibody/target molecule, emissions spectra, filter sets, camera settings, tissue type, and proposed data analysis pipeline. A variety of mIF methods, including hapten-based, cyclic tyramide-based amplification and DNA barcode-based detection allow higher sensitivity and higher order multiplexing beyond the traditional species barriers imposed by secondary antibody-based detection. Emerging methods such as CODEX (Akoya, Inc.) (Goltsev et al., 2018), MACsima (Miltenyi Biotec), Orion (Rarecyte, Inc.), GeoMx Digital Spatial Profiling (Nanostring, Inc.) (Toki et al., 2019), and Visium FFPE (10x Genomics) generate higher-plex spatial analysis (20–40 or more markers on a single section), but we speculate these techniques are better suited for discovery rather than immediate clinical applications until challenges associated with long turnaround times, high cost per sample, sample destruction, and stringent validation requirements are overcome.

Among the most widely used mIF method, especially in immuno-oncology, is Tyramide Signal Amplification (TSA) (Opal, Akoya, Inc.), a cyclic staining protocol using tyramide-conjugated fluorophores (Stack et al., 2014). Briefly, the TSA method amplifies fluorescent signals through a polymer-HRP detection system similar to traditional IHC, but instead of using DAB to deposit chromogen, HRP activates tyramide to covalently bind multiple tyrosine residues near the epitope of interest. Non-covalently bound antibodies are then stripped using heat, while tyramide-linked fluorophores accumulate on the tissue with each cycle of staining. This staining/amplification cycle is then repeated up to 7 more times (generating up to an 8-plex image) with different antibody/fluorophore combinations, with consideration to order of target detection as well as rigorous controls required during assay development and with each experiment to ensure accurate detection of each marker. Once an assay is developed, the advantages of this technique are its

simplicity, enhanced sensitivity relative to fluorophore-linked secondary antibodies, high specificity, and compatibility with most fluorescent microscopy systems. Spectral unmixing, discussed above, is an obligate requirement in the Opal workflow. With multiple rounds of epitope retrieval, tissue integrity may become compromised, limiting assay plexy and precluding use of the mIF slide for additional assays such as H&E staining. A recent improvement in the TSA method using a stripping buffer instead of heat underscores the importance of maintaining tissue integrity for any mIF analysis (Willemsen et al., 2021).

One recently developed method with several advantages over cyclic TSA-amplification is Ultivue's InSituPlex (ISP) technology (**Figure 1**). Antibodies against four different targets are each conjugated to a unique DNA barcode sequence. After a single antigen retrieval step, all antibody-DNA conjugates are applied to the slide. The barcodes on each antibody are then amplified *in situ*, avoiding secondary antibodies that can exhibit unwanted cross-reactivity. Next, fluorescent probes complementary to each barcode label each target, enhancing sensitivity. ISP has been automated on autostainers (BOND RX, Leica Biosystems), and slides can be imaged on a variety of fluorescent scanners and analyzed using any image analysis software. ISP can be performed in multiples of 4-plex (e.g., 8, 12, 16 plex) by applying all barcoded antibodies simultaneously and then detecting four fluorophores (plus nuclear counterstain to detect DNA and mark cells) per cycle. ISP features a rapid, low-complexity, easily automated workflow with pre-optimized, highly sensitive assays that can deliver reproducible results comparable to other methods (Humphries et al., 2020), but with high throughput and faster assay development times than TSA-based assays. Because ISP uses standard, gentle antigen retrieval, following mIF staining the slide can then be stained for H&E and the resulting WSI precisely merged with mIF data, allowing association of every cell in the H&E section with its marker profile (**Figure 2**).

Quantitative analysis of multiplex fluorescence images. Image analysis software is required to analyze the massive datasets created by whole slide mIF. A subdiscipline of computer vision, image analysis can be applied to WSI to quantify marker pixel counts or structures in regions of interest (such as tumor vs. nontumor) selected manually or in an automated fashion using marker status or AI. Various cell types, defined by the presence or absence of one or more markers, can be quantified in the tissue section by number, location, density, proximity to other cell types or structures, or any other metric of interest. Tissue image analysis using rules-based machine learning algorithms has been used for decades in research, yet the few FDA-cleared clinical applications for image analysis of IHC are mostly restricted to algorithms that quantify CDx markers such as Her2 and ER/PR (Abels et al., 2019; Aeffner et al., 2019; Zuraw et al., 2020; Digital Pathology Association, 2021). Recently, deep learning-based AI algorithms have been employed to analyze large collections of H&E tissue slides to identify tissue features such as various types of cancer and to predict molecular lesions such as specific gene mutations (Couture, 2019; Chen et al., 2020; Rana et al., 2020; Echle et al., 2021; van der Laak et al., 2021), providing proofs of concept that image analysis can detect information in WSIs that are not detectable by a trained human observer. We hypothesize that unambiguous assignment of multi-marker cell phenotype to every cell in the tissue section, achieved by precise coregistration of H&E and mIF images, will augment interpretation of the H&E section, whether read by a human pathologist or an AI algorithm.

Regions of interest. One major area of relevance to cancer diagnostics concerns specification of regions of interest (ROI) in each tissue sample. Pathologists use (and are legally required to view) representative sections of all stained tissue blocks, typically by H&E and IHCs, to render a diagnosis; to do otherwise, by intentional or unintentional omission of tissues for review, increases likelihood of misdiagnosis and constitutes grounds for malpractice. For TME assessment in immuno-oncology, how many and which areas of the slide to analyze remains largely undefined. Beyond the categories of hot, warm, and cold tumors based on location and density of inflammatory infiltrates (Bonaventura et al., 2019) - more recently referred to as inflamed, immune excluded, and immune desert, respectively (Hegde and Chen, 2020) - many tumors exhibit heterogeneity and intermediate attributes between these categories, and even tumors classified as "hot" exhibit heterogeneity unrecognized by traditional IHC analysis (Shembrey et al., 2019). To accommodate such heterogeneity and estimate critical parameters, pathologists have historically relied on identification of relevant random or defined "fields of view" (FOVs), such as when estimating mitotic rates to grade sarcomas (Neuville et al., 2014). Should TME analysis be based on the whole slide or on specific FOVs? If the latter, how many FOVs, and how should they be selected: randomly, with consideration paid to tumor architecture, or by specific criteria? For example, since the invasive front is a region where tumor cells can be visualized interacting with adjacent non-neoplastic tissue, it seems intuitive that invasive front FOVs should be analyzed to estimate risk of metastasis (Eiro et al., 2012). However, different driver mechanisms and intercellular interactions may be operative within the tumor mass and its invasive front, and different mechanisms may be dominant in different areas of the invasive front (Lawson et al., 2018), so either the entire invasive front should be analyzed, or FOV selection should be guided by criteria linked to the pathogenic mechanism being evaluated or by less biased image analysis or AI techniques. In either case, we believe WSIs will need to serve as input for FOV selection, whether chosen by a human pathologist or by computer software.

Whole slide imaging systems for diagnostic use and the "pixel pathway." When considering how mIF might enter diagnostic practice it is important to consider how health authorities such as the FDA have approached regulation of WSI systems using brightfield microscopy. Over 2 decades ago, whole slide scanners that create high resolution images from standard pathology tissue slides were marketed for research and educational purposes, with the perceived promise (and among some, fear) that they would someday augment or even replace manual microscopy in diagnostic practice. Such was born, as an extension of efforts around telepathology for remote diagnosis in the 1980s and 1990s, the field of "digital pathology" (Soenksen,

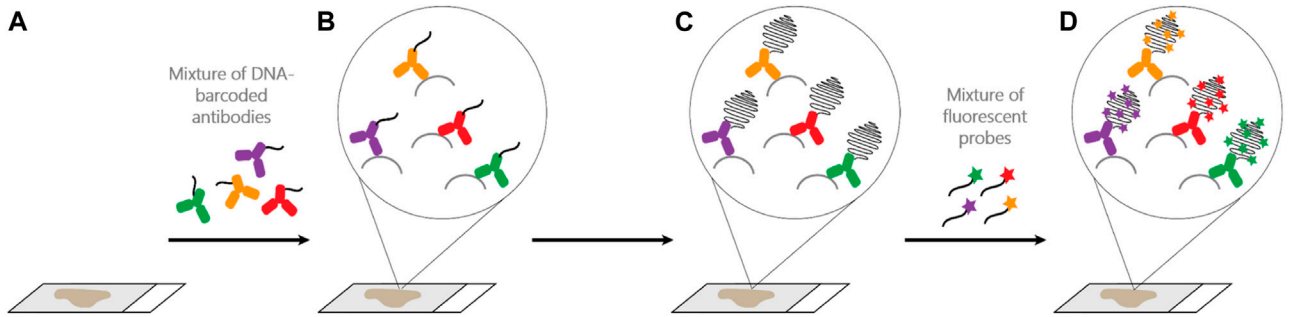

FIGURE 1 | Ultivue InSituPlex (ISP) assay workflow. **(A,B)**: Four different DNA-barcoded antibodies are applied to a FFPE tissue section. **(B,C)**: Barcode amplification. **(D)**: Targets are labeled through hybridization of fluorescent probes to their respective barcodes. Higher plex staining (greater than 4-plex) is possible by initial application of all antibodies, each with a unique barcode, to the tissue and then detecting 4 markers per cycle, separated by gentle DNA exchange steps (not shown).

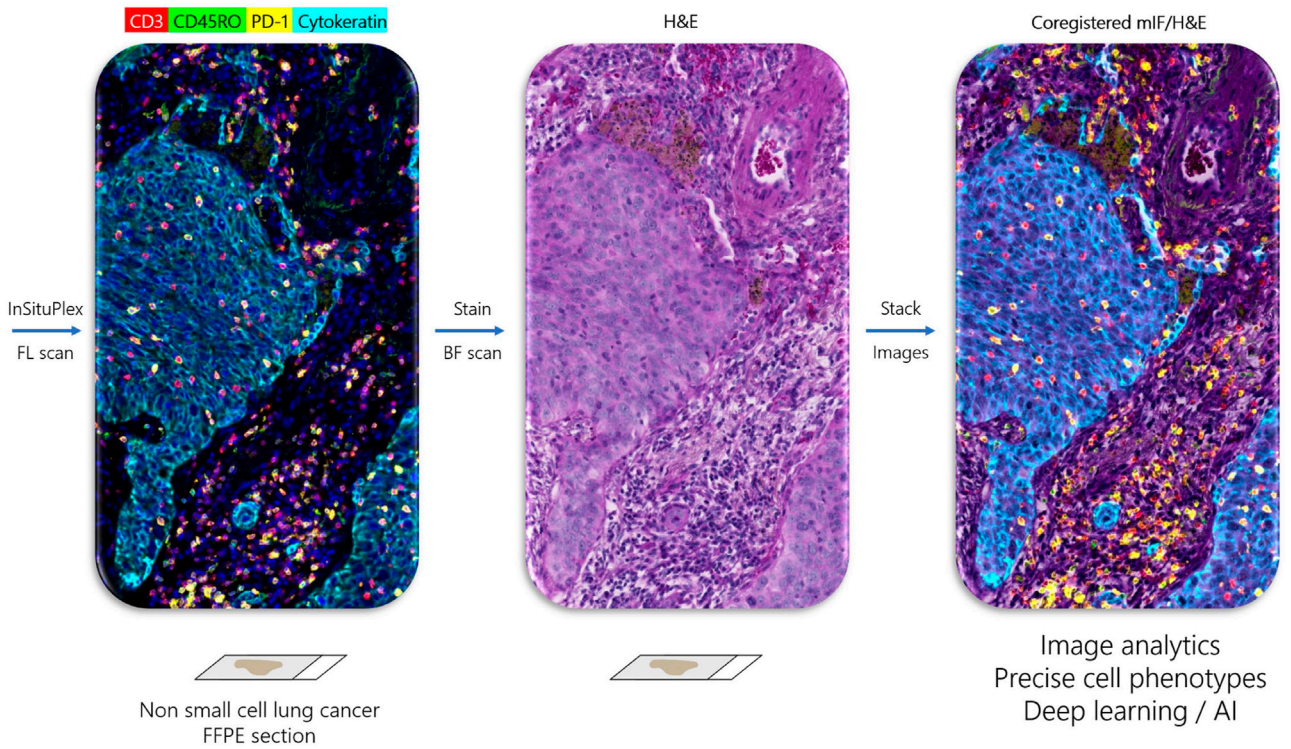

FIGURE 2 | Ultivue InSituPlex workflow enables coregistration of multiplex IF and H&E tissue images. Left panel shows image of non-small cell lung cancer stained with four-marker panel including CD3$^+$ T cells (red), CD45RO+ memory T cells (green), PD-1+ exhausted T cells (yellow), and Cytokeratin positive carcinoma cells (cyan) obtained by fluorescent (FL) scan. H&E stain on same section (middle panel) obtained by brightfield (BF) scan. Right panel is coregistered overlay of multiplex and H&E images, which allows assignment of marker phenotype to every cell in the H&E section, which may be used for integrated image analytics and training of deep learning networks.

2009; Weinstein et al., 2019). Slide digitization enabled quantitation of tissue parameters by image analysis, described above. However, at that time there were no digital pathology systems approved as IVDs for primary diagnosis by FDA. Several years of negotiations between the Digital Pathology Association (DPA), College of American Pathologists (CAP), various scanner manufacturers, and the FDA eventually led to WSI system definition and performance standards that could be used as a basis of FDA approval (Abels and Pantanowitz, 2017). For a WSI system to achieve FDA clearance for diagnostic use, it was agreed that over 2000 cases of the variety seen in a typical surgical pathology clinical practice needed to be assessed by over a dozen pathologists using many, physically separate (but identically specified) WSI systems. A WSI system consists of three

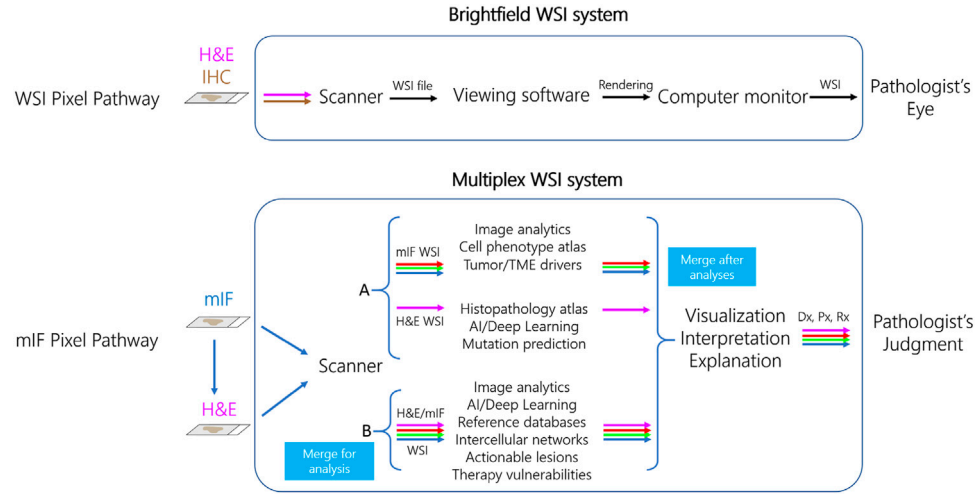

FIGURE 3 | Pixel pathways for diagnostic whole slide imaging (WSI) and multiplex immunofluorescence (mIF) systems. In the current FDA WSI system paradigm **(top row)**, image pixels are traced sequentially through a three-component system that includes brightfield scanner, viewing software, and computer monitor to be interpreted by the Pathologist. In a proposed cell-phenotype centric mIF system **(bottom row)**, the pixel pathway originates with scanning of mIF and then H&E stains on the same slide, a capability of Ultivue's ISP technology. In model A **(top)**, mIF and H&E images are separately analyzed using the indicated tools, and then images are merged after analysis. In model B **(bottom)**, merged mIF and H&E images are subject to a novel data pipeline such as cell-based annotation of H&E sections for analysis by deep learning, allowing earlier definition of each cell's phenotype in the system's pixel pathway. Both models converge so the Pathologist can visualize the merged image with analyses, followed by judgment of the diagnostic (Dx), prognostic (Px), and predictive (Rx) explanations and interpretations when issuing the patient's diagnostic report.

separate but connected devices including the slide scanner, viewing software, and computer monitor (**Figure 3**) (Abels and Pantanowitz, 2017). At the heart of defining a WSI system for manufacture, distribution, and promotion was its "pixel pathway," the path of each image pixel as it transited through the WSI system—from the tissue slide to the pathologist's eye. The pixel pathway concept served several purposes: 1) as an initial step toward WSI system standardization, 2) generation of diagnostic accuracy data to show that diagnoses made using different WSI systems were noninferior to diagnoses made by manual microscopy, and 3) identification of various system failure modes and the potential to attribute system failures (e.g., a false positive or false negative diagnosis) to a root cause such as a specific component of the WSI system itself, the pathologist, or to an intrinsically challenging differential diagnosis such as dysplasia vs. carcinoma *in situ*. To date, only two such WSI systems have been cleared for primary diagnosis by the FDA, the first by Philips in 2017 and the second by Leica Biosystems in 2019 (Mukhopadhyay et al., 2018; Bauer et al., 2020; Borowsky et al., 2020). These and other studies have engendered confidence among pathologists that using WSI is as safe as using their microscope for primary diagnosis. There remain widespread barriers to uptake of digital pathology systems, which will need to be addressed before mIF is accepted as a diagnostic tool. Primary among these is a lack of standardization and interoperability between different WSI components and systems (Marble et al., 2020), meaning that each WSI system has a distinct pixel pathway design. Moreover, for WSI systems to fulfill current standards requires device manufacturers to invest multiple years and millions of dollars in system development, specification, and validation - a long-time frame and large investment compared to the rapid technological advancements and decreasing costs of digital imaging technology and deployment options in individual labs under LDT enforcement discretion. Additional factors that need to be addressed include lack of incentives for digital pathology infrastructure investments and reimbursements (Lasiter et al., 2020), mouse-driven and ergonomically unfriendly "point and click" viewing software (Molin et al., 2015), creation of viable business cases for implementation (Lujan et al., 2021a), and a pathologist's fear of being tethered to a potentially unreliable computer system as opposed to a trusted manual microscope. Recognition of these issues was accelerated in 2020 by the COVID-19 pandemic, which prompted some institutions to rapidly validate their digital pathology systems for diagnostic use in order to maintain continuity of care (Hanna et al., 2020; Stathonikos et al., 2020; Samuelson et al., 2021; Lujan et al., 2021b), whereas other institutions relied on less rigorous system validation guided by the pathologist's ability to judge when images are of insufficient quality to make a diagnosis. A notable parallel concerns the application of telecytology (remote microscopic viewing of cytology specimens) for rapid onsite evaluation (ROSE) of adequacy of biopsy specimens, which is recommended to follow CAP guidelines for validation of diagnostic WSI systems (Pantanowitz et al., 2013; Lin et al., 2019; Evans et al., 2021).

Standardize cell phenotypes before pixel pathways. It has been proposed that widespread adoption of digital pathology in health care will require ecosystem-wide implementation of standards akin to those that enabled the field of diagnostic radiology to convert from film-based to digital platforms over a decade ago (Herrmann et al., 2018; Clunie, 2021). A pivotal element of radiology's digital conversion was establishing data format

standards and component interoperability standards that serve as a basis of device regulatory approval, such that unique system configurations and workflows can be established at each facility from interchangeable components that will perform in a predictable fashion when combined in a system. While some digital pathology standards exist, particularly around the emerging use of DICOM file formats, regulators and manufacturers have not yet agreed upon standards that can serve as basis of product development, testing, approvals, and marketing (Herrmann et al., 2018). As a result, many digital pathology systems used for primary diagnosis throughout the United States are distinct, classified as LDTs, because each system consists of a unique mix of components that may or may not be approved by the FDA for specific uses.

Given the myriad potential mIF system configurations and potential diagnostic uses, coupled with lack of standards in mIF and in digital pathology in general, we do not foresee all relevant stakeholders agreeing to a standardized "pixel pathway" for diagnostic mIF-based WSI systems any time soon. Instead of focusing on image pixels, since mIF is most commonly used to identify cell phenotypes defined by coexpression of multiple markers, one potential step towards standardization of mIF data would be to first standardize data formats at the level of identification and characterization of each individual cell in the sample, perhaps in a manner analogous to how flow cytometry manufacturers created the Flow Cytometry Standard (FCS) data format (Spidlen et al., 2021), with addition of a cell position coordinate in the x-y tissue plane (including the relevant image patch) specifying the location of each cell in the tissue. Such "tissue cytometry" is not a new concept (Ecker and Steiner, 2004; Blenman and Bosenberg, 2019), but advances in multiplex technology, understanding of single cell biology and the role of pathogenic cell types in disease, increased computational power and AI, and a requirement to better characterize the TME are creating urgency around diagnostic use of multiplex staining. Irrespective of efforts to standardize mIF and digital pathology, each diagnostic mIF system used as a LDT will have a unique "pixel pathway" and data pipeline to identify cell phenotypes that could serve as a basis of in-laboratory verification and validation testing, as well as to identify failure modes and their root causes. Similarly, by analogy to brightfield WSI systems, stringent validation of single-site mIF systems used as LDTs should be far easier than the multisite/multisystem validation required of candidate mIF IVD systems. Nearly all FDA-approved CDx IVD tests, including those based on IHC or ISH, are class III risk class devices requiring premarket approval (PMA); however, an increasing number of FDA-approved CDx assays are classified as LDTs, but only one assay (PDGFRB FISH for imatinib eligibility) is tissue-based, the remainder being PCR or NGS-based (Jørgensen, 2021).

Use of immunofluorescence data in diagnostics. How might mIF data be analyzed in future diagnostics? At least two cell phenotype-centric models for mIF WSI system "pixel pathways" can be proposed (**Figure 3**). In one model ("A" in **Figure 3**), the H&E section and mIF data are subject to separate analysis pipelines and then merged after analysis. In line with many recent applications of AI to pathology, H&E image pixels and features are linked by supervised training of convolutional neural networks (CNNs) to data such as pathologist-annotated image features, specialist-rendered diagnosis, presence or absence of molecular lesions, prognosis, or treatment outcomes. In parallel, mIF is used to identify and quantify specific cell phenotypes and their locations in the biopsy (Wilson et al., 2021). This model is analogous to the current addition of non-histology-based biomarkers such as NGS panels to pathology diagnosis, with results integrated at interpretation and reporting stages. An alternative model ('B" in **Figure 3**) exploits ISP's ability to generate a merged H&E and mIF image (**Figure 2**) as input data to generate cell-level annotations of H&E slide images for training CNNs. We envision at least two advantages of model B. First, it eliminates the need for manual pathologist annotations of H&E images for algorithm training, widely viewed as a key limiting factor in global deployment of AI in pathology (van der Laak et al., 2021). Second, identifying the multi-marker profile of every cell in the H&E-stained tissue biopsy results in earlier identification of cell phenotypes in relation to their interpretation appearances and tissue distributions in the system's pixel pathway. There are a few examples using singleplex IHC to augment annotation of H&E sections for training AI [reviewed by van der Laak et al. (2021)], including use of cytokeratin IHC to aid identification of breast (Litjens et al., 2018) or prostate (Bulten et al., 2019) cancer cells, detection of mitoses using phosphohistone H3 (Tellez et al., 2018), and detection of breast cancer cells using cytokeratin and Ki67 IHC (Valkonen et al., 2020), and one recent example using mIF of tumor infiltrating lymphocyte (TIL) markers to predict driver mutations in colon cancer (Bian et al., 2021). In either model, mIF and H&E data could be merged by the scanner or by analysis software after scanning to be rendered for viewing and interpretation.

As mentioned, in addition to using H&E-stained tissues to train AI to assist with histopathology diagnoses, recent reports have shown that AI can predict a tumor's mutational status normally revealed by molecular diagnostic tests such as PCR or NGS (Burlutskiy et al., 2020). This has in turned raised the question – heretical to molecular pathologists - of whether molecular tests are necessary for diagnosis. We speculate that given the substantial cost of molecular testing, initial diagnostic uses of H&E interpretation by AI may serve to increase the diagnostic yield of molecular testing by screening out cases likely to yield a negative result (high sensitivity with 100% specificity). Similarly, it is unknown whether mIF will ultimately be necessary for diagnosis, i.e., whether specific cell phenotypes such as pathogenic macrophage subtypes or regulatory T cell subtypes currently identified only by multiplex methods can be recognized in H&E sections alone by properly trained AI, or whether multiplex staining will be required to identify such cells in every biopsy. Since H&E-based interpretation is so critical to diagnostic pathology, we anticipate that irrespective of the pixel pathway model of the mIF system, the pathologist will require direct coregistration of the H&E with the multiplex images so they can visualize complex cell phenotypes on the same tissue section they use to make the primary diagnosis.

Preparing for multiplex in clinical practice. Given the established use of IHC to detect markers in routine anatomic pathology, the promise of multiplex tissue analysis as a basis of new diagnostics, and the current regulatory landscape of digital pathology, we offer the following conjectures:

1) Unlike singleplex IHC, the complexity and diagnostic significance of multiplex data used to identify multi-marker cell phenotypes cannot be grasped by the pathologist without computational assistance. Therefore, pathologists must be trained on digital pathology software to visualize, quantify, and interpret multiplex tissue data.
2) Multiplex data needs to seamlessly integrate into the digital pathology work environment used for primary diagnosis, including integration with H&E-stained slide images, molecular studies, and other patient and slide metadata.
3) Manual fluorescence microscopy is not a preferred diagnostic modality for pathologists, meaning that expanded use of fluorescence detection in clinical practice will require a scanner to generate WSIs that can be viewed, manipulated, and analyzed by digital pathology software.
4) Interpretation of mIF data will require image analysis, augmented by explainable AI algorithms, to understand and interpret data and report diagnoses (Huss and Coupland, 2020; van der Laak et al., 2021).
5) Until Pathology adopts data formatting and component interoperability standards akin to Radiology, including integration of multiplex tissue data, end-to-end WSI systems used in a diagnostic capacity will likely be custom applications operating as LDTs in each laboratory site.
6) By analogy to brightfield WSI systems, health authorities such as FDA will require mIF WSI IVD systems to have a defined pixel pathway, from slide staining to stain visualization and interpretation. Fundamental differences in brightfield vs. fluorescent microscopy, the lack of standards around mIF systems, protocols, data collection and software analysis pipelines (especially if the WSI system provides decision support as a medical device), and a requirement for similar clinical interpretation across platforms and practice environments, implies that establishing standards to achieve clearances for a mIF WSI system (or even a for a stand-alone scanner) will be challenging.
7) Since a major goal of mIF analysis is to assess multiple marker colocalization in cells to identify and score specific cell phenotypes, we propose that efforts to standardize data should first focus, by analogy to flow cytometry, on standardizing definitions of specific cell phenotypes rather than on striving to create a standardized mIF pixel pathway.
8) Precise multi-marker annotation of every cell in the H&E slide by mIF data will augment training and performance of AI on H&E-stained tissue samples for some but not all relevant elements of tissue diagnosis. Optimal uses of AI on mIF data in diagnostic workflows have yet to be defined (Mungenast et al., 2021).
9) Pathologists must have greater access to digital pathology systems and software including image analysis/computational pathology tools in order to begin to integrate multiplex analysis of any kind into primary diagnosis.

Imagining the Pathologist's Future

As WSI scanners and viewing software gained a dedicated user base, the concept of the "pathologist cockpit" emerged as a model for digital pathology-based case sign out of the future (Soenksen, 2009). Just like an airplane cockpit, it was imagined that all the controls, dials and knobs, sticks and gadgets necessary for the pathologist to navigate from point A (tissue intake) to point B (the diagnostic report) would be laid out on multiple screens. A decade later, many centers have created multiscreen pathologist cockpits that bring pathology data and relevant software to the pathologist's fingertips. We can now imagine, in outline and with some detail, the pathologist's cockpit of the future: multiplex profiling will identify the phenotype of every cell in H&E tissue section; vast computational power will enable access to knowledge databases such as cell and tumor atlases; and AI will help the pathologist make sense of it all to better help clinicians select the best therapy for their patients. We expect that the next generation of pathologists, like sages on mountaintops, will be ever the wiser with an expanded ability to navigate disease.

CONCLUSION

Rules and regulations governing creation and deployment of diagnostic tests are of necessity geared to ensure patient safety and preserve equipoise in clinical investigations (Rabinstein et al., 2016; O'Neill et al., 2019), but regulations can also oppose innovation, thereby denying patient benefit. The potential of digital pathology to transform anatomic pathology practice is not limited to remote case sign-out or training AI to interpret H&E slides; its potential will be realized when knowledge about single cell phenotypes and disease driver pathways, unique to each patient and their disease and revealed by multiplex marker labeling methods, is available for every pathologist to interpret every patient's tissue biopsy. IHC has been a major contributor to understanding the roles of single cells and cell populations in diagnostic biopsies, but as currently practiced only allows interrogation of one marker, one molecular species at a time, and is incapable of identifying emerging cell types of importance defined by coexpression of multiple markers in the same subcellular compartment. Given the current regulatory landscape of diagnostic anatomic and digital pathology, the technical demands of multiplex assays, and lack of standardized mIF methods, we propose that retrospective analysis of clinical trial cohorts and development of diagnostic assays as LDTs in individual laboratories will increase assay confidence and generate real world evidence of clinical validity and, by inference clinical utility, which in turn will inform the optimal design, performance and testing of standardized diagnostic multiplex systems of the future.

AUTHOR CONTRIBUTIONS

KW conceived, drafted, and finalized the manuscript; DW, MM, KM, FL, and AZ drafted and edited the manuscript.

ACKNOWLEDGMENTS

Thanks to Pamela Guy, Amy Ly, Angela Vasaturo (Ultivue, Inc.) and Doug Woodruff (DWW Consulting) for manuscript feedback; George McNamara (Johns Hopkins) and Eric Walk (Roche, Inc.) for discussions and references pertaining to use of IHC and

multiplex technologies in clinical practice; Kim Blenman (Yale) for discussions about FCS; and the Alliance for Digital Pathology (Pathology Innovation Collaborative Community – PiCC) and the Anatomic Pathology Patient Interest Association (APPIA) for providing valuable forums for open discussion of regulatory issues impacting diagnostic tissue staining.

REFERENCES

Abels, E., Pantanowitz, L., Aeffner, F., Zarella, M. D., Laak, J., Bui, M. M., et al. (2019). Computational Pathology Definitions, Best Practices, and Recommendations for Regulatory Guidance: a white Paper from the Digital Pathology Association. *J. Pathol.* 249 (3), 286–294. doi:10.1002/path.5331

Abels, E., and Pantanowitz, L. (2017). Current State of the Regulatory Trajectory for Whole Slide Imaging Devices in the USA. *J. Pathol. Inform.* 8, 23. doi:10.4103/jpi.jpi_11_17

Aeffner, F., Zarella, M., Buchbinder, N., Bui, M., Goodman, M., Hartman, D., et al. (2019). Introduction to Digital Image Analysis in Whole-Slide Imaging: A White Paper from the Digital Pathology Association. *J. Pathol. Inform.* 10, 9. doi:10.4103/jpi.jpi_82_18

Agrawal, L., Engel, K. B., Greytak, S. R., and Moore, H. M. (2018). Understanding Preanalytical Variables and Their Effects on Clinical Biomarkers of Oncology and Immunotherapy. *Semin. Cancer Biol.* 52 (Pt 2), 26–38. doi:10.1016/j.semcancer.2017.12.008

Aldridge, S., and Teichmann, S. A. (2020). Single Cell Transcriptomics Comes of Age. *Nat. Commun.* 11 (1), 4307. doi:10.1038/s41467-020-18158-5

Angell, H. K., Bruni, D., Barrett, J. C., Herbst, R., and Galon, J. (2020). The Immunoscore: Colon Cancer and beyond. *Clin. Cancer Res.* 26 (2), 332–339. doi:10.1158/1078-0432.ccr-18-1851

Atkins, D., Reiffen, K.-A., Tegtmeier, C. L., Winther, H., Bonato, M. S., and Störkel, S. (2004). Immunohistochemical Detection of EGFR in Paraffin-Embedded Tumor Tissues. *J. Histochem. Cytochem.* 52 (7), 893–901. doi:10.1369/jhc.3a6195.2004

Baharlou, H., Canete, N. P., Cunningham, A. L., Harman, A. N., and Patrick, E. (2019). Mass Cytometry Imaging for the Study of Human Diseases-Applications and Data Analysis Strategies. *Front. Immunol.* 10, 2657. doi:10.3389/fimmu.2019.02657

Bank, P. C. D., Jacobs, L. H. J., van den Berg, S. A. A., van Deutekom, H. W. M., Hamann, D., Molenkamp, R., et al. (2020). The End of the Laboratory Developed Test as We Know it? Recommendations from a National Multidisciplinary Taskforce of Laboratory Specialists on the Interpretation of the IVDR and its Complications. *Clin. Chem. Lab. Med.*

Bauer, T., Behling, C., Miller, D., Chang, B., Viktorova, E., Magari, R., et al. (2020). Precise Identification of Cell and Tissue Features Important for Histopathologic Diagnosis by a Whole Slide Imaging System. *J. Pathol. Inform.* 11, 3. doi:10.4103/jpi.jpi_47_19

Bian, C., Wang, Y., Lu, Z., An, Y., Wang, H., Kong, L., et al. (2021). ImmunoAIzer: A Deep Learning-Based Computational Framework to Characterize Cell Distribution and Gene Mutation in Tumor Microenvironment. *Cancers (Basel)* 13 (7). doi:10.3390/cancers13071659

Blenman, K. R. M., and Bosenberg, M. W. (2019). Immune Cell and Cell Cluster Phenotyping, Quantitation, and Visualization Using In Silico Multiplexed Images and Tissue Cytometry. *Cytometry* 95 (4), 399–410. doi:10.1002/cyto.a.23668

Bogen, S., Vani, K., and Sompuram, S. (2009). Molecular Mechanisms of Antigen Retrieval: Antigen Retrieval Reverses Steric Interference Caused by Formalin-Induced Cross-Links. *Biotech. Histochem.* 84 (5), 207–215. doi:10.3109/10520290903039078

Bonaventura, P., Shekarian, T., Alcazer, V., Valladeau-Guilemond, J., Valsesia-Wittmann, S., Amigorena, S., et al. (2019). Cold Tumors: A Therapeutic Challenge for Immunotherapy. *Front. Immunol.* 10, 168. doi:10.3389/fimmu.2019.00168

Borowsky, A. D., Glassy, E. F., Wallace, W. D., Kallichanda, N. S., Behling, C. A., Miller, D. V., et al. (2020). Digital Whole Slide Imaging Compared with Light Microscopy for Primary Diagnosis in Surgical Pathology. *Arch. Pathol. Lab. Med.* 144 (10), 1245–1253. doi:10.5858/arpa.2019-0569-oa

Bruni, D., Angell, H. K., and Galon, J. (2020). The Immune Contexture and Immunoscore in Cancer Prognosis and Therapeutic Efficacy. *Nat. Rev. Cancer* 20 (11), 662–680. doi:10.1038/s41568-020-0285-7

Bulle, A., and Lim, K. H. (2020). Beyond Just a Tight Fortress: Contribution of Stroma to Epithelial-Mesenchymal Transition in Pancreatic Cancer. *Signal. Transduct Target. Ther.* 5 (1), 249. doi:10.1038/s41392-020-00341-1

Bulten, W., Bandi, P., Hoven, J., Loo, R. V., Lotz, J., Weiss, N., et al. (2019). Epithelium Segmentation Using Deep Learning in H&E-stained Prostate Specimens with Immunohistochemistry as Reference Standard. *Sci. Rep.* 9 (1), 864. doi:10.1038/s41598-018-37257-4

Burlutskiy, N., Waring, P., and Hipp, J. (2020). The Revival of the H&E with Artificial Intelligence. *J. Clin. Anat. Pathol.* 5 (2). doi:10.47275/2332-4864-108

Carossino, M., Ip, H. S., Richt, J. A., Shultz, K., Harper, K., Loynachan, A. T., et al. (2020). Detection of SARS-CoV-2 by RNAscope *In Situ* Hybridization and Immunohistochemistry Techniques. *Arch. Virol.* 165 (10), 2373–2377. doi:10.1007/s00705-020-04737-w

Chaudhary, R., Slebos, R. J. C., Song, F., McCleary-Sharpe, K. P., Masannat, J., Tan, A. C., et al. (2021). Effects of Checkpoint Kinase 1 Inhibition by Prexasertib on the Tumor Immune Microenvironment of Head and Neck Squamous Cell Carcinoma. *Mol. Carcinogenesis* 60 (2), 138–150. doi:10.1002/mc.23275

Chen, M., Zhang, B., Topatana, W., Cao, J., Zhu, H., Juengpanich, S., et al. (2020). Classification and Mutation Prediction Based on Histopathology H&E Images in Liver Cancer Using Deep Learning. *NPJ Precis Oncol.* 4, 14. doi:10.1038/s41698-020-0120-3

Chen, M., and Zhao, H. (2019). Next-generation Sequencing in Liquid Biopsy: Cancer Screening and Early Detection. *Hum. Genomics* 13 (1), 34. doi:10.1186/s40246-019-0220-8

Clunie, D. A. (2021). DICOM Format and Protocol Standardization-A Core Requirement for Digital Pathology Success. *Toxicol. Pathol.* 49 (4), 738–749. doi:10.1177/0192623320965893

College of American Pathologists Laboratory Accreditation Program (2017). Available from: https://www.cap.org/laboratory-improvement/accreditation/laboratory-accreditation-program.

Compton, C. C., Robb, J. A., Anderson, M. W., Berry, A. B., Birdsong, G. G., Bloom, K. J., et al. (2019). Preanalytics and Precision Pathology: Pathology Practices to Ensure Molecular Integrity of Cancer Patient Biospecimens for Precision Medicine. *Arch. Pathol. Lab. Med.* 143 (11), 1346–1363. doi:10.5858/arpa.2019-0009-sa

Couture, H. (2019). A Deeper Understanding of Breast Cancer. *Scientific Am.*, 2019.

Couzin-Frankel, J. (2013). Cancer Immunotherapy. *Science* 342 (6165), 1432–1433. doi:10.1126/science.342.6165.1432

Cui, M., and Zhang, D. Y. (2021). Artificial Intelligence and Computational Pathology. *Lab. Invest.*

Czarnecka, A. M., Sobczuk, P., Kostrzanowski, M., Spalek, M., Chojnacka, M., Szumera-Cieckiewicz, A., et al. (2020). Epithelioid Sarcoma-From Genetics to Clinical Practice. *Cancers (Basel)* 12 (8). doi:10.3390/cancers12082112

de Vries, N. L., Mahfouz, A., Koning, F., and de Miranda, N. (2020). Unraveling the Complexity of the Cancer Microenvironment with Multidimensional Genomic and Cytometric Technologies. *Front. Oncol.* 10, 1254. doi:10.3389/fonc.2020.01254

Debus, E., Moll, R., Franke, W. W., Weber, K., and Osborn, M. (1984). Immunohistochemical Distinction of Human Carcinomas by Cytokeratin Typing with Monoclonal Antibodies. *Am. J. Pathol.* 114 (1), 121–130.

Dickinson, M. E., Bearman, G., Tille, S., Lansford, R., and Fraser, S. E. (2001). Multi-spectral Imaging and Linear Unmixing Add a Whole New Dimension to Laser Scanning Fluorescence Microscopy. *Biotechniques* 31 (6), 1272–1278. doi:10.2144/01316bt01

Digestive System Tumours (2019). *WHO Classification of Tumours*. 5th ed. Lyon, France: IARC Publications.

Dimitriou, N., Arandjelovic, O., and Caie, P. D. (2019). Deep Learning for Whole Slide Image Analysis: An Overview. *Front. Med. (Lausanne).* 6, 264. doi:10.3389/fmed.2019.00264

Digital Pathology Association (2021). 510(k) Image Analysis Algorithm Clearances: Digital Pathology Association. Available from: https://digitalpathologyassociation.org/_data/cms_files/files/DPA_Regulatory-FDA-510k_list.pdf.

Dunstan, R. W., Wharton, K. A., Jr., Quigley, C., and Lowe, A. (2011). The Use of Immunohistochemistry for Biomarker Assessment-Can it Compete with Other Technologies?. *Toxicol. Pathol.* 39 (6), 988–1002. doi:10.1177/0192623311419163

Echle, A., Rindtorff, N. T., Brinker, T. J., Luedde, T., Pearson, A. T., and Kather, J. N. (2021). Deep Learning in Cancer Pathology: a New Generation of Clinical Biomarkers. *Br. J. Cancer* 124 (4), 686–696. doi:10.1038/s41416-020-01122-x

Ecker, R. C., and Steiner, G. E. (2004). Microscopy-based Multicolor Tissue Cytometry at the Single-Cell Level. *Cytometry* 59A (2), 182–190. doi:10.1002/cyto.a.20052

Eiro, N., Pidal, I., Fernandez-Garcia, B., Junquera, S., Lamelas, M. L., del Casar, J. M., et al. (2012). Impact of CD68/(CD3+CD20) Ratio at the Invasive Front of Primary Tumors on Distant Metastasis Development in Breast Cancer. *PLoS One* 7 (12), e52796. doi:10.1371/journal.pone.0052796

Evans, A. J., Brown, R. W., Bui, M. M., Chlipala, E. A., Lacchetti, C., Milner, D. A., et al. (2021). Validating Whole Slide Imaging Systems for Diagnostic Purposes in Pathology: Guideline Update from the College of American Pathologists in Collaboration with the American Society for Clinical Pathology and the Association for Pathology Informatics. *Arch. Pathol. Lab. Med.*. doi:10.5858/arpa.2020-0723-cp

Fetsch, P. A., and Abati, A. (2010). The Clinical Immunohistochemistry Laboratory: Regulations and Troubleshooting Guidelines. *Methods Mol. Biol.* 588, 399–412. doi:10.1007/978-1-59745-324-0_43

Francisco-Cruz, A., Parra, E. R., Tetzlaff, M. T., and Wistuba, II (2020). Multiplex Immunofluorescence Assays. *Methods Mol. Biol.* 2055, 467–495. doi:10.1007/978-1-4939-9773-2_22

Galon, J., Costes, A., Sanchez-Cabo, F., Kirilovsky, A., Mlecnik, B., Lagorce-Pages, C., et al. (2006). Type, Density, and Location of Immune Cells within Human Colorectal Tumors Predict Clinical Outcome. *Science* 313 (5795), 1960–1964. doi:10.1126/science.1129139

Ganesh, K., and Massagué, J. (2018). TGF-β Inhibition and Immunotherapy: Checkmate. *Immunity* 48 (4), 626–628. doi:10.1016/j.immuni.2018.03.037

Genzen, J. R., Mohlman, J. S., Lynch, J. L., Squires, M. W., and Weiss, R. L. (2017). Laboratory-Developed Tests: A Legislative and Regulatory Review. *Clin. Chem.* 63 (10), 1575–1584. doi:10.1373/clinchem.2017.275164

Genzen, J. R. (2019). Regulation of Laboratory-Developed Tests. *Am. J. Clin. Pathol.* 152 (2), 122–131. doi:10.1093/ajcp/aqz096

Goltsev, Y., Samusik, N., Kennedy-Darling, J., Bhate, S., Hale, M., Vazquez, G., et al. (2018). Deep Profiling of Mouse Splenic Architecture with CODEX Multiplexed Imaging. *Cell* 174 (4), 968–981. doi:10.1016/j.cell.2018.07.010

Gordon, S. R. (1988). Use of Selected Excitation Filters for Enhancement of Diaminobenzidine Photomicroscopy. *J. Histochem. Cytochem.* 36 (6), 701–704. doi:10.1177/36.6.3367053

Grogan, T. M. (1992). Automated Immunohistochemical Analysis. *Am. J. Clin. Pathol.* 98 (4 Suppl. 1), S35–S38.

Guidance for Industry (1998). "Guidance for Submission of Immunohistochemistry Applications to the FDA," in *DHHS F, CDRH, Immunology Branch.*

Gundle, K. R., Deutsch, G. B., Goodman, H. J., Pollack, S. M., Thompson, M. J., Davis, J. L., et al. (2020). Multiplexed Evaluation of Microdosed Antineoplastic AgentsIn Situin the Tumor Microenvironment of Patients with Soft Tissue Sarcoma. *Clin. Cancer Res.* 26 (15), 3958–3968. doi:10.1158/1078-0432.ccr-20-0614

Gurcan, M. N., Boucheron, L. E., Can, A., Madabhushi, A., Rajpoot, N. M., and Yener, B. (2009). Histopathological Image Analysis: a Review. *IEEE Rev. Biomed. Eng.* 2, 147–171. doi:10.1109/rbme.2009.2034865

Hack, S. P., Zhu, A. X., and Wang, Y. (2020). Augmenting Anticancer Immunity through Combined Targeting of Angiogenic and PD-1/pd-L1 Pathways: Challenges and Opportunities. *Front. Immunol.* 11, 598877. doi:10.3389/fimmu.2020.598877

Hanna, M. G., Reuter, V. E., Ardon, O., Kim, D., Sirintrapun, S. J., Schüffler, P. J., et al. (2020). Validation of a Digital Pathology System Including Remote Review during the COVID-19 Pandemic. *Mod. Pathol.* 33 (11), 2115–2127. doi:10.1038/s41379-020-0601-5

Hegde, P. S., and Chen, D. S. (2020). Top 10 Challenges in Cancer Immunotherapy. *Immunity* 52 (1), 17–35. doi:10.1016/j.immuni.2019.12.011

Herrmann, M. D., Clunie, D. A., Fedorov, A., Doyle, S. W., Pieper, S., Klepeis, V., et al. (2018). Implementing the DICOM Standard for Digital Pathology. *J. Pathol. Inform.* 9, 37. doi:10.4103/jpi.jpi_42_18

Hofman, P., Badoual, C., Henderson, F., Berland, L., Hamila, M., Long-Mira, E., et al. (2019). Multiplexed Immunohistochemistry for Molecular and Immune Profiling in Lung Cancer-Just about Ready for Prime-Time?. *Cancers (Basel)* 11 (3). doi:10.3390/cancers11030283

Huang, R., Lasiter, L., Bard, A., Quinn, B., Young, C., Salgado, R., et al. (2021). National Maintenance Cost for Precision Diagnostics under the Verifying Accurate Leading-Edge *In Vitro* Clinical Test Development (VALID) Act of 2020. *JCO Oncol. Pract.*, OP2000862. doi:10.1200/OP.20.00862

Huey, R. W., Makawita, S., Xiao, L., Matamoros, A., Estrella, J. S., Overman, M. J., et al. (2019). Sarcomatoid Carcinoma Presenting as Cancers of Unknown Primary: a Clinicopathological Portrait. *BMC Cancer* 19 (1), 965. doi:10.1186/s12885-019-6155-6

Humphries, M. P., Bingham, V., Abdullahi Sidi, F., Craig, S. G., McQuaid, S., James, J., et al. (2020). Improving the Diagnostic Accuracy of the PD-L1 Test with Image Analysis and Multiplex Hybridization. *Cancers (Basel).* 12 (5). doi:10.3390/cancers12051114

Huss, R., and Coupland, S. E. (2020). Software-assisted Decision Support in Digital Histopathology. *J. Pathol.* 250 (5), 685–692. doi:10.1002/path.5388

Inamura, K. (2018). Update on Immunohistochemistry for the Diagnosis of Lung Cancer. *Cancers (Basel)* 10 (3). doi:10.3390/cancers10030072

Ji, A. L., Rubin, A. J., Thrane, K., Jiang, S., Reynolds, D. L., Meyers, R. M., et al. (2020). Multimodal Analysis of Composition and Spatial Architecture in Human Squamous Cell Carcinoma. *Cell* 182 (2), 497–514. doi:10.1016/j.cell.2020.05.039

Jørgensen, J. T. (2016). Companion and Complementary Diagnostics: Clinical and Regulatory Perspectives. *Trends Cancer* 2 (12), 706–712. doi:10.1016/j.trecan.2016.10.013

Jørgensen, J. T. (2021). The Current Landscape of the FDA Approved Companion Diagnostics. *Transl Oncol.* 14 (6), 101063. doi:10.1016/j.tranon.2021.101063

Kohlberger, T., Liu, Y., Moran, M., Chen, P.-H., Brown, T., Hipp, J., et al. (2019). Whole-Slide Image Focus Quality: Automatic Assessment and Impact on AI Cancer Detection. *J. Pathol. Inform.* 10, 39. doi:10.4103/jpi.jpi_11_19

Konnick, E. Q. (2020). The Regulatory Landscape of Precision Oncology Laboratory Medicine in the United States - Perspective on the Past 5 Years and Considerations for Future Regulation. *Pract. Lab. Med.* 21, e00172. doi:10.1016/j.plabm.2020.e00172

Lasiter, L., Samboy, J., Leibowitz, C., Mathews, C., Hoskyns, S., and Abels, E. (2020). Aligning Reimbursement for Digital Pathology with its Value. *J. Precision Med.*

Lawson, D. A., Kessenbrock, K., Davis, R. T., Pervolarakis, N., and Werb, Z. (2018). Tumour Heterogeneity and Metastasis at Single-Cell Resolution. *Nat. Cel Biol* 20 (12), 1349–1360. doi:10.1038/s41556-018-0236-7

Lazarus, J., Akiska, Y., Perusina Lanfranca, M., Delrosario, L., Sun, L., Long, D., et al. (2019). Optimization, Design and Avoiding Pitfalls in Manual Multiplex Fluorescent Immunohistochemistry. *J. Vis. Exp.* 149. doi:10.3791/59915

Li, J. Y., Chen, Y. P., Li, Y. Q., Liu, N., and Ma, J. (2021). Chemotherapeutic and Targeted Agents Can Modulate the Tumor Microenvironment and Increase the Efficacy of Immune Checkpoint Blockades. *Mol. Cancer* 20 (1), 27. doi:10.1186/s12943-021-01317-7

Lin, J. R., Izar, B., Wang, S., Yapp, C., Mei, S., Shah, P. M., et al. (2018). Highly Multiplexed Immunofluorescence Imaging of Human Tissues and Tumors Using T-CyCIF and Conventional Optical Microscopes. *Elife* 7. doi:10.7554/elife.31657

Lin, O., Rudomina, D., Feratovic, R., and Sirintrapun, S. J. (2019). Rapid On-Site Evaluation Using Telecytology: A Major Cancer center Experience. *Diagn. Cytopathology* 47 (1), 15–19. doi:10.1002/dc.23925

Litjens, G., Bandi, P., Ehteshami Bejnordi, B., Geessink, O., Balkenhol, M., Bult, P., et al. (2018). 1399 H&E-stained sentinel Lymph Node Sections of Breast Cancer Patients: the CAMELYON Dataset. *Gigascience* 7 (6). doi:10.1093/gigascience/giy065

Lujan, G., Quigley, J. C., Hartman, D., Parwani, A., Roehmholdt, B., Meter, B. V., et al. (2021). Dissecting the Business Case for Adoption and Implementation of Digital Pathology: A white Paper from the Digital Pathology Association. *J. Pathol. Inform.* 12 (1), 17. doi:10.4103/jpi.jpi_67_20

Lujan, G. M., Savage, J., Shana'ah, A., Yearsley, M., Thomas, D., Allenby, P., et al. (2021). Digital Pathology Initiatives and Experience of a Large Academic Institution during the Coronavirus Disease 2019 (COVID-19) Pandemic. *Arch. Pathol. Lab. Med.* doi:10.5858/arpa.2020-0715-sa

Marble, H. D., Huang, R., Dudgeon, S. N., Lowe, A., Herrmann, M. D., Blakely, S., et al. (2020). A Regulatory Science Initiative to Harmonize and Standardize Digital Pathology and Machine Learning Processes to Speed up Clinical Innovation to Patients. *J. Pathol. Inform.* 11, 22. doi:10.4103/jpi.jpi_27_20

Marx, V. (2019). A Dream of Single-Cell Proteomics. *Nat. Methods* 16 (9), 809–812. doi:10.1038/s41592-019-0540-6

Marx, V. (2021). Method of the Year: Spatially Resolved Transcriptomics. *Nat. Methods* 18 (1), 9–14. doi:10.1038/s41592-020-01033-y

McGinnis, L. M., Ibarra-Lopez, V., Rost, S., and Ziai, J. (2021). Clinical and Research Applications of Multiplexed Immunohistochemistry and *In Situ* Hybridization. *J. Pathol.*

Medical Devices (1998). Medical Devices; Classification/reclassification of Immunohistochemistry Reagents and Kits--FDA. Final Rule. *Fed. Regist.* 63 (106), 30132–30142.

Molin, J., Lundström, C., and Fjeld, M. (2015). A Comparative Study of Input Devices for Digital Slide Navigation. *J. Pathol. Inform.* 6, 7. doi:10.4103/2153-3539.151894

Morrison, L. E., Lefever, M. R., Behman, L. J., Leibold, T., Roberts, E. A., Horchner, U. B., et al. (2020). Brightfield Multiplex Immunohistochemistry with Multispectral Imaging. *Lab. Invest.* 100 (8), 1124–1136. doi:10.1038/s41374-020-0429-0

Mortezaee, K. (2021). Enriched Cancer Stem Cells, Dense Stroma, and Cold Immunity: Interrelated Events in Pancreatic Cancer. *J. Biochem. Mol. Toxicol.*, e22708.

Mukhopadhyay, S., Feldman, M. D., Abels, E., Ashfaq, R., Beltaifa, S., Cacciabeve, N. G., et al. (2018). Whole Slide Imaging versus Microscopy for Primary Diagnosis in Surgical Pathology. *Am. J. Surg. Pathol.* 42 (1), 39–52. doi:10.1097/pas.0000000000000948

Mungenast, F., Fernando, A., Nica, R., Boghiu, B., Lungu, B., Batra, J., et al. (2021). Next-Generation Digital Histopathology of the Tumor Microenvironment. *Genes* 12 (4). doi:10.3390/genes12040538

Najafi, M., Mortezaee, K., and Ahadi, R. (2019). Cancer Stem Cell (A)symmetry & Plasticity: Tumorigenesis and Therapy Relevance. *Life Sci.* 231, 116520. doi:10.1016/j.lfs.2019.05.076

Neuville, A., Chibon, F., and Coindre, J.-M. (2014). Grading of Soft Tissue Sarcomas: from Histological to Molecular Assessment. *Pathology* 46 (2), 113–120. doi:10.1097/pat.0000000000000048

New York State Clinical Laboratory Evaluation Program (2021). Available from: https://www.wadsworth.org/regulatory/clep.

Nicholas, N. S., Apollonio, B., and Ramsay, A. G. (2016). Tumor Microenvironment (TME)-driven Immune Suppression in B Cell Malignancy. *Biochim. Biophys. Acta (Bba) - Mol. Cel Res.* 1863 (3), 471–482. doi:10.1016/j.bbamcr.2015.11.003

Nwanze, J., Siddiqui, M. T., Stevens, K. A., Saxe, D., and Cohen, C. (2017). MYC Immunohistochemistry Predicts MYC Rearrangements by FISH. *Front. Oncol.* 7, 209. doi:10.3389/fonc.2017.00209

O'Neill, T., Miksad, R., Miller, D., Maloney, L., John, A., Hiller, C., et al. (2019). ISPOR, the FDA, and the Evolving Regulatory Science of Medical Device Products. *Value in Health* 22 (7), 754–761. doi:10.1016/j.jval.2019.03.020

Ouyang, W., and O'Garra, A. (2019). IL-10 Family Cytokines IL-10 and IL-22: from Basic Science to Clinical Translation. *Immunity* 50 (4), 871–891. doi:10.1016/j.immuni.2019.03.020

Pantanowitz, L., Sinard, J. H., Henricks, W. H., Fatheree, L. A., Carter, A. B., Contis, L., et al. (2013). Validating Whole Slide Imaging for Diagnostic Purposes in Pathology: Guideline from the College of American Pathologists Pathology and Laboratory Quality Center. *Arch. Pathol. Lab. Med.* 137 (12), 1710–1722. doi:10.5858/arpa.2013-0093-cp

Parra, E. R., Francisco-Cruz, A., and Wistuba, II (2019). State-of-the-Art of Profiling Immune Contexture in the Era of Multiplexed Staining and Digital Analysis to Study Paraffin Tumor Tissues. *Cancers (Basel).* 11 (2). doi:10.3390/cancers11020247

Perou, C. M., Parker, J. S., Prat, A., Ellis, M. J., and Bernard, P. S. (2010). Clinical Implementation of the Intrinsic Subtypes of Breast Cancer. *Lancet Oncol.* 11 (8), 718–719. doi:10.1016/s1470-2045(10)70176-5

Prichard, J. W. (2014). Overview of Automated Immunohistochemistry. *Arch. Pathol. Lab. Med.* 138 (12), 1578–1582. doi:10.5858/arpa.2014-0083-ra

Rabinstein, A. A., Brinjikji, W., and Kallmes, D. F. (2016). Equipoise in Clinical Trials. *Circ. Res.* 119 (7), 798–800. doi:10.1161/circresaha.116.309594

Rameshbabu, S., Labadie, B. W., Argulian, A., and Patnaik, A. (2021). Targeting Innate Immunity in Cancer Therapy. *Vaccines (Basel).* 9 (2). doi:10.3390/vaccines9020138

Rana, A., Lowe, A., Lithgow, M., Horback, K., Janovitz, T., Da Silva, A., et al. (2020). Use of Deep Learning to Develop and Analyze Computational Hematoxylin and Eosin Staining of Prostate Core Biopsy Images for Tumor Diagnosis. *JAMA Netw. Open* 3 (5), e205111. doi:10.1001/jamanetworkopen.2020.5111

Regev, A., Teichmann, S. A., Lander, E. S., Amit, I., Benoist, C., Birney, E., et al. (2017). The Human Cell Atlas. *Elife* 6. doi:10.7554/elife.27041

Rimm, D. L. (2006). What Brown Cannot Do for You. *Nat. Biotechnol.* 24 (8), 914–916. doi:10.1038/nbt0806-914

Roach, C., Zhang, N., Corigliano, E., Jansson, M., Toland, G., Ponto, G., et al. (2016). Development of a Companion Diagnostic PD-L1 Immunohistochemistry Assay for Pembrolizumab Therapy in Non-small-cell Lung Cancer. *Appl. Immunohistochem. Mol. Morphol.* 24 (6), 392–397. doi:10.1097/pai.0000000000000408

Rodig, S. J., Gusenleitner, D., Jackson, D. G., Gjini, E., Giobbie-Hurder, A., Jin, C., et al. (2018). MHC Proteins Confer Differential Sensitivity to CTLA-4 and PD-1 Blockade in Untreated Metastatic Melanoma. *Sci. Transl Med.* 10 (450). doi:10.1126/scitranslmed.aar3342

Samuelson, M. I., Chen, S. J., Boukhar, S. A., Schnieders, E. M., Walhof, M. L., Bellizzi, A. M., et al. (2021). Rapid Validation of Whole-Slide Imaging for Primary Histopathology Diagnosis. *Am. J. Clin. Pathol.* 155 (5), 638–648. doi:10.1093/ajcp/aqaa280

Santiago, T., Tarek, N., Boulos, F., Hayes, C., Jeha, S., Raimondi, S., et al. (2019). Correlation between MYCN Gene Status and MYCN Protein Expression in Neuroblastoma: A Pilot Study to Propose the Use of MYCN Immunohistochemistry in Limited-Resource Areas. *Jgo* 5, 1–7. doi:10.1200/jgo.19.00135

Sathe, A., Grimes, S. M., Lau, B. T., Chen, J., Suarez, C., Huang, R. J., et al. (2020). Single-Cell Genomic Characterization Reveals the Cellular Reprogramming of the Gastric Tumor Microenvironment. *Clin. Cancer Res.* 26 (11), 2640–2653. doi:10.1158/1078-0432.ccr-19-3231

Scheerens, H., Malong, A., Bassett, K., Boyd, Z., Gupta, V., Harris, J., et al. (2017). Current Status of Companion and Complementary Diagnostics: Strategic Considerations for Development and Launch. *Clin. Translational Sci.* 10 (2), 84–92. doi:10.1111/cts.12455

Schneider, F., Maurer, C., and Friedberg, R. C. (2017). International Organization for Standardization (ISO) 15189. *Ann. Lab. Med.* 37 (5), 365–370. doi:10.3343/alm.2017.37.5.365

Schwarze, J. K., Awada, G., Cras, L., Tijtgat, J., Forsyth, R., Dufait, I., et al. (2020). Intratumoral Combinatorial Administration of CD1c (BDCA-1)(+) Myeloid Dendritic Cells Plus Ipilimumab and Avelumab in Combination with Intravenous Low-Dose Nivolumab in Patients with Advanced Solid Tumors: A Phase IB Clinical Trial. *Vaccines (Basel).* 8 (4). doi:10.3390/vaccines8040670

Scott, D. W. (2015). Cell-of-Origin in Diffuse Large B-Cell Lymphoma: Are the Assays Ready for the Clinic?. *Am. Soc. Clin. Oncol. Educ. Book*, e458–e466. doi:10.14694/edbook_am.2015.35.e458

Shah, A. A., David Bourne, T., and Murali, R. (2013). BAP1 Protein Loss by Immunohistochemistry: a Potentially Useful Tool for Prognostic Prediction in Patients with Uveal Melanoma. *Pathology* 45 (7), 651–656. doi:10.1097/pat.0000000000000002

Shelton, J., Purgina, B. M., Cipriani, N. A., Dupont, W. D., Plummer, D., and Lewis, J. S., Jr (2017). p16 Immunohistochemistry in Oropharyngeal Squamous Cell Carcinoma: a Comparison of Antibody Clones Using Patient Outcomes and High-Risk Human Papillomavirus RNA Status. *Mod. Pathol.* 30 (9), 1194–1203. doi:10.1038/modpathol.2017.31

Shembrey, C., Huntington, N. D., and Hollande, F. (2019). Impact of Tumor and Immunological Heterogeneity on the Anti-cancer Immune Response. *Cancers (Basel)* 11 (9). doi:10.3390/cancers11091217

Siow, Z. R., De Boer, R., Lindeman, G., and Mann, G. B. (2018). Spotlight on the Utility of the Oncotype DX® Breast Cancer Assay. *Int J Womens Health* 10, 89–100. doi:10.2147/ijwh.s124520

Soenksen, D. (2009). Digital Pathology at the Crossroads of Major Health Care Trends: Corporate Innovation as an Engine for Change. *Arch. Pathol. Lab. Med.* 133 (4), 555–559. doi:10.5858/133.4.555

Solomon, J. P., Linkov, I., Rosado, A., Mullaney, K., Rosen, E. Y., Frosina, D., et al. (2020). NTRK Fusion Detection across Multiple Assays and 33,997 Cases: Diagnostic Implications and Pitfalls. *Mod. Pathol.* 33 (1), 38–46. doi:10.1038/s41379-019-0324-7

Sompuram, S. R., Vani, K., Hafer, L. J., and Bogen, S. A. (2006). Antibodies Immunoreactive with Formalin-Fixed Tissue Antigens Recognize Linear Protein Epitopes. *Am. J. Clin. Pathol.* 125 (1), 82–90. doi:10.1309/6h0arqf7k3y608eh

Spidlen, J., Moore, W., Parks, D., Goldberg, M., Blenman, K., Cavenaugh, J. S., et al. (2021). Data File Standard for Flow Cytometry, Version FCS 3.2. *Cytometry* 99 (1), 100–102. doi:10.1002/cyto.a.24225

Stack, E. C., Wang, C., Roman, K. A., and Hoyt, C. C. (2014). Multiplexed Immunohistochemistry, Imaging, and Quantitation: a Review, with an Assessment of Tyramide Signal Amplification, Multispectral Imaging and Multiplex Analysis. *Methods* 70 (1), 46–58. doi:10.1016/j.ymeth.2014.08.016

Stathonikos, N., van Varsseveld, N. C., Vink, A., van Dijk, M. R., Nguyen, T. Q., Leng, W. W. J. d., et al. (2020). Digital Pathology in the Time of corona. *J. Clin. Pathol.* 73 (11), 706–712. doi:10.1136/jclinpath-2020-206845

Stein, S., Henze, L., Poch, T., Carambia, A., Krech, T., Preti, M., et al. (2021). IL-17A/F Enable Cholangiocytes to Restrict T Cell-Driven Experimental Cholangitis by Upregulating PD-L1 Expression. *J. Hepatol.* 74 (4), 919–930. doi:10.1016/j.jhep.2020.10.035

Stenzinger, A., and Weichert, W. (2020). Einfluss der neuen In-vitro-Diagnostik-Regulation (IVDR) der Europäischen Union auf die Pathologie. Was ist wichtig?. *Pathologe* 41 (Suppl. 2), 129–133. doi:10.1007/s00292-020-00867-9

Surace, M., DaCosta, K., Huntley, A., Zhao, W., Bagnall, C., Brown, C., et al. (2019). Automated Multiplex Immunofluorescence Panel for Immuno-Oncology Studies on Formalin-Fixed Carcinoma Tissue Specimens. *J. Vis. Exp.* 143. doi:10.3791/58390

Tacha, D. E., and Miller, R. T. (2004). Use of p63/P504S Monoclonal Antibody Cocktail in Immunohistochemical Staining of Prostate Tissue. *Appl. Immunohistochem. Mol. Morphol.* 12 (1), 75–78. doi:10.1097/00129039-200403000-00014

Tan, W. C. C., Nerurkar, S. N., Cai, H. Y., Ng, H. H. M., Wu, D., Wee, Y. T. F., et al. (2020). Overview of Multiplex Immunohistochemistry/immunofluorescence Techniques in the Era of Cancer Immunotherapy. *Cancer Commun.* 40 (4), 135–153. doi:10.1002/cac2.12023

Taube, J. M., Akturk, G., Angelo, M., Engle, E. L., Gnjatic, S., Greenbaum, S., et al. (2020). The Society for Immunotherapy of Cancer Statement on Best Practices for Multiplex Immunohistochemistry (IHC) and Immunofluorescence (IF) Staining and Validation. *J. Immunother. Cancer* 8 (1). doi:10.1136/jitc-2019-000155

Taylor, C. R. (1980). Immunohistologic Studies of Lymphoma: Past, Present, and Future. *J. Histochem. Cytochem.* 28 (8), 777–787. doi:10.1177/28.8.7003004

Tellez, D., Balkenhol, M., Otte-Holler, I., van de Loo, R., Vogels, R., Bult, P., et al. (2018). Whole-Slide Mitosis Detection in H&E Breast Histology Using PHH3 as a Reference to Train Distilled Stain-Invariant Convolutional Networks. *IEEE Trans. Med. Imaging* 37, 2126–2136. doi:10.1109/TMI.2018.2820199

Tetzlaff, M. T., Pattanaprichakul, P., Wargo, J., Fox, P. S., Patel, K. P., Estrella, J. S., et al. (2015). Utility of BRAF V600E Immunohistochemistry Expression Pattern as a Surrogate of BRAF Mutation Status in 154 Patients with Advanced Melanoma. *Hum. Pathol.* 46 (8), 1101–1110. doi:10.1016/j.humpath.2015.04.012

Toki, M. I., Merritt, C. R., Wong, P. F., Smithy, J. W., Kluger, H. M., Syrigos, K. N., et al. (2019). High-Plex Predictive Marker Discovery for Melanoma Immunotherapy-Treated Patients Using Digital Spatial Profiling. *Clin. Cancer Res.* 25 (18), 5503–5512. doi:10.1158/1078-0432.ccr-19-0104

Tsutsumi, Y. (2021). Pitfalls and Caveats in Applying Chromogenic Immunostaining to Histopathological Diagnosis. *Cells* 10 (6). doi:10.3390/cells10061501

Valkonen, M., Isola, J., Ylinen, O., Muhonen, V., Saxlin, A., Tolonen, T., et al. (2020). Cytokeratin-Supervised Deep Learning for Automatic Recognition of Epithelial Cells in Breast Cancers Stained for ER, PR, and Ki-67. *IEEE Trans. Med. Imaging* 39 (2), 534–542. doi:10.1109/tmi.2019.2933656

van der Laak, J., Litjens, G., and Ciompi, F. (2021). Deep Learning in Histopathology: the Path to the Clinic. *Nat. Med.* 27 (5), 775–784. doi:10.1038/s41591-021-01343-4

Vani, K., Sompuram, S. R., Schaedle, A. K., Balasubramanian, A., and Bogen, S. A. (2017). Analytic Response Curves of Clinical Breast Cancer IHC Tests. *J. Histochem. Cytochem.* 65 (5), 273–283. doi:10.1369/0022155417694869

Virchow, R. (1858). *Die Celllularpathologie*. London: John Churchill.

Vitale, I., Manic, G., Coussens, L. M., Kroemer, G., and Galluzzi, L. (2019). Macrophages and Metabolism in the Tumor Microenvironment. *Cel Metab.* 30 (1), 36–50. doi:10.1016/j.cmet.2019.06.001

Vitale, I., Shema, E., Loi, S., and Galluzzi, L. (2021). Intratumoral Heterogeneity in Cancer Progression and Response to Immunotherapy. *Nat. Med.* 27 (2), 212–224. doi:10.1038/s41591-021-01233-9

Wang, F., Flanagan, J., Su, N., Wang, L. C., Bui, S., Nielson, A., et al. (2012). RNAscope: a Novel *In Situ* RNA Analysis Platform for Formalin-Fixed, Paraffin-Embedded Tissues. *J. Mol. Diagn.* 14 (1), 22–29. doi:10.1016/j.jmoldx.2011.08.002

Webster, J. D., and Dunstan, R. W. (2014). Whole-Slide Imaging and Automated Image Analysis. *Vet. Pathol.* 51 (1), 211–223. doi:10.1177/0300985813503570

Weinstein, R., Holcomb, M., and Krupinski, E. (2019). Invention and Early History of Telepathology (1985-2000). *J. Pathol. Inform.* 10, 1. doi:10.4103/jpi.jpi_71_18

Willemsen, M., Krebbers, G., Bekkenk, M. W., Teunissen, M. B. M., and Luiten, R. M. (2021). Improvement of Opal Multiplex Immunofluorescence Workflow for Human Tissue Sections. *J. Histochem. Cytochem.*, 221554211007793.

Wilson, C. M., Ospina, O. E., Townsend, M. K., Nguyen, J., Moran Segura, C., Schildkraut, J. M., et al. (2021). Challenges and Opportunities in the Statistical Analysis of Multiplex Immunofluorescence Data. *Cancers (Basel).* 13 (12). doi:10.3390/cancers13123031

Wolff, A. C., Hammond, M. E. H., Allison, K. H., Harvey, B. E., McShane, L. M., and Dowsett, M. (2018). HER2 Testing in Breast Cancer: American Society of Clinical Oncology/College of American Pathologists Clinical Practice Guideline Focused Update Summary. *Jop* 14 (7), 437–441. doi:10.1200/jop.18.00206

Wong, H.-l., Christie, M., Gately, L., Tie, J., Lee, B., Semira, C., et al. (2018). Mismatch Repair Deficiency Assessment by Immunohistochemistry: for Lynch Syndrome Screening and beyond. *Future Oncol.* 14 (26), 2725–2739. doi:10.2217/fon-2018-0319

Xu-Monette, Z. Y., Zhang, M., Li, J., and Young, K. H. (2017). PD-1/PD-L1 Blockade: Have We Found the Key to Unleash the Antitumor Immune Response?. *Front. Immunol.* 8, 1597. doi:10.3389/fimmu.2017.01597

Yan, N., Zhang, Y., Guo, X., Yuan, D., Tian, G., and Yang, J. (2020). A Review on Cancer of Unknown Primary Origin: The Role of Molecular Biomarkers in the Identification of Unknown Primary Origin. *Methods Mol. Biol.* 2204, 109–119. doi:10.1007/978-1-0716-0904-0_10

Yan, W. H., Jiang, X. N., Wang, W. G., Sun, Y. F., Wo, Y. X., Luo, Z. Z., et al. (2020). Cell-of-Origin Subtyping of Diffuse Large B-Cell Lymphoma by Using a qPCR-Based Gene Expression Assay on Formalin-Fixed Paraffin-Embedded Tissues. *Front. Oncol.* 10, 803. doi:10.3389/fonc.2020.00803

Yemelyanova, A., Vang, R., Kshirsagar, M., Lu, D., Marks, M. A., Shih, I. M., et al. (2011). Immunohistochemical Staining Patterns of P53 Can Serve as a Surrogate Marker for TP53 Mutations in Ovarian Carcinoma: an Immunohistochemical and Nucleotide Sequencing Analysis. *Mod. Pathol.* 24 (9), 1248–1253. doi:10.1038/modpathol.2011.85

Zimak, J., Schweller, R. M., Duose, D. Y., Hittelman, W. N., and Diehl, M. R. (2012). Programming *In Situ* Immunofluorescence Intensities through Interchangeable Reactions of Dynamic DNA Complexes. *Chembiochem* 13 (18), 2722–2728. doi:10.1002/cbic.201200525

Zuraw, A., Staup, M., Klopfleisch, R., Aeffner, F., Brown, D., Westerling-Bui, T., et al. (2020). Developing a Qualification and Verification Strategy for Digital Tissue Image Analysis in Toxicological Pathology. *Toxicol. Pathol.*, 192623320980310.

Conflict of Interest: KAW, DW, MM, KM, and FL are employees of and shareholders in, and AZ a consultant for, Ultivue, Inc.

Publisher's Note: All claims expressed in this article are solely those of the authors and do not necessarily represent those of their affiliated organizations, or those of the publisher, the editors and the reviewers. Any product that may be evaluated in this article, or claim that may be made by its manufacturer, is not guaranteed or endorsed by the publisher.

frontiers in Molecular Biosciences

ORIGINAL RESEARCH
published: 30 July 2021
doi: 10.3389/fmolb.2021.661222

Pathology Quality Control for Multiplex Immunofluorescence and Image Analysis Assessment in Longitudinal Studies

*Rossana Lazcano, Frank Rojas, Caddie Laberiano, Sharia Hernandez and Edwin Roger Parra**

Department of Translational Molecular Pathology, The University of Texas MD Anderson Cancer Center, Houston, TX, United States

Immune profiling of formalin-fixed, paraffin-embedded tissues using multiplex immunofluorescence (mIF) staining and image analysis methodology allows for the study of several biomarkers on a single slide. The pathology quality control (PQC) for tumor tissue immune profiling using digital image analysis of core needle biopsies is an important step in any laboratory to avoid wasting time and materials. Although there are currently no established inclusion and exclusion criteria for samples used in this type of assay, a PQC is necessary to achieve accurate and reproducible data. We retrospectively reviewed PQC data from hematoxylin and eosin (H&E) slides and from mIF image analysis samples obtained during 2019. We reviewed a total of 931 reports from core needle biopsy samples; 123 (13.21%) were excluded during the mIF PQC. The most common causes of exclusion were the absence of malignant cells or fewer than 100 malignant cells in the entire section (n = 42, 34.15%), tissue size smaller than 4 × 1 mm (n = 16, 13.01%), fibrotic tissue without inflammatory cells (n = 12, 9.76%), and necrotic tissue (n = 11, 8.94%). Baseline excluded samples had more fibrosis (90 vs 10%) and less necrosis (5 vs 90%) compared with post-treatment excluded samples. The most common excluded organ site of the biopsy was the liver (n = 19, 15.45%), followed by soft tissue (n = 17, 13.82%) and the abdominal region (n = 15, 12.20%). We showed that the PQC is an important step for image analysis and that the absence of malignant cells is the most limiting sample characteristic for mIF image analysis. We also discuss other challenges that pathologists need to consider to report reliable and reproducible image analysis data.

Keywords: digital image analysis, biopsy, quality control, pathology, multiplex immunofluorescence

OPEN ACCESS

Edited by:
Joe Yeong,
*Institute of Molecular and Cell Biology (A*STAR), Singapore*

Reviewed by:
Lixue Cao,
Guangdong Provincial People's Hospital, China
Sizun Jiang,
Harvard Medical School, United States

****Correspondence:***
Edwin Roger Parra
erparra@mdanderson.org

Specialty section:
This article was submitted to Molecular Diagnostics and Therapeutics, a section of the journal Frontiers in Molecular Biosciences

Received: *30 January 2021*
Accepted: *19 July 2021*
Published: *30 July 2021*

Citation:
Lazcano R, Rojas F, Laberiano C, Hernandez S and Parra ER (2021) Pathology Quality Control for Multiplex Immunofluorescence and Image Analysis Assessment in Longitudinal Studies. Front. Mol. Biosci. 8:661222. doi: 10.3389/fmolb.2021.661222

INTRODUCTION

Pathology quality control (PQC) consists of multiple technical steps that evaluate and measure the quality of a sampling process (Adyanthaya and Jose, 2013). PQC also provides consistent checks to identify and address errors and obtain accurate, precise, and reproducible data (Mangino, 2006; Greig, 2019). A retrospective analysis at the National Cancer Institute Developmental Therapeutics Clinic found that 74% of the core needle biopsies performed in pharmacodynamic studies that included fluorescence and mass spectrometry analyses passed their quality control criteria (Ferry-Galow et al., 2016; Parchment and Doroshow, 2016). The study used hematoxylin and eosin (H&E)

slide-based analyses as the first PQC step and found that the lack of malignant cells (MCs) excluded the largest number of samples.

In the last 5 years, the immune profiling of formalin-fixed, paraffin-embedded (FFPE) tissues using multiplex immunofluorescence (mIF) staining and digital image analysis methodologies has arisen as a new technology to study several biomarkers on a single slide in longitudinal studies (Francisco-Cruz et al., 2020). However, an efficient PQC process developed by pathologists with experience in digital image analysis is needed. This type of PQC for image analysis and mIF is necessary to avoid expending unnecessary resources and laboratory personnel time (Parra et al., 2020) and to obtain high-quality and reproducible results.

The success of any research study that uses FFPE tissues depends on the quality of the samples. Therefore, it is important to establish minimum parameters for biopsy sample quality that should be met before the staining process begins (Ferry-Galow et al., 2018). Core needle biopsy samples are generally around 1.58 mm in diameter and 12.7 mm long, although their size can vary. The small size of these samples makes them the most challenging for digital image analysis because it is more likely for a significant proportion of the sample to be damaged during cutting, staining, and scanning, especially when sensitive staining methodologies such as mIF are used. Yet, these tissues are invaluable material for longitudinal studies, so efforts to obtain quality data, which is important for translational studies, should be maximized.

The goal of this manuscript is to maximize the workflow of the PQC for digital image analysis. Thus, we retrospectively studied this assessment to standardize the process, to minimize time and cost expenditures, and to guarantee high-quality and reproducible results using mIF and digital image analysis.

MATERIALS AND METHODS

From 4,371 biopsies collected by the Adaptive patient-oriented longitudinal learning and optimization program from different research programs at The University of Texas MD Anderson Cancer Center from January through December of 2019, we retrospectively reviewed the PQC reports based on the H&E slides of 931 core needle biopsies from longitudinal studies. Biopsies from different time points were included in this study (608 baseline biopsies and 323 post-treatment biopsies), and all the samples had been processed for mIF and digital image analysis to study the tumor microenvironment, including the presence of cytokeratins, SOX10, and GFAP to characterize malignant cells in different organs; immune checkpoint markers (i.e., PD-L1, B7-H3, B7-H4, IDO-1, VISTA, LAG3, ICOS, TIM3, and OX40); tumor-infiltrating lymphocyte markers (i.e., CD3, CD8, CD45RO, granzyme B, PD-1, and FOXP3); and markers to characterize myeloid-derived suppressor cells (i.e., CD68, CD66b, CD14, CD33, Arg-1, and CD11b), and these samples were placed in panels similar to those previously published (Parra et al., 2021).

Five principal characteristics as annotated in the H&E PQC reports of the biopsies were analyzed: 1) tissue size (length and width), 2) percentage of tumor area with respect to the total size of the sample, 3) percentage of MCs in the tumor area of the sample, 4) percentage of necrotic area, and 5) percentage of fibrosis. In parallel, the PQC of the digital image analysis was retrieved from the final data reports of the mIF panels and reviewed. Similar characteristics were analyzed on the mIF slides. For the cases in which image analysis could not be performed, the comments containing the criterion of exclusion were retrieved instead. All the data from the H&E and digital image analysis PQCs were tabulated, and the results are shown below.

RESULTS

None of the 931 core needle biopsies evaluated were excluded during the H&E PQC, while 123 biopsies (13.21%) were excluded during the digital image analysis PQC at low magnification (10x) (**Figures 1**, **2**). The range of excluded samples per project was 3.45–24.17%. Post-treatment samples were more frequently excluded (62 of 323, 19.20%) compared to the baseline samples (61 of 608, 10.03%). An important characteristic of the samples was their size. The median length was 12 mm (range, 1–24 mm), and the median width was around 1 mm (range, 0.8–1.2 mm). However, we observed that the median length of the samples excluded due to small size was 1.25 mm (range, 0.5–4 mm), and the median width was similar for included and excluded samples.

After we retrieved the annotated characteristics of the samples from the H&E PQC reports, we compared the baseline and post-treatment characteristics of the excluded and included samples. (See examples on **Figure 3**). In the excluded baseline biopsies, the median percentages of tumor area and MCs in the tumor area were both 0% (range, 0–60%). For the included baseline biopsies, the median tumor content area was 95% (range, 30–100%), and the median percentage of MCs in the tumor area was 60% (range, 5–100%). Interestingly, we observed that the excluded baseline samples had tumor areas with a median of 90% fibrotic areas compared to only 20% fibrotic areas in the included baseline samples. The percentage of necrosis was similar in the excluded and included samples. Furthermore, in the excluded post-treatment biopsies, the median tumor area was 10% and the percentage of MCs in the tumor area was 5%. In the included post-treatment samples, the median tumor area was 20% and the percentage of MCs in the tumor area was 50%. We also found a higher percentage of necrotic area in the excluded samples than in the included samples (median, 90 versus 25%, respectively). However, the percentage of fibrotic area was lower in the excluded post-treatment biopsies as shown in (**Table 1**).

When we reviewed the digital image analysis PQC reports for the excluded samples, the most common causes of exclusion were absence of MCs or fewer than 100 MCs (n = 42, 34.15%), small tissue sample size (n = 16, 13.01%), mostly fibrotic tissue without inflammatory cells (n = 12, 9.76%), and mostly necrotic tissue (n = 11, 8.94%). The less common reasons for exclusion were fragmentation conditions (n = 2, 1.63%); crushed cell artifact (n = 2, 1.63%); staining artifact, apparently for oxidation and

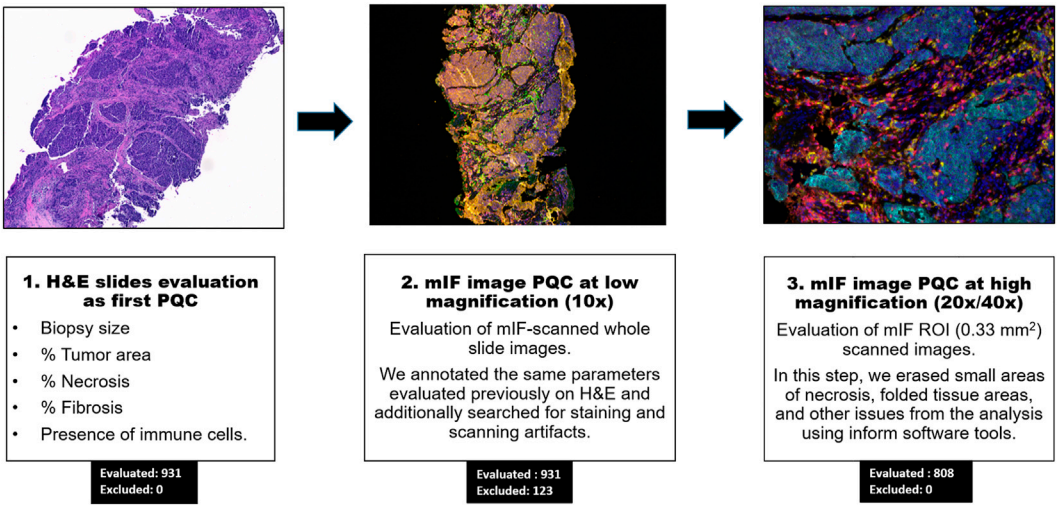

FIGURE 1 | Workflow of pathology quality control (PQC) for core needle biopsy sample assessment for multiplex immunofluorescence and digital image analysis. Showing the overall three steps of PQC, including assessment of the hematoxylin and eosin (H&E) slides for PQC, image analysis PQC at 10x magnification, and image analysis PQC of region of interest (ROI) images at 20x/40x magnification. The numbers of cases evaluated and excluded at each step are indicated.

desiccation of the sample (n = 2, 1.63%) and hemorrhagic tissue (n = 1, 0.81%); (**Table 2** and **Figure 4**). Although most of the samples showed one of the previously mentioned predominant causes for exclusion, some samples showed more than one cause for exclusion. For these samples, the most frequent combinatory factors were few or no MCs and mostly fibrotic tissue without inflammatory cells (n = 7, 5.69%) as well as mostly necrotic and fibrotic tissue without inflammatory cells (n = 4, 3.25%) (**Table 2**).

With respect to the site of the biopsy, the liver had the most samples excluded (19 of 123, 15.45%), followed by soft tissues (17 of 123, 13.82%) and the abdominal region (15 of 123, 12.20%). The remaining excluded samples came from a wide range of anatomic locations, such as the breast, cervix, gastrointestinal tract, lung, and lymph node, and none of these sites alone accounted for more than 10% of the total excluded samples (**Table 3**). It was possible to identify differences in the causes of exclusion in the context of the biopsy location. For example, liver biopsies were excluded more frequently due to fibrotic areas without inflammation, whereas soft tissue samples were excluded more frequently for having few or no MCs (**Figure 5**).

DISCUSSION

This study shows that different characteristics of core needle biopsies can impede digital image analysis, and PQC specific to digital image analysis can help guarantee high-quality and reproducible data. In this study, we observed that sample size, tumor content, percentage of necrosis, and percentage of fibrosis are important in quality control of physical and scanned H&E slides as well as scanned mIF slides. We also showed that a systematic PQC assessment of core needle biopsies is important to maintain the quality of the biopsies for image analysis.

According to our study, tissue size and tumor content were the most challenging and important characteristics for determining which samples could undergo digital image analysis to study the phenotypes expressed by the tumor immune microenvironment and MCs. We showed that 34.15% of the samples were excluded owing to the absence of MCs or low tumor content, and 13.01% of the samples were excluded owing to small sample size. These excluded samples had a median size of 1.25 x 1 mm. Similar to a previous study in which the most important exclusion criteria was the absence of MCs, 44% of the biopsy specimens evaluated in this study contained less than 25% viable MCs (Pisano et al., 2001). As we expected, in these core needle biopsy samples the most important measure that differentiated excluded and included biopsies was sample length, given that sample widths were determined by the different needle diameters as well as the fixation process.

As previously published (Parra et al., 2020), we noted that a tumor content of at least 10% in a biopsy sample that is at least 2 × 1 mm is enough to perform image analysis; however, we can successfully stain samples as small as 0.5 mm^2. The idea that these samples are representative of the entire tumor microenvironment is still controversial due to intratumoral heterogeneity in biomarker expression (Nicoś et al., 2020). Thus, we recommend an area of analysis at least 1 mm^2 to obtain reliable data from this type of sample, but this minimum area will vary depending on the tumor content of the sample (Padmanabhan et al., 2017). For example, in the literature there are publications that considered samples 10 mm in length to be adequate for the diagnosis of prostate cancer (Cicione et al., 2012) and 15 mm in length adequate for the diagnosis of liver disease (Palmer et al., 2014). Another study using mIF on pre-treatment biopsies and post-treatment tumor resections of breast carcinoma found that adequate tissue sampling, with at least 15 regions of interest, was necessary to

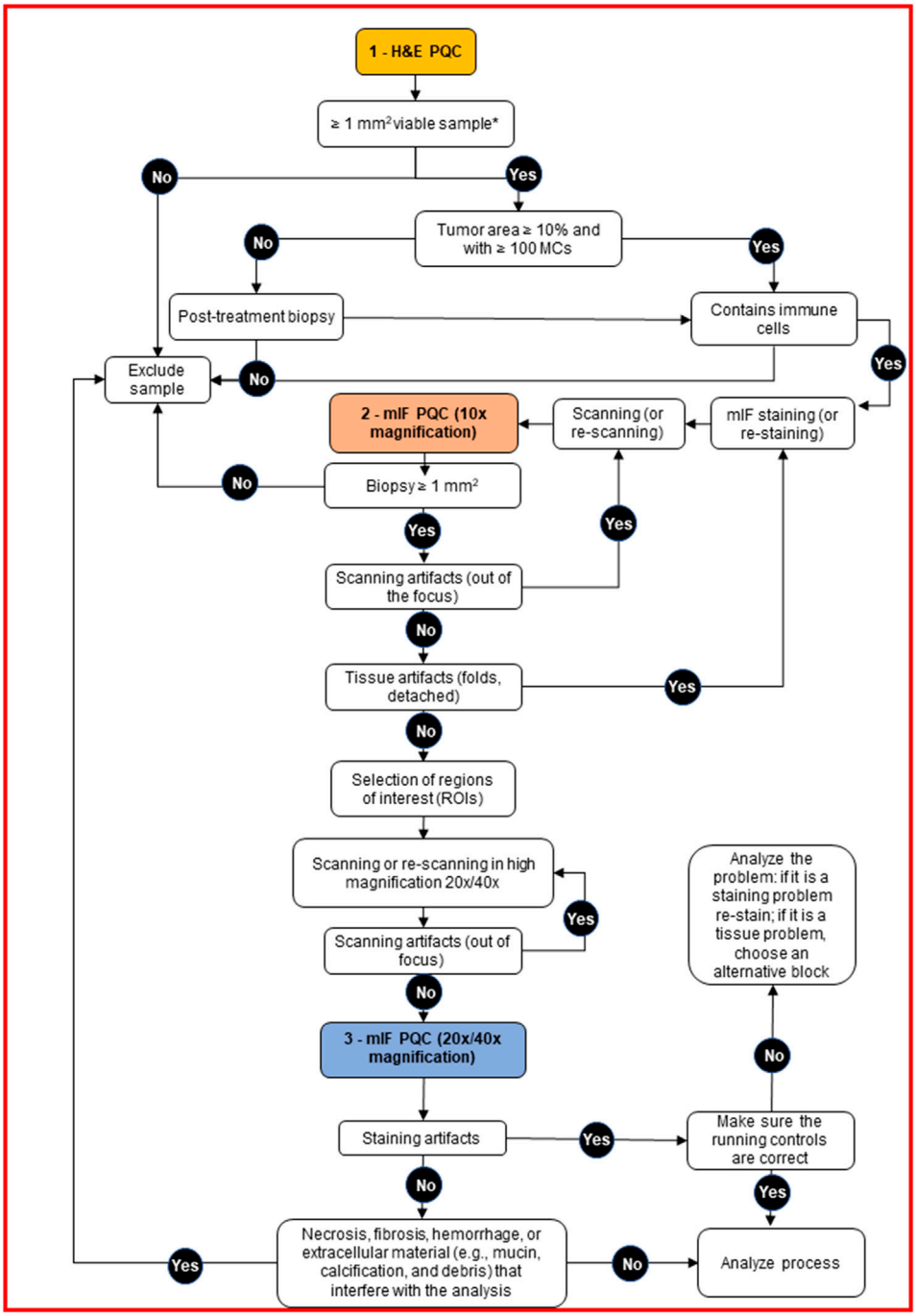

FIGURE 2 | Decision tree for pathology quality control (PQC) of core needle biopsy sample assessment for multiplex immunofluorescence and digital image analysis. The tree shows the detailed protocol with corresponding decisions for the pathologist to make during the three PQC steps. H&E, hematoxylin and eosin; MCs, malignant cells; mIF, multiplex immunofluorescence.

have a strong correlation between the tumor-infiltrating lymphocytes and PD-L1 markers included in an mIF panel and the H&E/PD-L1 clone SP142 clinical assays (Sanchez et al., 2021). However, there are not standardized image analysis PQC protocols to determine the minimum sample size needed for immunoprofiling, and more studies are warranted to address this need. We believe that each sample should be evaluated separately, according to its type (whole section or core needle biopsy) and the study aims.

When comparing baseline and post-treatment biopsies, the median tumor content was 90 vs 20%, respectively. While an adequate tumor presence is required in baseline biopsy samples,

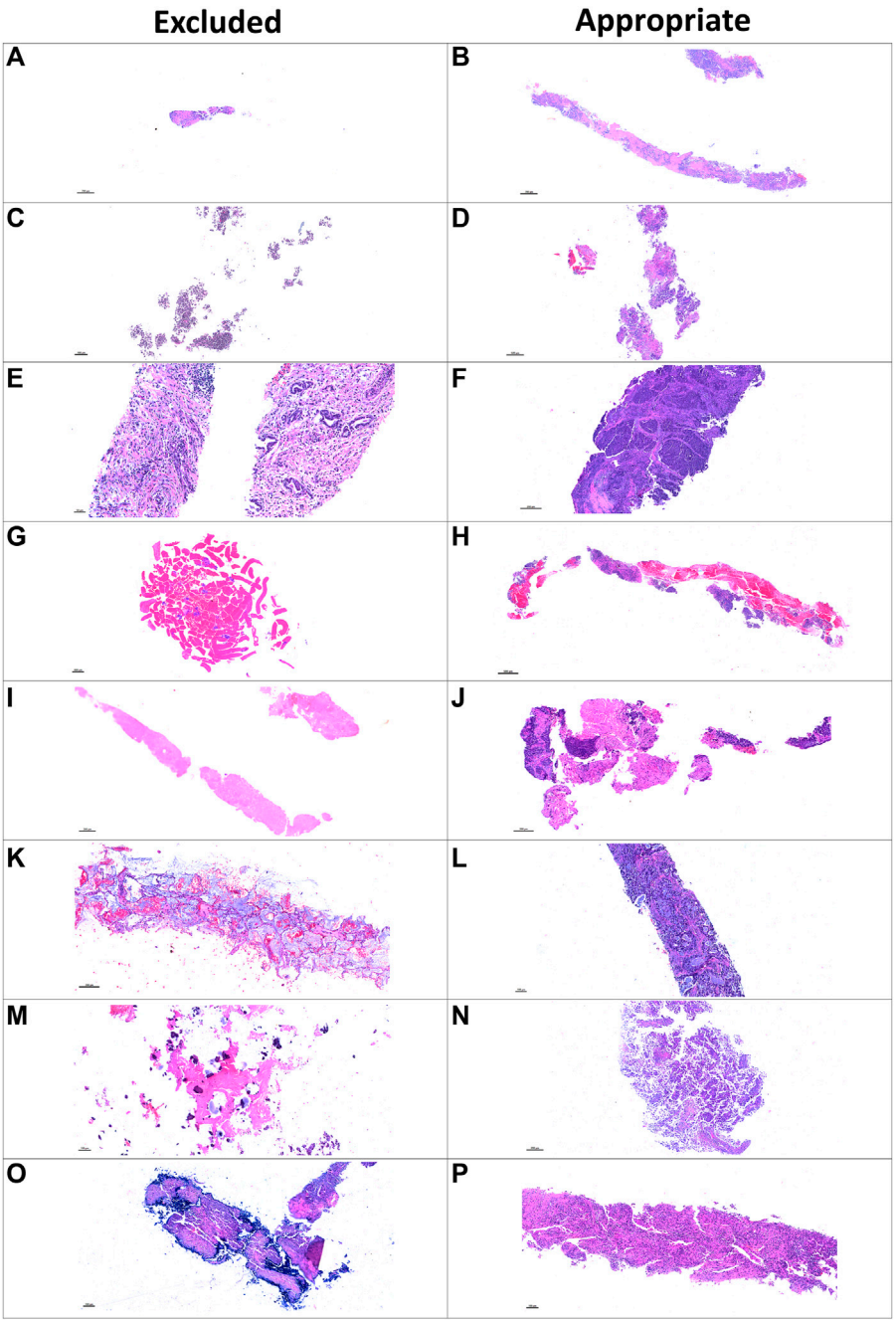

FIGURE 3 | Microphotographs of representative examples of excluded and included core needle biopsies using hematoxylin and eosin slides for pathology quality control. Excluded examples (*left column*) compared with samples considered appropriate for image analysis (*right column*). Small sample size **(A)** compared with a large, adequate sample **(B)**. Sample without malignant cells and only with normal tissue **(C)** compared with a sample with adequate amount of malignant cells **(D)**. Sample with extensive fragmentation **(E)** compared with another fragmented sample that could be included in the analysis **(F)**. Small sample with extensive hemorrhagic area **(G)** compared with another large sample with extensive hemorrhagic area but also with enough tumor content **(H)**. Sample with extensive necrotic area **(I)** compared with another similarly sized sample with enough tumor content for analysis **(J)**. Sample with mucinous and scattered malignant cells **(K)** compared with a sample considered appropriate for image analysis **(L)**. Sample with predominant fibrosis and calcification **(M)** compared with an adequate tumor-containing sample **(N)**. A biopsy with artifact of desiccation **(O)** compared with a well-preserved biopsy **(P)**.

fewer MCs or an absence of tumor cells in cases with complete pathological response after treatment is appropriate in post-treatment biopsy samples. Regarding the minimum number of MCs needed to analyze specific marker clones that are expressed by MCs, such as PD-L1, at least 100 MCs are recommended to obtain consistent and reliable data (Tsao

TABLE 1 | General overview of pathology quality control characteristics in our cohort (*N* = 931) divided by baseline (*N* = 608) and post-treatment (*N* = 323) core needle biopsies.

Biopsy timepoint	Status	N	Characteristic of the sample, median percentage			
			Tumor area	Malignant cells	Fibrosis	Necrosis
Baseline	Included	547	95	60	20	10
	Excluded	61	0	0	90	5
Post-treatment	Included	261	20	50	25	25
	Excluded	62	10	5	10	90

TABLE 2 | Characteristics of exclusion criteria observed during digital image analysis PQC (N = 123).

One exclusion criterion	Extent	N (%)
No or fewer than 100 MCs	Entire sample	42 (34.15)
Small biopsy size (< 1 mm^2)	Entire sample	16 (13.01)
Tissue availability after staining	Entire sample	14 (11.38)
Fibrotic tissue without inflammatory cells	More than 80%	12 (9.76)
Necrotic tissue	More than 80%	11 (8.94)
Fragmented biopsy	Entire sample	2 (1.63)
Staining artifact of oxidation/desiccation	Entire sample	2 (1.63)
Crushed cells artifact	Entire sample	2 (1.63)
Mostly hemorrhagic tissue	Entire sample	1 (0.81)
Two exclusion criteria		
No MCs or fewer than 100 MCs and fibrotic tissue without inflammatory cells	More than 80%	7 (5.69)
Necrotic tissue and fibrotic tissue without inflammatory cells	Entire sample	4 (3.25)
Fragmented biopsy and staining artifact of oxidation/desiccation	Entire sample	3 (2.44)
Small biopsy size and necrotic tissue	More than 80%	2 (1.63)
Necrotic tissue and crushed cells artifact	Entire sample	2 (1.63)
Small biopsy size and fibrotic tissue without inflammatory cells	More than 80%	1 (0.81)
No MCs or fewer than 100 MCs and necrotic tissue	More than 80%	1 (0.81)
Staining artifact of oxidation/desiccation and crushed cells artifact	Entire tissue	1 (0.81)
Total	**123**	**123 (100)**

PQC, pathology quality control; MC, malignant cell.

et al., 2018; Francisco-Cruz et al., 2020). However, there is not a consensus regarding the minimum number of MCs needed for image analysis of different markers expressed by MCs. According to our experience, we believe that a minimum of 100 MCs is needed to consider a sample as representative for digital image analysis. If the sample has fewer than 100 MCs, then we consider it to be inadequate to perform image analysis to study markers expressed by those cells. It is important to consider that when performing immune profiling for longitudinal studies, we work not only with baseline biopsies that need to contain enough MCs but also with post-treatment biopsies that many times lack enough MCs because of the effects of treatment. In these cases and when the study is not related to a specific marker expressed by MCs, exclusion of the sample shoud also be based on criteria other than the number of MCs, including the proportion of inflammatory cells, especially T-cells that play an important role in the tumor immune response, and other components such as fibrosis, edema, or necrosis (Hellmann et al., 2014).

The presence of inflammation in the tumor and stroma compartment is required when the aim of the study is to quantify the immune microenvironment (Parra et al., 2020). However, there is a lack of consensus on the areas that adequately show the inflammatory microenvironment. Thus, the pathologist must subjectively define an adequate area. After the mIF slides are scanned, the pathologist should always try to select the entire tumor area in the sample. However, they must capture at least 1 mm^2 of the regions of interest (Parra et al., 2020) to obtain reliable data

In our daily routine, we always look for characteristics such as inflammatory cells forming aggregates, as tertiary lymphoid structures (Sautès-Fridman et al., 2019) or in a diffuse distribution, as these can direct the analysis toward a reliable minimum quantity of cell phenotypes to obtain comprehensive data to be correlated with the clinicopathologic component. However, there is not a universal minimum number of cell phenotypes considered to be an adequate representation of the sample, partly because this number depends on the biological characteristics of the tumor and because we are often limited by software, which requires a minimum of five cells expressing a marker per sample to start the image analysis process.

Fibrotic samples without inflammatory cells are another important cause of exclusion. In our cohort, we excluded 9.76% of our samples because of this criterion in both baseline and post-

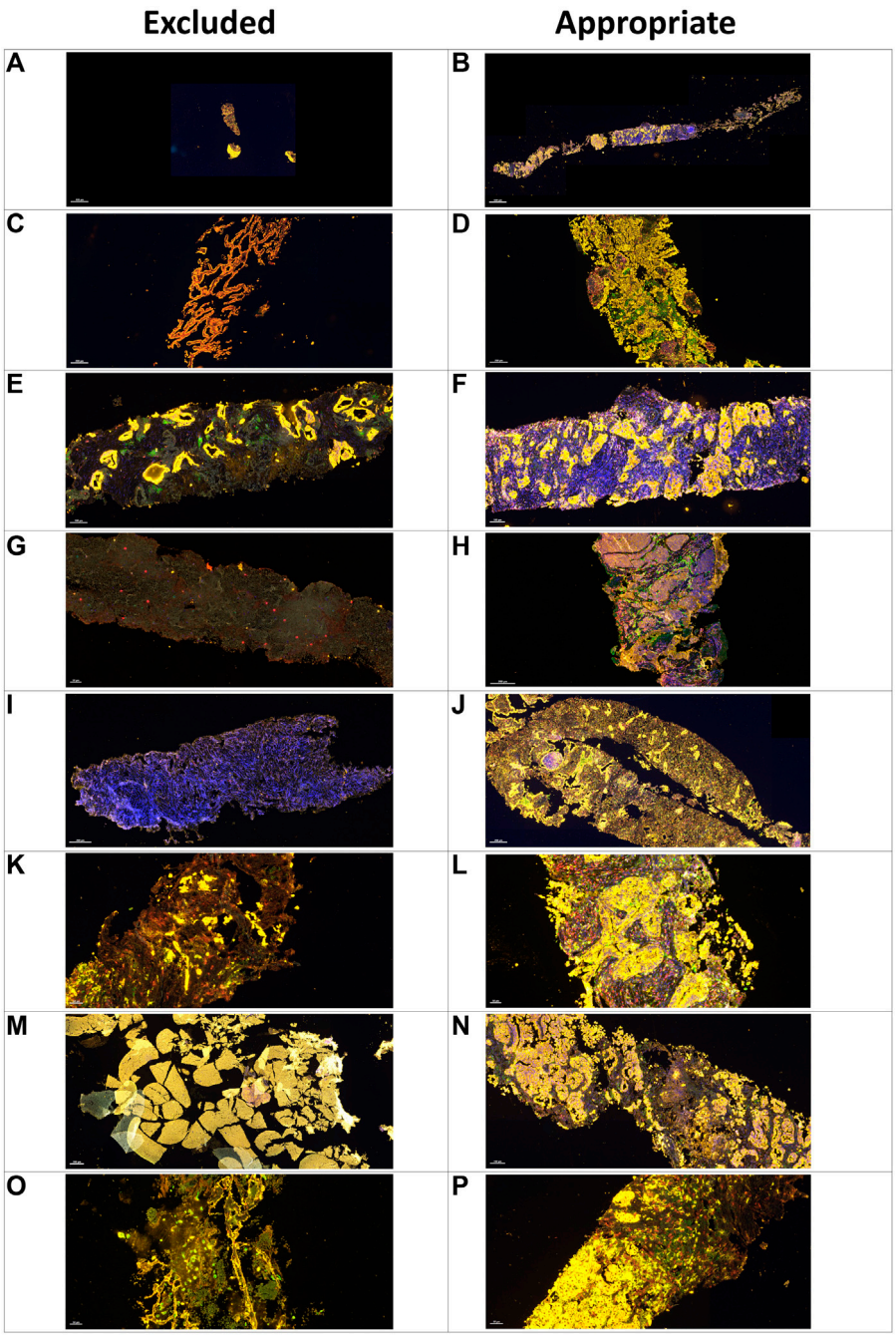

FIGURE 4 | Microphotographs of representative examples of excluded and included core needle biopsies in multiplex immunofluorescence slides using digital image analysis assessment for pathology quality control. Excluded examples (*Left column*) compared with samples considered appropriate for image analysis (*right column*). A small sample **(A)** compared with a large sample with adequate amount of tumor content in *yellow* **(B)**. Sample without malignant cells and with only normal tissue in *yellow* **(C)** compared with nets of malignant cells in *yellow* **(D)**. Nets of malignant cells in *yellow* in the middle of extensive fibrotic areas with lack of inflammatory cells **(E)** compared with a sample with a large amount of inflammatory cells **(F)**. Sample with extensive necrotic area in *grayish green* **(G)** compared with a sample without necrotic areas **(H)**. Sample with staining artifact showing the lack of marker expression **(I)** compared with another sample with adequate staining **(J)**. Sample with crushed cells artifact **(K)** compared with a sample with clear individualization of the different cells **(L)**. A hemorrhagic sample **(M)** compared with a sample with adequate tumor tissue **(N)**. A sample with mostly mucinous material and few tumor cells **(O)** compared with another sample with a regular amount of tumor cells **(P)**.

treatment samples. However, we found that our baseline and post-treatment samples had similar fibrotic content (20–25%). Curiously, we found that excluded baseline samples had more fibrotic content than excluded post-treatment samples (90 versus 10%, respectively). As expected, one of the important exclusion factors for post-treatment samples was necrosis, which was often a

TABLE 3 | Location of excluded core needle biopsies.

Location	N (%)
Connective tissue, head and neck	7 (5.69)
Ovary	2 (1.63)
Abdomen	15 (12.20)
Soft tissue	17 (13.82)
Brain	6 (4.88)
Breast	2 (1.63)
Cervix	3 (2.44)
Esophagus	1 (0.81)
Gastroesophageal junction	1 (0.81)
Kidney	6 (4.88)
Liver	19 (15.45)
Lung	8 (6.50)
Lymph node	7 (5.69)
Omentum	1 (0.81)
Bone	2 (1.63)
Pancreas	1 (0.81)
Parotid gland	1 (0.81)
Pelvis	1 (0.81)
Peritoneum	7 (5.69)
Pleura	3 (2.44)
Retroperitoneum	8 (6.50)
Sternum	1 (0.81)
Stomach	1 (0.81)
Thyroid gland	3 (2.44)
Total	123 (100)

result of the treatments' effects on tumors. Although this characteristic is often evaluated as a positive sign of treatment response, it is a limiting factor for digital image analysis (Parra et al., 2020).

Tissue artifact-related sample exclusion was less frequent (1.63%). When the H&E PQC is performed properly, these tissue artifacts could be related to the effects of surgical trauma, tissue ischemia, poor fixation, cutting procedures, or scanning problems (Flamminio et al., 2011). Even subtle artifacts can have large implications for the algorithms used to recognize positive biomarkers, resulting in inaccuracies. For this reason, there have been many attempts to create digital pathology tools for automated PQC (Ameisen et al., 2013; Senaras et al., 2018; Bengtsson and Ranefall, 2019). Software for automated PQC that employs image metrics and identifies H&E scanned slides with gross technical artifacts exists, but it is not suitable for use on mIF-stained slides (Janowczyk et al., 2019).

We also observed that some specific organ site characteristics can interfere with the image analysis and thus are extremely important in digital imaging analysis PQC. The most often excluded biopsy site was the liver, with extensive fibrosis as the most common exclusion criterion. Soft tissue samples were excluded the second most often, mainly for absence of or few MCs. Nevertheless, these high rates of exclusion could be related to the high numbers of liver and soft tissue projects included in our study. Each location or organ has its own technical specifications for obtaining an adequate sample. For example, for breast cancers, some authors have described that the use of the semi-automated needle yielded a 23% rate of inadequate results compared to 9% when using an automated needle to obtain breast samples (Sridharan et al., 2015). Different needle sizes are

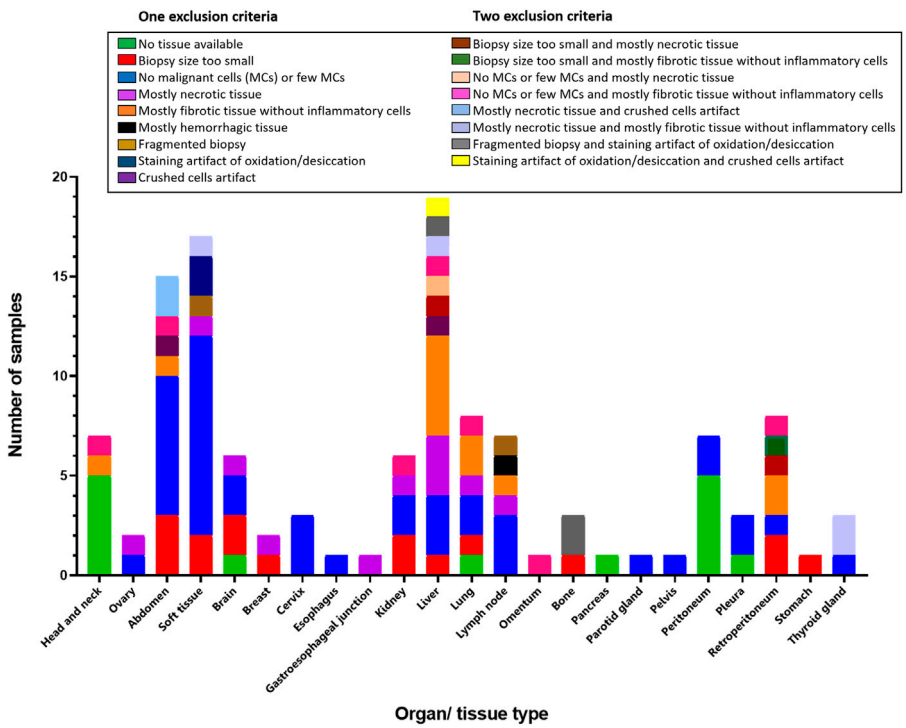

FIGURE 5 | Bar graph showing localization and exclusion criteria of the samples. Inset box containing the exclusion criteria divided in one or two criteria.

recommended depending on the organ and its vascularization status to avoid the risk of hemorrhage, especially in liver samples (Hall et al., 2017; Hoang et al., 2018). However, the use of different needle sizes did not to affect the quality of the biopsy of breast tissue (Huang et al., 2017). For these reasons, each specialist must analyze the risks and benefits of the selected biopsy technique and its effect on the quality of samples.

Finally, other tissue characteristics that should be avoided for the mIF analysis but were not found to be exclusion criteria in the current study are the presence of noncellular materials, e.g., glandular secretions; intra-alveolar material, which may contain inflammatory cells and debris; cartilage; bone tissue, in which decalcification may affect tissue staining; and adipose tissue, which can lead to tissue detachment during the staining process (Parra et al., 2021).

In conclusion, PQC for digital image analysis for mIF is extremely important to obtain reliable results. However, consensus and guidelines are necessary to produce reliable data in multi-institutional longitudinal studies. Evaluation of H&E slides at the beginning of any process as well as evaluation of mIF image slides for digital image analysis is fundamental and should consider the study design and material received, including the markers included in the mIF panels.

DATA AVAILABILITY STATEMENT

The raw data supporting the conclusion of this article will be made available by the authors, without undue reservation.

ETHICS STATEMENT

Ethical review and approval was not required for the study on human participants in accordance with the local legislation and institutional requirements. The patients/participants provided their written informed consent to participate in this study.

AUTHOR CONTRIBUTIONS

RL and EP conceived the idea and the theme of this manuscript and developed this manuscript. RL wrote most of this manuscript. FR, CL, and SH contributed to the writing of this manuscript with their expertise on pathology quality control and tissue immune profiling using digital image analysis. EP developed the technology in our laboratory and edited the manuscript according to his experience.

FUNDING

This study was supported in part by the scientific and financial support for the CIMAC-CIDC Network provided through the National Cancer Institute (NCI) Cooperative Agreement U24CA224285 of The University of Texas MD Anderson Cancer Center CIMAC and for the Translational Molecular Pathology Immunoprofiling Platform, as well as by National Institutes of Health/NCI through Cancer Center Support Grant P30CA016672 (Institutional Tissue Bank) and SPORE grant 5P50CA070907-18 from the Cancer Prevention and Research Institute of Texas through MIRA RP160668.

ACKNOWLEDGMENTS

The author acknowledges the Multiplex Immunoflourescence and Digital Pathology Laboratory at Department of Translational Molecular Pathology, The University of Texas MD Anderson Cancer Center who contribute daily to quality multiplex immunoflourescence and IHC processing. We also thank Dawn Chalaire, Associate Director, and Ashli Nguyen-Villarreal, Associate Scientific Editor, in the Research Medical Library at The University of Texas MD Anderson Cancer Center, for editing this article.

REFERENCES

Adyanthaya, S., and Jose, M. (2013). Quality and Safety Aspects in Histopathology Laboratory. *J. Oral Maxillofac. Pathol.* 17 (3), 402–407. doi:10.4103/0973-029X.125207

Ameisen, D., Deroulers, C., Perrier, V., Yunès, J.-B., Bouhidel, F., Battistella, M., et al. (2013). Stack or Trash? Quality Assessment of Virtual Slides. *Diagn. Pathol.* 8 (Suppl. 1), S23. doi:10.1186/1746-1596-8-s1-s23

Bengtsson, E., and Ranefall, P. (2019). Image Analysis in Digital Pathology: Combining Automated Assessment of Ki67 Staining Quality with Calculation of Ki67 Cell Proliferation Index. *Cytometry* 95 (7), 714–716. doi:10.1002/cyto.a.23685

Cicione, A., Cantiello, F., De Nunzio, C., Tubaro, A., and Damiano, R. (2012). Prostate Biopsy Quality Is Independent of Needle Size: A Randomized Single-Center Prospective Study. *Urol. Int.* 89 (1), 57–60. doi:10.1159/000339250

Ferry-Galow, K. V., Datta, V., Makhlouf, H. R., Wright, J., Wood, B. J., Levy, E., et al. (2018). What Can Be Done to Improve Research Biopsy Quality in Oncology Clinical Trials?. *J. Oncol. Pract.* 14, JOP1800092. doi:10.1200/JOP.18.00092

Ferry-Galow, K. V., Makhlouf, H. R., Wilsker, D. F., Lawrence, S. M., Pfister, T. D., Marrero, A. M., et al. (2016). The Root Causes of Pharmacodynamic Assay Failure. *Semin. Oncol.* 43 (4), 484–491. doi:10.1053/j.seminoncol.2016.06.006

Flamminio, F., Tosi, A. L., and Fellegara, G. (2011). Crushing Artifacts Resulting in Small Blue Cellular Clusters that Simulate Small Cell Carcinoma. *Int. J. Surg. Pathol.* 19 (4), 487–491. doi:10.1177/1066896911411187

Francisco-Cruz, A., Parra, E. R., Tetzlaff, M. T., and Wistuba, II (2020). Multiplex Immunofluorescence Assays. *Methods Mol. Biol.* 2055, 467–495. doi:10.1007/978-1-4939-9773-2_22

Greig, B. (2019). Quality Control of Immunophenotyping. *Methods Mol. Biol.* 2032, 227–279. doi:10.1007/978-1-4939-9650-6_14

Hall, T. C., Deakin, C., Atwal, G. S., and Singh, R. K. (2017). Adequacy of Percutaneous Non-Targeted Liver Biopsy Under Real-Time Ultrasound Guidance when Comparing the Biopince and Achieve Biopsy Needle. *Br. J. Radiol.* 90 (1080), 20170397. doi:10.1259/bjr.20170397

Hellmann, M. D., Chaft, J. E., William, W. N., Jr., Rusch, V., Pisters, K. M. W., Kalhor, N., et al. (2014). Pathological Response after Neoadjuvant Chemotherapy in Resectable Non-Small-Cell Lung Cancers: Proposal for the Use of Major Pathological Response as a Surrogate Endpoint. *Lancet Oncol.* 15 (1), e42–e50. doi:10.1016/s1470-2045(13)70334-6

Hoang, N. S., Ge, B. H., Pan, L. Y., Ozawa, M. G., Kong, C. S., Louie, J. D., et al. (2018). Determining the Optimal Number of Core Needle Biopsy Passes for Molecular Diagnostics. *Cardiovasc. Intervent Radiol.* 41 (3), 489–495. doi:10.1007/s00270-017-1861-4

Huang, M. L., Hess, K., Candelaria, R. P., Eghtedari, M., Adrada, B. E., Sneige, N., et al. (2017). Comparison of the Accuracy of US-Guided Biopsy of Breast Masses Performed with 14-gauge, 16-gauge and 18-gauge Automated Cutting Needle Biopsy Devices, and Review of the Literature. *Eur. Radiol.* 27 (7), 2928–2933. doi:10.1007/s00330-016-4651-5

Janowczyk, A., Zuo, R., Gilmore, H., Feldman, M., and Madabhushi, A. (2019). HistoQC: An Open-Source Quality Control Tool for Digital Pathology Slides. *JCO Clin. Cancer Inform.* 3, 1–7. doi:10.1200/cci.18.00157

Mangino, J. (2006). IPCC Good Practice Guidance and Uncertainty Management in National Greenhouse Gas Inventories. *Simon Eggelston LB, Kyoko Miwa, Todd Ngara, Kiyoto Tanabe*. Tokyo, Japan: Intergovernmental Panel on Climate Change (IPCC) by the Institute for Global Environmental Strategies.

Nicoś, M., Krawczyk, P., Crosetto, N., and Milanowski, J. (2020). The Role of Intratumor Heterogeneity in the Response of Metastatic Non-Small Cell Lung Cancer to Immune Checkpoint Inhibitors. *Front. Oncol.* 10, 569202. doi:10.3389/fonc.2020.569202

Padmanabhan, V., Steinmetz, H. B., Rizzo, E. J., Erskine, A. J., Fairbank, T. L., de Abreu, F. B., et al. (2017). Improving Adequacy of Small Biopsy and Fine-Needle Aspiration Specimens for Molecular Testing by Next-Generation Sequencing in Patients with Lung Cancer: A Quality Improvement Study at Dartmouth-Hitchcock Medical Center. *Arch. Pathol. Lab. Med.* 141 (3), 402–409. doi:10.5858/arpa.2016-0096-oa

Palmer, T., Georgiades, I., Treanor, D., Wright, A., Shah, M., Khosla, R., et al. (2014). Improved Tissue Sections for Medical Liver Biopsies: A Comparison of 16 vs 18 G Biopsy needles Using Digital Pathology. *J. Clin. Pathol.* 67 (5), 415–419. doi:10.1136/jclinpath-2013-201954

Parchment, R. E., and Doroshow, J. H. (2016). Theory and Practice of Clinical Pharmacodynamics in Oncology Drug Development. *Semin. Oncol.* 43 (4), 427–435. doi:10.1053/j.seminoncol.2016.07.001

Parra, E. R., Ferrufino-Schmidt, M. C., Tamegnon, A., Zhang, J., Solis, L., Jiang, M., et al. (2021). Immuno-profiling and Cellular Spatial Analysis Using Five Immune Oncology Multiplex Immunofluorescence Panels for Paraffin Tumor Tissue. *Sci. Rep.* 11 (1), 8511. doi:10.1038/s41598-021-88156-0

Parra, E. R., Jiang, M., Solis, L., Mino, B., Laberiano, C., Hernandez, S., et al. (2020). Procedural Requirements and Recommendations for Multiplex Immunofluorescence Tyramide Signal Amplification Assays to Support Translational Oncology Studies. *Cancers (Basel).* 12 (2), 255. doi:10.3390/cancers12020255

Pisano, E. D., Fajardo, L. L., Caudry, D. J., Sneige, N., Frable, W. J., Berg, W. A., et al. (2001). Fine-Needle Aspiration Biopsy of Nonpalpable Breast Lesions in a Multicenter Clinical Trial: Results from the Radiologic Diagnostic Oncology Group V. *Radiology* 219 (3), 785–792. doi:10.1148/radiology.219.3.r01jn28785

Sanchez, K., Kim, I., Chun, B., Pucilowska, J., Redmond, W. L., Urba, W. J., et al. (2021). Multiplex Immunofluorescence to Measure Dynamic Changes in Tumor-Infiltrating Lymphocytes and PD-L1 in Early-Stage Breast Cancer. *Breast Cancer Res.* 23 (1), 2. doi:10.1186/s13058-020-01378-4

Sautès-Fridman, C., Petitprez, F., Calderaro, J., and Fridman, W. H. (2019). Tertiary Lymphoid Structures in the Era of Cancer Immunotherapy. *Nat. Rev. Cancer* 19 (6), 307–325. doi:10.1038/s41568-019-0144-6

Senaras, C., Niazi, M. K. K., Lozanski, G., and Gurcan, M. N. (2018). DeepFocus: Detection of Out-Of-Focus Regions in Whole Slide Digital Images Using Deep Learning. *PLoS One* 13 (10), e0205387. doi:10.1371/journal.pone.0205387

Sridharan, R., Yunos, S. M., Aziz, S., Hussain, R. I., Alhabshi, S. M., Suria Hayati, M. P., et al. (2015). Comparison on the Use of Semi-Automated and Automated Core Biopsy Needle in Ultrasound Guided Breast Biopsy. *Med. J. Malaysia* 70, 326–333.

Tsao, M. S., Kerr, K. M., Kockx, M., Beasley, M.-B., Borczuk, A. C., Botling, J., et al. (2018). PD-L1 Immunohistochemistry Comparability Study in Real-Life Clinical Samples: Results of Blueprint Phase 2 Project. *J. Thorac. Oncol.* 13 (9), 1302–1311. doi:10.1016/j.jtho.2018.05.013

Conflict of Interest: The authors declare that the research was conducted in the absence of any commercial or financial relationships that could be construed as a potential conflict of interest.

Publisher's Note: All claims expressed in this article are solely those of the authors and do not necessarily represent those of their affiliated organizations, or those of the publisher, the editors and the reviewers. Any product that may be evaluated in this article, or claim that may be made by its manufacturer, is not guaranteed or endorsed by the publisher.

frontiers in Molecular Biosciences

REVIEW
published: 31 August 2021
doi: 10.3389/fmolb.2021.660202

Best Practices for Technical Reproducibility Assessment of Multiplex Immunofluorescence

*Caddie Laberiano-Fernández, Sharia Hernández-Ruiz, Frank Rojas and Edwin Roger Parra **

Department of Translational Molecular Pathology, The University of Texas MD Anderson Cancer Center, Houston, TX, United States

Multiplex immunofluorescence (mIF) tyramide signal amplification is a new and useful tool for the study of cancer that combines the staining of multiple markers in a single slide. Several technical requirements are important to performing high-quality staining and analysis and to obtaining high internal and external reproducibility of the results. This review manuscript aimed to describe the mIF panel workflow and discuss the challenges and solutions for ensuring that mIF panels have the highest reproducibility possible. Although this platform has shown high flexibility in cancer studies, it presents several challenges in pre-analytic, analytic, and post-analytic evaluation, as well as with external comparisons. Adequate antibody selection, antibody optimization and validation, panel design, staining optimization and validation, analysis strategies, and correct data generation are important for reproducibility and to minimize or identify possible issues during the mIF staining process that sometimes are not completely under our control, such as the tissue fixation process, storage, and cutting procedures.

Keywords: reproducibility, standardization, analytical evaluation, clinical application, multiplex immunofluorescence

OPEN ACCESS

Edited by:
Joe Yeong,
*Institute of Molecular and Cell Biology (A*STAR), Singapore*

Reviewed by:
Dong Ren,
The First Affiliated Hospital of Sun Yat-sen University, China
Brian Beliveau,
University of Washington, United States

***Correspondence:**
Edwin Roger Parra
erparra@mdanderson.org

Specialty section:
This article was submitted to Molecular Diagnostics and Therapeutics, a section of the journal Frontiers in Molecular Biosciences

Received: *29 January 2021*
Accepted: *11 August 2021*
Published: *31 August 2021*

Citation:
Laberiano-Fernández C, Hernández-Ruiz S, Rojas F and Parra ER (2021) Best Practices for Technical Reproducibility Assessment of Multiplex Immunofluorescence. Front. Mol. Biosci. 8:660202. doi: 10.3389/fmolb.2021.660202

INTRODUCTION

Multiplex immunofluorescence (mIF) tyramide signal amplification (TSA) is a new and useful tool for the study of cancer that combines the staining with multispectral imaging analysis technology, allows the design of mIF panels for up to six biomarkers, characterizes the co-expression of markers (cell phenotypes), and quantifies these markers overall with the use of a nuclear counterstain (DAPI) in a single slide (Parra et al., 2019; Francisco-Cruz et al., 2020b). Different mIF panels can be created using this technology to study the tissue microenvironment. The multispectral fluorescence microscope, along with the combined markers and individual fluorophores, is used to create a multispectral image that facilitates the analysis. By incorporating image analysis software, the images generated by the scanners can be easily analyzed and the cellular populations quantified (Parra et al., 2021a). mIF facilitates assessments at the cellular level of different proteins, as well as their spatial arrangement, and thus enables precision medicine in immuno-oncology, translational research, and clinical practice by elucidating the immune response of the human body to diverse tumors and showing differences in the pre- and post-treatment tissue.

Using mIF, it is possible to study the co-expression between markers to identify distinct cell populations and pathways and their relationships in different tissues and in turn to determine their roles in clinical outcomes (Parra, 2021). In that way, targetable biomarker pathways, such as PD-1/PD-L1, can be studied to verify the effect of immune therapies in the tumor microenvironment and

their clinical benefit (Velcheti et al., 2014; Schalper et al., 2015; Parra et al., 2018a; Barua et al., 2018). This technology therefore has an important role in translational oncology research (Stauber et al., 2010; Steiner et al., 2014; Sood et al., 2016; Rost et al., 2017; Gorris et al., 2018) and facilitating our understanding of the disease (Blom et al., 2017; Hofman et al., 2019). mIF also has applicability for diseases other than cancer, and it is well suited for prognostication at early stages of pathogenesis, when key signaling protein levels and activities are perturbed (Dejima et al., 2021). On the clinical side, there is high demand to incorporate mIF in a Clinical Laboratory Improvement Amendments (CLIA) certified as an innovative tool for diagnosis and prognosis.

The mIF-TSA workflow starts with antibody selection, optimization, and validation and ends with a digital image analysis (Parra et al., 2020). It is important to refine, standardize, optimize, and validate the end-to-end workflow in mIF to obtain reproducible results to support large-scale multi-site trials and individual principal investigator projects and to enable their possible clinical application.

The reproducibility of results remains the cornerstone of modern science (Hewitt, 2016). Given reproducible results, considering possible technical and human problems, with adequate protocols, each laboratory or institution can proceed in the same direction, using published experiences as a reference. Pre-analytic, analytic, and post-analytic variables that may influence reproducibility, quality, and staining procedure should be considered (Rojo et al., 2009; Okoye and Nnatuanya, 2015; Rudbeck, 2015; Meyerholz and Beck, 2018). Most of the descriptions related to these variables are focused on immunohistochemistry (IHC) on the basis of a study by Engel and others, who recognized more than 60 variables in the pre-analytic stage alone (Engel and Moore, 2011) and some variables which can be considered are pre-fixation, reagent conditions, and slide preparation, but those same variables can also be applied for IF and mIF.

It was recognized over a decade ago that standardization is vital for reproducible and reliable results in IHC (Goldstein et al., 2007). Agencies such as the Biological Stain Commission, Clinical and Laboratory Standards Institute, The U.S. Food and Drug Administration, and the manufacturing sector have established guidelines, standards, and recommendations for reagents and package inserts (Taylor, 1992; Taylor, 1998; Taylor, 1999; Goldstein et al., 2007). Although all of this effort has improved the quality of IHC, most of the causative responsibility rests with the individual laboratory performing the analysis, specifically the lack of standardization and attention to quality assurance programs (Rhodes, 2003; Varma et al., 2004; Goldstein et al., 2007).

CLIA requirements for determining test performance specifications apply to all laboratory tests. All the improvements related to reproducibility can positively affect the CLIA evaluation. For IHC assays, accuracy, analytic sensitivity, and specificity are determined by analytic assay validation, which is theoretically achieved by testing a validation tissue set against a gold standard (Fitzgibbons et al., 2014). In the last year, we saw an increase in the use of this technique but the requirement aspects to be reproducible are not well established between the different centers and research groups. There are also few manuscripts about mIF reproducibility (Akturk et al., 2021; Taube et al., 2021) which have been published; thus, it is important to compare the results directly.

In the present article, we review and describe the difficulties in the reproducibility of the main workflow-related steps of the mIF technique and how to optimize the process.

PRE-ANALYTIC EVALUATION

To develop a reproducible mIF imaging platform, several technical requirements must be met: 1) rigorous tissue quality controls, 2) a balanced multiplex assay staining format, 3) the ability to quantitate multiple markers in a defined region of interest (considering a minimum number of areas selected), and 4) experimental reproducibility, both internally and across different laboratories (Shipitsin et al., 2014).

For all these considerations, the IHC and mIF staining and imaging protocols must be standardized, automated, and validated. Being able to adapt IHC workflows in mIF without extensive re-optimization saves time and avoids human error, making it useful for translational research and future clinical applications (Tumeh et al., 2014; Giraldo et al., 2018; Tan et al., 2020).

ANTIBODY SELECTION, OPTIMIZATION, AND CONTROLS GUIDING REPRODUCIBILITY

The staining protocol for mIF can begin with the selection of the antibodies and their optimization by IHC or IF according to the experience and confidence of the pathologist, especially when starting with IF instead of IHC (Carvajal-Hausdorf et al., 2015). In that way, the antibody selection for mIF panel design can be considered the first step for developing a panel and needs to be done by a multidisciplinary team, including pathologists, oncologists, and immunologists. Some antibodies can be selected because of their clinical implications, while other antibodies, such as those targeting immune checkpoint markers (Francisco-Cruz et al., 2020a) may be selected to answer specific scientific or research questions. Then, choosing the correct antibody's clones and their optimization by IHC or IF is crucial to detect specific epitopes. In parallel, the selection of correct controls, negative or positive, is essential to the valid interpretation of the staining (Engel and Moore, 2011), and it is one aspect by which methods can be systematically assessed in consecutive multiplexed assays to confirm reproducibility (Canadian Association of Pathologists-Association canadienne des pathologistes National Standards Committee et al., 2010; Stack et al., 2014). For antibody selection, each antibody's clonality must be considered regarding its advantages and disadvantages (**Table 1**). Monoclonal antibodies are often preferred for IHC and IF because of their higher specificity

TABLE 1 | Advantage and disadvantages of polyclonal and monoclonal antibodies.

	Antibody's type		
—	**Polyclonal**	**Monoclonal**	**Recombinant**
Advantage	Low cost to produce	Homogeneity is conserved between batches to ensure reproducible results	Improved reproducibility and control
	Quick turnaround time from antigen preparation to antibody harvesting	High specificity for single epitope	Antibodies can be produced rapidly
	Ability to detect multiple epitopes on an antigen	Less background	No host animals are need
	High affinity and sensitivity to detect low quantity proteins	Specificity of monoclonal antibodies make them efficient	Easier isotype conversion
	Preferred for detection of denatured proteins	Cross-reactivity with other molecules is reduced	
Disadvantage	Higher tolerance for differences in antigen	Significantly more expensive to produce	High cost to develop and produce
	Variability in each batch	Require more specialized training to create and have a much longer turnaround time	High degree of technical skills of the professionals is required
	Non-specific antibody	Cover only one epitope	
	Multiple epitopes cause high chance of cross-reactivity resulting in higher background	More sensitive to buffer conditions	

and reproducibility and lower background and lot-to-lot variability. They are usually generated against unique peptides of the target antigen, located in regions that are less affected by formalin fixation. In contrast, polyclonal antibodies bind to different epitopes on the same protein and are obtained from experimental animals through repetitive stimulation of the antigen. Finally, recombinant antibodies, produced by recombinant DNA technology, should also be considered.

Another aspect to evaluate is the potential impact of antibody sensitivity and specificity during the optimization process considering the antibodies must be verified by the user (Taylor, 1999). Besides, in the optimization process, staining intensity can be modified according to the results of a pre-analytic study, which may be affected by methodological variables such as tissue fixation, antibody specificity and dilution, antigen retrieval duration and type, and detection systems (Ng et al., 2018). For this reason, it is crucial to compare samples using external or internal control. While cell lines are useful for testing individual markers and defining their expression level, they are not completely appropriate to use as positive controls; the most rigorous are tissue controls (Hewitt et al., 2014), which can contain multiple proteins, unlike pure cell line preparations. In addition, negative controls are used to demonstrate that the reaction visualized is a result of the interaction of the epitope of the target molecule and the paratope of the antibody or affinity reagent, demonstrating the specificity of the antibody (Hewitt et al., 2014) during the run staining. Although antibodies must be prepared according to the vendors' instructions, the experience of laboratory members, under pathologist supervision, is important to determine optimal staining conditions and correct marker expression as part of quality control **Figure 1**). In this regard, the primary antibody should be titrated to an appropriate concentration that retains the specificity of the stain while removing any background signal or non-specific staining of the tissue. Antibodies that are prepared at a too high concentration can result in off-target staining (Anagnostou et al., 2010; Toki et al., 2017); an optimal concentration results in better accuracy and reproducibility (Toki et al., 2017; Taube et al., 2020). The adequate expression must be tested because some markers are able to stain more than one compartment of cells or other types of cells (e.g., PD-L1 could have cytoplasmic expression, but only membrane expression is considered positive staining, and it could be expressed in inflammatory cells besides the malignant cells) (Parra and Hernández Ruiz, 2021a) **(Figure 2)**.

STRATEGIES FOR ANTIBODY VALIDATION

One of the key factors for mIF panel reproducibility is to use antibodies that have been thoroughly optimized and validated for their application in research studies or for clinical applications. After antibody optimization by IHC or IF in control tissues, a good practice is applying those antibodies in a set of different tissues and organs including different common cancer types contained in tissue microarrays (TMAs) for quantitative measurement and antibody testing and validation. Although the construction of TMAs is often expensive for some laboratories (Taube et al., 2020), it is highly recommended to test the antibodies that will be integrated with an mIF panel in at least a set of cases for validation purposes, as a minimum requirement (Parra et al., 2017). The International Working Group for Antibody Validation proposed in total five different "pillars" to use for antibody validation with 1) genetic, 2) orthogonal, 3) independent antibody strategies, 4) expression of tagged proteins, and 5) immunocapture followed by mass spectrometry. It is recommended to consider at least one of these pillars as a minimum criterion for claiming that a selected protein has been adequately valid for a particular application (Uhlen et al., 2016). The most common and mainstay strategies are the orthogonal and the independent antibody strategy (Sivertsson et al., 2020). In the case of orthogonal validation (the most common), for an mIF panel validation, we use a non-antibody-based method to identify any effects or artifacts that

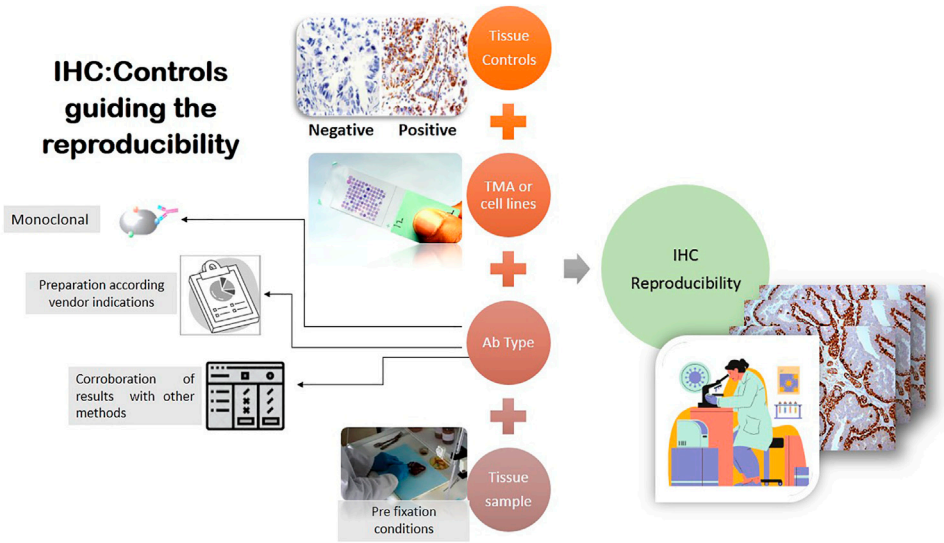

FIGURE 1 | One of the most important steps in obtaining reproducibility in mIF is evaluating antibodies in IHC. Different factors must be considered to provide the best results; studies of tissue controls, TMAs, or cell lines are needed to analyze the staining of each marker using vendors' instructions or via corroboration by other methods, such as Western blot analysis. The pre-analytical process can also affect the marker expression results; all of these factors together are part of IHC reproducibility.

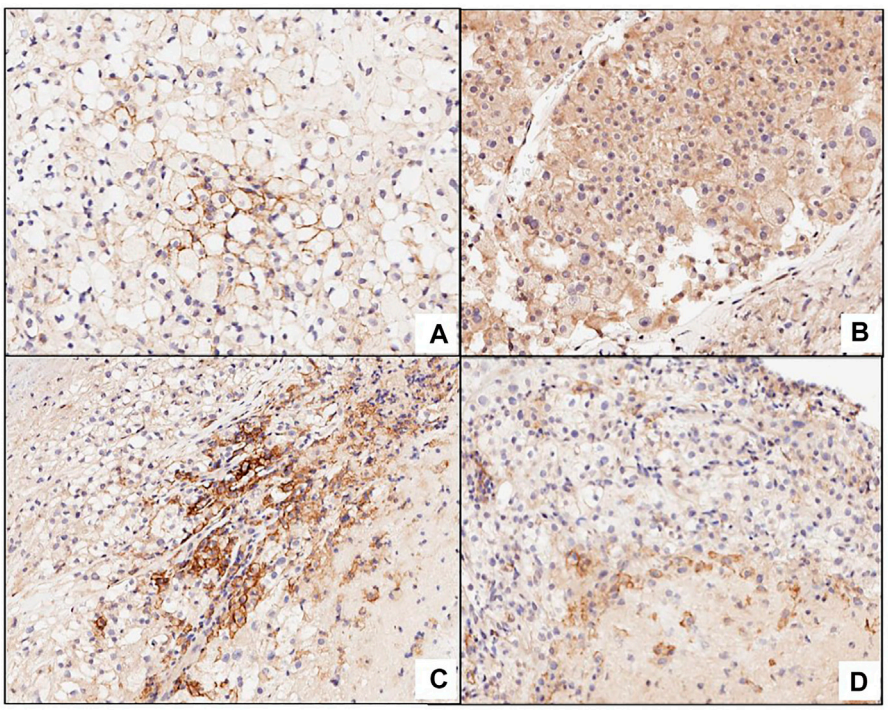

FIGURE 2 | Picture **(A)** shows a positive membrane staining in PD-L1 in clear renal cell carcinoma. Picture **(B)** expresses cytoplasmic staining that is not considered positive in the evaluation. C and D are false positive because both are expressing the marker in inflammatory cells or macrophages.

are directly related to the antibody or panel in question (Sivertsson et al., 2020). Depending on the antibodies targeted in a panel, non-antibody-based methods can include mining previously published results. Overall, it is possible studying expression analysis *via* genomics, transcriptomics, and proteomics techniques; or employing other established

TABLE 2 | Strategies and methods for antibody/multiplex immunofluorescence panel validation.

Strategy	Method	Advantage	Disadvantage
Genetic	*In situ* hybridization (ISH), CRISPR/CAS9 or siRNA/shRNA, Western blot	- Novel genes in spatial contest - The use of genome editing techniques is preferred - Provide a direct link between the gene, the target protein, and its detection by the antibody - Useful for examining antibody specificity for proteins that come from related genes	- Limited co-expression - Need functional knockdown reagents - Cannot be used for human tissue samples and body fluids (plasma and serum) - Time-consuming
Orthogonal	Fluorescent *in situ* hybridization (FISH), quantitative PCR, RNA-seq, Western blot	- Expression of the target protein is compared with an antibody-independent method - Co-expression in spatial context	- Limited probes and parameters - Need differential expression of target protein
Independent antibody	Immunofluorescence imaging, Immunohistochemistry, Western blot	- Co-expression can be in spatial context - The data generated using several antibodies (different epitopes) in the same protein is compared	- Limited parameters - Need antibodies with different epitopes
Tagged protein expression	Immunohistochemistry, Western blot	- Novel target in spatial context - Tagged proteins should be expressed at endogenous levels	- Limited co-expression - Overexpression of the target protein might mask the detection of off-target binding events - Limitations of this method are similar to those of the genetic approaches - Avoid potential artifacts introduced by the tag itself
Immunocapture followed by mass spectrometry	Immunoprecipitation, chromatin immunoprecipitation	- Fast, easily co-expression -This is one of the best methods for identifying off-target protein binding	- Many proteins have similar size - Difficulty in distinguishing direct interactors with the antibody versus proteins that form relevant complexes with the target protein - Some of the antibodies validated still do not perform in immunofluorescence assays

antibody-independent methods such as *in situ* hybridization or RNA sequencing. This strategy can also be used to ensure that any antibody validation performed in-house uses the most relevant biological models for the targets of interest. Although immunostaining techniques that are established in a lab, such as Western blot (Parra et al., 2018b), in positive and negative cell lines (Bordeaux et al., 2010) for research antibodies, can help provide a quick visual indication of antibody specificity (Parra et al., 2020; Parra and Hernández Ruiz, 2021b), it is always important and recommended that the antibody's data generated be supported by orthogonal testing. One way of achieving this is to mine publicly available databases (e.g., CCLE, BioGPS, Human Protein Atlas, DepMap Portal, COSMIC) for genomic and transcriptomic profiling information to clarify whether observed immunostaining results are relevant or are instead due to antibody-related artifacts (Cell Signaling, 2019; Ghandi et al., 2019; Broad Institute, 2021; COSMIC, 2021; The Human Protein Atlas, 2021).

About the independent antibody strategy, this is characterized by the use of independent antibodies, defined as a similar expression pattern determined by an independent antibody targeting a non-overlapping region of the similar protein (Sivertsson et al., 2020). Two or more independent antibodies that acknowledge a similar target may be used to assess antibody specificity in a range of assays. This approach requires that the expression patterns generated by the two antibodies correlate within a given application environment, which means that the two antibodies are able to bind to totally different regions of the protein and thus have different epitopes, minimizing the likelihood of off-target binding to a similar unrelated protein (Uhlen et al., 2016). Although diverse techniques can be used for antibody validation according to the necessities of the studies as described above, it is important to consider, when choosing one, its advantages and disadvantages, which are described in **Table 2**

MIF OPTIMIZATION AND CONTROL SELECTION

mIF panel development is essentially the consolidation of a single IF protocol in a multiplex protocol (Taube et al., 2020); it should ideally be performed using tissues with a full range of known expression patterns for the targets of interest, using the same positive and negative controls as described above for antibody optimization and validation. Careful project design is mandatory, as well as choosing correct, reliable, and very well optimized

antibodies to create a panel; other important variables for optimizing results include fresh tissue sections and regular or thin tissue slices (maximum, 4 μm) and adequately charged slides to avoid tissue detachment. It is important to use very well-known control tissues during each run of staining to detect possible errors in the mIF panel; for example, human reactive tonsil is frequently used during mIF optimization because we know the exact distribution of its different cell populations (Parra et al., 2017). Although it has been demonstrated that we can design panels containing up to eight antibody targets (Parra et al., 2021b), the complexity of handling will increase with the number of markers introduced in a panel. For the pre-analytical step, it is also necessary to consider individual marker signals; the subcellular location of the targets' expression (nuclear, membrane, and cytoplasmic); optimization of antigen retrieval conditions (pH and temperature); reagent titration (e.g., primary antibody, secondary antibody, and fluorophores); incubation conditions (time and temperature); and blocking of non-specific binding, following similar rigor to that described in the antibody validation.

Besides the factors mentioned before, two important aspects remain. First, because TSA reagents covalently bind to sites surrounding the antigen, they can potentially inhibit the binding of a subsequent primary antibody through steric hindrance. This phenomenon is considered an umbrella effect and tends to occur in situations where multiple markers reside in a single cell compartment, such as a $CD3^+$ $CD8^+$ PD-1+ T cell, where all three markers are expressed on the cell membrane. It is conceivable that if CD3 and/or CD8 comes before PD-1 in the panel, sufficient tyramide could be deposited to block the PD-1 antigen. If present, this phenomenon might also be diagnosed when the evaluation to singleplex IHC/IF is performed. A useful strategy to determine antibody/fluorophore interference or blocking is the drop controls method to find which one is causing the interference (Surace et al., 2019). To correct this situation, we can increase the primary antibody concentration(s), reduce TSA fluorophore concentration(s), and/or change the order of targets in the panel (Taube et al., 2020).

The second aspect to consider is crosstalk, which is an additional signal from the non-target fluorophore captured by the microscopic system (60, (Arppe et al., 2017). There are commonly recommended practices to cut back this effect; for example, crosstalk is often considerably reduced by choosing fluorophores whose excitation and emission spectra match those of the corresponding channels but minimally overlap those of non-corresponding ones. Alternatively, optimizing the filters of imaging channels, such as the adoption of excitation and emission filters with narrower bandwidths, can very effectively alleviate the crosstalk, although the signal strength might be sacrificed (Tie and Lu, 2020).

MULTISPECTRAL LIBRARY AND OPTICAL DETECTION

Multispectral libraries and their optical detection play an important role in determining the correct extraction of the photophore's signal according to their fluorescence wavelength. Exposure times need to be set up carefully to maintain a balance of the signal intensity across markers in the panel (Parra et al., 2020). Because we are working with multispectral imaging, additional considerations required for capturing the images include the generation of a spectral library, which will facilitate the discrimination and capture of the individual fluorescence signal using the correct spectra from each fluorophore (Francisco-Cruz et al., 2020b; Parra et al., 2021b; Viratham Pulsawatdi et al., 2020). The creation of the spectral library with a single stained sample for each individual fluorophore corresponding primary antibody will be important for the signal extraction (**Figure 3**). Also recommended for signal extraction is a marker with a highly prevalent antigen such as CD20, anti-sodium potassium ATPase, or vimentin, as well as rechecking this spectral library regularly depending on whether the scanner system uses a fluorescence bulb or LED light sources for the excitation. Finally, it is important that the signal extraction is from exogenous and endogenous autofluorescence in this methodology (Francisco-Cruz et al., 2020b). Other components in the scanner systems used for acquiring the images that must be considered when choosing the scanner system are multispectral range, fluorescence throughput, automation, and multiplexing capability, among others, to obtain high-quality images (**Table 3**).

PANEL VALIDATION

The final validation of the mIF panel requires the performance of intra-site and inter-site reproducibility studies prior to clinical use (Taube et al., 2020). At this point, the same TMA as used in the antibody validation is an optimal material for validation purposes. The experience with IHC is diverse, according to the marker, without a universal consensus, because each marker is different; in mIF, this knowledge is still being developed. Although automated staining can give us high reproducibility and is recommended for mIF staining, manual staining can be considered to process small quantities of slides at the same time to avoid errors and antibody variability caused by manual manipulation (Parra et al., 2017). Finally, similar strategies as mentioned for antibody validation can be applied for panel validation.

ANALYTIC EVALUATION

Diverse factors could affect the pre-analytical step, as mentioned previously; reagents, autostainer performance, section thickness variation, scanner performance, and change in quality and quantity of the cells between serial sections can influence the mIF analysis (Lee et al., 2020). For an IHC or mIF assay to be considered validated, at a minimum, it must be demonstrated to be accurate and precise, as well as reproducible from an analytic perspective and on pathologist interpretation (Taube et al., 2020).

Marker evaluation is a key aspect of reproducibility. Markers with abundant and specific cell expression, such as

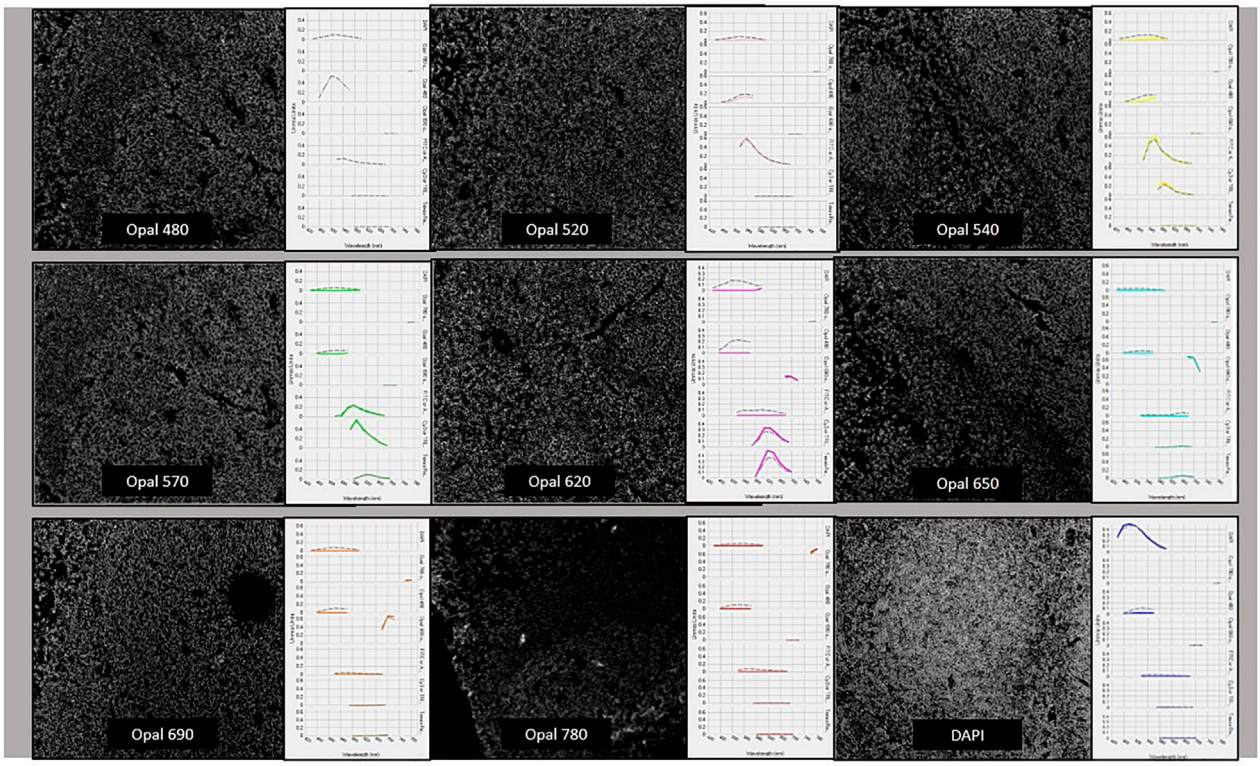

FIGURE 3 | Spectral library creation with the different fluorophores from the Opal-9 kit. Opal 480, Opal 520, Opal 540, Opal 570, Opal 620, Opal 650, and Opal 690, Opal 780, and DAPI were stained, optimized, and validated until we obtained similar dynamic ranges and specific wave peaks as is possible to see in this picture.

TABLE 3 | Differences scanners used for multiplex analysis.

Company	Scanner type	Image acquisition and scanning instrument	Corporate location/notes	Resolution	Image extraction	File type	Automatization
Leica Biosystems	BF and FL	Aperio Versa	Illinois, United States	0.468 µm per pixel with ×20 objective. 0.2um at 40x	WS	TIFF, JPEG	Semi-auto and auto
3DHistech	BF and FL	Pannoramic 250 FLASH III	Budapest, Hungary	0.172 and 0.087/ 0.325 and 0.162 pixels	WS	---	Auto
Ventana/ Roche	BF and FL	iScan	United States, International	24-bit true color	WS	TIFF/BIF	Auto and manual
PerkinElmer	MSI (BF and FL)	Vectra/Vectra Polaris	Boston, United States	10× (1.0 µm/pixel), 20× (0.5 µm/pixel) and 40× (0.25 um/pixel)	ROI	QPTIFF, IM3, JPEG, single-layer TIFF, BMP, PNG	Touchless automation with walk-away image acquisition
Olympus America	BF and FL	VS110, Nanozoomer (United States)	Japan, International	0.32 µm/pixel (20×/NA 0.75) - 0.16 µm/pixel (40×/NA 0.95)	WS	Compress images and save images in different file formats	Auto
Zeiss	BF and FL	AxioVision MosaiX	United States, Germany	5× (2.11 µm/pixel), 10× (1.05 µm/pixel), and 20× (0.53 µm/ pixel)	WS	AVI, BMP, J2K, JP2, JPG, LSM, MOV. PCT, PCX, PNG, PSD, TGA, TIF, WMF	Auto/manual

BF: bright field; FL: fluorescence: MALDI: matrix-assisted laser desorption/ionization; FOV: field of view; WS: whole section; ROI: region of interest.

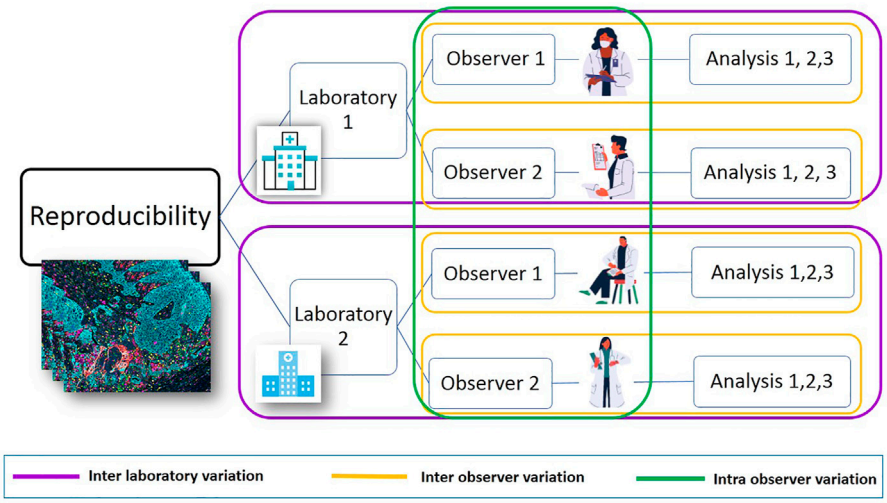

FIGURE 4 | Post-analytic reproducibility study. It is possible to address the flow of post-analytic studies that compare results between two or more sites. Each site can have different observers, and each can analyze slides or projects more than one time using image analysis. This algorithm makes it possible to find variability between laboratories. This workflow is useful for IHC/mIF and other techniques, improving the quality of the final results. It is highly recommended to publish the results and findings.

CD3, are easy to evaluate and will probably be consistent across serial sections when the expression is evaluated. For markers with variable geographic distribution across tissues and variable tumoral expression, such as PD-L1, reproducibility will be more challenging across serial sections (Parra et al., 2018b). To determine the reproducibility of markers in the mIF panel, we must consider that a group of markers is being evaluated and that those markers have specific cell phenotypes (marker co-expression) across different sections, according to the abundance of specific cell phenotypes (Lee et al., 2020). Marker reproducibility studies are easier in IHC compared with mIF because the evaluation is performed one by one; in mIF, it is harder to evaluate an entire panel using only one method, so the variability is related to the number of markers and their expression is extensive when specific phenotypes are evaluated.

Another drawback for mIF is high inter-observer variability for the same marker (Gerdes et al., 1984; Vincent-Salomon et al., 2007; Mohammed et al., 2012; Munzone et al., 2012; Cheng et al., 2015; Matsumoto et al., 2015). For instance, Ki-67 is a widely endorsed marker for a range of cancers Tumeh et al. (2014), but an issue has been raised concerning the reproducibility of IHC for Ki-67 and the implications of variability in clinical decision-making (Curigliano et al., 2017). Multiple research groups have demonstrated that inter-observer variability can be negated using digital analysis (Tan et al., 2020). There are different ideas as to the causes of between-pathologist variation; it may be the result of differences in each pathologist's clinical experience and technological competence (Barnes et al., 2017). In this case, the best approach may be to create a protocol of interpretation, with a consensus across all the groups. It will be useful to perform an objective analysis of each marker, or at least most markers. Having clear examples of false positives or false negatives can also be fundamental.

The selection of representative regions (hot spots) to score, cellular expression or intensity thresholding, binning, overall positive and negative slide rating, and cut-offs are additional challenges to consider in the post-analytic study.

While training and various quality systems have increased pathologists' scoring repeatability, reproducibility, and accuracy, there is still significant room for improvement (Terrenato et al., 2013; Lin and Chen, 2014; Nielsen, 2015), and the same challenges can arise even in image analysis (Barnes et al., 2017), especially when different laboratories use different image analysis systems. Although computational quantitation using digital image analysis algorithms may improve reader precision performance (Rexhepaj et al., 2008; Ghaznavi et al., 2013; Barnes et al., 2017), it is important to harmonize those systems between laboratories and create protocols to make the data more reproducible.

In digital analyses, the pathologist evaluates a digital image of the glass slide on a computer monitor and uses a computational algorithm to provide a result. The reader selects representative fields of view or regions of interest (ROIs) of the tumor that the algorithm analyzes to yield a score that is intended to represent the whole tumor (Barnes et al., 2017).

As tumors often harbor substantial cellular and spatial heterogeneity, it is essential to perform high-resolution multiplexed analysis across entire tumor sections. Other factors must also be considered when determining whether to select representative ROIs or the entire tissue. Analyzing the entire tumor can be time- and resource-consuming, so it is best is to select areas that are representative of the tumor's heterogeneity. The analysis of small ROIs or small tissue areas generates important variations and errors in the assessment of tumor and immune markers in cancer (Hofman et al., 2019). Other

TABLE 4 | Stages, challenge, and possible solutions for the best reproducibility of multiplex immunofluorescence panel.

Stage	Problem	Solution	Advantages of solutions	Disadvantages of solutions
Pre-analytical	Antibody specificity and staining	Use of positive and negative controls. Review of publications and experiences related to the Ab	Comparison with standardized process and other experiences	If the Ab does not have a previous protocol, it could result not reproducible
	Type of antibody and preparation	Preference by monoclonal antibody. Use specification of the vendor to prepare it	Better results	Not always is possible to monoclonal antibodies
	Optimization of panels in mIF	Test and work all the markers previously with IHC.	Comparison between IHC and mIF results	Some markers could not stain as the IHC
Analytical	Interpretation of markers	Standardized the interpretation of the most common markers	Interpretation well established	Some markers do not have protocols
	Consideration of areas of analysis and hotspots	Decide the number of representative areas of analysis and avoid select hotspots	Better representativeness	To have the right representative areas not always is possible. Number of ROIs could change depending on the type of tumor
	Type of image analysis	Do not expect to have the same result in all the different types of analysis technique. Consider the differences between software. Each one has its advantage and disadvantages		Experience-dependent
Post-analytical	Variability of intra- and inter-observer	Create protocols. If still persisting some variability, identify the problem	Standardization	Time-consuming and requires additional effort of the collaborators
	External and internal variability	Publish the results of each project. Take the experience of other laboratories to improve	Share knowledge	The new technologies do not have other experiences in other laboratories because they can be expensive

tumor types may have a higher degree of molecular heterogeneity, which may contribute to outcome (Rizzardi et al., 2016); analyzing a minimum area according to the complexity of each case is the most reasonable solution, but it is also important to have consensus between groups.

Given all of these challenges, laboratories that use mIF should standardize a minimum ROI or tissue area for analysis to generate accurate and reproducible results, considering the bibliographic data already available. The criteria to select areas of analysis should be compared in select representative areas, using the same method for evaluating each marker. In addition, although the algorithm can be locked, it will not always fit all the tumors; thus, it is possible to use an algorithm model as a base and make small changes according to the heterogeneity or type of tumor.

As each sample is complex, it is necessary to determine what factors should be excluded from the analysis (such as necrotic areas, hemorrhagic areas, non-preserved areas, unsatisfactory samples) and to standardize the reasons for exclusion to identify those that are unsatisfactory for mIF; in this way, only the cases without these considerations will be analyzed. The fewer the confusing factors are involved in the results, the easier it will be to standardize the workflow; each analysis could have less interobserver variability.

POST-ANALYTIC EVALUATION

After the pre-analytic and analytic evaluations, it is important to consider inside and outside evaluations. On the basis of our experience with IHC, although internal quality control procedures address daily reproducibility and are fundamental for monitoring performance in individual laboratories, external quality assessment is necessary to compare results from many laboratories by means of an external agency. This step allows the identification of insufficient stains and inappropriate protocols, as well as the identification of possible issues with interpretation (Vyberg et al., 2005; Copete et al., 2011). An external evaluation can provide an objective evaluation of staining results from many laboratories for a given epitope or biomarker, identify the best practice protocols to obtain optimal results, and systematically identify causes of insufficient results (Nielsen, 2015). A similar evaluation is expected to be performed for mIF panels.

Some of the challenges in the pre-analytical and analytical steps have included standardizing the post-analytic component of mIF quantitation, including the interpretation approach, representative region (hot spot) selection, cellular expression, intensity thresholding, and cut-offs. While training and quality systems have increased pathologists' scoring repeatability, reproducibility, and accuracy, there is still significant room for improvement (Barnes et al., 2017). The experiences of different institutions should be combined in a common effort to standardize tissue scoring.

The final device design and configuration should be verified, including accuracy, technical sensitivity, and specificity and precision (i.e., intra-assay run, inter-assay run, inter-lot variability, inter-reader variability, and inter-instrumentation variability). External analytical validation studies should then be performed to document reproducibility (**Figure 4**).

Several published reports have described mIF optimization panel methods for solid tumors, but few are fully automated or reproducible for large numbers of samples (Lee et al., 2020) or between multiple institutions. One study described a collaboration between six institutions to develop an automated six-plex assay that is focused on the PD-1/PD-L1 axis and assesses inter- and intra-site reproducibility, on the basis of the percentage of expression by immune cells, in serial sections of tonsils and a lung cancer TMA. This approach improved the reproducibility of PD-L1 and immune cells (Hoyt et al., 2019).

It is necessary to create groups or committees that include experts in mIF from different institutions to generate guidelines and recommendations for staining, optimization, and validation procedures for mIF technology that can help to harmonize this assay across different research laboratories and standardize its clinical application (**Table 4**). Finally, the goal is to establish only one protocol for all of the institutions that use this technology, making it possible to identify issues even when each lab has its own differences in the items related to pre-analytical and analytical evaluation; however, these differences must not be an excuse to not improve internal protocols or to justify incorrect results.

CONCLUSIONS

Reproducibility must be evaluated at each step of the process. Small mistakes could have a large impact on the final results and on reproducibility within and between laboratories. The use of standardized protocols is a good approach to avoid wrong results, poor workflow, or whatever issue could affect the quality and results.

AUTHOR CONTRIBUTIONS

CL wrote most of the manuscript. FR and SH contributed to the writing with their expertise on digital image analysis and immune profiling. EP conceived the idea of the manuscript, developed the technology in our laboratory, and edited the manuscript according to his experience.

FUNDING

This study was supported in part by the scientific and financial support for the CIMAC-CIDC Network provided through the National Cancer Institute (NCI) Cooperative Agreement U24CA224285 of The University of Texas MD Anderson Cancer Center CIMAC and for the Translational Molecular Pathology Immunoprofiling Platform, as well as by National Institutes of Health/NCI through Cancer Center Support Grant P30CA016672 (Institutional Tissue Bank) and SPORE grant 5P50CA070907-18 from the Cancer Prevention and Research Institute of Texas through MIRA RP160668.

ACKNOWLEDGMENTS

The authors would like to acknowledge the Translational Molecular Pathology Immunoprofiling Laboratory members, who contribute daily to quality multiplex IF and IHC processing. The manuscript was edited by Sarah Bronson of the Research Medical Library at The University of Texas MD Anderson Cancer Center.

REFERENCES

Akturk, G., Parra, E. R., Gjini, E., Lako, A., Lee, J. J., Neuberg, D., et al. (2021). Multiplex Tissue Imaging Harmonization: A Multicenter Experience from CIMAC-CIDC Immuno-Oncology Biomarkers Network. *Clin. Cancer Res.* doi:10.1158/1078-0432.ccr-21-2051

Anagnostou, V. K., Welsh, A. W., Giltnane, J. M., Siddiqui, S., Liceaga, C., Gustavson, M., et al. (2010). Analytic Variability in Immunohistochemistry Biomarker Studies. *Cancer Epidemiol. Biomarkers Prev.* 19 (4), 982–991. doi:10.1158/1055-9965.epi-10-0097

Arppe, R., Carro-Temboury, M. R., Hempel, C., Vosch, T., and Just Sørensen, T. (2017). Investigating Dye Performance and Crosstalk in Fluorescence Enabled Bioimaging Using a Model System. *PLoS One* 12 (11), e0188359. doi:10.1371/journal.pone.0188359

Barnes, M., Srinivas, C., Bai, I., Frederick, J., Liu, W., Sarkar, A., et al. (2017). Whole Tumor Section Quantitative Image Analysis Maximizes Between-Pathologists' Reproducibility for Clinical Immunohistochemistry-Based Biomarkers. *Lab. Invest.* 97 (12), 1508–1515. doi:10.1038/labinvest.2017.82

Barua, S., Solis, L., Parra, E. R., Uraoka, N., Jiang, M., Wang, H., et al. (2018). A Functional Spatial Analysis Platform for Discovery of Immunological Interactions Predictive of Low-Grade to High-Grade Transition of Pancreatic Intraductal Papillary Mucinous Neoplasms. *Cancer Inform.* 17, 1176935118782880. doi:10.1177/1176935118782880

Blom, S., Paavolainen, L., Bychkov, D., Turkki, R., Mäki-Teeri, P., Hemmes, A., et al. (2017). Systems Pathology by Multiplexed Immunohistochemistry and Whole-Slide Digital Image Analysis. *Sci. Rep.* 7 (1), 15580. doi:10.1038/s41598-017-15798-4

Bordeaux, J., Welsh, A. W., Agarwal, S., Killiam, E., Baquero, M. T., Hanna, J. A., et al. (2010). Antibody Validation. *Biotechniques* 48 (3), 197–209. doi:10.2144/000113382

Broad Institute (2021) Cancer Cell Line Encyclopedia. Available at: https://sites.broadinstitute.org/ccle/.

Canadian Association of Pathologists-Association canadienne des pathologistes National Standards CommitteeTorlakovic, E. E., Riddell, R., Banerjee, D., El-Zimaity, H., Pilavdzic, D., et al. (2010). Canadian Association of Pathologists-Association canadienne des pathologistes National Standards Committee/Immunohistochemistry: Best practice recommendations for standardization of immunohistochemistry tests. *Am. J. Clin. Pathol.* 133 (3), 354–365. doi:10.1309/AJCPDYZ1XMF4HJWK

Carvajal-Hausdorf, D. E., Schalper, K. A., Neumeister, V. M., and Rimm, D. L. (2015). Quantitative Measurement of Cancer Tissue Biomarkers in the Lab and in the Clinic. *Lab. Invest.* 95 (4), 385–396. doi:10.1038/labinvest.2014.157

Cell Signaling (2019). Hallmarks of Antibody Validation. Available at: https://www.korambiotech.com/wp-content/uploads/2021/06/Hallmarks-of-Antibody-Validation.pdf.

Cheng, C. L., Thike, A. A., Tan, S. Y. J., Chua, P. J., Bay, B. H., and Tan, P. H. (2015). Expression of FGFR1 Is an Independent Prognostic Factor in Triple-Negative Breast Cancer. *Breast Cancer Res. Treat.* 151 (1), 99–111. doi:10.1007/s10549-015-3371-x

Copete, M., Garratt, J., Gilks, B., Pilavdzic, D., Berendt, R., Bigras, G., et al. (2011). Inappropriate Calibration and Optimisation of Pan-Keratin (Pan-CK) and Low Molecular Weight Keratin (LMWCK) Immunohistochemistry Tests: Canadian Immunohistochemistry Quality Control (CIQC) Experience. *J. Clin. Pathol.* 64 (3), 220–225. doi:10.1136/jcp.2010.085258

COSMIC (2021). Catalogue of Somatic Mutations in Cancer (COSMIC). Available at: https://cancer.sanger.ac.uk/cosmic.

Curigliano, G., Burstein, H. J., Winer, E. P., Gnant, M., Dubsky, P., Loibl, S., et al. (2017). De-escalating and Escalating Treatments for Early-Stage Breast Cancer: the St. Gallen International Expert Consensus Conference on the Primary Therapy of Early Breast Cancer 2017. *Ann. Oncol.* 28 (8), 1700–1712. doi:10.1093/annonc/mdx308

Dejima, H., Hu, X., Chen, R., Zhang, J., Fujimoto, J., Parra, E. R., et al. (2021). Immune Evolution from Preneoplasia to Invasive Lung Adenocarcinomas and Underlying Molecular Features. *Nat. Commun.* 12 (1), 2722. doi:10.1038/s41467-021-22890-x

Engel, K. B., and Moore, H. M. (2011). Effects of Preanalytical Variables on the Detection of Proteins by Immunohistochemistry in Formalin-Fixed, Paraffin-Embedded Tissue. *Arch. Pathol. Lab. Med.* 135 (5), 537–543. doi:10.5858/2010-0702-rair.1

Fitzgibbons, P. L., Bradley, L. A., Fatheree, L. A., Alsabeh, R., Fulton, R. S., Goldsmith, J. D., et al. (2014). Principles of Analytic Validation of Immunohistochemical Assays: Guideline from the College of American Pathologists Pathology and Laboratory Quality Center. *Arch. Pathol. Lab. Med.* 138 (11), 1432–1443. doi:10.5858/arpa.2013-0610-cp

Francisco-Cruz, A., Parra, E., Tetziaff, M., and Wistuba, I. (2020a). "Multiplex Immunofluorescence Assays," *Biomarkers for Immunotherapy of Cancer* (New York: Springer), 467–495.

Francisco-Cruz, A., Parra, E. R., Tetzlaff, M. T., and Wistuba, II (2020b). Multiplex Immunofluorescence Assays. *Methods Mol. Biol.* 2055, 467–495. doi:10.1007/978-1-4939-9773-2_22

Gerdes, J., Dallenbach, F., Lennert, K., Lemke, H., and Stein, H. (1984). Growth Fractions in Malignant Non-hodgkin's Lymphomas (NHL) as Determinedin Situwith the Monoclonal Antibody Ki-67. *Hematol. Oncol.* 2 (4), 365–371. doi:10.1002/hon.2900020406

Ghandi, M., Huang, F. W., Jané-Valbuena, J., Kryukov, G. V., Lo, C. C., McDonald, E. R., et al. (2019). Next-generation Characterization of the Cancer Cell Line Encyclopedia. *Nature* 569 (7757), 503–508. doi:10.1038/s41586-019-1186-3

Ghaznavi, F., Evans, A., Madabhushi, A., and Feldman, M. (2013). Digital Imaging in Pathology: Whole-Slide Imaging and beyond. *Annu. Rev. Pathol. Mech. Dis.* 8, 331–359. doi:10.1146/annurev-pathol-011811-120902

Giraldo, N. A., Nguyen, P., Engle, E. L., Kaunitz, G. J., Cottrell, T. R., Berry, S., et al. (2018). Multidimensional, Quantitative Assessment of PD-1/PD-L1 Expression in Patients with Merkel Cell Carcinoma and Association with Response to Pembrolizumab. *J. Immunother. Cancer* 6 (1), 99. doi:10.1186/s40425-018-0404-0

Goldstein, N. S., Hewitt, S. M., Taylor, C. R., Yaziji, H., and Hicks, D. G.Members of Ad-Hoc Committee On Immunohistochemistry Standardization (2007). Recommendations for Improved Standardization of Immunohistochemistry. *Appl. Immunohistochem. Mol. Morphol.* 15 (2), 124–133. doi:10.1097/pai.0b013e31804c7283

Gorris, M. A. J., Halilovic, A., Rabold, K., van Duffelen, A., Wickramasinghe, I. N., Verweij, D., et al. (2018). Eight-Color Multiplex Immunohistochemistry for Simultaneous Detection of Multiple Immune Checkpoint Molecules within the Tumor Microenvironment. *J. Immunol.* 200 (1), 347–354. doi:10.4049/jimmunol.1701262

Hewitt, S. M., Baskin, D. G., Frevert, C. W., Stahl, W. L., and Rosa-Molinar, E. (2014). Controls for Immunohistochemistry. *J. Histochem. Cytochem.* 62 (10), 693–697. doi:10.1369/0022155414545224

Hewitt, S. M. (2016). Reproducibility. *J. Histochem. Cytochem.* 64 (4), 223. doi:10.1369/0022155416636547

Hofman, P., Badoual, C., Henderson, F., Berland, L., Hamila, M., Long-Mira, E., et al. (2019). Multiplexed Immunohistochemistry for Molecular and Immune Profiling in Lung Cancer-Just about Ready for Prime-Time? *Cancers (Basel)* 11 (3), 283. doi:10.3390/cancers11030283

Hoyt, C., Roman, K., Engle, L., Wang, C., Ballesteros-Merino, C., Jensen, S. M., et al. (2019). "Abstract LB-318: Multi-Institutional TSA-Amplified Multiplexed Immunofluorescence Reproducibility Evaluation (MITRE Study): Reproducibility Assessment of an Automated Multiplexed Immunofluorescence Slide Staining, Imaging, and Analysis Workflow. Cancer Research," Proceedings of AACR Annual Meeting 2019, Atlanta, GA, March 29–April 3, 2019. doi:10.1158/1538-7445.sabcs18-lb-318

Lee, C.-W., Ren, Y. J., Marella, M., Wang, M., Hartke, J., and Couto, S. S. (2020). Multiplex Immunofluorescence Staining and Image Analysis Assay for Diffuse Large B Cell Lymphoma. *J. Immunol. Methods* 478, 112714. doi:10.1016/j.jim.2019.112714

Lin, F., and Chen, Z. (2014). Standardization of Diagnostic Immunohistochemistry: Literature Review and Geisinger Experience. *Arch. Pathol. Lab. Med.* 138 (12), 1564–1577. doi:10.5858/arpa.2014-0074-ra

Matsumoto, H., Koo, S.-l., Dent, R., Tan, P. H., and Iqbal, J. (2015). Role of Inflammatory Infiltrates in Triple Negative Breast Cancer: Table 1. *J. Clin. Pathol.* 68 (7), 506–510. doi:10.1136/jclinpath-2015-202944

Meyerholz, D. K., and Beck, A. P. (2018). Principles and Approaches for Reproducible Scoring of Tissue Stains in Research. *Lab. Invest.* 98 (7), 844–855. doi:10.1038/s41374-018-0057-0

Mohammed, Z. M. A., McMillan, D. C., Elsberger, B., Going, J. J., Orange, C., Mallon, E., et al. (2012). Comparison of Visual and Automated Assessment of Ki-67 Proliferative Activity and Their Impact on Outcome in Primary Operable Invasive Ductal Breast Cancer. *Br. J. Cancer* 106 (2), 383–388. doi:10.1038/bjc.2011.569

Munzone, E., Botteri, E., Sciandivasci, A., Curigliano, G., Nolè, F., Mastropasqua, M., et al. (2012). Prognostic Value of Ki-67 Labeling index in Patients with Node-Negative, Triple-Negative Breast Cancer. *Breast Cancer Res. Treat.* 134 (1), 277–282. doi:10.1007/s10549-012-2040-6

Ng, S.-B., Fan, S., Choo, S.-N., Hoppe, M., Mai Phuong, H., De Mel, S., et al. (2018). Quantitative Analysis of a Multiplexed Immunofluorescence Panel in T-Cell Lymphoma. *SLAS TECHN. Transl. Life Sci. Innov.* 23 (3), 252–258. doi:10.1177/2472630317747197

Nielsen, S. (2015). External Quality Assessment for Immunohistochemistry: Experiences from NordiQC. *Biotech. Histochem.* 90 (5), 331–340. doi:10.3109/10520295.2015.1033462

Okoye, J. O., and Nnatuanya, N. I. (2015). Immunohistochemistry: a Revolutionary Technique in Laboratory Medicine. *Clin. Med. Diagn.* 5, 60–69. doi:10.5923/j.cmd.20150504.02

Parra, E. R., Francisco-Cruz, A., and Wistuba, II (2019). State-of-the-Art of Profiling Immune Contexture in the Era of Multiplexed Staining and Digital Analysis to Study Paraffin Tumor Tissues. *Cancers (Basel)* 11 (2). doi:10.3390/cancers11020247

Parra, E. R., Jiang, M., Solis, L., Mino, B., Laberiano, C., Hernandez, S., et al. (2020). Procedural Requirements and Recommendations for Multiplex Immunofluorescence Tyramide Signal Amplification Assays to Support Translational Oncology Studies. *Cancers (Basel)* 12 (2), 255. doi:10.3390/cancers12020255

Parra, E. R., Ferrufino-Schmidt, M. C., Tamegnon, A., Zhang, J., Solis, L., Jiang, M., et al. (2021a). Immuno-profiling and Cellular Spatial Analysis Using Five Immune Oncology Multiplex Immunofluorescence Panels for Paraffin Tumor Tissue. *Sci. Rep.* 11 (1), 8511. doi:10.1038/s41598-021-88156-0

Parra, E. R., and Hernández Ruiz, S. (2021a). Detection of Programmed Cell Death Ligand 1 Expression in Lung Cancer Clinical Samples by an Automated Immunohistochemistry System. *Methods Mol. Biol.* 2279, 35–47. doi:10.1007/978-1-0716-1278-1_4

Parra, E. R., and Hernández Ruiz, S. (2021b). Western Blot as a Support Technique for Immunohistochemistry to Detect Programmed Cell Death Ligand 1 Expression. *Methods Mol. Biol.* 2279, 49–57. doi:10.1007/978-1-0716-1278-1_5

Parra, E. R. (2021). Methods to Determine and Analyze the Cellular Spatial Distribution Extracted from Multiplex Immunofluorescence Data to Understand the Tumor Microenvironment. *Front. Mol. Biosci.* 8, 668340. doi:10.3389/fmolb.2021.668340

Parra, E. R., Uraoka, N., Jiang, M., Cook, P., Gibbons, D., Forget, M.-A., et al. (2017). Validation of Multiplex Immunofluorescence Panels Using Multispectral Microscopy for Immune-Profiling of Formalin-Fixed and Paraffin-Embedded Human Tumor Tissues. *Sci. Rep.* 7 (1), 13380. doi:10.1038/s41598-017-13942-8

Parra, E. R., Villalobos, P., Behrens, C., Jiang, M., Pataer, A., Swisher, S. G., et al. (2018a). Effect of Neoadjuvant Chemotherapy on the Immune Microenvironment in Non-small Cell Lung Carcinomas as Determined by Multiplex Immunofluorescence and Image Analysis Approaches. *J. Immunother. Cancer* 6 (1), 48. doi:10.1186/s40425-018-0368-0

Parra, E. R., Villalobos, P., Mino, B., and Rodriguez-Canales, J. (2018b). Comparison of Different Antibody Clones for Immunohistochemistry Detection of Programmed Cell Death Ligand 1 (PD-L1) on Non-Small Cell Lung Carcinoma. *Appl. Immunohistochem. Mol. Morphol.* 26 (2), 83–93. doi:10.1097/pai.0000000000000531

Parra, E. R., Zhai, J., Tamegnon, A., Zhou, N., Pandurengan, R. K., Barreto, C., et al. (2021b). Identification of Distinct Immune Landscapes Using an Automated Nine-Color Multiplex Immunofluorescence Staining Panel and Image Analysis in Paraffin Tumor Tissues. *Sci. Rep.* 11 (1), 4530. doi:10.1038/s41598-021-83858-x

Rexhepaj, E., Brennan, D. J., Holloway, P., Kay, E. W., McCann, A. H., Landberg, G., et al. (2008). Novel Image Analysis Approach for Quantifying Expression of Nuclear Proteins Assessed by Immunohistochemistry: Application to Measurement of Oestrogen and Progesterone Receptor Levels in Breast Cancer. *Breast Cancer Res.* 10 (5), R89. doi:10.1186/bcr2187

Rhodes, A. (2003). Quality Assurance in Immunohistochemistry. *Am. J. Surg. Pathol.* 27 (9), 1284–1285. doi:10.1097/00000478-200309000-00015

Rizzardi, A. E., Zhang, X., Vogel, R. I., Kolb, S., Geybels, M. S., Leung, Y.-K., et al. (2016). Quantitative Comparison and Reproducibility of Pathologist Scoring and Digital Image Analysis of Estrogen Receptor β2 Immunohistochemistry in Prostate Cancer. *Diagn. Pathol.* 11 (1), 63. doi:10.1186/s13000-016-0511-5

Rojo, M. G., Bueno, G., and Slodkowska, J. (2009). Review of Imaging Solutions for Integrated Quantitative Immunohistochemistry in the Pathology Daily Practice. *Folia Histochem. Cytobiol.* 47 (3), 349–354. doi:10.2478/v10042-008-0114-4

Rost, S., Giltnane, J., Bordeaux, J. M., Hitzman, C., Koeppen, H., and Liu, S. D. (2017). Erratum: Multiplexed Ion Beam Imaging Analysis for Quantitation of Protein Expresssion in Cancer Tissue Sections. *Lab. Invest.* 97 (10), 1263. doi:10.1038/labinvest.2017.94

Rudbeck, L. (2015). Adding Quality to Your Qualitative IHC. *MLO Med. Lab. Obs* 47 (12), 18–21.

Schalper, K. A., Brown, J., Carvajal-Hausdorf, D., McLaughlin, J., Velcheti, V., Syrigos, K. N., et al. (2015). Objective Measurement and Clinical Significance of TILs in Non-small Cell Lung Cancer. *J. Natl. Cancer Inst.* 107 (3), dju435. doi:10.1093/jnci/dju435

Shipitsin, M., Small, C., Giladi, E., Siddiqui, S., Choudhury, S., Hussain, S., et al. (2014). Automated Quantitative Multiplex Immunofluorescence *In Situ* Imaging Identifies Phospho-S6 and Phospho-PRAS40 as Predictive Protein Biomarkers for Prostate Cancer Lethality. *Proteome Sci.* 12, 40. doi:10.1186/1477-5956-12-40

Sivertsson, Å., Lindström, E., Oksvold, P., Katona, B., Hikmet, F., Vuu, J., et al. (2020). Enhanced Validation of Antibodies Enables the Discovery of Missing Proteins. *J. Proteome Res.* 19 (12), 4766–4781. doi:10.1021/acs.jproteome.0c00486

Sood, A., Miller, A. M., Brogi, E., Sui, Y., Armenia, J., McDonough, E., et al. (2016). Multiplexed Immunofluorescence Delineates Proteomic Cancer Cell States Associated with Metabolism. *JCI Insight* 1 (6), e87030. doi:10.1172/jci.insight.87030

Stack, E. C., Wang, C., Roman, K. A., and Hoyt, C. C. (2014). Multiplexed Immunohistochemistry, Imaging, and Quantitation: a Review, with an Assessment of Tyramide Signal Amplification, Multispectral Imaging and Multiplex Analysis. *Methods* 70 (1), 46–58. doi:10.1016/j.ymeth.2014.08.016

Stauber, J., MacAleese, L., Franck, J., Claude, E., Snel, M., Kaletas, B. K., et al. (2010). On-tissue Protein Identification and Imaging by MALDI-Ion Mobility Mass Spectrometry. *J. Am. Soc. Mass. Spectrom.* 21 (3), 338–347. doi:10.1016/j.jasms.2009.09.016

Steiner, C., Ducret, A., Tille, J. C., Thomas, M., McKee, T. A., Rubbia-Brandt, L., et al. (2014). Applications of Mass Spectrometry for Quantitative Protein Analysis in Formalin-Fixed Paraffin-Embedded Tissues. *Proteomics* 14 (4-5), 441–451. doi:10.1002/pmic.201300311

Surace, M., DaCosta, K., Huntley, A., Zhao, W., Bagnall, C., Brown, C., et al. (2019). Automated Multiplex Immunofluorescence Panel for Immuno-Oncology Studies on Formalin-Fixed Carcinoma Tissue Specimens. *J. Vis. Exp.* 143. doi:10.3791/58390

Tan, W. C. C., Nerurkar, S. N., Cai, H. Y., Ng, H. H. M., Wu, D., Wee, Y. T. F., et al. (2020). Overview of Multiplex Immunohistochemistry/immunofluorescence Techniques in the Era of Cancer Immunotherapy. *Cancer Commun.* 40 (4), 135–153. doi:10.1002/cac2.12023

Taube, J. M., Akturk, G., Angelo, M., Engle, E. L., Gnjatic, S., Greenbaum, S., et al. (2020). The Society for Immunotherapy of Cancer Statement on Best Practices for Multiplex Immunohistochemistry (IHC) and Immunofluorescence (IF) Staining and Validation. *J. Immunother. Cancer* 8 (1), e000155. doi:10.1136/jitc-2019-000155

Taube, J. M., Roman, K., Engle, E. L., Wang, C., Ballesteros-Merino, C., Jensen, S. M., et al. (2021). Multi-institutional TSA-Amplified Multiplexed Immunofluorescence Reproducibility Evaluation (MITRE) Study. *J. Immunother. Cancer* 9 (7), e002197. doi:10.1136/jitc-2020-002197

Taylor, C. R. (1999). FDA Issues Final Rule for Classification and Reclassification of Immunochemistry Reagents and Kits. *Am. J. Clin. Pathol.* 111 (4), 443–444. doi:10.1093/ajcp/111.4.443

Taylor, C. R. (1998). Report from the Biological Stain Commission: FDA Issues Final Rule for Classification/reclassification of Immunochemistry (IHC) Reagents and Kits. *Biotech. Histochem.* 73 (4), 175–177. doi:10.3109/10520299809141107

Taylor, C. R. (1992). Report of the Immunohistochemistry Steering Committee of the Biological Stain Commission. "Proposed Format: Package Insert for Immunohistochemistry Products". *Biotech. Histochem.* 67 (6), 323–338. doi:10.3109/10520299209110045

Terrenato, I., Arena, V., Pizzamiglio, S., Pennacchia, I., Perracchio, L., Buglioni, S., et al. (2013). External Quality Assessment (EQA) Program for the Preanalytical and Analytical Immunohistochemical Determination of HER2 in Breast Cancer: an Experience on a Regional Scale. *J. Exp. Clin. Cancer Res.* 32, 58. doi:10.1186/1756-9966-32-58

The Human Protein Atlas (2021). The Human Protein Atlas Project 2021. Available at: https://www.proteinatlas.org/.

Tie, H. C., and Lu, L. (2020). How to Quantitatively Measure, Assess and Correct the Fluorescence Crosstalk in the Wide-Field Microscopy. *bioRxiv* [Epub ahead of print]. doi:10.1101/2020.05.20.105627

Toki, M. I., Cecchi, F., Hembrough, T., Syrigos, K. N., and Rimm, D. L. (2017). Proof of the Quantitative Potential of Immunofluorescence by Mass Spectrometry. *Lab. Invest.* 97 (3), 329–334. doi:10.1038/labinvest.2016.148

Tumeh, P. C., Harview, C. L., Yearley, J. H., Shintaku, I. P., Taylor, E. J. M., Robert, L., et al. (2014). PD-1 Blockade Induces Responses by Inhibiting Adaptive Immune Resistance. *Nature* 515 (7528), 568–571. doi:10.1038/nature13954

Uhlen, M., Bandrowski, A., Carr, S., Edwards, A., Ellenberg, J., Lundberg, E., et al. (2016). A Proposal for Validation of Antibodies. *Nat. Methods* 13 (10), 823–827. doi:10.1038/nmeth.3995

Varma, M., Berney, D. M., Jasani, B., and Rhodes, A. (2004). Technical Variations in Prostatic Immunohistochemistry: Need for Standardisation and Stringent Quality Assurance in PSA and PSAP Immunostaining. *J. Clin. Pathol.* 57 (7), 687–690. doi:10.1136/jcp.2003.014894

Velcheti, V., Schalper, K. A., Carvajal, D. E., Anagnostou, V. K., Syrigos, K. N., Sznol, M., et al. (2014). Programmed Death Ligand-1 Expression in Non-small Cell Lung Cancer. *Lab. Invest.* 94 (1), 107–116. doi:10.1038/labinvest.2013.130

Vincent-Salomon, A., Gruel, N., Lucchesi, C., MacGrogan, G., Dendale, R., Sigal-Zafrani, B., et al. (2007). Identification of Typical Medullary Breast Carcinoma as a Genomic Sub-group of Basal-like Carcinomas, a Heterogeneous New Molecular Entity. *Breast Cancer Res.* 9 (2), R24. doi:10.1186/bcr1666

Viratham Pulsawatdi, A., Craig, S. G., Bingham, V., McCombe, K., Humphries, M. P., Senevirathne, S., et al. (2020). A Robust Multiplex Immunofluorescence and Digital Pathology Workflow for the Characterisation of the Tumour Immune Microenvironment. *Mol. Oncol.* 14 (10), 2384–2402. doi:10.1002/1878-0261.12764

Vyberg, M., Torlakovic, E., Seidal, T., Risberg, B., Helin, H., and Nielsen, S. (2005). Nordic Immunohistochemical Quality Control. *Croat. Med. J.* 46 (3), 368–371.

Conflict of Interest: The authors declare that the research was conducted in the absence of any commercial or financial relationships that could be construed as a potential conflict of interest.

Publisher's Note: All claims expressed in this article are solely those of the authors and do not necessarily represent those of their affiliated organizations, or those of the publisher, the editors, and the reviewers. Any product that may be evaluated in this article, or claim that may be made by its manufacturer, is not guaranteed or endorsed by the publisher.

frontiers in Molecular Biosciences

METHODS
published: 21 September 2021
doi: 10.3389/fmolb.2021.673042

Fluorescent Multiplex Immunohistochemistry Coupled With Other State-Of-The-Art Techniques to Systematically Characterize the Tumor Immune Microenvironment

*Anaïs Boisson[1], Grégory Noël[1], Manuel Saiselet[2], Joël Rodrigues-Vitória[2], Noémie Thomas[1], Mireille Langouo Fontsa[1], Doïna Sofronii[1], Céline Naveaux[1], Hugues Duvillier[3], Ligia Craciun[4], Denis Larsimont[4], Ahmad Awada[5], Vincent Detours[2], Karen Willard-Gallo[1] and Soizic Garaud[1]**

[1]Molecular Immunology Unit, Institut Jules Bordet, Université Libre de Bruxelles, Brussels, Belgium, [2]IRIBHM, Université Libre de Bruxelles, Brussels, Belgium, [3]Flow Cytometry Facility, Institut Jules Bordet, Université Libre de Bruxelles, Brussels, Belgium, [4]Department of Pathology, Institut Jules Bordet, Université Libre de Bruxelles, Brussels, Belgium, [5]Oncology Medicine Department, Institut Jules Bordet, Université Libre de Bruxelles, Brussels, Belgium

Our expanding knowledge of the interactions between tumor cells and their microenvironment has helped to revolutionize cancer treatments, including the more recent development of immunotherapies. Immune cells are an important component of the tumor microenvironment that influence progression and treatment responses, particularly to the new immunotherapies. Technological advances that help to decipher the complexity and diversity of the tumor immune microenvironment (TIME) are increasingly used in translational research and biomarker studies. Current techniques that facilitate TIME evaluation include flow cytometry, multiplex bead-based immunoassays, chromogenic immunohistochemistry (IHC), fluorescent multiplex IHC, immunofluorescence, and spatial transcriptomics. This article offers an overview of our representative data, discusses the application of each approach to studies of the TIME, including their advantages and challenges, and reviews the potential clinical applications. Flow cytometry and chromogenic and fluorescent multiplex IHC were used to immune profile a HER2+ breast cancer, illustrating some points. Spatial transcriptomic analysis of a luminal B breast tumor demonstrated that important additional insight can be gained from this new technique. Finally, the development of a multiplex panel to identify proliferating B cells, TFH, and TFR cells on the same tissue section demonstrates their co-localization in tertiary lymphoid structures.

Keywords: tumor immune microenvironment, breast cancer, tumor-infiltrating lymphocytes, tertiary lymphoid structure, fluorescent multiplex immunohistochemistry

OPEN ACCESS

Edited by:
Joe Yeong,
*Institute of Molecular and Cell Biology (A*STAR), Singapore*

Reviewed by:
Jabed Iqbal,
Singapore General Hospital, Singapore
Colt Egelston,
City of Hope National Medical Center, United States

****Correspondence:***
Soizic Garaud
soizic.garaud@bordet.be

Specialty section:
This article was submitted to Molecular Diagnostics and Therapeutics, a section of the journal Frontiers in Molecular Biosciences

Received: *26 February 2021*
Accepted: *11 August 2021*
Published: *21 September 2021*

Citation:
Boisson A, Noël G, Saiselet M, Rodrigues-Vitória J, Thomas N, Fontsa ML, Sofronii D, Naveaux C, Duvillier H, Craciun L, Larsimont D, Awada A, Detours V, Willard-Gallo K and Garaud S (2021) Fluorescent Multiplex Immunohistochemistry Coupled With Other State-Of-The-Art Techniques to Systematically Characterize the Tumor Immune Microenvironment. Front. Mol. Biosci. 8:673042. doi: 10.3389/fmolb.2021.673042

INTRODUCTION

The tumor immune microenvironment (TIME) plays a critical role in cancer development, progression, and treatment responses. It is defined by the immune cells, antigens, and soluble factors (including cytokines, chemokines, and immunoglobulins) that surround and influence tumor cells. The molecular and cellular composition of the TIME influences disease outcome via the balance between pro- and anti-tumor innate and adaptive immune responses. Human tumor-infiltrating lymphocytes (TILs) such as $CD8^+$ cytotoxic T cells, conventional $CD4^+$ T cells, T follicular helper cells (T_{FH}) (van der Leun et al., 2020), B cells (Wouters and Nelson, 2018), and natural killer cells (Stabile et al., 2017) are generally associated with favorable (anti-tumor) immune responses, together with γδ T cells (Lo Presti et al., 2020) and eosinophils (Grisaru-Tal et al., 2020). Many studies also show that tumor-associated macrophages and neutrophils, myeloid-derived suppressor cells, and regulatory T (Treg) cells are key drivers of cancer progression via their ability to promote tumor cell functions such as proliferation, aggressiveness, and dissemination in parallel with suppression of T cell-mediated anti-tumor immunity (Lecot et al., 2019; Ohue and Nishikawa, 2019; Davidov et al., 2020). A caveat is that immune cells are functionally heterogeneous and plastic with most capable of divergent behavior based on their activation status and the surrounding microenvironment.

Beyond the TIME composition, studying the location and spatial distribution of immune cells can provide a framework for understanding tumor biology and identifying potential predictive biomarkers. Spatial characteristics of tumors can be initially stratified based on tissue architecture such as intratumoral, peritumoral (or stromal) areas, and the invasive margin. In human breast cancer (BC), both intratumoral and stromal TIL have been consistently and significantly associated with overall survival (OS) in the $HER2^+$ and triple-negative subgroups (Dieci et al., 2015; Hendry et al., 2017). Recent studies of TIL subsets in BC revealed stromal $CD3^+$ T cells and $FOXP3^+$ Treg were associated with disease-free survival (DFS) but not their intratumoral counterpart while both intratumoral and stromal $CD8^+$ cytotoxic T cells predict longer DFS (Koletsa et al., 2020). Recent studies of tumor and immune spatial distribution at the single-cell level demonstrated a significant correlation with disease outcomes. For example, T cells and proliferating tumor cells were found in close proximity in immunoedited colorectal cancer metastases whereas short distances were seen between T cells and PD-$L1^+$ cells in non-immunoedited metastases (Angelova et al., 2018). Analysis of matched primary and recurrent head and neck squamous cell carcinoma detected $CD8^+$ T cell exclusion from tumor nests and close proximity between Treg or myeloid cells with tumor cells at relapse (Banik et al., 2020). TIL in the invasive margin or stroma can form tertiary lymphoid structure (TLS), which are similar to secondary lymphoid organs with a T cell zone adjacent to a B cell follicle that contains germinal center B cells, T_{FH} cells (Garaud et al., 2019), and mature dendritic cells (Dieu-Nosjean et al., 2008). A TLS presence is associated with favorable clinical outcomes (Dieu-Nosjean et al., 2008; Silina et al., 2018) and responses to immune checkpoint blockade (Cabrita et al., 2020; Helmink et al., 2020; Petitprez et al., 2020). The TLS maturation stage also harbors important prognostic information on the risk of disease recurrence (Posch et al., 2018; Silina et al., 2018). This means that deeper compositional and spatial analysis of immune cells infiltrating the tumor is needed to achieve a better understanding of effective anti-tumor immunity and discover new potential biomarkers.

Recent technological advances for phenotypic and transcriptional analysis of individual cells in the context of their spatial distribution are new, powerful tools for studying the TIME and identifying potential biomarkers. Fluorescent multiplex immunohistochemistry (mIHC) can simultaneously evaluate multiple biological markers on a single formalin-fixed, paraffin-embedded (FFPE) section. The objective of this review is to comparatively evaluate mIHC relative to more established TIME analytical techniques. We will consider their relative strengths and limitations as well as use our laboratory's studies of the BC immune microenvironment (as an example for other solid tumors) to showcase how mIHC can help to generate a more complete picture.

Tumor Immune Microenvironment Evaluation Using Fresh Specimens

Archival FFPE blocks are the most readily available source of tissue samples for translational research but fresh and frozen samples, including biopsies and surgical tissue specimens, are increasingly being collected for tumor microenvironment analysis. Our laboratory developed a methodology for the rapid isolation of intact lymphoid cells from normal and abnormal tissues in an effort to evaluate them proximate to their native state (Garaud et al., 2014). Briefly, the tissue is mechanically dissociated without enzymatic digestion to prepare single-cell suspensions. Lymphoid cells can be easily used for cell sorting, isolation, cryopreservation, and/or phenotypic analysis. Additionally, because this is an enzyme-free method, the primary tissue supernatant from the homogenates can be used to characterize and compare cytokines, chemokines, immunoglobulins, and antigens present in normal and malignant tissues (Garaud et al., 2018; Garaud et al., 2019).

Flow Cytometry

Flow cytometry is a broadly applied, reliable technique for quantitative and qualitative multi-parametric analysis of single cells in solution. Traditional flow cytometers can detect up to 20 parameters (size, granularity, and 18 fluorescent detectors); however, advances in fluorochromes and instrumentation now make it possible to perform experiments with 30 + parameters. In oncoimmunology, flow cytometry has been used for years to routinely classify hematological malignancies via the analysis of immune subpopulations using lineage markers, including T cell markers (CD3, CD4, CD8), B cell markers (CD19, CD20), monocyte markers (CD14, CD11b), and NK cell markers (CD56, CD161) in parallel. Flow cytometry using these and

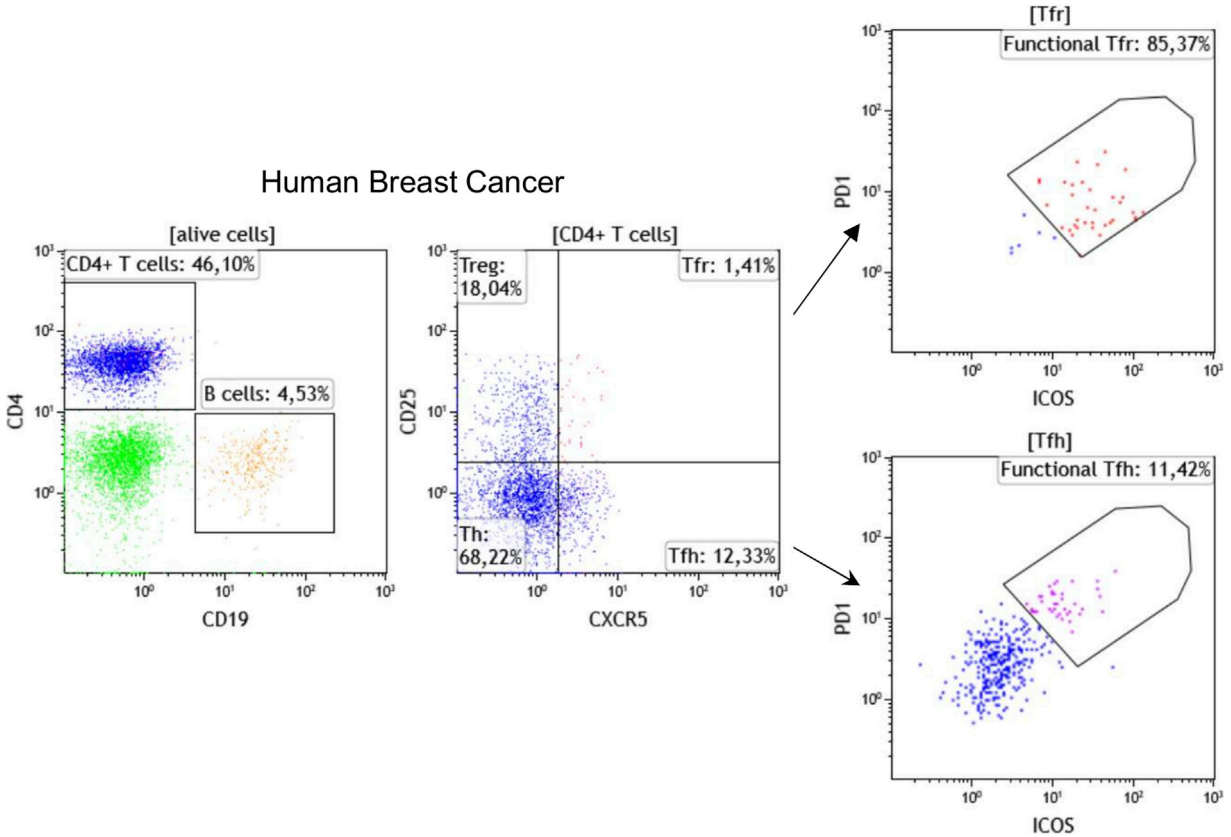

FIGURE 1 | Immunophenotyping of T_{FH} and T_{FR} cells by flow cytometry using fresh breast cancer tissues. Representative dot plots show the percentage of $CD19^+$ B cells, $CD4^+$ T cells, $CD25^-CXCR5^-CD4^+$ helper T cells (Th), $CD25^+CXCR5^-CD4^+$ regulatory T (Treg), $CD25^+CXCR5^+CD4^+$ T_{FR}, and $CD25^-CXCR5^+CD4^+$ T_{FH} cells. The functionality of T_{FH} and T_{FR} cells has been demonstrated to be linked with PD-1 and ICOS expression levels.

other markers including those related to immune cell differentiation, maturation, activation, functionality, and antigen specificity are now also used to characterize the TIME. Our laboratory has established >30 panels, each with up to 10 fluorescent markers, specifically designed for flow cytometric analysis of immune subpopulations in blood and tissues from cancer patients. In addition, we use flow cytometry to identify the most reliable markers to be tested for mIHC. A recent example is our addition of CXCR5, the CXCL13 receptor, which is an important TLS chemokine, to classical lineage markers for the characterization of TLS-associated lymphoid cells (Noël G., in press). **Figure 1** shows a representative strategy for flow cytometric immunophenotyping of $CD3^+CD4^+CXCR5^+CD25^-$ T_{FH} and $CD3^+CD4^+CXCR5^+CD25^+$ follicular regulatory T (T_{FR}) TIL in fresh BC tissue. Furthermore, the active state of these specialized $CD4^+$ T cell subpopulations can be achieved using PD-1 and ICOS expression levels to identify functional PD-$1^{hi}ICOS^{int}$ T_{FH} and functional PD-$1^{int}ICOS^{hi}$ T_{FR} TIL (Shi et al., 2018; Xing et al., 2020; Noël G., in press). These flow cytometry data will be used to build our chromogenic and fluorescent mIHC panels.

Multiplexed Bead-Based Immunoassays

Immune cells and their soluble mediators, including cytokines, chemokines, and immunoglobulins, are key players in human tumor progression and can be numerically and functionally altered both in the periphery and in the tumor microenvironment. Immunoassays are exemplified by the widely used ELISA, one of the most commonly used techniques for detecting soluble mediators. The development of multiplexed bead-based immunoassays has led to their emergence as a new standard for detecting and quantifying a broad variety of immune mediators using small amounts of blood or bodily fluid samples. This approach is based on fluorescent microspheres (beads) in a sandwich immunoassay, which can simultaneously detection up to 500 markers (depending on system design) using a dual-laser analytical flow cytometer. Soluble mediators in the TIME can be effectively analyzed using multiplex bead-based immunoassays to examine primary tumor tissue supernatants from the homogenates (Garaud et al., 2014; Garaud et al., 2018; Garaud et al., 2019; Ray et al., 2020; Autenshlyus et al., 2021).

Challenges

The greatest challenge in examining TIL in fresh tumor samples is access to sufficient quantities of tissue for flow cytometric analysis. Additionally, these analyses can yield inconsistencies depending upon how the tissues are handled during the

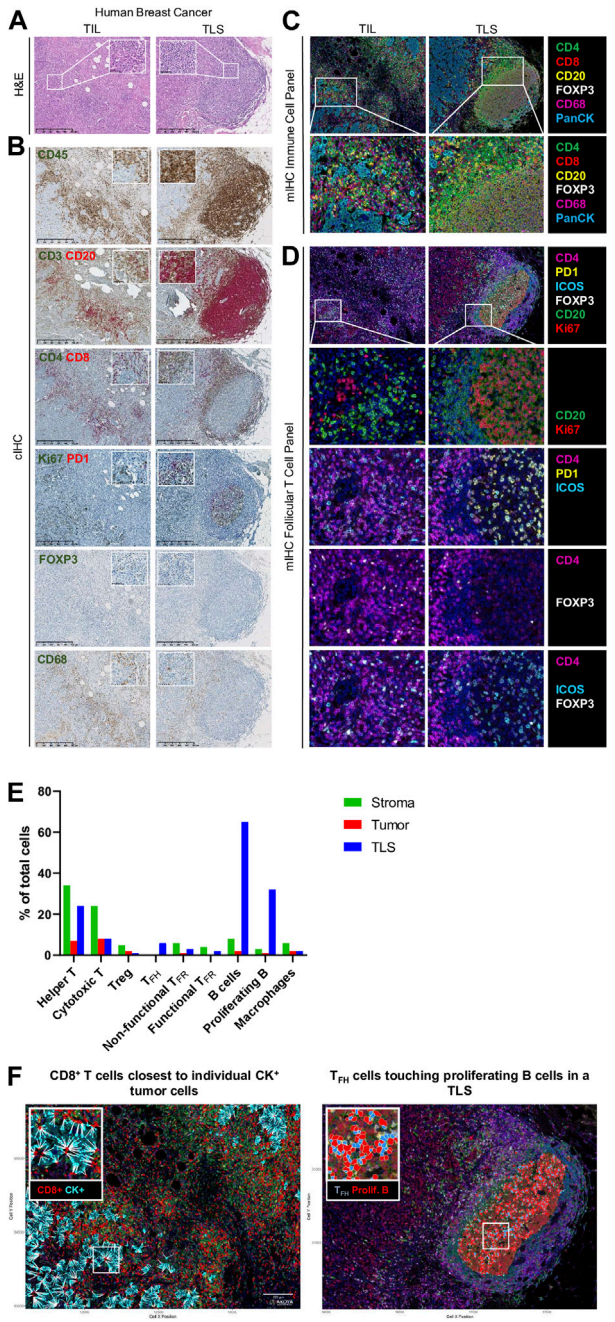

FIGURE 2 | Immune profiling of breast cancer. **(A–D)** Representative images of tumor-infiltrating lymphocyte (TIL) and tertiary lymphoid structure (TLS) in FFPE breast cancer sections detected by **(A)** hematoxylin and eosin staining (H&E), **(B)** chromogenic IHC (cIHC), and **(C, D)** multiplex IHC (mIHC). **(E)** Quantification of immune cells in stromal, tumoral, and TLS areas using InForm and PhenoptrReports. **(F)** Spatial distribution of immune cells including $CD8^+$ T cells closest to individual CK^+ tumor cells and T_{FH} cells touching proliferating B cells in a TLS. H&E and cIHC slides were scanned at ×40 magnification and the images are displayed at ×5 and ×40 magnification. mIHC slides were scanned at ×20 magnification.

pre-analytical phase, which can be affected by a variety of parameters including the length of time from biopsy/surgery to sample preparation, ischemia, temperature, and storage. Preparation of fresh tissues can also be limited by the availability of specialized equipment, including a vertical laminar flow hood, a tissue dissociator, and/or a flow cytometer. Thus, at the present time, this approach remains a research tool that needs to evolve further before it can be considered for routine clinical practice, as currently done for hematological malignancies.

Although multiplexed flow cytometry can facilitate detailed characterization of TIME complexity, this approach does not provide information on spatial relationships. This can be achieved by using complementary approaches in parallel such as conventional or mIHC to examine TIL organization and distribution within the TIME.

Tumor Immune Microenvironment Evaluation Using Formalin-Fixed, Paraffin-Embedded Tissue Specimens

FFPE tissue blocks are widely prepared in the routine pathology lab for chromogenic IHC (cIHC) staining as a part of diagnostic testing. Pathology departments archive vast numbers of FFPE blocks, but currently comparatively few frozen tissues, making the former a readily available resource for studying biomarkers.

Chromogenic Immunohistochemistry

Assessment of the immune infiltrate in diverse solid tumor types on hematoxylin and eosin- (H&E-) stained tissue sections is widely used for diagnosis and to provide prognostic and predictive information. TIL evaluation for early BC was the first to be recommended for routine characterization and reporting at the St. Gallen Consensus Conference 2019 (Balic et al., 2019). This analysis is based on a standardized method established by the International Immuno-Oncology Biomarkers Working Group (Hendry et al., 2017). While H&E staining is suitably reproducible and accurate for global TIL scoring (**Figure 2A**), our previous data revealed its lack of accuracy and reproducibility for TLS assessment (Buisseret et al., 2017a). Additionally, H&E-stained tissues do not provide any information on immune subsets in TIME.

CIHC is a relatively easy, inexpensive, and established technique based on antibody-mediated target antigen recognition that is detected using enzymes, such as horseradish peroxidase (HRP) or alkaline phosphatase (AP) to catalyze a color-producing reaction. Most frequently, detection is done using the 3, 3′-diaminobenzidine (DAB) chromogen, which precipitates in brown. Single detection methods are most commonly used to identify a particular biomarker of interest; however, the availability of new chromogens has led to the development of dual, triplex, and multiplex staining when the target antigens are not on the same cells or subcellular localization (i.e., cell membrane and nucleus). Studies of the BC TIME in our lab were facilitated through the development of numerous single and dual cIHC panels (Gu-Trantien et al., 2013; Buisseret et al., 2017b; Solinas et al., 2017). Dual cIHC is based on two consecutive stains of a single tissue section using DAB followed by AP Red detection on the BenchMark XT autostainer (Ventana Medical Systems) (Buisseret et al.,

2017b). An example of a BC immune infiltrate, previously analyzed as fresh tissue by flow cytometry and stained by various single and dual cIHC markers, is shown in **Figure 2B**. These images reveal the ready global detection using dual IHC for the majority of TIL with CD3 and CD20 or $CD4^+$ and $CD8^+$ T cell distribution as well as the location of $CD20^+$ B cells and $CD68^+$ macrophages and the organization of TIL in TLS. The advantages of using various cIHC panels include the preservation of tissue antigenicity, the automated process, and the ready visualization of DAB and Red precipitates using a brightfield microscope. The main limitations of this approach are the limited number of targets evaluated and the depletion of multiple tissue sections for single or dual marker analysis. More recently, multiplexed methodologies have gained popularity because they identify many biomarkers on the same tissue section simultaneously. These approaches include sequential immunoperoxidase labeling and erasing (SIMPLE) using alcohol-soluble peroxidase substrate 3-amino-9-ethylcarbazole combined with an antibody-antigen dissociation (Glass et al., 2009) and multiplexed consecutive IHC-staining on a single slide (MICSSS) that employs iterative cycles of tagging, image scanning, and destaining of the chromogenic substrate on a tissue section (Remark et al., 2016), which can visualize up to five or ten markers, respectively.

Immunofluorescence

Immunofluorescent (IF) techniques rely on antibodies tagged with a fluorescent dye to label antigens via their recognition and binding to specific epitopes. Direct and indirect IF are routinely employed, with direct detection done via a fluorophore-primary antibody conjugate and indirect detection requiring first recognition by the primary antibody followed by a fluorophore-conjugated secondary antibody directed to it. The advantage of direct IF is the rapidity of a single step that permits simultaneous staining with numerous antibodies from the same species. Indirect IF on the other hand has the advantage of higher sensitivity via the signal amplification generated by using secondary antibodies but is limited by the necessity to use antibodies from different species. Direct and indirect IF can be combined to amplify the signal for weaker targets and stain multiple primary antibodies from the same species concurrently.

Fluorescent Multiplex Immunohistochemistry

Fluorescent mIHC has developed into a feasible approach as a result of technological advances and cIHC/IF limitations. The simultaneous detection of multiple markers on a single section provides a comprehensive view of tissue composition, cellular functionality, subpopulation densities, and cell-cell interactions, to name a few, and is helping to drive mIHC development. Among different mIHC approaches, the Perkin Elmer/Akoya Biosciences Phenoptics™ system is currently capable of detecting up to eight biomarkers plus DAPI (nuclear cell counterstain). This system is based on sequential staining using tyramide signal amplification (TSA) to increase the signal 10-times more than conventional IHC (Faget and Hnasko, 2015). Further, the fluorescent deposit is covalently bound to tyrosine residues on or immediately surrounding the target epitope via activation of the tyramide by the HRP conjugated secondary antibody. This covalent bond enables both primary and secondary antibodies to be stripped from the tissue section via successive rounds of heat treatment (microwave, water bath, steamer, HIER platform, etc.), which has the added benefit of limiting antibody cross-reactivity and non-specific staining. The advantages of fluorescent mIHC include detection of low abundant proteins and using antibodies from the same species.

Our lab currently uses the Vectra® Polaris™ Automated Quantitative Pathology Imaging System for acquisition, which allows the visualization, analysis, quantification, and phenotyping of immune and other cells *in situ* via the integrated inForm and phenoptr/phenoptrReports tissue analysis software packages (Akoya Biosciences®). Multispectral acquisition can also be performed using a Zeiss LSM confocal microscope equipped with a PMT spectral 34-channel QUASAR (Carl Zeiss). The advantages of Akoya's platform include the unmixing of overlapping fluorophore emission spectra when using the spectral library containing each fluorophore employed, subtraction of tissue auto-fluorescence, and a fully integrated workflow. Furthermore, phenoptrReports provides the quality of the unmixing spectral library, signal strength, and crosstalk, which enables researchers to more readily optimize their multiplexed staining assays for best-in-class quantitative analysis. Additional stand-alone image analysis software packages are also available that can analyze multispectral images, including the HALO® Image Analysis Platform (Indica Labs), Visiopharm's AI-powered Phenotyping module (VISIOPHARM®), QuPath (Bankhead et al., 2017), and ImageJ. We developed our own mIHC panels to better characterize the BC TIME by testing various commercially available antibodies for optimal labeling of immune cell subpopulations. The first panel is used to locate the major T cell subpopulations, B cells, and macrophages (**Figure 2C**). Consecutive FFPE BC tissue sections from tumors previously analyzed using flow cytometry (fresh tissue) and cIHC (FFPE) are stained manually. The multispectral images for major immune subpopulations show massive stromal infiltration by $CD4^+$ and $CD8^+$ TIL together with $CD20^+$ TIL-B and $CD68^+$ macrophages in association with a TLS (**Figures 2C,E**). Another panel was designed to detect $CD4^+$ follicular helper subpopulations in TLS, which includes functional T_{FH} TIL ($PD\text{-}1^{hi}ICOS^+$, non-functional T_{FH} TIL are $PD\text{-}1^{lo/int}ICOS^{lo}$), functional T_{FR} TIL ($ICOS^+FOXP3^+$), and non-functional T_{FR} TIL ($ICOS^-FOXP3^+$) together with $Ki67^+CD20^+$ proliferating TIL-B (**Figures 2D,E**) (Noël G., in press). Proliferating B cells and T_{FH} were not observed in TIL outside of a TLS. The spatial distribution of these immune cells was analyzed using phenoptrReports to identify $CD8^+$ TIL nearest to CK^+ tumor cells and T_{FH} TIL touching proliferating B cells in the TLS (**Figure 2F**). All of the mIHC data we generated were consistent and complementary with our FACS and cIHC data for the same tumor in terms of immune cell detection, activation status, and localization within the BC TIME.

Challenges

While tissue imaging is widely used to investigate immune cell phenotypes and their spatial relationships, its principal

limitations are the restricted number of targets analyzed on a single slide and the dynamic range of marker intensity. For the latter, protein must be expressed above a minimal threshold and then scoring is based on the presence or absence of markers or a semi-quantitative H-score. TSA-based reagents for mIHC are more advantageous in this regard because they amplify the signal intensity and covalently bind the fluorophore to the target; however, there is still a risk of interference. TSA interference can derive from overactive tyramide deposits leading to a reduction or inhibition of antigen recognition via steric hindrance (umbrella effect) and/or tyrosine depletion, particularly when two or more markers are at the same cellular site [26]. Spectral bleeding, an artifact where the signal from one channel interferes with the channel being imaged, leads to false-positive staining and occurs between spectrally proximate fluorophores if the signal intensity is not well balanced [26]. In addition, the acquisition and characterization of mIHC images require both a multispectral imaging system and image analysis software. Research efforts to overcome these limitations include using DNA-barcoded antibodies such as the InSituPlex® Technology (ULTIVUE), the CODEX® system (AKOYA Biosciences®), and Digital Spatial Profiling (DSP) technologies (NanoString®). Tissue management, fixation procedures, storage conditions, and sectioning can also affect staining. Multiplex panel development thus requires optimization and validation (detailed below) to produce reproducible, reliable, and high-quality stained tissues.

Beyond technical limitations, image acquisition and analysis need to be standardized to reduce the likelihood of misinterpretation. First, whole-slide analysis, excluding necrotic areas, normal tissues, or vessels, should be favored whenever possible. The region of interest should be confirmed by a trained pathologist and fully cover individual fields for analysis. For larger tissues, the size of data tables can be reduced by randomly placing individual fields on a grid covering 50% or 25% of the region of interest using the phenochart viewer. Second, image analysis using mIHC provides information about the spatial organization including proximity between different types of cells; however, these analyses can be affected by the density of cells. Recent studies of the immune microenvironment during metastatic progression revealed shorter distances between T cells and proliferating tumor cells in immunoedited metastasis compared to unedited metastasis (Angelova et al., 2018). In addition, the tumor compartment should be taken into account in analysis such as the invasive margin or the center of the tumor as immune infiltration varies between these areas. To overcome this limitation, proximity analysis should be performed in tissues/areas with similar cell densities.

DEVELOPMENT OF A MULTIPLEXED PANEL FOR T FOLLICULAR HELPER CELLS

Our active development of mIHC panels for our studies has highlighted the essential factors one needs to consider when optimizing and validating a panel that includes three markers expressed at the membrane on the same cellular subpopulation. As an example, we describe our panel for characterizing follicular cells in TLS, which includes proliferating B cells, T_{FH}, and T_{FR} cells stained manually with antibodies to CD4, PD-1, ICOS, FOXP3, CD20, Ki67, and DAPI on FFPE sections. Multispectral images were acquired on a Vectra® Polaris™, analyzed with InForm software, and the quality report and marker quantification were generated with the phenoptrReports package.

TABLE 1 | Antibody-Opal pairing strategy.

Opal	Opal brightness rankings	Spectral bleed	Initial pairing
Opal 520	Highest		PD1/CD4/ICOS
Opal 540	Medium		CD20
Opal 570	Medium		Ki67/FOXP3
Opal 620	Medium		PD1/CD4/ICOS
Opal 650	Highest		PD1/CD4/ICOS
Opal 690	Lowest		Ki67/FOXP3

The table shows the strategy used for antibody-Opal pairing. The co-localized surface markers (PD-1, CD4 and ICOS) were associated with the brightest Opals using the rankings on the Vectra Polaris scanner. The markers not expressed in the same cellular compartment were associated with Opals that are more subject to spectral bleed with the Vectra Polaris scanner (black boxes).

Monoplex Assay Development

The first step in the development of an mIHC panel is to define the proper staining parameters for a single antibody and Opal pair using monoplex slides. Library slide development and primary antibody optimizations for antigen retrieval, titration, epitope sensitivity, and antibody stripping efficiency will be not addressed here as they are detailed in Akoya Biosciences® development guide and common for mIHC panel development. Human tonsil and BC FFPE tissue sections were used in the monoplex assays while multiplex assays were performed only on BC tissue sections.

Pairing Opal Fluorophores With Primary Antibodies

Following Akoya's recommendation, the pairing of an Opal fluorophore with an individual marker necessitates accounting for the Opal's brightness on the Vectra Polaris scanner (**Table 1**). Low marker expression should be assigned a brighter fluorophore, while more abundant markers work with dimmer fluorophores. We paired three membrane markers, CD4, PD-1, and ICOS, with high and medium fluorophores without spectral bleeding in the panel. This design allows us to minimize the quantity of Opal deposition while maintaining balanced signals and thereby maximally reducing tyrosine depletion or a potential umbrella effect. Misinterpretation due to spectral bleeding between Opal 540/570 and Opal 650/690, which are frequently observed with the Vectra Polaris scanner, can be avoided by selecting markers that are not expressed in the same cellular compartment such as CD20-Opal 540 and Ki67-Opal 570 or FOXP3-Opal 570. To fix the Opal pairing, we determined the Opal intensity count (OIC) for each combination using the InForm software count tool and plotting the autoexposure

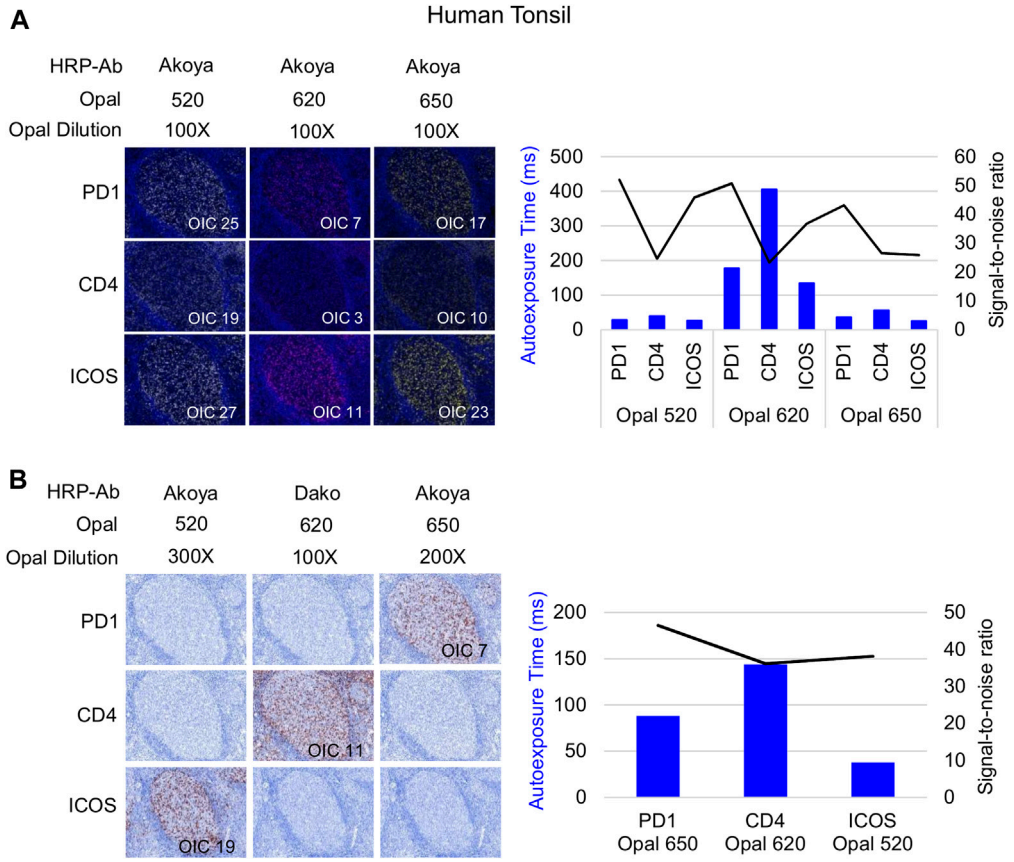

FIGURE 3 | Antibody-Opal pairing and signal balance of three markers co-localized on the cell surface. **(A)** Composite images of consecutive monoplex FFPE tonsil sections stained with PD-1, CD4, or ICOS with Opal 520, 620, or 650. The graph shows the autoexposure times (blue bars) and the signal-to-noise ratio (black curve) for each pairing. The signal-to-noise ratio was calculated via dividing the Opal intensity count (OIC) by the Opal background obtained in InForm. **(B)** Simulated DAB IHC images of optimized monoplex staining in **(A)**. The graphic shows the autoexposure times (blue bars) and the signal-to-noise ratio (black curve) of optimized monoplex staining determined by InForm. The slides were scanned at ×20 magnification with the Vectra Polaris and the composite images were analyzed with InForm software (v.2.4.8) and PhenoptrReports (Kent S Johnson (2020). phenoptr: inForm Helper Functions. R package v.0.2.6. https://akoyabio.github.io/phenoptr/).

time and signal-to-noise ratio (**Figure 3A**). The lowest autoexposure time and highest signal-to-noise ratio are highly recommended, which is why we decided to pair ICOS with Opal 520 and PD-1 with Opal 650. Alternatively, the pairing of CD4 with Opal 620 was not optimal at a low OIC, high autoexposure time and low signal-to-noise ratio; therefore, we used a secondary HRP antibody from Dako (EnVision$^+$ System-HRP Labelled Polymer Anti-Rabbit) to address this issue. Finally, to adjust Opal intensity levels, Akoya recommends a signal-to-noise ratio >10 with an OIC between 5 and 20 and an autoexposure time <150 m s. Based on Akoya's recommendations, a first monoplex adjustment was performed by testing dilutions of Opal 520 and 650. Optimized monoplex stainings visualized as simulated DAB IHC images within the same InForm project detected no spectral bleeding (no false staining) in the other Opal channels for all markers tested (**Figure 3B**).

Staining Order

Once the Opal pairing and preliminary signal balancing are completed, a staining sequence based on the epitope sensitivity and stripping efficiency of each primary antibody must be defined. When a given mIHC panel targets co-localized markers (i.e., in the same cellular compartment), the order of staining also must be defined by evaluating TSA interference. The optimization for three markers that can be co-expressed on the cell membrane, ICOS, PD-1, and CD4, is used here as an example. The impact of TSA interference (umbrella effect and/or tyrosine depletion) on multiplex staining was evaluated for monoplex and multiplex slides using sequential tonsil sections stained in different orders, visualized, and then analyzed using InForm and phenoptrReports. The number of detectable cells was determined for the same germinal center (GC) on both monoplex and multiplex slides. For each multispectral image, tissue segmentation, cell segmentation, and cell phenotyping were used to identify and quantify the cell density (positive cells/mm^2) and the Opal mean expression (OME) for each GC marker (**Figure 4A**). GCs, transient structures that form in secondary and tertiary lymphoid structures (tonsils and BC, respectively), were selected for quantification because T_{FH} cells (PD-1$^+$ICOS$^+$CD4$^+$) principally reside there and variation in cell

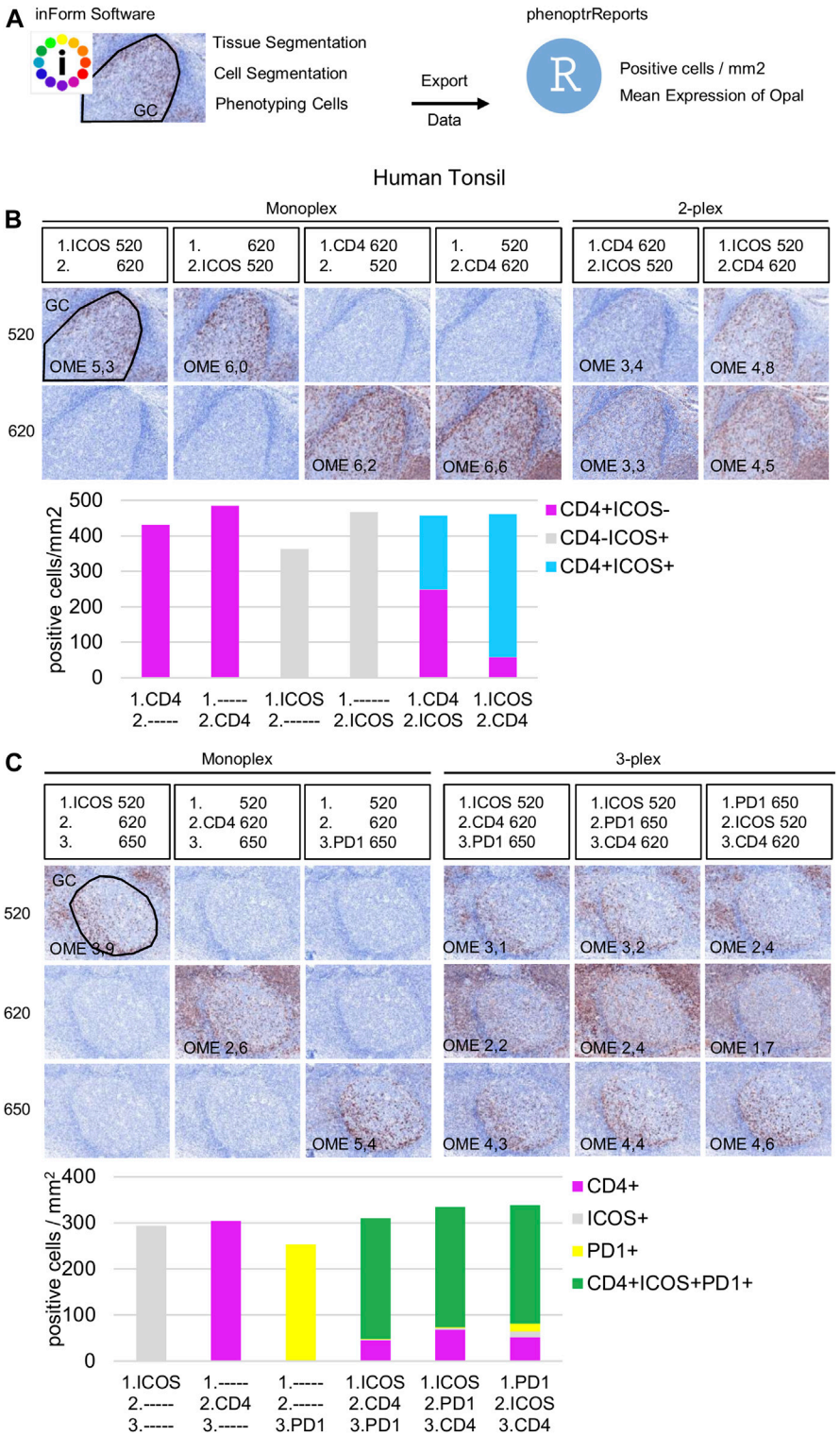

FIGURE 4 | Staining order optimization of three markers co-localized on the cell surface. **(A)** Workflow used to segment tissue regions, segment cells, and phenotype cells with the InForm software before quantifying cell density (positive cells/mm2) and Opal mean expression (OME) using PhenoptrReports on a germinal center (black line). **(B)** Simulated DAB IHC images of monoplex and 2-plex slides staining of consecutive FFPE tonsil sections alternating the position of CD4 and ICOS. The cell densities of $CD4^+ICOS^-$ (magenta), $CD4^-ICOS^+$ (grey), and $CD4^+ICOS^+$ (cyan) were quantified in the monoplex and 2-plex slides. **(C)** Simulated DAB IHC images of monoplex and 3-plex slides stained on consecutive FFPE tonsil sections, including PD-1 in first, second, or third position in the ICOS > CD4 staining order. The cell densities of total $CD4^+$ (magenta), total $ICOS^+$ (grey), total $PD1^+$ (yellow), and $CD4^+ICOS^+PD\text{-}1^+$ (green) were quantified in the monoplex and 3-plex slides. The slides were scanned at ×20 magnification with the Vectra Polaris and the composite images were analyzed with InForm software (v.2.4.8) and PhenoptrReports (Kent S Johnson (2020). phenoptr: inForm Helper Functions. R package v.0.2.6. https://akoyabio.github.io/phenoptr/).

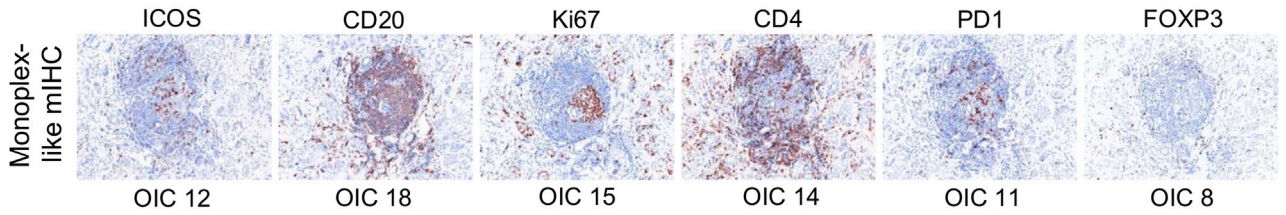

CDF \ Component	Opal 520	Opal 540	Opal 570	Opal 620	Opal 650	Opal 690
Unstained Tissue	0,7%	0,9%	0,1%	0,0%	0,0%	0,0%
ICOS Opal 520 100X		1,4%	0,1%	2,4%	0,3%	0,3%
CD20 Opal 540 150X	2,6%		1,6%	0,4%	0,4%	1,4%
Ki67 Opal 570 100X	0,0%	0,2%		3,4%	0,1%	0,1%
CD4 Opal 620 100X	0,0%	0,0%	0,1%		1,3%	1,8%
PD1 Opal 650 150X	0,0%	0,0%	0,0%	0,8%		0,5%
FOXP3 Opal 690 75X	1,4%	0,2%	0,7%	0,4%	1,0%	

FIGURE 5 | Evaluation of signal balance and crosstalk interference. Simulated DAB IHC images of monoplex stained slides of FFPE breast cancer sections to look like an mIHC slide by replacing the other primary antibodies with diluent. The unmixing quality report table shows the crosstalk from non-signal Opals for each component. The crosstalk values for a component are acceptable for phenotype classification and expression level assessment if all percentages in the component's column are <5%. The slides were scanned at ×20 magnification with the Vectra Polaris and the composite images were analyzed with InForm software (v.2.4.8) and PhenoptrReports (Kent S Johnson (2020). phenoptr: inForm Helper Functions. R package v.0.2.6. https://akoyabio.github.io/phenoptr/).

density or OME from TSA interference was more easily detected at this site.

Potential interference between co-localized CD4 and ICOS was first analyzed in consecutive FFPE tonsil sections (**Figure 4B**). Cell density quantification on the 2-plex slides revealed a reduction of $ICOS^+CD4^+$ cell densities associated with increased $CD4^+$ cell density when CD4 was stained before ICOS (CD4>ICOS) compared with the inverse (ICOS > CD4). The density of total $ICOS^+$ cells in the 2-plex ICOS > CD4 slide was similar to the monoplex slide, but this was not true for the 2-plex CD4>ICOS slide, while the densities of total $CD4^+$ cells in both 2-plex slides were similar to the monoplex slides. Even if $ICOS^+CD4^+$ cells are detectable on the 2-plex slides independent of the staining order, this result suggests that Opal 620 deposition on the CD4 epitope partially masks the recognition site of the ICOS epitope when CD4 and ICOS are on the membrane of the same cell. Moreover, in the 2-plex slides, there is a greater reduction in OME 520 when CD4 is stained first, confirming that TSA interference occurs due to CD4-Opal 620 (**Figure 4B**). Reduction of OME 520 can be fixed by the increasing Opal 520 concentration but the $ICOS^+$ $CD4^+$ cell density reduction can be only resolved by staining ICOS before CD4 in the multiplex sequence.

Slides were next stained in 3-plex to optimize the staining order for PD-1 in the ICOS > CD4 sequence (**Figure 4C**). Multiplexed slides reveal that staining PD-1 in the first position increases $PD\text{-}1^+$ cell density and decreases OME 520 and 620 (ICOS and CD4, respectively) compared to other staining orders. Based on these data we chose ICOS > CD4 > PD-1 for the staining order.

Signal Balance Assessment and Crosstalk Interference

Signal levels should be within a factor of three between one another to minimize interference, particularly for spectrally adjacent fluorophores. Evaluation of signal balance is achieved by starting with tonsil monoplex slides, the OIC tool in InForm, and the unmixing quality report in phenoptrReports. Akoya recommends starting the optimization with an Opal concentration of 100X and then adjusting fluorescent intensity signals by increasing or decreasing Opal concentrations. If signals are still too weak, different primary or secondary antibodies can be used or the Opal pairing, additional or more aggressive antigen retrieval methods, and longer primary or secondary antibody incubation times can also be tested. Tumor tissues show variable and heterogeneous target expression compared with tonsils (or other secondary lymphoid tissues) so it is important to evaluate the staining procedure in the target tissue. Monoplex BC slides were subjected to cycles of microwave treatment to simulate multiplex staining and then analyzed by InForm to determine the OIC for each Opal and phenoptrReports to determine crosstalk using the unmixing quality report tool (**Figure 5**). In contrast to tonsil tissue, ICOS and PD-1 are expressed at lower levels in tumor tissues. Opal 520 and 650 therefore needed to be increased to 100X and 150X, respectively, to restore signal balancing between all of the Opals.

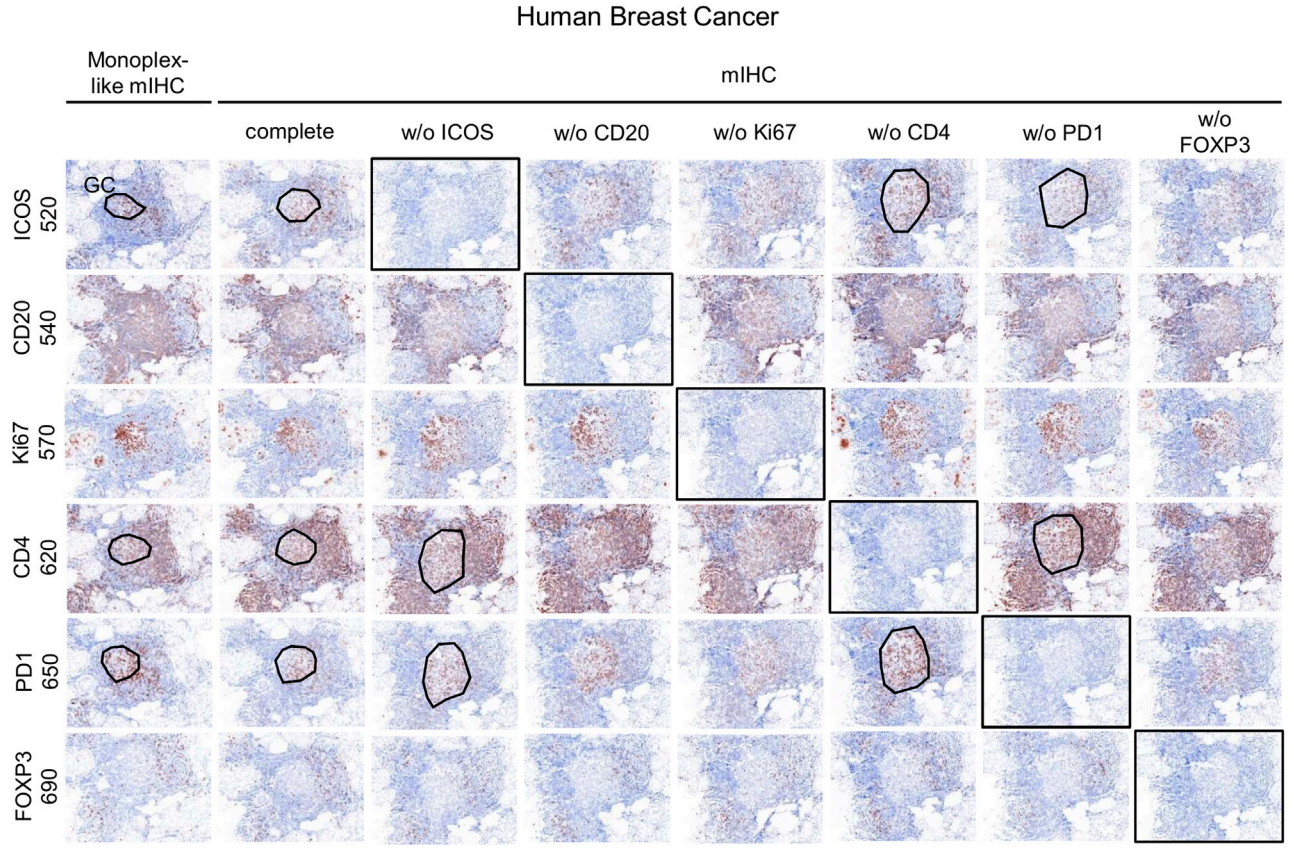

FIGURE 6 | Evaluation of the mIHC using drop controls. Simulated DAB IHC images of monoplex, mIHC, and drop control slides stained on consecutive FFPE breast tumor sections.

Increasing the Opal concentrations for co-localized markers can produce new TSA interference; therefore, it is better to optimize directly using the tissue of interest unless there are limited amounts of these tissues available. The development and validation of an mIHC panel with six markers plus DAPI require a minimum of 70 (4 μm) tissue sections so it is best to use a surrogate tissue if possible when the target tissue is a valuable resource. The Opal dilutions were also adjusted for Opal 540 and Opal 690 so that they were within the target brightness range required. The table of crosstalk by component revealed 2.6% crosstalk for CD20-Opal 540 in ICOS-Opal 520 and 3.4% crosstalk for Ki67-Opal 570 in CD4-Opal 620, both due to spectral bleeding or an unmixing error. 2.4% crosstalk for ICOS-Opal 520 in CD4-Opal 620 was also detected, which was not due to spectral bleeding because Opal 520 and 620 are spectrally distinct. CD4-Opal 620 follows ICOS-Opal 520 staining in the multiplex sequence suggesting that this crosstalk results from inadequate stripping of the ICOS antibody. However, crosstalk values below 5% are acceptable for phenotypic classification and expression level assessment.

Multiplex Assay Development

Once the monoplex slides were optimized, we looked for potential artifacts in the multiplex staining, such as spectral bleeding and TSA interference. The monoplex and drop controls were compared with the full multiplex panel (**Figures 6**, **7**). The drop controls were identical to the full multiplex except for the absence of one primary antibody in each control slide (Surace et al., 2019). Ideally, each drop control should generate no signal in the dropped channel and no changes in intensity and cell densities. We validated the absence of a signal in all dropped channels (**Figure 6**). To validate the staining on T_{FH} cells co-expressing CD4, PD-1, and ICOS, cell density and OME were determined within the TLS GC (black line) using the InForm and phenoptrReports software (**Figures 7A,B**). We observed no significant changes in cell density in the drop controls compared to the full multiplex panel. Alternatively, for T_{FH} cells in the GC of a TLS, the absence of CD4 increased the OME 520 and 650 (ICOS and PD-1, respectively) while the absence of PD-1 increased the OME 620 (CD4) and consequently decreased the OME 520 (ICOS). These data show an absence of spectral bleed in all Opal channels and weak TSA interference on T_{FH} cells due to Opal 620 and Opal 650 deposition, which impacts the Opal intensities without affecting T_{FH} cell density quantification. As an example, Opal 620 intensity levels on $CD4^+$ cells and $PD\text{-}1^+CD4^+$ cells should not be compared because PD-1-Opal 650 staining leads to reduced CD4-Opal 620 intensities from TSA interference, even if CD4 was stained prior to PD-1 in the mIHC panel

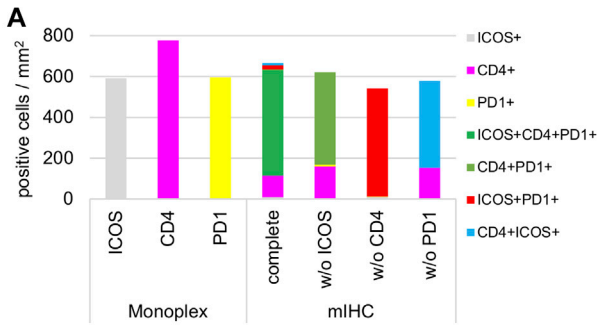

B

	OME on Tfh cells in GC TLS			
	mIHC			
	complete	w/o ICOS	w/o CD4	w/o PD1
Opal 520	2,8		3,3	2,1
Opal 620	3,4	3,7		4,6
Opal 650	2,9	2,7	3,9	

FIGURE 7 | Cell density and Opal expression quantification of drop control slides. **(A)** Cell density quantification of $CD4^+$, $ICOS^+$, $PD\text{-}1^+$, and T_{FH} subpopulations ($ICOS^+CD4^+PD\text{-}1^+$, $CD4^+PD\text{-}1^+$, $ICOS^+PD\text{-}1^+$, $CD4^+ICOS^+$) on monoplex slides, the mIHC slide and drop control slides without (w/o) ICOS, CD4, or PD-1. Each condition was quantified following the workflow shown in **Figure 4A** in a TLS GC (black dotted line in **Figure 6**). **(B)** Quantification of 520, 620, and 650 Opal mean expression (OME) on T_{FH} cells from an mIHC slide and drop control slides without (w/o) ICOS, CD4, PD-1 staining. Each condition was quantified followed the workflow as described above. The slides were scanned at ×20 magnification with the Vectra Polaris and the composite images were analyzed with InForm software (v.2.4.8).

sequence. As illustrated in **Figure 2D**, CD4 intensity is higher at the TLS border than in the GC due to the absence of PD-1 co-expression on these $CD4^+$ T cells. This OME variation is due to TSA interference and highlights the fact that marker intensity level quantification on different cell phenotypes requires robust validation.

TIME Evaluation From Frozen Specimens

While FFPE blocks remain the most readily available source for investigating the TIME, frozen specimens are increasingly being archived to use for staining, spatial transcriptomics (ST), or other approaches where the fixation process destroys or masks some epitopes. Frozen tissues can therefore be used to examine more labile factors and their spatial relationships within the TIME as well as identifying new biomarkers. The main advantages of frozen tissue sections include the preservation of proteins in their native state, which permits a faster staining protocol without the retrieval step and their reliability for molecular analyses such as DNA and RNA sequencing.

Immunofluorescence/Immunohistochemistry

Using frozen tissue sections does not require any pre-treatment including deparaffinization, hydration, and antigen retrieval; however, an additional step of fixation should be added before staining. The optimal fixative for the selected target tissue should be determined from a group that includes cold acetone, methanol, or 4% formaldehyde. mIHC using TSA amplification is not recommended for frozen tissue sections because microwave treatments will destroy tissue morphology. Using HRP blocking reagents to quash peroxidase can be an alternative to microwave treatment.

Spatial Transcriptomics

Despite recent technological advances in mIHC/IF, the number of markers that can be simultaneously detected is limited, particularly when compared with genomic techniques. Next-generation sequencing enables high throughput whole-genome or whole-transcriptome sequencing; however, these approaches do not provide spatial information. These limitations are being circumvented by ST, an emerging approach designed to transcriptionally profile spatial relationships in gene expression patterns using cancer tissues, with one example being the recent Visium platform introduced by 10X Genomics. This technique provides quantitative visualization and transcriptome analysis using intact fresh-frozen tissues sections and spatially barcoded oligo-deoxythymidine microarrays (Stahl et al., 2016; Vickovic et al., 2019). Following cDNA synthesis, the resulting barcoded cDNA libraries are sequenced using standard RNA-seq technologies. Unique barcodes (UMIs) are used to assign expression data to specific positions on the slide.

An initial examination of the spatial relationship for immune genes in human BC was achieved using the ST technology on a fresh-frozen section from an invasive lobular carcinoma (**Figure 8**). Using the Seurat algorithm, an open-source R toolkit for single-cell genomics, five clusters were drawn using non-linear dimension reduction (UMAP) in BC (**Figures 8A,B**) (Butler et al., 2018; Stuart et al., 2019). Interestingly, by superimposing the clusters onto the histological tissue image, an overlap between cluster four and an annotated TLS (based on H&E staining) was observed (**Figure 8C**). Spatial heatmaps confirmed the expression of immune markers previously identified by flow cytometry and mIHC within TLS such as *MS4A1* encoding CD20, *CD4*, and *CD8A*, as well as their immune activity with the expression of *FOXP3*, *PDCD1* encoding PD-1, and *ICOS* (**Figure 8D**). Next, we performed a heatmap of the top ten differentially expressed genes in TLS, defined by manual annotation, versus the remaining tumor tissue (**Figure 8E**). These data identify common gene expression profiles between TLS that differ from the expression profiles of the remaining tumor tissue. Finally, we selected two different immune cell signatures; the T_{FH} and Th1 signatures previously described by our group (Gu-Trantien et al., 2013), to portray the relative enrichment of T_{FH} and Th1 cells within the tumor microenvironment (**Figure 8F**). The T_{FH} signature was found to be intermediately expressed in two of the four annotated TLS and highly expressed in one, while the Th1 signature was expressed highly in all TLS. These results corroborate previous data from flow cytometry and mIHC, while giving new insights on the spatial distribution.

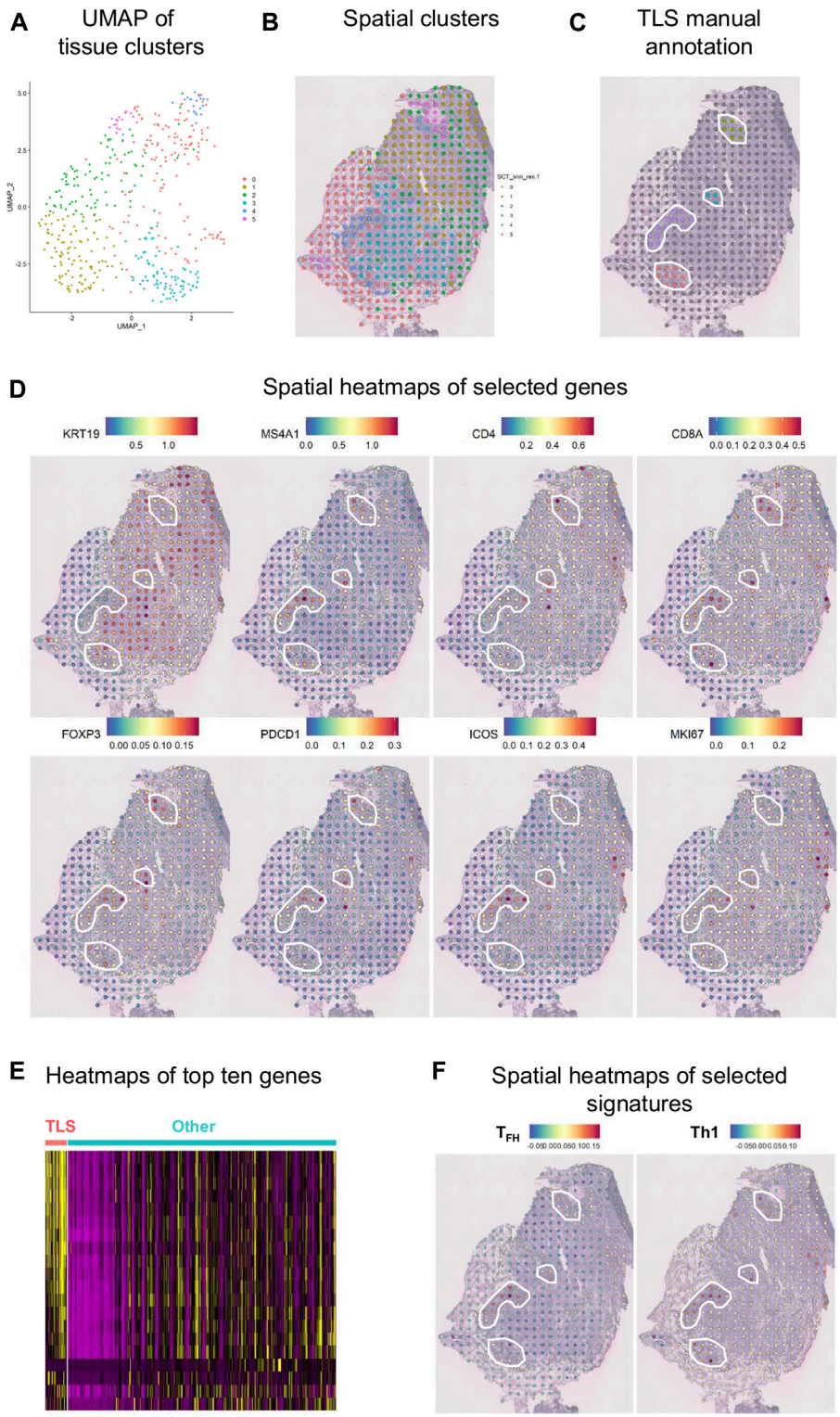

FIGURE 8 | Spatial gene expression in breast cancer. **(A)** UMAP representation of global gene expression in individual spots from a fresh-frozen section of an invasive lobular carcinoma created five distinct clusters with unbiased Seurat clustering. **(B)** The features were placed back onto the H&E staining. **(C)** Four TLS were histologically annotated on brightfield images of H&E-stained tissue sections (white line). **(D)** Visualization of eight selected genes as spatial heatmaps. **(E)** A heatmap of the top ten differentially expressed genes in the annotated TLS compared with the remaining tumor tissue. **(F)** Spatial heatmaps of T_{FH} and Th1 signatures.

TABLE 2 | Summary of technologies to investigate the TIME.

Method	Flow cytometry	Chromogenic IHC	Multiplex IHC	Spatial transcriptomics
Sample type	Fresh/frozen cells	FFPE/frozen tissue	FFPE tissue	Frozen tissue
Number of markers	18^{+}	2^{+}	Up to 8	Whole transcriptome
Detection system	Antibody	Enzymatic reaction	Enzymatic reaction	Barcoded primers
Read out	Fluorescent	Chromogenic	Fluorescent	Sequencing
Co-expression	Yes	No	2^{+}	Not applicable
Soluble mediators	Yes	No	No	No
Cost	$	$	$$	$$$
Spatial information	No	Yes	Yes	Yes
Observer	Scientist/biologist	Scientist/pathologist	Scientist/pathologist	Bio-informatician
Clinical relevant	No	Yes	Yes	No

Challenges

Some of the disadvantages of frozen tissue samples are the pre-analytical variables such as time of collection, preservation, and storage in the −80 °C freezer. Tissues need to be frozen as fast as possible once the sample is collected. Moreover, frozen tissue samples rapidly deteriorate at room temperature. The tissue histological quality is lower compared with FFPE samples, and tissues that are frozen incorrectly can form vacuoles. For these reasons, frozen tissue collections remain a smaller component of tumor banks compared to FFPE samples. Coupled with sampling restrictions, one of the major limitations of ST technology is its 50–100 μm resolution, even though the Visium platform expands the spatial resolution 5-fold beyond the first-generation of ST. The recent development of Slide-seq, a method for transferring RNA from tissue sections onto a surface covered in 10 μm DNA-barcoded beads with known positions, overcomes this limitation with a single-cell resolution and holds great promise for the future (Rodriques et al., 2019).

DISCUSSION

Overall, there are a variety of methodologies that can be used to explore the TIME for discovering the important cellular relationships or identifying relevant biomarkers, but each has distinct advantages and disadvantages. Many of these approaches are considered complementary to one another. In this manuscript, we detailed a number of experimental approaches that are particularly apt for investigating tumor tissues, focusing on TILs and TLS including T_{FH} and T_{FR} cells resident in BC-associated TLS. We further demonstrated it is possible to validate an mIHC panel that includes three co-localized surface markers. Using our rapid and simple non-enzymatic tissue dissociation protocol (Garaud et al., 2014), fresh tissue specimens can be used for TIL phenotyping, analysis of immune soluble mediators, and other characteristics of the TIME (**Table 2**). Flow cytometry, designed for the analysis of co-expressed markers on single cells, can be standardized for routine analysis and is relatively inexpensive. Because flow cytometric analyses do not provide spatial data, complementary approaches such as IHC/IF must be performed in parallel to obtain this information. cIHC is a useful tool, well established in routine clinical practice, and useful for characterizing individual markers and gaining spatial information on their location in the TIME. The main advantage of cIHC is its use to stain sections from FFPE blocks and their ready visualization with a brightfield microscope, something that is practicable in most pathology labs. In contrast to flow cytometry, cIHC is not capable of staining multiple markers to examine their co-localization. Two markers, usually on distinct cellular subpopulations or different subcellular locations, can be labeled on the same section in experienced labs while three markers are quite rare, which is why cIHC is not recommended when tissue is limited. The development of mIHC, using the TSA technology, has been driven by the need to circumvent sample limitation and the demand for spatial relationship information in a single tissue section. mIHC can presently detect up to eight markers on the same FFPE section. Image analysis software, designed to analyze these fluorescently labeled tissues, is an excellent tool to help scientists and pathologists examine complex cellular phenotypes in a spatial context. The downside of multiplex panel development is that it is time-consuming and requires a dedicated scientist to oversee the efforts and the detection of marker co-expression can be challenging. Despite that caveat, mIHC has emerged as a powerful tool for biomarker discovery and its continued evolution is likely to take it into routine clinical practice in the not-so-distant future. This will require careful assay optimization and validation to ensure robust and reproducible data across laboratories. Moreover, the specificity and sensitivity of mIHC still need to be validated along with consistency between those analyzing the images and need to have experienced pathologists, immunologists, and image analysis experts working together. Finally, while ST technology is a look into a future with full transcriptome analysis in whole tissue sections, major technical limitations do not accommodate its current use in clinical practice. These include the need for fresh-frozen tissues, single-cell spatial resolution that is not yet achieved, lower sensitivity compared with classical *in situ* hybridization analysis, high costs, and the required bio-informatics expertise.

DATA AVAILABILITY STATEMENT

The raw data supporting the conclusions of this article will be made available by the authors, without undue reservation.

ETHICS STATEMENT

The studies involving human participants were reviewed and approved by the Institut Jules Bordet. The patients/participants provided their written informed consent to participate in this study.

AUTHOR CONTRIBUTIONS

AB, SG, and GN conceived the research and designed experiments with support from KW-G; AB, MS, and SG performed the majority of experiments with specialized help from CN and HD; AB, SG, and KW-G analyzed and interpreted the data; AB, GN, NT, MLF, DS, JRV, VD, KWG, and SG discussed the data; JR-V and VD analyzed ST data; LC and DL recruited and sampled patients; AA proposed important concepts; AB, KW-G, and SG wrote and revised the manuscript with all authors subsequently providing advice and approving the final manuscript.

REFERENCES

Angelova, M., Mlecnik, B., Vasaturo, A., Bindea, G., Fredriksen, T., Lafontaine, L., et al. (2018). Evolution of Metastases in Space and Time under Immune Selection. *Cell* 175 (3), 751–765 e716. doi:10.1016/j.cell.2018.09.018

Autenshlyus, A., Arkhipov, S., Mikhaylova, E., Marinkin, I., Arkhipova, V., Varaksin, N., et al. (2021). Analyzing the Relationship between the Cytokine Profile of Invasive Breast Carcinoma, its Histopathological Characteristics and Metastasis to Regional Lymph Nodes. *Sci. Rep.* 11 (1), 11359. doi:10.1038/s41598-021-90930-z

Balic, M., Thomssen, C., Würstlein, R., Gnant, M., and Harbeck, N. (2019). St. Gallen/Vienna 2019: A Brief Summary of the Consensus Discussion on the Optimal Primary Breast Cancer Treatment 2019: A Brief Summary of the Consensus Discussion on the Optimal Primary Breast Cancer Treatment. *Breast Care* 14 (2), 103–110. doi:10.1159/000499931

Banik, G., Betts, C. B., Liudahl, S. M., Sivagnanam, S., Kawashima, R., Cotechini, T., et al. (2020). High-dimensional Multiplexed Immunohistochemical Characterization of Immune Contexture in Human Cancers. *Methods Enzymol.* 635, 1–20. doi:10.1016/bs.mie.2019.05.039

Bankhead, P., Loughrey, M. B., Fernández, J. A., Dombrowski, Y., McArt, D. G., Dunne, P. D., et al. (2017). QuPath: Open Source Software for Digital Pathology Image Analysis. *Sci. Rep.* 7 (1), 16878. doi:10.1038/s41598-017-17204-5

Buisseret, L., Desmedt, C., Garaud, S., Fornili, M., Wang, X., Van den Eyden, G., et al. (2017a). Reliability of Tumor-Infiltrating Lymphocyte and Tertiary Lymphoid Structure Assessment in Human Breast Cancer. *Mod. Pathol.* 30 (9), 1204–1212. doi:10.1038/modpathol.2017.43

Buisseret, L., Garaud, S., de Wind, A., Van den Eynden, G., Boisson, A., Solinas, C., et al. (2017b). Tumor-infiltrating Lymphocyte Composition, Organization and PD-1/PD-L1 Expression Are Linked in Breast Cancer. *Oncoimmunology* 6 (1), e1257452. doi:10.1080/2162402X.2016.1257452

Butler, A., Hoffman, P., Smibert, P., Papalexi, E., and Satija, R. (2018). Integrating Single-Cell Transcriptomic Data across Different Conditions, Technologies, and Species. *Nat. Biotechnol.* 36 (5), 411–420. doi:10.1038/nbt.4096

Cabrita, R., Lauss, M., Sanna, A., Donia, M., Skaarup Larsen, M., Mitra, S., et al. (2020). Tertiary Lymphoid Structures Improve Immunotherapy and Survival in Melanoma. *Nature* 577 (7791), 561–565. doi:10.1038/s41586-019-1914-8

Davidov, V., Jensen, G., Mai, S., Chen, S.-H., and Pan, P.-Y. (2020). Analyzing One Cell at a TIME: Analysis of Myeloid Cell Contributions in the Tumor Immune Microenvironment. *Front. Immunol.* 11, 1842. doi:10.3389/fimmu.2020.01842

Dieci, M. V., Mathieu, M. C., Guarneri, V., Conte, P., Delaloge, S., Andre, F., et al. (2015). Prognostic and Predictive Value of Tumor-Infiltrating Lymphocytes in Two Phase III Randomized Adjuvant Breast Cancer Trials. *Ann. Oncol.* 26 (8), 1698–1704. doi:10.1093/annonc/mdv239

Dieu-Nosjean, M.-C., Antoine, M., Danel, C., Heudes, D., Wislez, M., Poulot, V., et al. (2008). Long-term Survival for Patients with Non-small-cell Lung Cancer with Intratumoral Lymphoid Structures. *Jco* 26 (27), 4410–4417. doi:10.1200/JCO.2007.15.0284

Faget, L., and Hnasko, T. S. (2015). Tyramide Signal Amplification for Immunofluorescent Enhancement. *Methods Mol. Biol.* 1318, 161–172. doi:10.1007/978-1-4939-2742-5_16

Garaud, S., Buisseret, L., Solinas, C., Gu-Trantien, C., de Wind, A., Van den Eynden, G., et al. (2019). Tumor-infiltrating B Cells Signal Functional Humoral Immune Responses in Breast Cancer. *JCI Insight* 4. doi:10.1172/jci.insight.129641

Garaud, S., Gu-Trantien, C., Lodewyckx, J.-N., Boisson, A., De Silva, P., Buisseret, L., et al. (2014). A Simple and Rapid Protocol to Non-enzymatically Dissociate Fresh Human Tissues for the Analysis of Infiltrating Lymphocytes. *JoVE* 6, 52392. doi:10.3791/52392

Garaud, S., Zayakin, P., Buisseret, L., Rulle, U., Silina, K., de Wind, A., et al. (2018). Antigen Specificity and Clinical Significance of IgG and IgA Autoantibodies Produced *In Situ* by Tumor-Infiltrating B Cells in Breast Cancer. *Front. Immunol.* 9, 2660. doi:10.3389/fimmu.2018.02660

Glass, G., Papin, J. A., and Mandell, J. W. (2009). SIMPLE: a Sequential Immunoperoxidase Labeling and Erasing Method. *J. Histochem. Cytochem.* 57 (10), 899–905. doi:10.1369/jhc.2009.953612

Grisaru-Tal, S., Itan, M., Klion, A. D., and Munitz, A. (2020). A New Dawn for Eosinophils in the Tumour Microenvironment. *Nat. Rev. Cancer* 20 (10), 594–607. doi:10.1038/s41568-020-0283-9

Gu-Trantien, C., Loi, S., Garaud, S., Equeter, C., Libin, M., de Wind, A., et al. (2013). CD4+ Follicular Helper T Cell Infiltration Predicts Breast Cancer Survival. *J. Clin. Invest.* 123 (7), 2873–2892. doi:10.1172/JCI67428

Helmink, B. A., Reddy, S. M., Gao, J., Zhang, S., Basar, R., Thakur, R., et al. (2020). B Cells and Tertiary Lymphoid Structures Promote Immunotherapy Response. *Nature* 577 (7791), 549–555. doi:10.1038/s41586-019-1922-8

Hendry, S., Salgado, R., Gevaert, T., Russell, P. A., John, T., Thapa, B., et al. (2017). Assessing Tumor-Infiltrating Lymphocytes in Solid Tumors: A Practical Review for Pathologists and Proposal for a Standardized Method from the International Immunooncology Biomarkers Working Group: Part 1: Assessing the Host Immune Response, TILs in Invasive Breast Carcinoma and Ductal Carcinoma *In Situ*, Metastatic Tumor Deposits and Areas for Further Research. *Adv. Anat. Pathol.* 24 (5), 235–251. doi:10.1097/PAP.0000000000000162

Koletsa, T., Kotoula, V., Koliou, G.-A., Manousou, K., Chrisafi, S., Zagouri, F., et al. (2020). Prognostic Impact of Stromal and Intratumoral CD3, CD8 and FOXP3 in Adjuvantly Treated Breast Cancer: Do They Add Information over Stromal Tumor-Infiltrating Lymphocyte Density? *Cancer Immunol. Immunother.* 69 (8), 1549–1564. doi:10.1007/s00262-020-02557-0

Lecot, P., Sarabi, M., Pereira Abrantes, M., Mussard, J., Koenderman, L., Caux, C., et al. (2019). Neutrophil Heterogeneity in Cancer: From Biology to Therapies. *Front. Immunol.* 10, 2155. doi:10.3389/fimmu.2019.02155

Lo Presti, E., Dieli, F., Fournié, J. J., and Meraviglia, S. (2020). Deciphering Human γδ T Cell Response in Cancer: Lessons from Tumor-infiltrating γδ T Cells. *Immunol. Rev.* 298 (1), 153–164. doi:10.1111/imr.12904

Noël, G., Garaud, S., De Silva, P., de Wind, A., Van den Eynden, G., Salgado, R., et al. (in press). Functional Th1-Oriented Tfh Cells Infiltrating Human Breast Cancer Promote Effective Adaptive Immunity. *J. Clin. Invest.*, 139905. doi:10.1172/JCI139905

Ohue, Y., and Nishikawa, H. (2019). Regulatory T (Treg) Cells in Cancer: Can Treg Cells Be a New Therapeutic Target? *Cancer Sci.* 110 (7), 2080–2089. doi:10.1111/cas.14069

Petitprez, F., de Reyniès, A., Keung, E. Z., Chen, T. W.-W., Sun, C.-M., Calderaro, J., et al. (2020). B Cells Are Associated with Survival and Immunotherapy Response in Sarcoma. *Nature* 577 (7791), 556–560. doi:10.1038/s41586-019-1906-8

Posch, F., Silina, K., Leibl, S., Mündlein, A., Moch, H., Siebenhüner, A., et al. (2018). Maturation of Tertiary Lymphoid Structures and Recurrence of Stage II and III Colorectal Cancer. *Oncoimmunology* 7 (2), e1378844. doi:10.1080/2162402X.2017.1378844

Ray, A. L., Nofchissey, R. A., Khan, M. A., Reidy, M. A., Lerner, M. R., Wu, X., et al. (2020). The Role of Sex in the Innate and Adaptive Immune Environment of Metastatic Colorectal Cancer. *Br. J. Cancer* 123 (4), 624–632. doi:10.1038/s41416-020-0913-8

Remark, R., Merghoub, T., Grabe, N., Litjens, G., Damotte, D., Wolchok, J. D., et al. (2016). In-depth Tissue Profiling Using Multiplexed Immunohistochemical Consecutive Staining on Single Slide. *Sci. Immunol.* 1 (1), aaf6925. doi:10.1126/sciimmunol.aaf6925

Rodriques, S. G., Stickels, R. R., Goeva, A., Martin, C. A., Murray, E., Vanderburg, C. R., et al. (2019). Slide-seq: A Scalable Technology for Measuring Genome-wide Expression at High Spatial Resolution. *Science* 363 (6434), 1463–1467. doi:10.1126/science.aaw1219

Shi, J., Hou, S., Fang, Q., Liu, X., Liu, X., and Qi, H. (2018). PD-1 Controls Follicular T Helper Cell Positioning and Function. *Immunity* 49 (2), 264–274 e264. doi:10.1016/j.immuni.2018.06.012

Siliņa, K., Soltermann, A., Attar, F. M., Casanova, R., Uckeley, Z. M., Thut, H., et al. (2018). Germinal Centers Determine the Prognostic Relevance of Tertiary Lymphoid Structures and Are Impaired by Corticosteroids in Lung Squamous Cell Carcinoma. *Cancer Res.* 78 (5), 1308–1320. doi:10.1158/0008-5472.CAN-17-1987

Solinas, C., Garaud, S., De Silva, P., Boisson, A., Van den Eynden, G., de Wind, A., et al. (2017). Immune Checkpoint Molecules on Tumor-Infiltrating Lymphocytes and Their Association with Tertiary Lymphoid Structures in Human Breast Cancer. *Front. Immunol.* 8, 1412. doi:10.3389/fimmu.2017.01412

Stabile, H., Fionda, C., Gismondi, A., and Santoni, A. (2017). Role of Distinct Natural Killer Cell Subsets in Anticancer Response. *Front. Immunol.* 8, 293. doi:10.3389/fimmu.2017.00293

Ståhl, P. L., Salmén, F., Vickovic, S., Lundmark, A., Navarro, J. F., Magnusson, J., et al. (2016). Visualization and Analysis of Gene Expression in Tissue Sections by Spatial Transcriptomics. *Science* 353 (6294), 78–82. doi:10.1126/science.aaf2403

Stuart, T., Butler, A., Hoffman, P., Hafemeister, C., Papalexi, E., Mauck, W. M., 3rd, et al. (2019). Comprehensive Integration of Single-Cell Data. *Cell* 177 (7), 1888–1902 e1821. doi:10.1016/j.cell.2019.05.031

Surace, M., DaCosta, K., Huntley, A., Zhao, W., Bagnall, C., Brown, C., et al. (2019). Automated Multiplex Immunofluorescence Panel for Immuno-Oncology Studies on Formalin-Fixed Carcinoma Tissue Specimens. *JoVE* 143. doi:10.3791/58390

van der Leun, A. M., Thommen, D. S., and Schumacher, T. N. (2020). CD8+ T Cell States in Human Cancer: Insights from Single-Cell Analysis. *Nat. Rev. Cancer* 20 (4), 218–232. doi:10.1038/s41568-019-0235-4

Vickovic, S., Eraslan, G., Salmén, F., Klughammer, J., Stenbeck, L., Schapiro, D., et al. (2019). High-definition Spatial Transcriptomics for *In Situ* Tissue Profiling. *Nat. Methods* 16 (10), 987–990. doi:10.1038/s41592-019-0548-y

Wouters, M. C. A., and Nelson, B. H. (2018). Prognostic Significance of Tumor-Infiltrating B Cells and Plasma Cells in Human Cancer. *Clin. Cancer Res.* 24 (24), 6125–6135. doi:10.1158/1078-0432.CCR-18-1481

Xing, M., Feng, Y., Yao, J., Lv, H., Chen, Y., He, H., et al. (2020). Induction of Peripheral Blood T Follicular Helper Cells Expressing ICOS Correlates with Antibody Response to Hepatitis B Vaccination. *J. Med. Virol.* 92 (1), 62–70. doi:10.1002/jmv.25585

Conflict of Interest: The authors declare that the research was conducted in the absence of any commercial or financial relationships that could be construed as a potential conflict of interest.

Publisher's Note: All claims expressed in this article are solely those of the authors and do not necessarily represent those of their affiliated organizations, or those of the publisher, the editors, and the reviewers. Any product that may be evaluated in this article, or claim that may be made by its manufacturer, is not guaranteed or endorsed by the publisher.

frontiers in Molecular Biosciences

ORIGINAL RESEARCH
published: 26 October 2021
doi: 10.3389/fmolb.2021.658932

Immune Response in Myocardial Injury: *In Situ* Hybridization and Immunohistochemistry Techniques for SARS-CoV-2 Detection in COVID-19 Autopsies

Pek Yoon Chong[1], Jabed Iqbal[2], Joe Yeong[3], Tar Choon Aw[1], Kian Sing Chan[4] and Paul Chui[5]*

[1]Department of Pathology, Sengkang General Hospital, Singapore, Singapore, [2]Department of Anatomical Pathology, Singapore General Hospital, Singapore, Singapore, [3]Institute of Molecular and Cell Biology, A-STAR, Singapore, Singapore, [4]Department of Molecular Pathology, Singapore General Hospital, Singapore, Singapore, [5]Health Science Authority, Singapore, Singapore

OPEN ACCESS

Edited by:
Matteo Becatti, University of Firenze, Italy

Reviewed by:
Kewal Krishan, Panjab University, India
Alessio Biagioni, University of Florence, Italy

***Correspondence:**
Jabed Iqbal
jabed.iqbal@singhealth.com.sg

Specialty section:
This article was submitted to Molecular Diagnostics and Therapeutics, a section of the journal Frontiers in Molecular Biosciences

Received: *26 January 2021*
Accepted: *28 September 2021*
Published: *26 October 2021*

Citation:
Chong PY, Iqbal J, Yeong J, Aw TC, Chan KS and Chui P (2021) Immune Response in Myocardial Injury: In Situ Hybridization and Immunohistochemistry Techniques for SARS-CoV-2 Detection in COVID-19 Autopsies. Front. Mol. Biosci. 8:658932. doi: 10.3389/fmolb.2021.658932

Coronavirus disease-19 (COVID-19) is caused by the newly discovered coronavirus, severe acute respiratory syndrome coronavirus 2 (SARS-CoV-2). While the lung remains the primary target site of COVID-19 injury, damage to myocardium, and other organs also contribute to the morbidity and mortality of this disease. There is also increasing demand to visualize viral components within tissue specimens. Here we discuss the cardiac autopsy findings of 12 intensive care unit (ICU) naïve and PCR-positive COVID-19 cases using a combination of histological, Immunohistochemical/immunofluorescent and molecular techniques. We performed SARS-CoV-2 qRT-PCR on fresh tissue from all cases; RNA-ISH and IHC for SARS-CoV-2 were performed on selected cases using FFPE tissue from heart. Eight of these patients also had positive post-mortem serology for SARS-CoV-2. Histopathologic changes in the coronary vessels and inflammation of the myocardium as well as in the endocardium were documented which support the reports of a cardiac component to the viral infection. As in the pulmonary reports, widespread platelet and fibrin thrombi were also identified in the cardiac tissue. In keeping with vaccine-induced activation of virus-specific $CD4^+$ and $CD8^+$ T cells, and release of cytokines such as interferon-gamma (IFNγ), we observed similar immune cellular distribution and cytokines in these patients. Immunohistochemical and immunofluorescent localisation for the viral Spike (S-protein) protein and the nucleocapsid protein (NP) were performed; presence of these aggregates may possibly contribute to cardiac ischemia and even remodelling.

Keywords: PCR, COVID-19, autopsy, multiplex, serology

INTRODUCTION

SARS-CoV-2 (Covid 19), a novel corona virus was first implicated as the cause of a rapidly spreading infectious upper respiratory illness in late 2019 (Zhu et al., 2020) resulting in an exponential increase in global infections (WHO, 2020). There is much to be done as thenatural history of this disease has yet to be elucidated and whilst there has been an emphasis on pulmonary findings, there are now

TABLE 1 | Patient characteristics and autopsy findings.

case No.	1	2	3	4	5	6	7	8	9	10	11	12
Gender	**M**	**M**	**M**	**M**	**M**	**M**	**M**	**M**	**M**	**M**	**M**	**M**
AGE	32	46	47	53	30	41	41	48	27	42	69	59
BMI	25.28	19.05	20.62	26.67	16.11	27.1	21.87	18.94	22.41	18.31	21.48	31.7
Ante mortem test (PCR)	YES	YES	NA	NA	NA	YES	NEG	YES	YES	YES	YES	YES
TEST TO DEATH INTERVAL (DAYS)	6 HRS	4 DAYS	NA	NA	NA	42 DAYS	NA	38 DAYS	19 DAYS	47–48 DAYS	1 DAY	41 DAYS
PRIOR MEDICAL CONDITIONS	NIL	NIL	NIL	NIL	NIL	Not known	Not known	Not known	NIL	Not known	DM TYPE 2. HYPT. HYPOTHYROID. OBESE. CKD	Nil
CIRCUMSTANCES OF DEATH	SUDDEN DEATH	Fell from Height	SUDDEN DEATH	SUDDEN DEATH	SUDDEN DEATH	SUDDEN DEATH	SUDDEN DEATH	SUDDEN DEATH	Fell from height	SUDDEN DEATH, DECOMPOSED	ARI; SUDDEN DEATH	SUDDEN DEATH
HEART WT (gm)	345	235	419	410	245	404	245	340	222	244	463	398
HEART GENERAL DESCRIPTION	SOFT AND FLABBY.	SOFT AND FLABBY.	SOFT AND FLABBY	TRANSMURAL RUPTURE, ANTERIOR-ANTEROSEPTAL WALL, JUNCTION OF UPPER 2/3 AND DISTAL 1/3 LV.	SOFT AND FLABBY	SOFT AND FLABBY, FIBRINOUS ADHESIONS OVER RA, RV ENDOCARDIUM	GROSSLY NORMAL	GROSSLY NORMAL	GROSSLY NORMAL	DECOMPOSED	HEART ENLARGED	HEART ENLARGED
CORONARY arteries	LCA: PINPOINT RESIDUAL LUMEN	NORMAL.	LCA ATHEROSCLEROTIC WITH 50% OCCLUSION OF LAD.	LAD 10–25%. DARK RED THROMBUS, TOTAL OCCLUSION	LAD-ORGANISING THROMBUS.	MILD ATHEROSCLEROSIS						
LAD 10–25%	PROX LAD 75%-	LCA 25/ LAD 90/ LCX 75/ RCA PINPOINT	NAD	LAD 10–25	LCA 10 LAD 90- FIRST DIAGONAL PINPOINT	LCA 50 LAD25						
SEROLOGY (IgM + IgG)	CLOTTED	CLOTTED	POSITIVE; COI 2.22	POSITIVE; COI 2.38	CLOTTED	POSITIVE; COI 89.8	POSITIVE; COI 9.91	POSITIVE; COI 114	POSITIVE; COI21.5	UNSUITABLE FOR ANALYSIS	NO; COI 0.534	POSITIVE; COI:8.73
Swab (Nasal)	DETECTED	DETECTED	PRESUMPTIVE POSITIVE	NOT DETECTED	DETECTED	NOT DETECTED	NEGATIVE	NEGATIVE	NEGATIVE	DETECTED	DETECTED	NEGATIVE
Swab (PNS)	DETECTED	DETECTED	DETECTED	DETECTED	PRESUMPTIVE POSITIVE	NOT DETECTED	DETECTED	DETECTED	DETECTED	DETECTED	DETECTED	NEGATIVE
Swab (Tracheal)	DETECTED	DETECTED	PRESUMPTIVE POSITIVE	NOT DETECTED	DETECTED	NOT DETECTED	NEGATIVE	NEGATIVE	DETECTED	NEGATIVE	DETECTED	NEGATIVE
Swab (Ileal)	DETECTED	DETECTED	NOT DETECTED	INCONCLUSIVE	DETECTED	DETECTED	NEGATIVE	NEGATIVE	NEGATIVE	DETECTED. STRONG POSITIVE	PRESUMPTIVE POSITIVE	NEGATIVE
Swab (CNS)	DETECTED	DETECTED	NOT DETECTED	NOT DETECTED	NOT DETECTED	NOT DETECTED	NEGATIVE	NEGATIVE	NEGATIVE	NEGATIVE	DETECTED	NEGATIVE

LCA; Left coronary artery, LAD: Left anterior descending artery, PROX LAD: Proximal Left anterior descending artery, LCX: Left circumflex artery, RCA: right coronary artery.

increasing reports that Covid-19 may also affect the cardiovascular and other organ systems (Babapoor-Farrokhran et al., 2020; Barton et al., 2020). In fact, Yang et al. reported death of a small number of patients who died within a short period of time after admission, in other words, sudden death (Yang et al., 2021). Moreover, sudden cardiac arrest and death had been reported as early as 2020 despite improvement of general condition and constitutional symptoms (Shirazi et al., 2021).

Much about the pathogenesis of SARS-CoV-2 and the heart remains unknown (Siripanthong et al., 2020). Angiotensin (AT) converting enzyme 2 (ACE2), known as the cellular receptor for SARS-CoV-2 is ubiquitously expressed with the highest levels detected in the cardiovascular system (cardiomyocytes, cardiac fibroblasts, vascular smooth muscle cells and endothelial cells) as well as intestine, kidneys and lungs (Grifoni et al., 2020; Le Bert et al., 2020). We discuss the cardiac (and vascular) pathology seen in twelve cases of sudden death in patients who were also Covid-19 positive. We document possible evolution of the disease with little or no medical intervention in a study of these autopsy cases. We also aim to document the cellular immune response observed in the COVID-19 patients.

METHODS

In our series of twelve male autopsy cases, ten cases were sudden unexplained deaths. Case 1 had presented to his physician with anosmia, had a swab taken and was sent home where he was found collapsed the next day before the test results were known. The remaining 9 cases had a variety of complains including chest pain, epigastric pain or discomfort. Case 10 was last heard complaining of chest pain but was found dead 2 days later. Of these only two cases had known premorbid illnesses on record. Case 8 had a history of hypertension whilst case 11, who was unemployed, is the only case with documented premorbid conditions of poorly controlled diabetes and hypertension. He was being managed by his physician for 2 weeks of fever and cough before being tested positive for Covid-19. He collapsed at home a day later.

Two cases were unnatural deaths, having fallen from height (case 2 was admitted to hospital for

observation after 5 days of fever and a positive test, whilst case 9 was admitted in a facility for

well and asymptomatic Covid-19 patients.

All subjects, except for case 11, worked in the construction industry. None of the 12 cases.

Presented with severe respiratory symptoms nor required supplemental oxygen. In cases where clinical history was not available, we have taken the date of the first positive PCR test as the most probable start point of COVID-19 infection and have stratified the patients accordingly.

All twelve cases were referred to Health Sciences Authority for autopsy (mean age = 44.1 year range:27–69 years) (**Table 1**) under the Second Schedule of the Coroners Act Cap 63A (Revised Edition 2012 Singapore Statutes). All autopsies were carried out either in biosafety level (BL)-BSL3 or BSL4 autopsy facilities. All subjects were male.

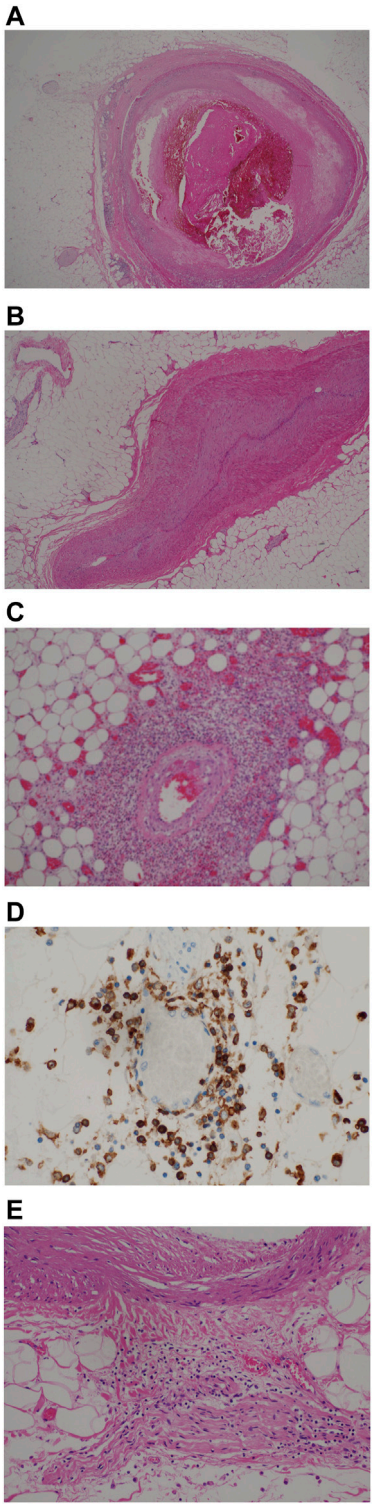

FIGURE 1 | (A) Coronary vessel with fresh fibrin thrombus, moderate inflammation, mild fibrosis (H&E, x200). **(B)** apposition of vascular endothelium (H&E, x200). **(C)** Perivascular inflammation around epicardial vessel (H&E, x200). **(D)** CD4-positive T-cells in perivascular tissue, 200x. **(E)** Perivascular inflammation extending to adipose tissue and involving peripheral nerve (H&E, x200).

TABLE 2 | Microscopic findings; key: Light yellow <7 days; Pink >7 days.

case no	1	2	3	4	5	7	11	9	6	8	10	12
Interval from ante-mortem PCR to autopsy	6 h	4 days	NA	NA	NA	NA	1 day	19	42 days	38 days	47–48 days	41 days
Epicardial vessel lumen	occluded	occluded (lumen closed by apposition)	occluded	occluded	occluded	80%	occluded atherosclerotic with inflammatory infiltrates	myointimal thickening	myointimal thickening	myointimal thickening	myointimal thickening	myointimal thickening
Fresh thrombus	yes	no	yes	yes	yes	no	no	no	no	no	no	no
Fibrin thrombi	yes	yes	yes	yes	yes	Yes	yes	yes	Yes	yes	Autolytic changes	yes
Perivascular inflammation	Yes 3 + mixed inflammatory cells	yes 1 + lymphocytic infiltration	yes 2 + lymphocytic infiltration	Yes 1 + lymphocytic infiltration	Yes 2 + mixed inflammatory cells	yes	Lymphoid aggregates	1 + lymphocytic infiltration	1 + lymphocytic infiltration	Lymphoid aggregates	Autolytic changes	Lymphoid aggregates
Myocardium inflammatory infiltrate	2 + lymphocytic	no	3 + lymphocytes and eosinophils	1 + Lymphocytes	3 + lymphocytes and eosinophils	2 + lymphocytes	scanty lymphocytes	1 + LYMPHOCYTES	2 + lymphocytes	1 + lymphocytes	Autolytic changes	1 + lymphocytes, eosinophils

FIGURE 2 | (A) Remodeling of myocardial vesels showing myointimal hypertrophy/thickening with perivascular lymphoid aggregates (H&E, x200). **(B)** Perivascular inflammation involving epicardial vessel (H&E, x200).

RESULTS

Vasculature

The findings are stratified with respect to known or estimated duration of symptoms. The earlier group comprised 5 cases with symptom duration ranging between <12 h and 5 days. In 4 of these, we observed complete occlusion of the coronary artery by fresh fibrin thrombi; the epicardial coronary vessels showed pre-existing mild atherosclerosis (**Figure 1A**). In a fifth patient (case 2), we observed that the patency of the arterial lumen was compromised by apposition of the endothelium (**Figure 1B**).

An inflammatory infiltrate was seen around epicardial vessels of varying diameter, predominantly in a perivascular location, extending into the outer layers of the vessel wall and outwards into the pericardial adipose tissue (**Figure 1C**, patient 3, **Table 2**). On cross sections, the interface of the more intense inflammatory infiltrates imbued a stellate appearance. The inflammatory cells were predominantly lymphoid in nature, particularly

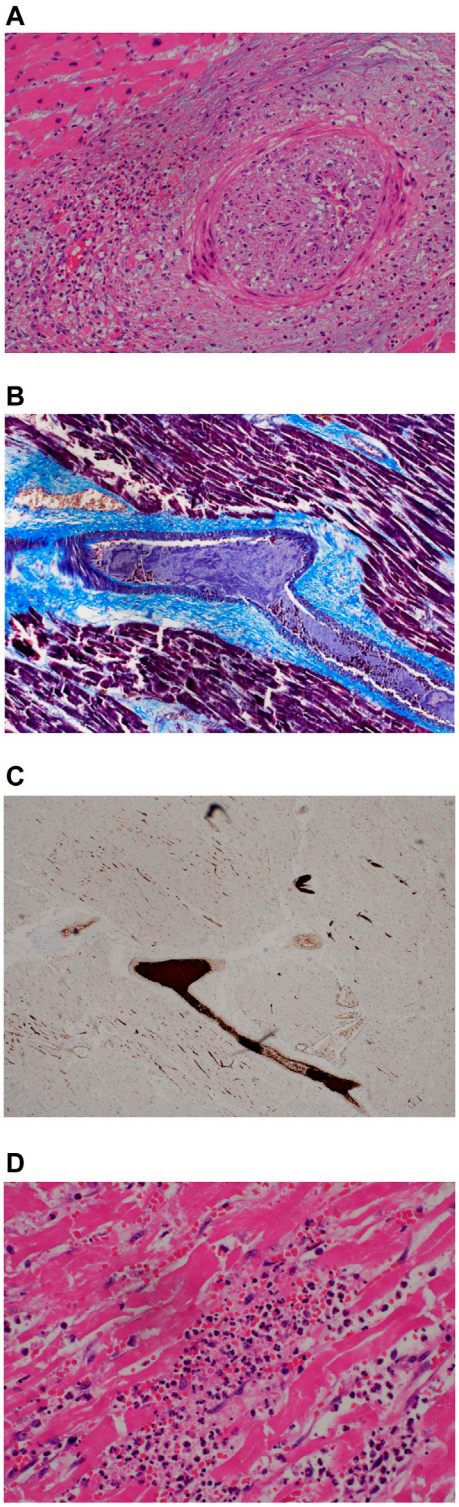

FIGURE 3 | (A) Occlusion of coronary artery lumen by proliferation of spindled cells (H&E, x200). **(B)** Fibrin thrombi. MSB stain (200x). **(C)** Platelet thrombi, CD61 immunohistochemical stain (200x).

CD4-positive (IHC) with scanty CD8-positive T-cells and CD20-positive B cells (**Figure 1D**). In some cases, the latter two subtypes of lymphocytes were virtually absent. Except for two cases where the eosinophilic infiltrate was heavy, eosinophils and monocytes were also noted in smaller amounts. Involvement of nerves by chronic inflammation were also seen **Figure 1E**.

In cases where symptoms persisted for more than 14 days, the inflammatory infiltrate was less prominent. The coronary vessels showed medial and intimal hypertrophy with focal dilatation, outpouching or tortuosity of vessels giving an irregular appearance (**Figure 2A**, case 5 A fine perivascular fibrosis was seen around both thin and thick-walled vessels of varying diameters including capillary vessels. The pericardial adipose tissue was involved in the inflammation in all cases, irrespective of duration of symptoms (**Figure 2B**).

Myocardium

The perivascular inflammatory infiltrate described previously was observed to follow the vessels into the myocardium and could be seen extending along the longitudinal axis of the vessels. In some cases, the inflammatory infiltrates were seen around the

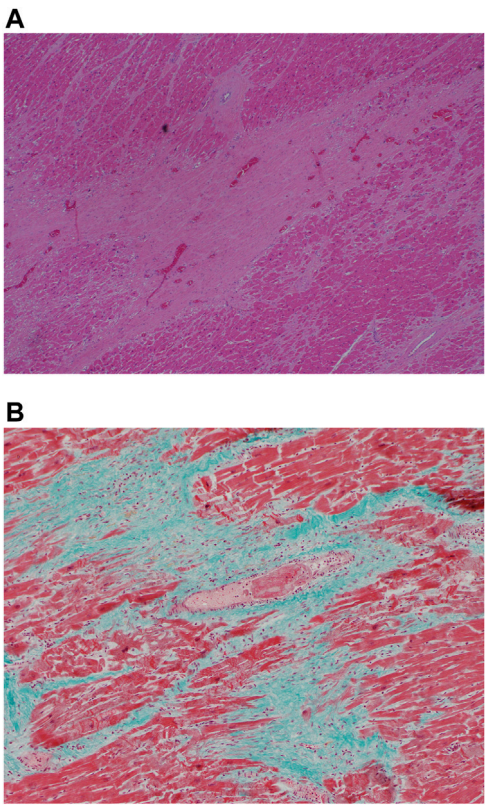

FIGURE 4 | (A) Myocarditis with myocyte necrosis (H&E, x200). **(B)** Stellate myocardial fibrosis (H&E, 200x). **(C)** Masson trichrome stain confirming fibrosis (200x).

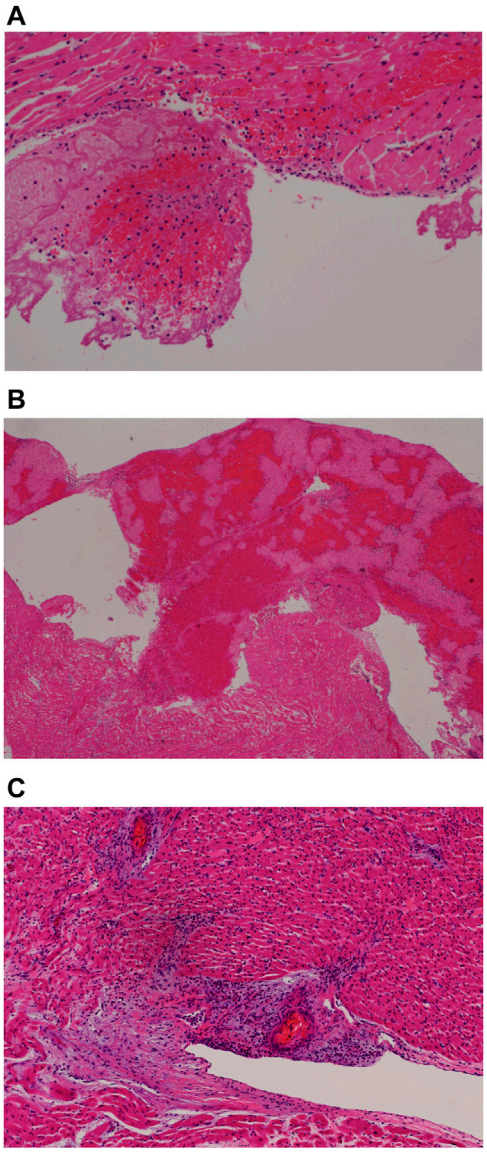

FIGURE 5 | (A) Endocardial fresh blood clot (H&E, 200x). **(B)** Endocardial organizing thrombus (H&E, 200x). **(C)** Endocarditis (H&E, 200x).

perivascular spaces, within the wall and lumen. Again, the lymphoid cells were predominantly of CD4 lineage with virtually no CD8-positive T-cells or CD20-positive B-cells. Obliteration of the vascular lumen by a proliferation of spindled myofibroblasts was seen in one case (**Figure 3A**, case 5).

Extensive fibrin and platelet thrombi were noted in the myocardial vessels as well as in the myocardial microvasculature. Mature fibrin thrombi were observed with MSB stains (**Figure 3B**); intravascular platelet aggregates were demonstrated by CD61 antibody (**Figure 3C**).

Myocarditis as evidenced by chronic inflammation and myocyte necrosiswas marked in 4 of the 5 earlier cases but could be seen in patchy fashion even in the later cases (**Figure 4A**, case 3) The inflammatory cells comprised a mixed population of lymphoid cells, neutrophils, eosinophils and monocytes; eosinophils were prominent in case 3,. Granulation tissue reaction with presence of reactive stromal cells was demonstrated in 2 of the earlier cases whilst a patchy stellate myocardial fibrosis was noted in the later cases (more than 7 days) (**Figure 4B,C**, case 8). This fibrosis could also be seen sweeping along the long axis of the myocardial vessels appearing to mirror the inflammatory infiltrate in the earlier cases. Within the fibrous tissue, thin-walled vessels were noted. It is unclear if these vessels represent residual vasculature or neovascularization. (**Figure 4D**, case 8).

Endocardium

Focal infiltration of the endocardial lining by mononuclear cells was noted in the earlier cases (**Figure 5A–C**, case 5).

RNAscope in-Situ Hybridization

RNAscope assay following the manufacturer's protocols was applied to five cases. Weak positive signals were detected within myocytes in three cases (cases 2,3 and 5). Co-localization of SARS-CoV-2 with its entry receptor ACE2 and serine protease TMPRSS2 (type II transmembrane serine protease) in different cell types, using RNAscope *in situ* hybridization, was found in various compartments of the heart, such as endothelial smooth muscle, myocardium, fibroblastic and inflammatory cells (**Figure 6**).

Immunohistochemistry

Detection of viral NP in myocardium was attempted using immunohistochemistry and identified in two cases including one case with coexisting myocardial viral S protein on RNAscope assay. The second case was 38 days post-covid-19 infection and viral NP-protein was detected within the vascular lumen as well as the immediate perivascular space (**Figure 7**, case 8).

mIHC/IF

We investigated the presence of the SARS-COV2 NP protein (Shirazi et al., 2021; Siripanthong et al., 2020; Le Bert et al., 2020; Grifoni et al., 2020) and the associated immune microenvironment by using multiplex IHC/IF technique (Ni et al., 2020; Thieme et al., 2020; Stack et al., 2014; Abel et al., 2014; Lovisa et al., 2015; Garnelo et al., 2015; Yeong et al., 2017; Garnelo et al., 2017; Esbona et al., 2016; Mlecnik et al., 2016; Nghiem et al., 2016; Feng et al., 2016; Lim et al., 2018). The SARS-COV2 NP protein was found predominantly near the perivascular regions colocalizing with receptors of SARS-COV2, ie ACE2 and TMPRSS2 (Yeong et al., 2019; Lam et al., 2019) (**Figure 3**). Interestingly, the pathogenic cytokines such as IL-6 (Xu et al., 2020a; Hoffmann et al., 2020; Qin et al., 2020; Wang et al., 2020) and IL-1β (Huang et al., 2020a; Xu et al., 2020a; Diao et al., 2020; Shi et al., 2020) were also detected in close proximity in the background of fibrosis highlighted by the expression of Collagen I and III (Liao et al., 2020; Wen et al., 2020).. (**Figure 8**)

We further demonstrated that some of the $ACE2^{+}$ cells were macrophages which are in line with previous reports (Delpino and Quarleri, 2020; George et al., 2020). Colocalization of the pathogenic cytokine GM-CSF (Diao et al., 2020) as well as surrounding T-cells were also observed in the proximity (**Figure 9**, case 8).

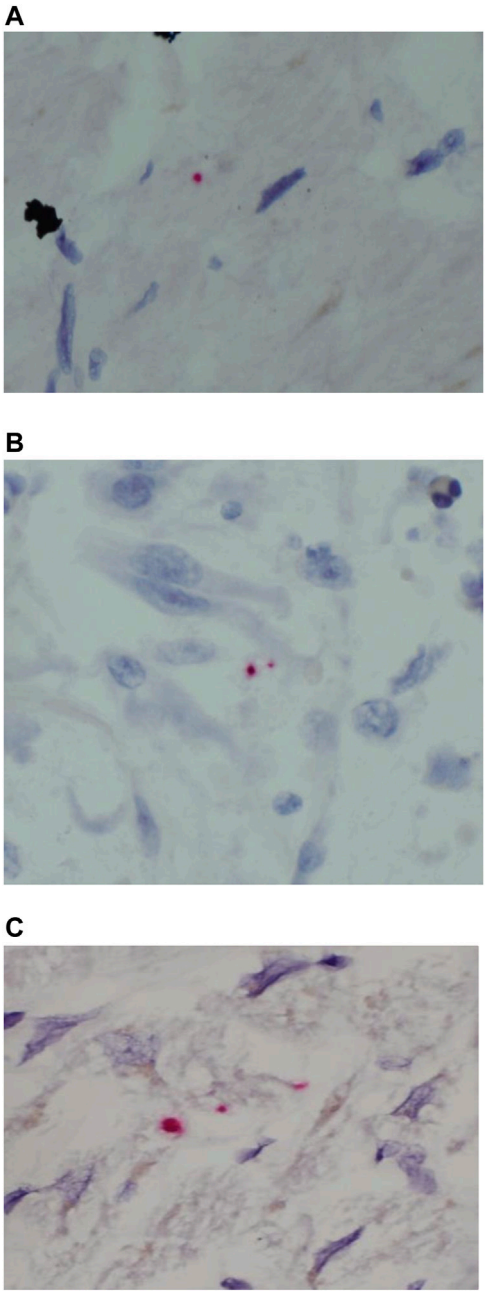

FIGURE 6 | SARS-CoV-2 ISH in myocardium from the autopsy of patients who died secondary to COVID-19 infection. **(A–C)** Positive reactions for the probes directed against SARS-CoV-2 S-protein (red dot) original magnifications ×400).

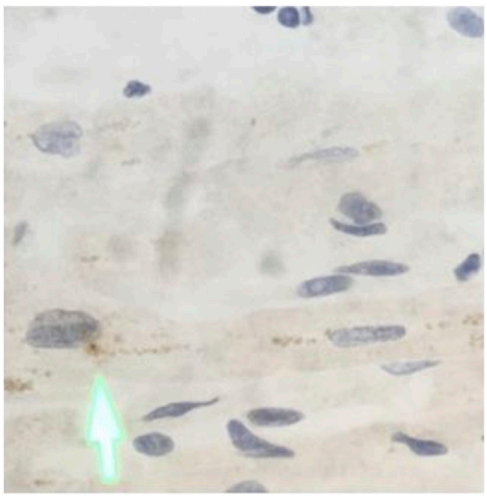

FIGURE 7 | Immunohistochemical analysis in myocardium from the autopsy of patient who died secondary to COVID-19 infection **(A)** SARS-CoV-2 is positive (arrow) in the myocardial tissue, original magnifications ×400.

Furthermore, we interrogated the immune phenotype of the T-cells present in the peri-vascular regions whereby Th2 cells, highlighted by absence of GATA3 nuclear stain, were virtually absent (Robinson et al., 2020). However, few T-cells demonstrated a Th-1 cell-like phenotype which expressed pathogenic cytokines such as interferon-gamma (Zheng and Flavell, 1997; Xu et al., 2020a; Diao et al., 2020; Weiskopf et al., 2020; Yao et al., 2020). Some of the T-cells expressed granzme-B signifying the effector function of cytotoxic T cells (Thevarajan et al., 2020; WHO, 2020; Zheng et al., 2020), as well as CD38 which has been widely reported as one of the SARS-COV2-specific T-cell marker (Huang et al., 2020a; Xu et al., 2020b; Craver et al., 2020; Thevarajan et al., 2020; Wang et al., 2020) (**Figure 10**, case 8).

SARS-CoV-Ab Serology

COI values for 7 of the 8 patients were clearly positive ranging from 2.22 to 114; it was 0.534 in the remaining patient. The range in 362 prepandemic male (age: mean, SD - 43.3, 14.5 years) sera on this assay was 0.066–0.373 (data not shown).

DISCUSSION

We document 12 autopsy cases with cardiac changes. Four of these cases had histologic evidence of myocarditis with marked predominantly lymphocytic and some eosinophilic infiltrates. The presence of SARS NP protein in a perivascular location, the proximity of T-cells and cytokine GM-CSF bum IHC/IF appears to corroborate changes observed at the light miscroscopy. Whether these changes were purely due to an underlying ischemic heart disease or whether the process was exacerbated by the viral infection is unclear.

Myocardial cells are a potential target of SARS-CoV-2, and myocarditis has been reported in a limited series in China, where 7% of deaths were attributed to myocardial damage with circulatory failure without a clear, definite diagnosis of myocarditis (Cheung et al., 2020). Others have described fulminant myocarditis in the setting of high viral load, with autopsy findings of myocardial inflammatory infiltrate, but without evidence of myocardial COVID-19 disease (Robinson et al., 2020). Although much of the published literature has focussed on the pulmonary changes, findings from our autopsy

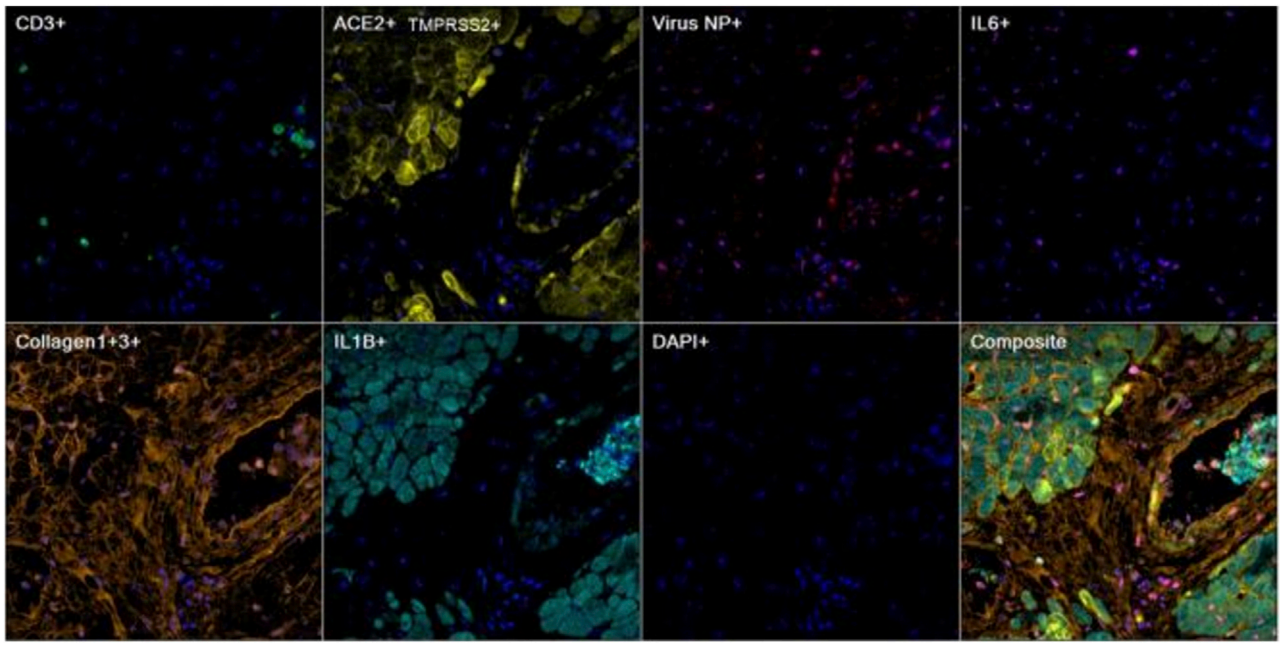

FIGURE 8 | Representative images of heart tissue stained using multiplex immunohistochemistry/immunofluorescence (mIHC/IF) [CD3 (green), ACE2/TMPRSS2 (yellow), Virus NP (red), IL6 (magenta), Collagen1+3 (orange), IL1B (cyan), DAPI (blue)] (Magnification, 400X).

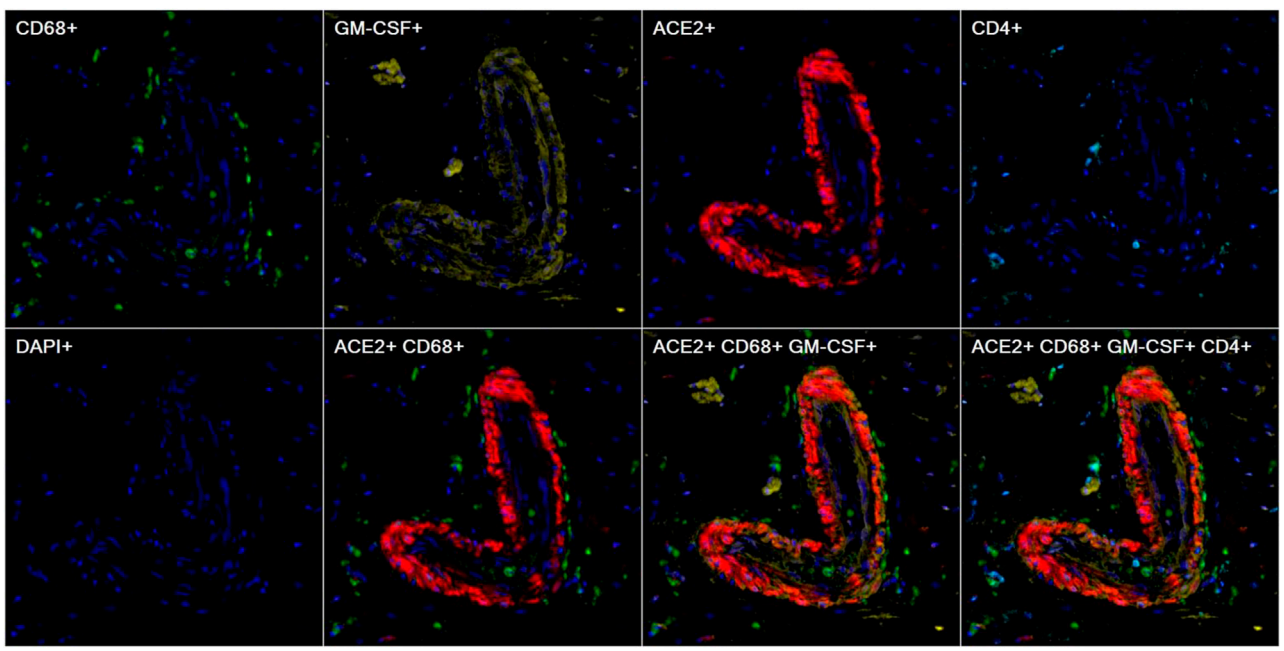

FIGURE 9 | Representative images of heart tissue stained using multiplex immunohistochemistry/immunofluorescence (mIHC/IF) [CD68 (green), GM-CSF (yellow), ACE2 (red), CD4 (cyan), DAPI (blue)] (Magnification, 200X).

series demonstrate that significant cardiac pathology may be associated with COVID-19 infection. It has already been postulated that in addition to coronary plaque destabilization and hypoxia, the possible mechanisms of COVID-19-related myocardial injury could be direct damage to the cardiomyocytes, chronic inflammation, myocardial interstitial fibrosis, interferon-mediated immune response and exaggerated cytokine response by T-cells (Babapoor-Farrokhran et al., 2020).

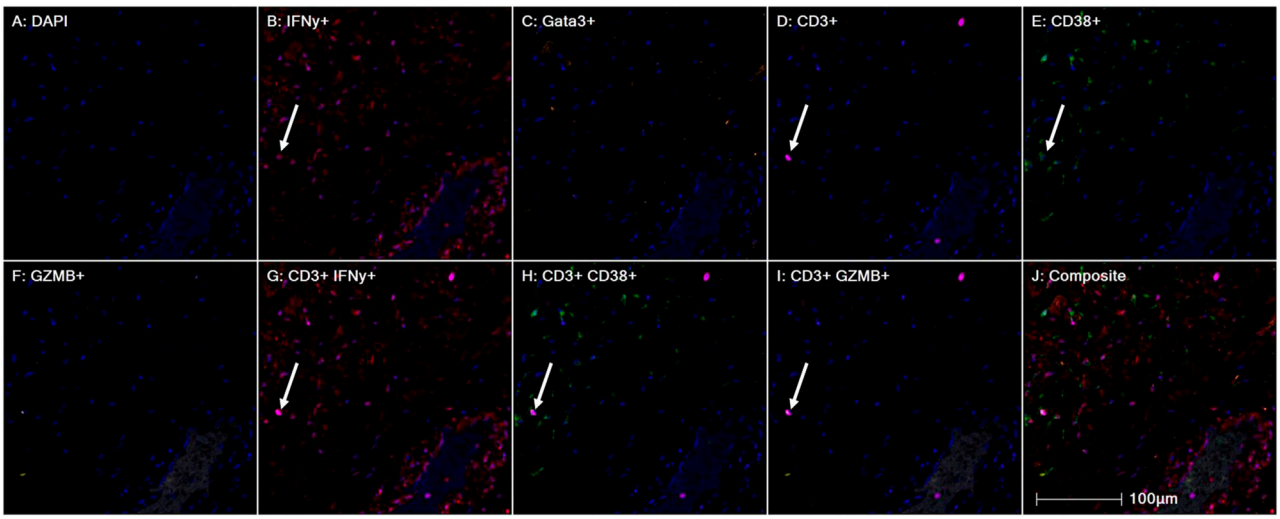

FIGURE 10 | Representative images of heart tissue stained using multiplex immunohistochemistry/immunofluorescence (mIHC/IF) Interferon gamma (red), GATA3 (orange), CD3 (magenta), CD38 (green), Granzyme B (yellow) (Magnification, 200X).

The records of the Forensic Department, Singapore show that in 2018, a total of 1,414 cases were autopsied and 18 were certified as myocarditis. In 2019 there were 1,262 cases of which 23 were certified as myocarditis. 131 cases were certified as Coronary heart disease in 2018 and 108 in 2019. A small autopsy series of four non-COVID-19 deceased patients during the same period did not reveal any significant myocardial inflammation (**Supplementary Table S2**).

In SARS autopsies (Chong et al., 2004) we reported pulmonary thromboembolic, deep vein thrombosis, and marantic valvular vegetations with widespread intravascular fibrin thrombi. As the SARS patients had a history of admission to intensive care units (ICU), it could be argued that these changes were related to ICU support and therapy. However, our current cases are all ICU-naïve.

SARS-CoV-2 is known to use the ACE2 receptor as a channel for entrance into the cell as receptors have been reported to be present in cardiac smooth muscle, vascular smooth muscle and endothelial cells as well as pneumocytes and enterocytes (Dandekar and Perlman, 2005; Yajima and Knowlton, 2009). It is possible that the virus enters these cells including the cardiac myocytes and that the immediate innate cytokine response may cause the initial myocardial damage early in the infection and that the arrival of the T-lymphocytes would further intensify this. Our studies have been able to demonstrate viral signals within the cardiac myocytes using both ISH and mIF assays. The latter has also demonstrated increased cytokine and interferon activity within the myocardium in perivascular locations co-locating with SARS-CoV-2specific T cells as well as macrophages. We note that in staining for the ACE2 receptor, the distribution of these receptors is not uniform throughout the cardiac and vascular samples. This underlying variation may underscore the heterogenous distribution of cardiac injury seen in our cases.

Yajima and Knowlton (2009); Wick et al. (2004) Immunohistochemical findings in our cases suggest the presence of virus within the vessel lumen and wall as well as within immediate perivascular space together with the presence of activated lymphocytes and cytokine activity (**Figure 4**). Macrophage/monocytes are known to be able to transport Corona viruses and studies have also suggested that T-lymphocytes may be similarly infected (Wick et al., 2004; Yajima and Knowlton, 2009). Hence whether this vascular inflammation is a direct reaction to the existence of the virus within the endothelium or a combination of dysregulated T cell, cytokine and humoral response remains to be seen. Consequently, it is tempting to propose that the observed perivascular and intravascular inflammation modulates the vascular integrity leading to vascular remodelling in the long-term.

The cytokine and inflammatory cell activity within the lumen are interesting as this suggests injury to the endothelial lining. Our cases show widespread platelet and fibrin thrombi within myocardial vessels and the myocardial microvasculature which appears to persist even in cases with a prolonged disease. The presence of possible NP protein signals within the lumen of the vessel may also suggest persistence of viral presence in circulating monocytes as another stimulus for the microembolic phenomena (**Figure 4**).

One of our cases also showed marked fibroblastic activity within intramyocardial vessels, suggesting possibly immune-mediated injury to endothelial lining possibly contributing to a stenosing lesion (Thieme et al., 2020). In recent years, pro-fibrotic role of the innate immune system has become apparent. Early events of fibrosis comprise inflammatory changes (Wick et al., 2010), including recruitment of mononuclear inflammatory infiltrates. Although, the initial events in activation of host defence mechanisms are still largely unknown, It has been proposed that viral myocarditis may have several phases from predisposition or susceptibility of the cardiac myocyte to infection, entry and active viral replication in the myocyte,

persistence of the viral genome without detectable replication and remodelling without detectable viral genome (Varga et al., 2020).

Using mIF methods, we have demonstrated presence of IL-1B and IL6 activity within collagen fibers in the regions of myocardial fibrosis, both of which have been known to play a profibrotic role (Huang et al., 2020a; Patil et al., 2020). It is possible that profibrotic cytokines and mediators released during myocarditis phase in susceptible individuals activate fibroblasts and stimulate fibroblast differentiation leading to subsequent cardiac remodelling. One further interesting point is the persistent epicardial adipose tissue injury seen in all cases manifested by small aggregates of $CD4^+$ T-lymphocytes around small thin-walled vessels and edematous tissue in the early cases to patchy aggregates of lymphocytes and contraction of the epicardial layer. As this epicardial adipose tissue has been postulated to be active in secretion of endocrine and paracrine substances, this persistent inflammation at this location may further compound vascular injury (Huang et al., 2020b).

Interestingly, use for SARS-CoV2 antibody titer has not been reported before for forensic purposes. The Roche assay detects total antibodies to the nucleocapsid protein. The results are reported as a cut-off index (COI); COI >1.4 are considered positive. This suggests that the COI of 0.534 may represent a subclinical antibody titer. Our findings suggest a possible forensic application for the Roche serology test.

Although direct SARS-CoV-2-induced myocardial is a consideration, COVID-19-associated cardiac damage is widely attributed to exaggerated immune response. One of the early reports describing myocardial inflammation in SARS-CoV-2 infection reported fulminant myocarditis with elevated IL-6 levels along with other cardiac injury markers (Wong et al., 2004). Various cohort-based studies also showed an increased cytokine production during COVID-19 infection, and cytokine storm in these patients was found to be associated with the disease severity and patient survival (Molenkamp et al., 2020). The immune response in SARS patients is mainly mediated through the Th1-cell activity as opposed to SARS-CoV-2 infection, where an imbalance between both Th1 and Th2 activity was found to support the inflammatory surge (Peiris et al., 2003; Corman et al., 2021). Overall, evidence from the published studies and ours implies that the SARS-CoV-2-induced inflammatory response may be a possible cause of cardiac damage in patients and could be targeted for therapeutic interventions. The robust elicitation of IFNγ-producing $CD4^+$ T cells in our studies indicates that a cellular immune response with potential anti-viral properties mirrors the strong neutralizing antibody and cytokine response seen in vaccine trials (Sahin et al., 2020). More recently, Bearse *et al* demonstrated that cardiac infection with SARS-CoV-2 was common among patients succumbing to COVID-19 infection. This study also showed that SARS-CoV-2-associated cardiac infection was associated with more cardiac inflammation and electrocardiographic changes (Bearse et al., 2021). Nonbiologic immunosuppression is associated with lower incidences of myocarditis and cardiac infection by SARS-CoV-2. In our series none of the patients received COVID-19 specific treatment.

Decrease of eosinophils was a critical event described in sudden deaths, which is consistent with previous report that eosinophils may predict the outcome of COVID-19 progression (Babapoor-Farrokhran et al., 2020). Patients with high percentage of neutrophils or neutrophils count had an increased risk of sudden death, probably due to cytokine storm activated by neutrophils (Wu et al., 2020). Unfortunately we did not have corroborating evidence to monitor immune cell counts or inflammatory biomarkers.

Exposure and susceptibility to COVID-19 are partly influenced by occupation and working environment. Migrant workers as in our cohort constituted a significant proportion of the workforce in sectors that have remained active throughout the crisis, such as construction work, logistics and deliveries. Several confounding factors such as inability to work in isolation, lack of access to private transportation, close physical proximity with coworkers and in some instances lack of adequate protective equipment render these workers particularly susceptible.

Although our study only examined male patients, the observed myocarditis is still concordant with other studies. In one study, the overall risk of patients with COVID-19 was nearly 16 times the risk for myocarditis compared with patients who did not have COVID-19. Patients with myocarditis were more commonly male (59.3 versus 41.7%). Despite the limitations, the observed myocardial lesions in our cohort may still be concordant with other studies (Boehmer et al., 2021).

Despite limited existing evidence, our study may provide relevant clues to associate sudden death of COVID-19 patients and potential risk factors. However, several limitations should be considered in our study: 1) it was a retrospective, single-center study and we were not able to conduct all radiographic or laboratory examinations in our subjects 2) interpretation of our findings might be limited by the small sample size 3) data collected for each patient may not be uniform as they represented different disease stages, which might lead to bias in clinical characteristics. Finally, as this is a descriptive/observational study, further mechanistic explanation needs to be clarified. Despite these limitations, our study demonstrated some insights into the characteristics of COVID-19 patients potentially at risk of sudden death. This would help physicians to effectively triage patients with particularly poor prognosis on admission to reduce the fatality rate.

CONCLUSION

Understanding the pathogenesis of COVID-19 infection is vital to the proper management of this disease. Conventional autopsy studies combined with state-of-the art molecular techniques are an integral part of this process. Here we highlight the incidence of increased cardiac and vascular events in COVID-19-infection which may underlie inflammatory syndromes (Wong et al., 2004) and raise the possibility for long term complications of potentially cardiotropic and persistent virus. Either persistent viraemia or migration of infected immune cells from the extracardiac locations likely occurs in COVID-19 patients which may exacerbate underlying ischemic myocardial injury. The

association of COVID19 NP protein with endothelial cells, cardiac smooth muscle cells warrants further investigation particularly in COVID19 recovering patients. The possible contribution to susceptibility of cardiac complications by gender, nutrition, genetics or viral mutation should also be considered.

METHODOLOGY

Real-Time Polymerase Chain Reaction

The inoculated swabs were tested at Singapore General Hospital Molecular Laboratory either using the automated Roche Cobas 6,800 System (Roche Molecular Systems, Inc., Branchburg, NJ) cobas SARS CoV-2 test, a dual-target (E gene and ORF1) qualitative real-time RT-PCR assay, or using our in-house developed SARS CoV-2 RT-PCR assay targeting the SARS-CoV-2 E-gene region (modified from the protocol published by Corman et al. (2021).

Multiplex Immunohistochemistry/ Immunofluorescence

mIHC/IF was performed using an Opal Multiplex fIHC kit (Akoya Bioscience, Menlo Park, California, USA), as previously described by our group and in other studies (Abel et al., 2014; Stack et al., 2014; Garnelo et al., 2015; Lovisa et al., 2015; Esbona et al., 2016; Garnelo et al., 2017; Yeong et al., 2017; Grifoni et al., 2020; Le Bert et al., 2020; Ni et al., 2020; Siripanthong et al., 2020; Thieme et al., 2020; Shirazi et al., 2021). Slides were labelled with primary antibodies, followed by appropriate secondary antibodies (see **Supplementary Table S1**). Particularly for this panel, we followed the detailed protocol that our group previous reported as protocol manuscript (Nghiem et al., 2016) and hereby briefly described.

FFPE tissue sections were cut onto Bond Plus slides (Leica Biosystems Richmond) and heated at 60°C for 20 min (Feng et al., 2016). Tissue slides were then subjected to deparaffinisation, rehydration and heat-induced epitope retrieval (HIER) using a Leica Bond Max autostainer (Leica Biosystems Melbourne), prior to endogenous peroxidase blocking (Leica Biosystems Newcastle). Slides were incubated with primary antibodies followed by application of polymeric HRP-conjugated secondary antibodies (Leica Biosystems Newcastle). An appropriate Opal fluorophore-conjugated Tyramide signal amplification (TSA) (Akoya Bioscience, Menlo Park, California, United States) was then added at 1:100 dilution. Slides were rinsed with washing buffer after each step. Following TSA deposition, slides were again subjected to HIER to strip the tissue-bound primary/ secondary antibody complexes and ready for labelling of the next marker. These steps were repeated until all six markers were labelled and finally added with spectral DAPI (Akoya Bioscience, Menlo Park, California, United States) at 1:10 dilution. Slides were mounted in ProLong Diamond Anti-fade Mountant (Molecular Probes, Life Technologies, United States) and cured in the dark at room temperature for 24 h. Images (viable tumour regions were selected by pathologists) were acquired for each case using a Vectra three pathology imaging system microscope (Akoya Bioscience, Menlo Park, California, United States) then analysed and scored by pathologist with inForm software (version 2.4.2; Akoya Bioscience, Menlo Park, California, United States) (Zheng and Flavell, 1997; Weiskopf et al., 2020) as well as HALO TM (Indica Labs) (Xu et al., 2020a; Hoffmann et al., 2020).

RNA in-Situ Hybridization

For RNAscope RNA-ISH (Advanced Cell Diagnostics) analysis of EBNA1, standard RNAscope manufacturer's protocols were followed using the RNAscope H2O2 and protease pretreatment kit (ACD, reference# 322,381), RNAscope Target retrieval buffer (ACD, reference# 322,000), and appropriate positive and negative RNA probes for controls.

Immunohistochemistry

IHC was performed on the FFPE tissue samples as previously described (Mlecnik et al., 2016; Qin et al., 2020; Wang et al., 2020). Tissue sections (4 μm thick) were labelled with antibodies targeting SARS-CoV-2 NP, as listed in **Supplementary Table S1**. Appropriate controls were included. To evaluate the antibody-labelled sections, images were captured using an IntelliSite Ultra-Fast Scanner (Philips, Eindhoven, Netherlands).

SARS-CoV-Ab Serology

Post-mortem arterial blood from all 8 COVID19 RT-PCR positive patients was tested SARS-CoV-Ab was measured on the Cobas e801 immunoassay analyzer (Roche). This assay measures total antibodies directed against the nucleocapsid protein. The assay has a specificity of 99.9% (714/715) and a sensitivity of 48.2% within the first week after positive RT-PCR results (n = 189) rising to 97.1% 14 days post-PCR diagnosis (n = 70). COI>1.0 are considered positive. for SARS-CoV-2 antibodies on the Roche Cobas e801 analyzer as per the manufacturer's instructions. The performance of this Roche assay has been evaluated and verified recently (Lau et al., 2020).

DATA AVAILABILITY STATEMENT

The raw data supporting the conclusions of this article will be made available by the authors, without undue reservation.

ETHICS STATEMENT

SingHealth CIRB Committee waived the requirement for ethical approval and written informed consent for participants in this study because this application involves the use of de-identified slides that cannot be readily identified in accordance with the national legislation and the institutional requirements.

AUTHOR CONTRIBUTIONS

KC: Optimization, validation and reporting RT-PCR assay TA: Optimization, validation and reporting serology assay JY: Optimization, validation and reporting of multiplex immunoassays PC: Conducting autopsy and reviewing histology slides JI and PYC: Reviewing histology slides.

All authors whose names appear on the submission.

1) made substantial contributions to the conception of the work, acquisition, analysis, or interpretation of data.
2) drafted the work or revised it critically for important intellectual content
3) approved the version to be published and
4) agree to be accountable for all aspects of the work

SUPPLEMENTARY MATERIAL

The Supplementary Material for this article can be found online at: https://www.frontiersin.org/articles/10.3389/fmolb.2021.658932/full#supplementary-material

REFERENCES

Abel, E. J., Bauman, T. M., Weiker, M., Shi, F., Downs, T. M., Jarrard, D. F., et al. (2014). Analysis and Validation of Tissue Biomarkers for Renal Cell Carcinoma Using Automated High-Throughput Evaluation of Protein Expression. *Hum. Pathol.* 45 (5), 1092–1099. doi:10.1016/j.humpath.2014.01.008

Babapoor-Farrokhran, S., GillWalker, D. J., Rasekhi, R. T., Bozorgnia, B., and Amanullah, A. (2020). Myocardial Injury and COVID-19: Possible Mechanisms. *Life Sci.* 253, 117723. doi:10.1016/j.lfs.2020.117723

Barton, L. M., Duval, E. J., Stroberg, E., Ghosh, S., and Mukhopadhyay, S. (2020). COVID-19 Autopsies, Oklahoma, USA. *Am. J. Clin. Pathol.* 153, 725–733. doi:10.1093/ajcp/aqaa062

Bearse, M., Hung, Y. P., Krauson, A. J., Bonanno, L., Boyraz, B., Harris, C. K., et al. (2021). Factors Associated with Myocardial SARS-CoV-2 Infection, Myocarditis, and Cardiac Inflammation in Patients with COVID-19. *Mod. Pathol.* 34, 1345–1357. doi:10.1038/s41379-021-00790-1

Boehmer, T. K., Kompaniyets, L., Lavery, A. M., Hsu, J., Ko, J. Y., Yusuf, H., et al. (2021). Association between COVID-19 and Myocarditis Using Hospital-Based Administrative Data - United States, March 2020-January 2021. *MMWR Morb. Mortal. Wkly. Rep.* 70, 1228–1232. doi:10.15585/mmwr.mm7035e5

Cheung, E. W., Zachariah, P., Gorelik, M., Boneparth, A., Kernie, S. G., Orange, J. S., et al. (2020). Multisystem Inflammatory Syndrome Related to COVID-19 in Previously Healthy Children and Adolescents in New York City. *JAMA* 324, 294–296. doi:10.1001/jama.2020.10374

Chong, P. Y., Chui, P., Ling, A. E., Franks, T. J., Tai, D. Y. H., Leo, Y. S., et al. (2004). Analysis of Deaths during the Severe Acute Respiratory Syndrome (SARS) Epidemic in Singapore: Challenges in Determining a SARS Diagnosis. *Arch. Pathol. Lab. Med.* 128 (2), 195–204. doi:10.5858/2004-128-195-aoddts

Corman, V. M., Landt, O., and Kaiser, M. (2021). The Cytokine Storm and COVID-19. *J. Med. Virol.* 25 (1), 250–256. doi:10.1002/jmv.26232

Craver, R., Huber, S., Sandomirsky, M., McKenna, D., Schieffelin, J., and Finger, L. (2020). Fatal Eosinophilic Myocarditis in a Healthy 17-Year-Old Male with Severe Acute Respiratory Syndrome Coronavirus 2 (SARS-CoV-2c). *Fetal Pediatr. Pathol.* 39, 263–268. doi:10.1080/15513815.2020.1761491

Dandekar, A. A., and Perlman, S. (2005). Immunopathogenesis of Coronavirus Infections: Implications for SARS. *Nat. Rev. Immunol.* 5 (12), 917–927. doi:10.1038/nri1732

Delpino, M. V., and Quarleri, J. (2020). SARS-CoV-2 Pathogenesis: Imbalance in the Renin-Angiotensin System Favors Lung Fibrosis. *Front. Cel. Infect. Microbiol.* 10, 340. doi:10.3389/fcimb.2020.00340

Diao, B., Wang, C., Tan, Y., Chen, X., Liu, Y., Ning, L., et al. (2020). Reduction and Functional Exhaustion of T Cells in Patients with Coronavirus Disease 2019 (COVID-19). *Front. Immunol.* 11, 827. doi:10.3389/fimmu.2020.00827

Esbona, K., Inman, D., Saha, S., Jeffery, J., Schedin, P., Wilke, L., et al. (2016). COX-2 Modulates Mammary Tumor Progression in Response to Collagen Density. *Breast Cancer Res.* 18 (1), 35. doi:10.1186/s13058-016-0695-3

Feng, Z., Jensen, S. M., Messenheimer, D. J., Farhad, M., Neuberger, M., Bifulco, C. B., et al. (2016). Multispectral Imaging of T and B Cells in Murine Spleen and Tumor. *J. Immunol.* 196 (9), 3943–3950. doi:10.4049/jimmunol.1502635

Garnelo, M., Tan, A., Her, Z., Yeong, J., Lim, C. J., Chen, J., et al. (2015). Interaction between Tumour-Infiltrating B Cells and T Cells Controls the Progression of Hepatocellular Carcinoma. *Gut* 66 (310814), 342–351. doi:10.1136/gutjnl-2015-310814

Garnelo, M., Tan, A., Her, Z., Yeong, J., Lim, C. J., Chen, J., et al. (2017). Interaction between Tumour-Infiltrating B Cells and T Cells Controls the Progression of Hepatocellular Carcinoma. *Gut* 66 (2), 342–351. doi:10.1136/gutjnl-2015-310814

George, P. M., Wells, A. U., and Jenkins, R. G. (2020). Pulmonary Fibrosis and COVID-19: The Potential Role for Antifibrotic Therapy. *Lancet Respir. Med.* 8, 807–815. doi:10.1016/S2213-2600(20)30225-3

Grifoni, A., Weiskopf, D., Ramirez, S. I., Mateus, J., Dan, J. M., Moderbacher, C. R., et al. (2020). Targets of T Cell Responses to SARS-CoV-2 Coronavirus in Humans with COVID-19 Disease and Unexposed Individuals. *Cell* 181, 1489–1501. doi:10.1016/j.cell.2020.05.015

Hoffmann, M., Kleine-Weber, H., Schroeder, S., Krüger, N., Herrler, T., Erichsen, S., et al. (2020). SARS-CoV-2 Cell Entry Depends on ACE2 and TMPRSS2 and Is Blocked by a Clinically Proven Protease Inhibitor. *Cell* 181 (2), 271–280. doi:10.1016/j.cell.2020.02.052

Huang, C., Wang, Y., Li, X., Ren, L., Zhao, J., Hu, Y., et al. (2020a). Clinical Features of Patients Infected with 2019 Novel Coronavirus in Wuhan, China. *The Lancet* 395 (10223), 497–506. doi:10.1016/s0140-6736(20)30183-5

Huang, H.-I., Lin, J.-Y., Chiang, H.-C., Huang, P.-N., Lin, Q.-D., and Shih, S.-R. (2020b). Exosomes Facilitate Transmission of Enterovirus A71 from Human Intestinal Epithelial Cells. *J. Infect. Dis.* 222 (3), 456–469. doi:10.1093/infdis/jiaa174

Lam, J. H., Ng, H. H. M., Lim, C. J., Sim, X. N., Malavasi, F., Li, H., et al. (2019). Expression of CD38 on Macrophages Predicts Improved Prognosis in Hepatocellular Carcinoma. *Front. Immunol.* 10, 2093. doi:10.3389/fimmu.2019.02093

Lau, C. S., Hoo, S. P., Yew, S. F., Ong, S. K., Lum, L. T., Heng, P. Y., et al. (2020). Evaluation of an Electrochemiluminescent SARS-CoV-2 Antibody Assay. *J. Appl. Lab. Med.* 5, 1313–1323. doi:10.1093/jalm/jfaa134

Le Bert, N., Tan, A. T., Kunasegaran, K., Tham, C. Y. L., Hafezi, M., Chia, A., et al. (2020). SARS-CoV-2-specific T Cell Immunity in Cases of COVID-19 and SARS, and Uninfected Controls. *Nature* 584, 457–462. doi:10.1038/s41586-020-2550-z

Liao, M., Liu, Y., Yuan, J., Wen, Y., Xu, G., Zhao, J., et al. (2020). The Landscape of Lung Bronchoalveolar Immune Cells in COVID-19 Revealed by Single-Cell RNA Sequencing. *Nat. Med.* 26, 842–844. doi:10.1101/2020.02.23.20026690

Lim, J. C. T., Yeong, J. P. S., Lim, C. J., Ong, C. C. H., Wong, S. C., Chew, V. S. P., et al. (2018). An Automated Staining Protocol for Seven-Colour Immunofluorescence of Human Tissue Sections for Diagnostic and Prognostic Use. *Pathology* 50 (3), 333–341. doi:10.1016/j.pathol.2017.11.087

Lovisa, S., LeBleu, V. S., Tampe, B., Sugimoto, H., Vadnagara, K., Carstens, J. L., et al. (2015). Epithelial-to-Mesenchymal Transition Induces Cell Cycle Arrest and Parenchymal Damage in Renal Fibrosis. *Nat. Med.* 21 (9), 998–1009. doi:10.1038/nm.3902

Mlecnik, B., Bindea, G., Kirilovsky, A., Angell, H. K., Obenauf, A. C., Tosolini, M., et al. (2016). The Tumor Microenvironment and Immunoscore Are Critical Determinants of Dissemination to Distant Metastasis. *Sci. Transl. Med.* 8 (327), 327ra26. doi:10.1126/scitranslmed.aad6352

Molenkamp, R., Meijer, A., Chu, D. K., Bleicker, T., Brünink, S., Schneider, J., et al. (2020). Detection of 2019 Novel Coronavirus (2019-nCoV) by Real-Time RT-

PCR. *Euro Surveill.* 25 (3), 2000045. doi:10.2807/1560-7917.ES.2020.25.3.2000045

Nghiem, P. T., Bhatia, S., Lipson, E. J., Kudchadkar, R. R., Miller, N. J., Annamalai, L., et al. (2016). PD-1 Blockade with Pembrolizumab in Advanced Merkel-Cell Carcinoma. *N. Engl. J. Med.* 374 (26), 2542–2552. doi:10.1056/nejmoa1603702

Ni, L., Ye, F., Cheng, M.-L., Feng, Y., Deng, Y.-Q., Zhao, H., et al. (2020). Detection of SARS-CoV-2-specific Humoral and Cellular Immunity in COVID-19 Convalescent Individuals. *Immunity* 52, 971–977. doi:10.1016/j.immuni.2020.04.023

Patil, M., Singh, S., Henderson, J., and Krishnamurthy, P. (2020). Mechanisms of COVID-19-induced Cardiovascular Disease: Is Sepsis or Exosome the Missing Link?. *J. Cel Physiol* 236, 3366–3382. doi:10.1002/jcp.30109

Peiris, J., Lai, S., Poon, L., Guan, Y., Yam, L., Lim, W., et al. (2003). Coronavirus as a Possible Cause of Severe Acute Respiratory Syndrome. *The Lancet* 361, 1319–1325. doi:10.1016/s0140-6736(03)13077-2

Qin, C., Zhou, L., Hu, Z., Zhang, S., Yang, S., Tao, Y., et al. (2020). Dysregulation of Immune Response in Patients with Coronavirus 2019 (COVID-19) in Wuhan, China. *Clin. Infect. Dis.* 71, 762–768. doi:10.1093/cid/ciaa248

Robinson, E. L., Alkass, K., Bergmann, O., Maguire, J. J., Roderick, H. L., and Davenport, A. P. (2020). Genes Encoding ACE2, TMPRSS2 and Related Proteins Mediating SARS-CoV-2 Viral Entry Are Upregulated with Age in Human Cardiomyocytes. *J. Mol. Cell Cardiol.* 147, 88–91. doi:10.1016/j.yjmcc.2020.08.009

Sahin, U., Muik, A., Derhovanessian, E., Vogler, I., Kranz, L. M., Vormehr, M., et al. (2020). COVID-19 Vaccine BNT162b1 Elicits Human Antibody and TH1 T Cell Responses. *Nature* 586, 594–599. doi:10.1038/s41586-020-2814-7

Shi, Y., Tan, M., Chen, X., Liu, Y., Huang, J., Ou, J., et al. (2020). Immunopathological Characteristics of Coronavirus Disease 2019 Cases in Guangzhou, China. *medRxiv* 160, 261–268. doi:10.1101/2020.03.12.20034736

Shirazi, S., Mami, S., Mohtadi, N., Ghaysouri, A., Tavan, H., Nazari, A., et al. (2021). Sudden Cardiac Death in COVID-19 Patients, a Report of Three Cases. *Future Cardiol.* 17 (1), 113–118. doi:10.2217/fca-2020-0082

Siripanthong, B., Nazarian, S., Muser, D., Deo, R., Santangeli, P., Khanji, M. Y., et al. (2020). Recognizing COVID-19-Related Myocarditis: The Possible Pathophysiology and Proposed Guideline for Diagnosis and Management. *Heart Rhythm* 17, 1463–1471. doi:10.1016/j.hrthm.2020.05.001

Stack, E. C., Wang, C., Roman, K. A., and Hoyt, C. C. (2014). Multiplexed Immunohistochemistry, Imaging, and Quantitation: a Review, with an Assessment of Tyramide Signal Amplification, Multispectral Imaging and Multiplex Analysis. *Methods* 70 (1), 46–58. doi:10.1016/j.ymeth.2014.08.016

Thevarajan, I., Nguyen, T. H. O., Koutsakos, M., Druce, J., Caly, L., van de Sandt, C. E., et al. (2020). Breadth of Concomitant Immune Responses Prior to Patient Recovery: A Case Report of Non-Severe COVID-19. *Nat. Med.* 26 (4), 453–455. doi:10.1038/s41591-020-0819-2

Thieme, C. J., Anft, M., Paniskaki, K., Blazquez-Navarro, A., Doevelaar, A., Seibert, F. S., et al. (2020). The SARS-CoV-2 T-Cell Immunity Is Directed against the Spike, Membrane, and Nucleocapsid Protein and Associated with COVID 19 Severity. *Cell Rep. Med.* 1 (6), 10092. doi:10.1101/2020.05.13.20100636

Varga, Z., Flammer, A. J., Steiger, P., Haberecker, M., Andermatt, R., Zinkernagel, A. S., et al. (2020). Endothelial Cell Infection and Endotheliitis in COVID-19. *The Lancet* 395, 1417–1418. doi:10.1016/s0140-6736(20)30937-5

Wang, C., Xie, J., Zhao, L., Fei, X., Zhang, H., Tan, Y., et al. (2020). Alveolar Macrophage Dysfunction and Cytokine Storm in the Pathogenesis of Two Severe COVID-19 Patients. *EBioMedicine* 57, 102833. doi:10.1016/j.ebiom.2020.102833

Weiskopf, D., Schmitz, K., Raadsen, M., Grifoni, A., Okba, N., Endeman, H., et al. (2020). Phenotype of SARS-CoV-2-specific T-Cells in COVID-19 Patients with Acute Respiratory Distress Syndrome. *Sci Immunol.* 5 (48), eabd2071. doi:10.1126/sciimmunol.abd2071

Wen, W., Su, W., Tang, H., Le, W., Zhang, X., Zheng, Y., et al. (2020). Immune Cell Profiling of COVID-19 Patients in the Recovery Stage by Single-Cell Sequencing. *Cell Discov* 6 (1), 31. doi:10.1038/s41421-020-0168-9

WHO (2020). Available at: www.who.int/emergencies/diseases/novel-coronavirus-2-19/interactive-timeline#event-71 accessioned (Accessed Aug 20, 2020).

Wick, G., Backovic, A., Rabensteiner, E., Plank, N., Schwentner, C., and Sgonc, R. (2010). The Immunology of Fibrosis: Innate and Adaptive Responses. *Trends Immunol.* 31 (3), 110–119. doi:10.1016/j.it.2009.12.001

Wick, G., Knoflach, M., and Xu, Q. (2004). Autoimmune and Inflammatory Mechanisms in Atherosclerosis. *Annu. Rev. Immunol.* 22, 361–403. doi:10.1146/annurev.immunol.22.012703.104644

Wong, C. K., Lam, C. W. K., Wu, A. K. L., Ip, W. K., Lee, N. L. S., Chan, I. H. S., et al. (2004). Plasma Inflammatory Cytokines and Chemokines in Severe Acute Respiratory Syndrome. *Clin. Exp. Immunol.* 136 (1), 95–103. doi:10.1111/j.1365-2249.2004.02415.x

Wu, C., Chen, X., Cai, Y., Xia, J. a., Zhou, X., Xu, S., et al. (2020). Risk Factors Associated with Acute Respiratory Distress Syndrome and Death in Patients with Coronavirus Disease 2019 Pneumonia in Wuhan, China. *JAMA Intern. Med.* 180, 934–943. doi:10.1001/jamainternmed.2020.0994

Xu, X., Chen, P., Wang, J., Feng, J., Zhou, H., Li, X., et al. (2020). Evolution of the Novel Coronavirus from the Ongoing Wuhan Outbreak and Modeling of its Spike Protein for Risk of Human Transmission. *Sci. China Life Sci.* 63 (1674-7305), 457–460. doi:10.1007/s11427-020-1637-5

Xu, Z., Shi, L., Wang, Y., Zhang, J., Huang, L., Zhang, C., et al. (2020). Pathological Findings of COVID-19 Associated with Acute Respiratory Distress Syndrome. *Lancet Respir. Med.* 8 (4), 420–422. doi:10.1016/s2213-2600(20)30076-x

Yajima, T., and Knowlton, K. U. (2009). Viral Myocarditis. *Circulation* 119, 2615–2624. doi:10.1161/circulationaha.108.766022

Yang, N., Tian, K., Jin, M., Zhang, X., Zhang, F., Shi, X., et al. (2021). Sudden Death of COVID-19 Patients in Wuhan, China: A Retrospective Cohort Study. *J. Glob. Health* 11, 05006. doi:10.7189/jogh.11.05006

Yao, X. H., Li, T. Y., He, Z. C., Ping, Y. F., Liu, H. W., Yu, S. C., et al. (2020). A Pathological Report of Three COVID-19 Cases by Minimal Invasive Autopsies. *Zhonghua Bing Li Xue Za Zhi* 49 (5), 411–417. doi:10.3760/cma.j.cn112151-20200312-00193

Yeong, J., Lim, J. C. T., Lee, B., Li, H., Ong, C. C. H., Thike, A. A., et al. (2019). Prognostic Value of CD8 + PD-1+ Immune Infiltrates and PDCD1 Gene Expression in Triple Negative Breast Cancer. *J. Immunotherapy Cancer* 7 (1), 34. doi:10.1186/s40425-019-0499-y

Yeong, J., Thike, A. A., Lim, J. C. T., Lee, B., Li, H., Wong, S.-C., et al. (2017). Higher Densities of Foxp3+ Regulatory T Cells Are Associated with Better Prognosis in Triple-Negative Breast Cancer. *Breast Cancer Res. Treat.* 163 (1), 21–35. doi:10.1007/s10549-017-4161-4

Zheng, M., Gao, Y., Wang, G., Song, G., Liu, S., Sun, D., et al. (2020). Functional Exhaustion of Antiviral Lymphocytes in COVID-19 Patients. *Cell Mol Immunol* 17, 533–535. doi:10.1038/s41423-020-0402-2

Zheng, W.-P., and Flavell, R. A. (1997). The Transcription Factor GATA-3 Is Necessary and Sufficient for Th2 Cytokine Gene Expression in CD4 T Cells. *Cell* 89 (4), 587–596. doi:10.1016/s0092-8674(00)80240-8

Zhu, N., Zhang, D., Wang, W., Li, X., Yang, B., Song, J., et al. (2020). A Novel Coronavirus from Patients with Pneumonia in China, 2019. *N. Engl. J. Med.* 382, 727–733. doi:10.1056/NEJMoa2001017

Conflict of Interest: The authors declare that the research was conducted in the absence of any commercial or financial relationships that could be construed as a potential conflict of interest.

Publisher's Note: All claims expressed in this article are solely those of the authors and do not necessarily represent those of their affiliated organizations, or those of the publisher, the editors and the reviewers. Any product that may be evaluated in this article, or claim that may be made by its manufacturer, is not guaranteed or endorsed by the publisher.

Advantages of publishing in Frontiers

OPEN ACCESS
Articles are free to read for greatest visibility and readership

FAST PUBLICATION
Around 90 days from submission to decision

HIGH QUALITY PEER-REVIEW
Rigorous, collaborative, and constructive peer-review

TRANSPARENT PEER-REVIEW
Editors and reviewers acknowledged by name on published articles

Frontiers
Avenue du Tribunal-Fédéral 34
1005 Lausanne | Switzerland

Visit us: www.frontiersin.org
Contact us: frontiersin.org/about/contact

REPRODUCIBILITY OF RESEARCH
Support open data and methods to enhance research reproducibility

DIGITAL PUBLISHING
Articles designed for optimal readership across devices

FOLLOW US
@frontiersin

IMPACT METRICS
Advanced article metrics track visibility across digital media

EXTENSIVE PROMOTION
Marketing and promotion of impactful research

LOOP RESEARCH NETWORK
Our network increases your article's readership